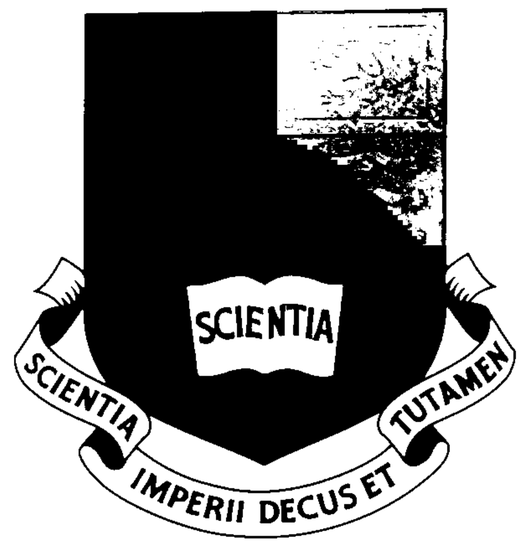
Imperial College
London



MODELLING OF FLOWS IN VERTICAL PIPES AND ITS APPLICATION TO MULTIPHASE FLOW METERING AT HIGH GAS CONTENT AND TO THE PREDICTION OF WELL PERFORMANCE

Gioia Falcone

A dissertation submitted to the University of London in fulfilment of the requirements for the degree of Doctor of Philosophy and the Diploma of Imperial College

Department of Chemical Engineering and Chemical Technology

Imperial College London

January 2006

BRL.
LONDON.
UNIV

ABSTRACT

This thesis is comprised of two main parts, which share a common two-phase flow modelling basis.

The first part is focussed on the problem of Multiphase Flow Metering (MFM) within the oil and gas industry. The focus is on the case of flow with high gas fractions, i.e. Wet Gas Metering, which is a specific problem area within the field of MFM. Both established and novel technologies, suitable to measure the flow rates of oil, gas and water in a three-phase flow, are critically reviewed and assessed within this thesis A novel wet gas metering concept, ANUMET, was developed as part of this Ph.D. work and protected by international patent. This concept is described in this thesis and some preliminary results are presented.

The second part of this thesis deals with the physical understanding of the phenomena occurring in well testing. This work was carried out within the aegis of a Joint Industrial Project (JIP) on well test analysis for gas-condensate reservoirs based on the pressure transient method. Analysis of pressure transient following a well shut-down is a well established reservoir evaluation method. However, much of the pressure data recorded during a well test may be dominated by wellbore effects that can mask reservoir characteristics and lead to erroneous well test interpretations. The work described in this thesis addresses the interpretation of pressure transient data to take account of these effects. The ultimate objective of the project of which the work described in this thesis forms a part is to achieve a full phenomenological model of the complex transient multiphase flow behaviour. In the work described here, a number of steps were made towards this ultimate objective as follows:

1. A series of simple experiments were supervised and analysed for the case of the isolation of a bubble flow in a vertical tube and for the case of shut-down of an experimental system aimed at simulation of the reservoir/well combination.

2. An existing code for phenomenological modelling of steady-state flows in a vertical tube (GRAMP2) was modified to predict well flows by linking it to a physical property package (Multiflash).
3. Work was carried out on providing a methodology for linking the reservoir and the well behaviour.
4. An analytical framework was developed for the transient behaviour of single-phase gas flow in a reservoir/well system.
5. Work was carried out on the full set of equations for a transient annular two-phase flow.

The way forward to the dynamic integration between the wellbore and the near-wellbore reservoir is suggested within this thesis.

Acknowledgements

I would like to thank everyone who helped during the course of my thesis.

In particular, Geoff Hewitt, for his endless enthusiasm and unique insight. Even though my industrial sponsors kept changing over the years, Geoff remained my constant point of reference. I will always feel privileged for being given the opportunity to work with him.

Also, I am extremely grateful to Colin Hale for his continuous technical advice and invaluable help with the experimental work in the laboratory, and to Liyun Lao for his collaboration to the testing of ANUMET in the LOTUS rig.

Finally, my special thanks go to Jader Barbosa for his generous contribution to this project, in particular to the enhancement of the GRAMP2 code and the development of the transient annular flow equations.

Table of Contents

CHAPTER 1 ..... **14**

Introduction **14**

1.1 The objective of the work 14

1.2 The nature of gas-liquid flows 15

1.3 Modelling methods for vertical gas-liquid flows 16

1.3.1 Bubble flow 18

1.3.2 Transition between bubble flow and slug flow 20

1.3.3 Slug flow 22

1.3.4 Transition from slug flow to churn flow 24

1.3.5 Churn flow 26

1.3.6 Churn/annular transition 27

1.3.7 Annular flow 28

1.3.8 Annular/wispy annular transition 35

1.3.9 Wispy annular flow 36

1.4 Structure of the thesis 38

CHAPTER 2 ..... **40**

State-of-the-art of Multiphase Flow Metering (MFM) **40**

2.1 Summary 40

2.2 Brief history of MFM 41

2.3 MFM applications 41

2.3.1 Layout of production facilities 41

2.3.2 Well testing 42

2.3.3 Reservoir management 42

2.3.4 Production allocation 42

2.3.5 Production monitoring 43

2.3.6 CAPEX and OPEX 43

2.3.7 Fiscal metering or custody transfer 44

2.4 How accurate can MFM be? 44

2.5 MFM installations worldwide 47

2.6 Fundamentals of MFM technologies 50

2.6.1 Dual energy gamma densitometry 51
2.6.2 Impedance and microwave techniques 54
2.6.3 Differential pressure devices 55
2.6.4 Cross correlation 56
2.7 Novel MFM technologies 58
2.8 Review of commercial MFM's 60
2.9 The future of MFM 65
2.9.1 Better accuracy, repeatability, and reliability 66
2.9.2 Clamp-on solutions for topsides and seabed applications 66
2.9.3 International Regulation on MFM accuracy requirements 66
2.9.4 Flow assurance via integration of technologies 67
2.9.5 Integrated solutions to optimise field recovery 69
2.9.6 Wet gas metering 70
2.10 Conclusions 71

CHAPTER 3 72
Wet Gas Metering and ANUMET 72
3.1 Summary 72
3.2 Introduction 73
3.2.1 Definition of wet gas and wet gas metering issues 73
3.3 The ANUMET system 77
3.3.1 Technical description 78
3.4 Experimental equipment and test procedure 88
3.4.1 The LOTUS rig 88
3.4.2 The experimental set up 90
3.5 Results 93
3.6 Conclusions 101

CHAPTER 4 102
Introduction to Well Test Analysis 102
4.1 Introduction to well test analysis 102
4.2 Well test analysis in gas condensate and volatile oil reservoirs 106
4.3 Wellbore phenomena during transient well testing 106
4.4 Conclusions 117

CHAPTER 5 ..... **118**

Experimental studies simulating well testing and their interpretation **118**

5.1 Background 118

5.2 Experimental studies simulating well testing 119

5.3 A model for transient bubbly flow 120

5.3.1 Well with bubbly flow in steady-state 121

5.3.2 Situation after shut-in 123

5.3.3 Implementation 124

5.4 Comparison with experiments of Al-Darmaki 124

5.5 Conclusions 126

CHAPTER 6 ..... **127**

Wellbore modelling as an aid to Well Test Analysis for Gas Condensate Reservoirs: GRAMP2 ..... **127**

6.1 Introduction 127

6.2 Background to GRAMP2 127

6.3 Enhancements to the code: compositional PVT characterisation 128

6.3.1 Building an interface between GRAMP2 and PVTi 129

6.3.2 Implementing EoS and flash calculations in GRAMP2 129

6.3.3 Building an interface between GRAMP2 and Multiflash 137

6.4 Enhancements to the code: temperature calculation 138

6.5 GRAMP2: new (compositional) version 138

6.6 Steady-state simulations using the new version of GRAMP2 154

6.6.1 Results of simulations 156

6.7 Conclusions 160

CHAPTER 7 ..... **162**

Work towards a transient phenomenological wellbore model **162**

7.1 Introduction 162

7.2 Current approach to integrated reservoir-wellbore systems 163

7.3 Link between wellbore conditions and efflux from the reservoir 165

7.4 Integrated approach to reservoir and wellbore equations for transient flows (single phase compressible fluid) 167

7.4.1 The equations for the well 167

7.4.2 The equations for the reservoir 168
7.4.3 Solution procedure 169
7.5 Transient annular flow 173
7.6 Conclusions 174

CHAPTER 8 175
Conclusions and recommendations for future work 175
8.1 Conclusions 175
8.1.1 MFM and wet gas metering 175
8.1.2 Work towards a transient reservoir/wellbore model 176
8.2 Recommendations for future work 177
8.2.1 Future work on MFM and wet gas metering 177
8.2.2 Future work towards a transient reservoir/wellbore model 177

Nomenclature 179

References 183

APPENDIX I 199
Experimental data gathered in LOTUS during ANUMET tests 199

APPENDIX II 205
Equations for transient two-phase annular flow 205

APPENDIX III 226
Selection of publications related to this Ph.D. work 226

List of Figures

CHAPTER 1

Fig.1 - 1: Flow regimes in gas-liquid flow in vertical tubes 15

Fig.1 - 2: Solutions for void fraction in vertical flow using the one-dimensional analysis method: (a) vertical co-current upflow; (b) vertical co-current downflow; (c) vertical counter-current flow (liquid down, gas up); (d) vertical counter-current flow (liquid up, gas down) 19

Fig.1 - 3: Variation of total pressure gradient with flow regime. Comparison of pressure gradient predictions with measurements for air-water flow 24

Fig.1 - 4: Flow reversal in the liquid film zone in churn flow 26

Fig.1 - 5: Repetitive wave formation and transport in churn flow 27

Fig.1 - 6: Data for liquid entrained fraction in the churn/annular transition region 28

Fig.1 - 7: Relationship between film friction factor and film Reynolds number for annular flow. Calculated by Hewitt and Hall-Taylor from the numerical integration results of Hewitt 29

Fig.1 - 8: Comparison of triangular relationship with experimental data for film flow rate of Gill et al. 30

Fig.1 - 9: Comparison of pressure gradient predictions with measurements for air-water flow 34

Fig.1 - 10: Comparison of film flow rates predicted by Hewitt and Govan with the experimental steam-water data of Nigmatulin 35

Fig.1 - 11: Comparison of predicted annular/wispy annular regime transition with transition line observed experimentally by Hewitt and Roberts 36

Fig.1 - 12: Development of frequency spectra for pressure gradient in air-water wispy annular flow 37

Fig.1 - 13: Peak frequencies in pressure gradient fluctuations in air-water wispy annular flow 37

Fig.1 - 14: Power spectral density for optical scattering with and without the film removed upstream of the scattering device 37

CHAPTER 2

Fig.2 - 1: The concept of "rangeability" for differential pressure devices 45

Fig.2 - 2: Schematic of a typical multiphase meter set-up 46

Fig.2 - 3: Growth rate of MFM installations 48

Fig.2 - 4: Estimated number of MFM installations up to 2004, including permanent installations and well testing applications 48

Fig.2 - 5: Current regional distribution of MFM installations 49

Fig.2 - 6: Absolute error in phase fraction for a two-phase system air-water 52

Fig.2 - 7: Absolute error in phase fraction for a two-phase system air-oil 53

Fig.2 - 8: Absolute error in phase fraction for a two-phase system oil-water 53

Fig.2 - 9: Effects of flow regime and void fraction on theoretical response 54

Fig.2 - 10: Effects of orifice/bonnet inserts upstream of a venturi 56

Fig.2 - 11: Cross correlation principle 56

Fig.2 - 12: The use of wellhead choke valves to monitor and predict well performance 69

CHAPTER 3

Fig.3 - 1: Classification of reservoir fluids 74

Fig.3 - 2: Multiphase mass fraction triangles showing liquid volume fraction lines at three gas densities 76

Fig.3 - 3: A proposed map for classifying a wet gas streams, on the basis of superficial velocity for gas and liquid. Three types of "wet gas" have been defined on the basis of the superficial velocity of gas/liquid, GVF and Lockhart Martinelli parameter 77

Fig.3 - 4: Twisted tape with "fish tail" end for separation of liquid drops in annular flow 78

Fig.3 - 5: Comparison between experimental and calculated (from the "triangular relationship") dimensionless film flow rates 80

Fig.3 - 6: Droplet separation by a "fish-tail" twisted tape device 81

Fig.3 - 7: Expansion / contraction device 82

Fig.3 - 8: Effect of expansion/contraction device on entrained fraction 83

Fig.3 - 9: Comparison of venturi pressure drop measured with venturi downstream of expansion/contraction device with that calculated from the homogeneous model 86

Fig.3 - 10: ANUMET metering concept 87

Fig.3 - 11: The LOTUS rig 88

Fig.3 - 12: Flow envelope for the LOTUS rig 89

Fig.3 - 13: The test section in the LOTUS rig 90

Fig.3 - 14: Calculated vs. measured liquid mass flux 94
Fig.3 - 15: Relative error of liquid mass flux (Measured-Calculated)/Measured 94
Fig.3 - 16: Calculated vs. measured gas mass flux (with correction for compressibility effects) 96
Fig.3 - 17: Calculated vs. measured gas mass flux (without correction for compressibility effects) 97
Fig.3 - 18: Error-minimising 'n' exponent vs. measured gas mass flux 98
Fig.3 - 19: Error minimising 'n' exponent vs. measured gas mass flux, plotted for one of the six sets of experiments 98
Fig.3 - 20: Error-minimising and de Leeuw 'n' exponent as a function of the gas Froude number 99
Fig.3 - 21: Error-minimising venturi discharge coefficient vs. stream quality 100

CHAPTER 4

Fig.4 - 1: Drawdown and build-up test sequence 103
Fig.4 - 2: Effect of wellbore storage on pressure tests 107
Fig.4 - 3: Log-log derivative plots, increasing wellbore storage due to phase redistribution in the wellbore 108
Fig.4 - 4: Decrease in near-wellbore liquid saturation below the dew point due to capillary number effects 110
Fig.4 - 5: Increase in near-wellbore gas relative permeability below the dew point due to capillary number effects 110
Fig.4 - 6: Variation of Gas Relative Permeability with Velocity in a Sandstone Core 111

CHAPTER 5

Fig.5 - 1: Comparison of predicted and observed pressure distributions during steady-state flow (in red) and after shut-in (in blue) 125
Fig.5 - 2: Comparison of predicted and observed times to reach steady-state after shut-in 125

CHAPTER 6

Fig.6 - 1: Workflow of GRAMP2 for annular flow regime 148
Fig.6 - 2: Simulated pressure and temperature vs. distance 156

Fig.6 - 3: Simulated void fraction and film thickness vs. distance 156
Fig.6 - 4: Simulated liquid and gas density vs. distance 157
Fig.6 - 5: Simulated gas and liquid viscosity vs. distance 157
Fig.6 - 6: Simulated stream quality and entrained fraction vs. distance 158
Fig.6 - 7: Simulated liquid and gas superficial velocity vs. distance 158
Fig.6 - 8: Compaq Visual FORTRAN workspace with GRAMP2 main programme and ancillary subroutines for the interface with Multiflash 161

CHAPTER 7

Fig.7 - 1: Workflow to investigate bottomhole IPR's during build-ups using Eclipse300 166
Fig.7 - 2: Typical procedure followed to simulate a build-up with Eclipse300 and corresponding output 166

CHAPTER 8

Fig.8 - 1: Experimental layout with pressure vessel and porous medium 178

List of Tables

CHAPTER 2

Table 2 - 1: Current commercial MFM's, WGM's and DMFM's 63

Table 2 - 2: Current commercial MFM's with/without flow conditioning 63

Table 2 - 3: Current commercial MFM's with/without gamma ray source 64

Table 2 - 4: Current commercial MFM's intrusive/non-intrusive 64

Table 2 - 5: Current commercial MFM's with/without cross-correlation 65

CHAPTER 6

Table 6 - 1: Well stream composition as implemented in Multiflash 154

Table 6 - 2: Input data fed to GRAMP2 155

CHAPTER 1

Introduction

1.1 The objective of the work

The overall objective of the work described in this thesis was to further develop modelling methods for gas-liquid flow and to apply these methods to two separate problems (both important in hydrocarbon recovery):

- The measurement of the phase flow rates in a gas-liquid flow. The focus of this application was on the case of flow with high gas fractions, flowing typically in the annular dispersed region;
- The development of a physical understanding of the phenomena occurring in wellbore testing. Here, the well is turned off at the beginning of the test and the subsequent behaviour of pressure, particularly downhole pressure (i.e. the pressure at the bottom of the well), is used to gain information about the state of the reservoir (i.e. the stratum containing the hydrocarbon products – gas and liquid).

An important related objective was to obtain experimental and field data to validate the analyses. In this context, the author carried out test work for validating the modelling of the first problem (two-phase flow metering) and participated in the supervision of two MSc projects and one DipIng project aimed at obtaining data relevant to the second area (well testing). Field data relating to the second application were acquired for a gas condensate field in the North Sea and were used in assessing the modelling of well performance and well testing.

1.2 The nature of gas-liquid flows

Gas-liquid flows are characterised by the types of interfacial distribution observed, known as *flow patterns* or *flow regimes*. The flow patterns depend on phase physical properties, phase flow rates, channel geometry and channel orientation. In the present work, the focus has been on flows in vertical channels of circular cross section and on one particular singularity in such channels, namely the venturi.

The flow patterns occurring in vertical gas-liquid flows are illustrated in **Fig.1 – 1** and are described as follows (Hewitt, 1982):

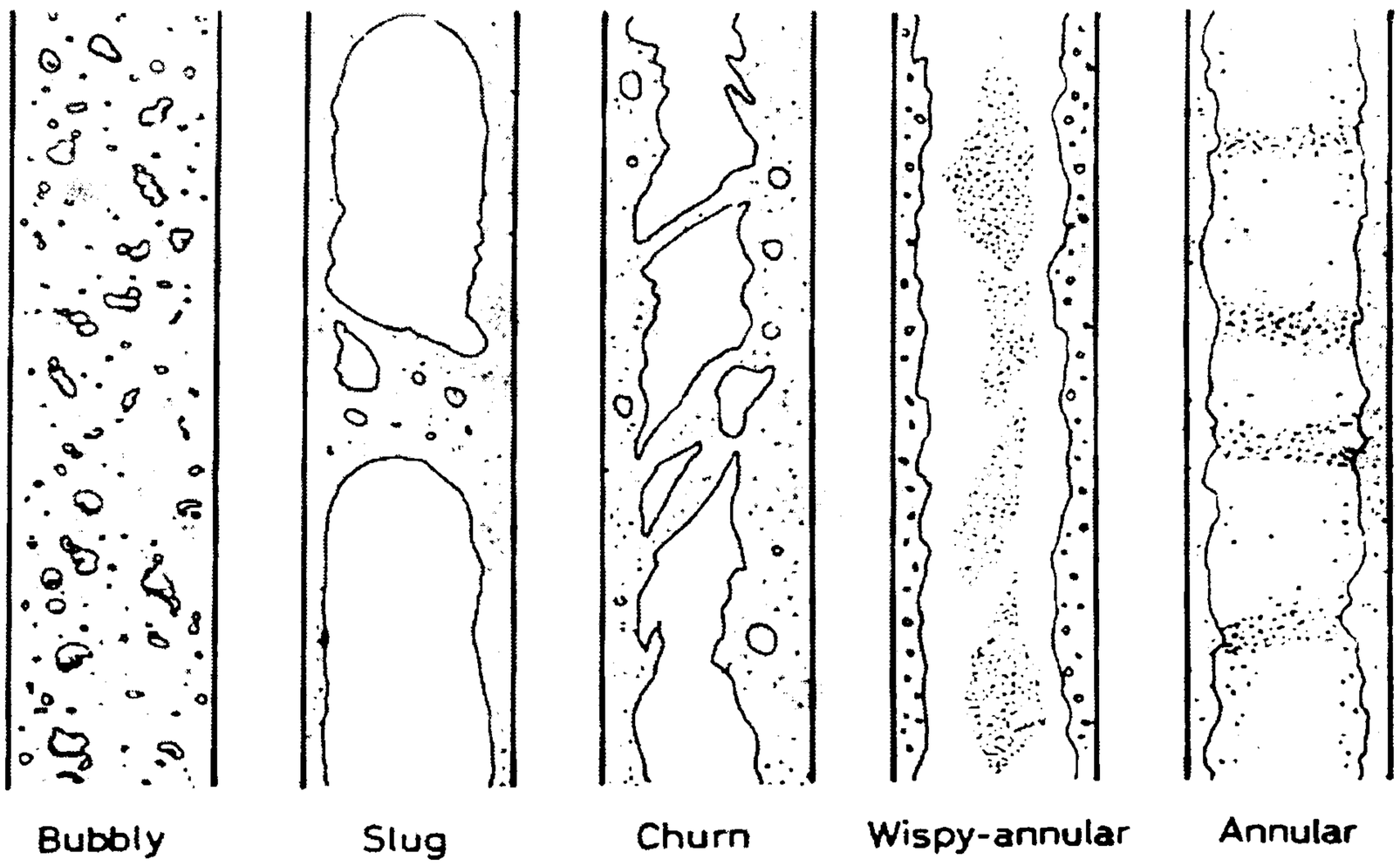


Fig.1 - 1: Flow regimes in gas-liquid flow in vertical tubes (Hewitt, 1982).

1. *Bubble flow*. The liquid phase is continuous and a dispersion of bubbles flows within the liquid continuum. This flow pattern typically occurs at relatively high liquid velocities and low gas velocities.
2. *Slug* (or *plug*) *flow*. At higher gas flows, bubble coalescence occurs and eventually the bubble diameter approaches that of the tube. When this occurs, large, characteristically bullet-shaped bubbles are formed, which may be separated by regions containing a dispersion of smaller bubbles. Typically, the liquid phase flows down the outside of the large bubbles in the form of a falling film, although the net flow of both liquid and gas can be upward.
3. *Churn flow*. It consists of very long gas bubbles and relatively small liquid slugs. With increasing flow velocity, a breakdown of the slug flow bubbles leads to an unstable flow regime in which there is, in wide-bore tubes, an oscillatory motion of the liquid upward and downward in the tube; thus the name churn flow. The oscillation may not occur in narrow-bore tubes and a smoother transition between the slug flow and annular flow regimes may be observed. Because of the high gas velocity, a wave or ripple motion is often observed at the bubble tail with tiny gas bubbles entrained in the liquid slug.
4. *Annular flow*. The liquid flows on the wall of the tube as a film and the gas phase flows in the centre. Usually, some of the liquid phase is entrained as small droplets in the gas core; it is also possible (although less common) for bubbles to be entrained in the liquid.
5. *Wispy annular flow*. As the liquid flow rate is increased, the concentration of drops in the gas core increases; ultimately, droplet coalescence in the core leads to large lumps or streaks (wisps) of liquid in the gas core. This regime is characteristic of flows with high mass flux.

1.3 Modelling methods for vertical gas-liquid flows

The general objective of modelling gas-liquid flows is to estimate the *pressure gradient* (i.e. the change of pressure per unit length of pipe). This pressure gradient $\left(\frac{dp}{dz}\right)$ is often considered to consist of three components, namely *gravitational pressure gradient* $\left(\frac{dp_g}{dz}\right)$, *frictional pressure gradient* $\left(\frac{dp_f}{dz}\right)$ and *accelerational*

pressure gradient $\left(\frac{dp_a}{dz}\right)$. In the classical *separated flow model* for steady-state flow in a constant cross-sectional area vertical duct, these terms are given as (Hewitt, 1982):

$$-\left.\frac{dp}{dz}\right|_g = [(1-\varepsilon_G)\rho_L + \varepsilon_G\rho_G]g \qquad \textbf{Eq.1 - 1}$$

$$-\left.\frac{dp}{dz}\right|_f = \frac{\tau_0 P}{A} \qquad \textbf{Eq.1 - 2}$$

$$-\left.\frac{dp}{dz}\right|_a = \dot{m}^2 \frac{d}{dz}\left[\frac{x^2}{\rho_G\varepsilon_G} + \frac{(1-x)^2}{\rho_L(1-\varepsilon_G)}\right] \qquad \textbf{Eq.1 - 3}$$

where g is the acceleration due to gravity, ε_G the volume fraction of the gas phase in-situ in the channel, ρ_L and ρ_G the gas and liquid densities, τ_0 the wall shear stress, P the channel periphery and A the channel cross-sectional area. $\dot{m}$ is the total mass flux and x the quality (fraction of the mass flux which is gas).

As will be seen from Section 1.2, the nature of two-phase gas-liquid flows is highly complex and the development of adequate models presents a severe challenge. Briefly, models can be categorised as follows:

1. Empirical models, in which data for frictional pressure gradient and void fraction are related to system variables through empirical equations.
2. Phenomenological models, in which observations are made of the flow patterns and models constructed (with appropriate closure laws) to represent the flow taking account of the features of the flow pattern.
3. Multifluid models. These have a formal structure which considers the governing equations (mass, momentum and energy) and solves these with appropriate closure laws (usually based on empirical data) for the particular situation. An example of a code based on this approach, and used in the oil industry, is OLGA (produced by Scandpower Ltd).
4. Interface tracking methods, in which the details of the interfacial structure are calculated by various techniques; a review of such methods is given by Hewitt and Reeks (2005).

The models pursued in the work described in this thesis are firmly in the second category, namely phenomenological models. For vertical flows, they may be summarised as described below.

1.3.1 Bubble flow

The apparent simplicity of bubble flow conceals the reality of extremely complex phenomena occurring, in particular in bubble-bubble interactions, bubble coalescence and bubble break-up. At the simplest level, phenomenological models for bubble flow attempt to take account of these interactions by semi-empirical correlations which recognise that the intensity of interactions increases as the bubble concentration (void fraction) increases. In the *one-dimensional* model for bubbly flow, the volume flux j_{GL} of the gas phase relative to a plane moving at the total superficial velocity $U = U_G + U_L$* is calculated. By continuity, j_{GL} is given by:

$$j_{GL} = U_G(1-\varepsilon_G) + \varepsilon_G U_L \qquad \textbf{Eq.1 - 4}$$

where ε_G is the void fraction. The flux of gas through this moving plane is also governed by physical considerations, including mutual interference between the bubbles, and a classical way of representing this physical situation is through the equation (Wallis, 1969):

$$j_{GL} = u_\infty \varepsilon_G (1-\varepsilon_G)^n \qquad \textbf{Eq.1 - 5}$$

where u_∞ is the rise velocity of a single bubble in a liquid and n is a constant which has a value of the order of 2.0. **Eq.1 - 4** and **Eq.1 - 5** must be satisfied simultaneously and the solution depends on the directions of the flows. These solutions are illustrated in **Fig.1 - 2**; for co-current upflow and co-current downflow, there is a single solution (though the co-current downflow demonstrates a higher void fraction as shown). For flows in which the gas flows up and the liquid flows down, there may be two solutions or a limiting condition ("flooding") in which only one solution occurs. At high liquid velocities, of course, there are no solutions for this case. The

---

* The superficial velocity of a phase is defined as the ratio of the volumetric flow rate of that phase and the cross-sectional area of the pipe.

situation of gas flowing down with liquid flowing up is unphysical as also shown in **Fig.1 - 2**.

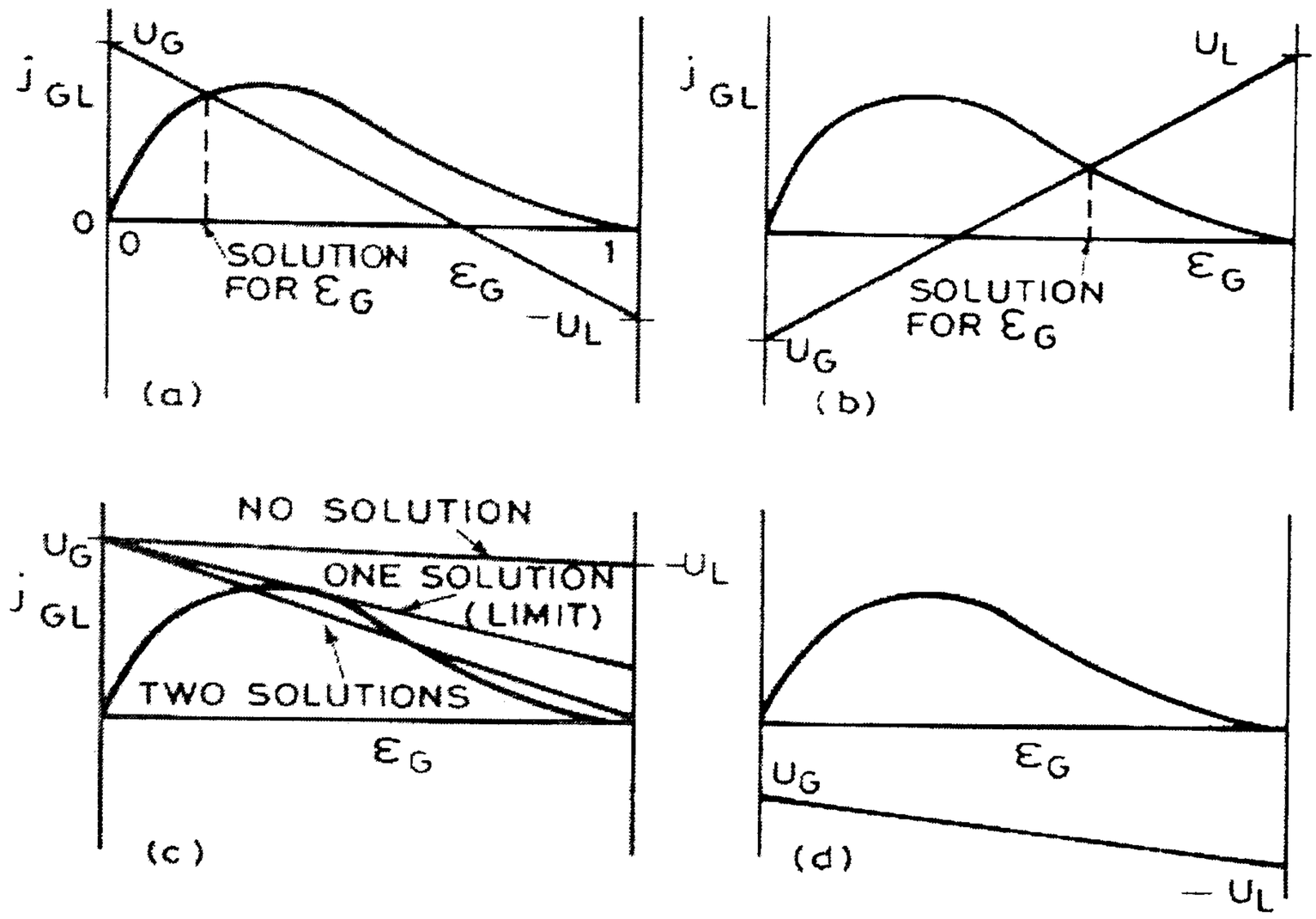


Fig.1 - 2: Solutions for void fraction in vertical flow using the one-dimensional analysis method: (a) vertical co-current upflow; (b) vertical co-current downflow; (c) vertical counter-current flow (liquid down, gas up); (d) vertical counter-current flow (liquid up, gas down) (Hewitt, 1982).

The one-dimensional analysis demonstrated in **Fig.1 - 2** assumes uniform velocity and void fraction across the channel cross section. In fact, void fraction distributions are usually highly non-uniform, with the void fraction near the wall being higher under some circumstances ("wall peaking") and, in other circumstances, the void fraction at the tube axis being highest. We may define an *average* value of a parameter F (which might be, for instance, local superficial velocity, local void fraction, local actual velocity) as follows:

$$\langle F \rangle = \frac{1}{A} \int_A F dA \qquad \textbf{Eq.1 - 6}$$

where A is the cross sectional area of the channel. We can also define a *weighted mean* value of F as follows:

$$\overline{F} = \frac{\langle \varepsilon_G F \rangle}{\langle \varepsilon_G \rangle} = \frac{(1/A)\int_A \varepsilon_G F dA}{(1/A)\int_A \varepsilon_G dA} \qquad \text{Eq.1 - 7}$$

The weighted mean gas velocity $\overline{u}_G$ is given by:

$$\overline{u}_G = C_0 \langle U \rangle + \frac{\langle \varepsilon_G u_{GU} \rangle}{\langle \varepsilon_G \rangle} \qquad \text{Eq.1 - 8}$$

where:

$$C_0 = \frac{\langle \varepsilon_G U \rangle}{\langle \varepsilon_G \rangle \langle U \rangle} = \frac{(1/A)\int_A \varepsilon_G U dA}{(1/A^2)\int_A U dA \int_A \varepsilon_G dA} \qquad \text{Eq.1 - 9}$$

where C_o is a *distribution parameter*, which has a value of the order of 1.2 for bubbly flows. u_{GU} is the local rise velocity of the gas bubbles relative to the mean flow and, in this model, need not be assumed to be constant as it was in the one-dimensional model. In fact, effective "slip" between the two phases can occur even if u_{GU} is zero across the channel, due to differences in the shapes of the velocity and void fraction profiles. Thus, in this case, the slip ratio is given by:

$$S = \frac{\langle 1 - \varepsilon_G \rangle}{1/C_o - \langle \varepsilon_G \rangle} \qquad \text{Eq.1 - 10}$$

In recent years, much work has been carried out on the phenomena occurring in bubbly flows with a wide range of local measurements (carried out using, for instance, point conductance probes and optical probes) and, increasingly, using computational methods to represent the detail motions and interfacial deformations of the bubbles.

1.3.2 Transition between bubble flow and slug flow

Basically, two main mechanisms have been proposed for the bubble/slug flow transition:

(1) Gradual growth of bubbles by coalescence, leading to spherical cap bubbles that are of the same order of size as the pipe and, hence, giving slug flow. Calculations on collision frequency were carried out by Radovcich and Moissis (1962). They hypothesised that the transition to slug flow became more likely when the collision frequency increased rapidly with void fraction in the range of 0.2-0.3. This has led to suggestions that the transition might typically occur at void fractions around 0.25. However, a counteracting influence is that of break-up of bubbles by turbulence and such a mechanism is included in the generic flow pattern map of Taitel and Dukler (1976).

(2) Bubble coalescence is a relatively slow process, governed by the drainage of a liquid film near the point of contact, and bubbles may separate before coalescence occurs. Thus, in more recent times, it has been suggested that an essential step is the formation of "void waves" in which regions of large bubble concentration occur and in which bubble separation is inhibited (thus giving more time for coalescence). An instability mechanism exists, leading to the growth of void waves (see, for example, Biesheuval and Gorissen (1988)) and predictions so that void waves grow significantly at void fractions consistent with the observed transition values.

If the bubble/slug transition occurs due to a gradual coalescence and growth of the bubbles, then there will be a significant effect of channel length on the transition void fraction. Observations reported by Hewitt (1990) showed that the critical void fraction for the bubble/slug transition increased and then decreased with increasing liquid velocity. More importantly, it was found that the limiting void fraction was independent of the channel length in the range 0.77 to 4.87m. This suggests that an instability mechanism, such as void waves rather than the gradual growth of bubbles, may be the explanation of the transition. However, this matter is still highly controversial, with more recent evidence partially supporting the gradual growth mechanism.

1.3.3 Slug flow

Flow that we describe here as "slug flow" is sometimes referred to as "plug flow" or "elongated bubble flow". An attempt is often made to make distinctions between various types of intermittent flows of this type on the basis of, say, the amount of gas entrained in the "slugs" (i.e., the liquid-continuous zones between the large gas bubbles). Certainly, at low velocities, the slugs are relatively gas-free and, as velocity increases, more and more small bubbles are entrained in them. In this context, the term "slug flow" is taken as covering the full gamut of these situations; making finer distinctions can be rather confusing.

In slug flow, an important parameter is the rise velocity (u_s) of a Taylor bubble in a static fluid. For low-viscosity fluids (e.g. water) and wide bore tubes (wider than 1 cm, say), u_s is given by:

$$u_s = 0.345\sqrt{gd} \qquad \textbf{Eq.1 - 11}$$

where g is the acceleration due to gravity and d the tube diameter. For higher viscosity fluids and smaller diameter tubes, account has to be taken of viscosity and surface tension, and a correlation for u_s was developed by Wallis (1962) as follows:

$$\frac{u_S}{\sqrt{gd}} = 0.345\left[1-\exp(0.029Vi)\right]\left(1-\exp\frac{3.37-E\ddot{o}}{m}\right) \qquad \textbf{Eq.1 - 12}$$

where the Viscosity Number, Vi, and the Eötvos Number, $E\ddot{o}$, are given by:

$$Vi = \frac{\left[d^3 g(\rho_L-\rho_G)\right]^{1/2}}{\eta_L} \qquad \textbf{Eq.1 - 13}$$

$$E\ddot{o} = \frac{gd^2(\rho_L-\rho_G)}{\sigma} \qquad \textbf{Eq.1 - 14}$$

where η_L is the liquid phase viscosity, ρ_L and ρ_G the liquid and gas phase densities and σ the surface tension. The parameter m in **Eq.1 – 12** is given by:

$$m = 10 \text{ for } Vi \geq 250 \qquad \textbf{Eq.1 - 15}$$

$$m = 69Vi^{-0.35} \text{ for } 18 \leq Vi \leq 250 \qquad \textbf{Eq.1 - 16}$$

$$m = 29 \text{ for } Vi \leq 18 \qquad \textbf{Eq.1 - 17}$$

For a slug flow (i.e. with simultaneous flow of liquid and gas), the gas velocity u_G is given by:

$$u_G = C_0 U + u_S \qquad \textbf{Eq.1 - 18}$$

where C_0 (a distribution parameter) has a typical value of 1.2. The void fraction ε_G in slug flow is simply given by U_G / u_G.

Two interesting features of slug flow are as follows:

(1) Though the flow in the liquid slugs is generally upwards, the liquid flow around the Taylor bubbles is downwards and this induces downwards flow near the wall near the top of the liquid slug. Thus, for a significant fraction of the time, the wall shear stress is negative and, in many cases, the *averaged* value of wall shear stress is also negative. This implies, curiously, a negative average frictional pressure gradient in slug flow; however, the total pressure gradient is usually governed by the gravitational component which is, of course, positive.

(2) In the top part of the liquid slug, since the velocity near the wall is downwards, the liquid velocity near the axis must, by continuity, be greater than the total superficial velocity. Thus, a Taylor bubble finding itself in this region will move rapidly towards the preceding Taylor bubble, leading to bubble coalescence. This phenomenon was investigated by Moissis and Griffith (1962) who showed that the ratio of

the velocity of the trailing to the leading bubble decreased to unity only after a separation distance (slug length) greater than around 8 diameters. Slug lengths smaller than this are, therefore, unstable.

1.3.4 Transition from slug flow to churn flow

Some insight into the slug/churn transition can be obtained by studying detailed measurements of total pressure gradient in a vertical tube, and the relationship between the total pressure gradient and the flow regime. Typical data of this form were obtained by Owen (1986) and are shown in **Fig.1 - 3** where the dimensionless pressure gradient is plotted as a function of dimensionless air flow rate. The latter is defined as:

$$U_G^* = U_G \sqrt{\frac{\rho_G}{gd(\rho_L - \rho_G)}} \qquad \textbf{Eq.1 - 19}$$

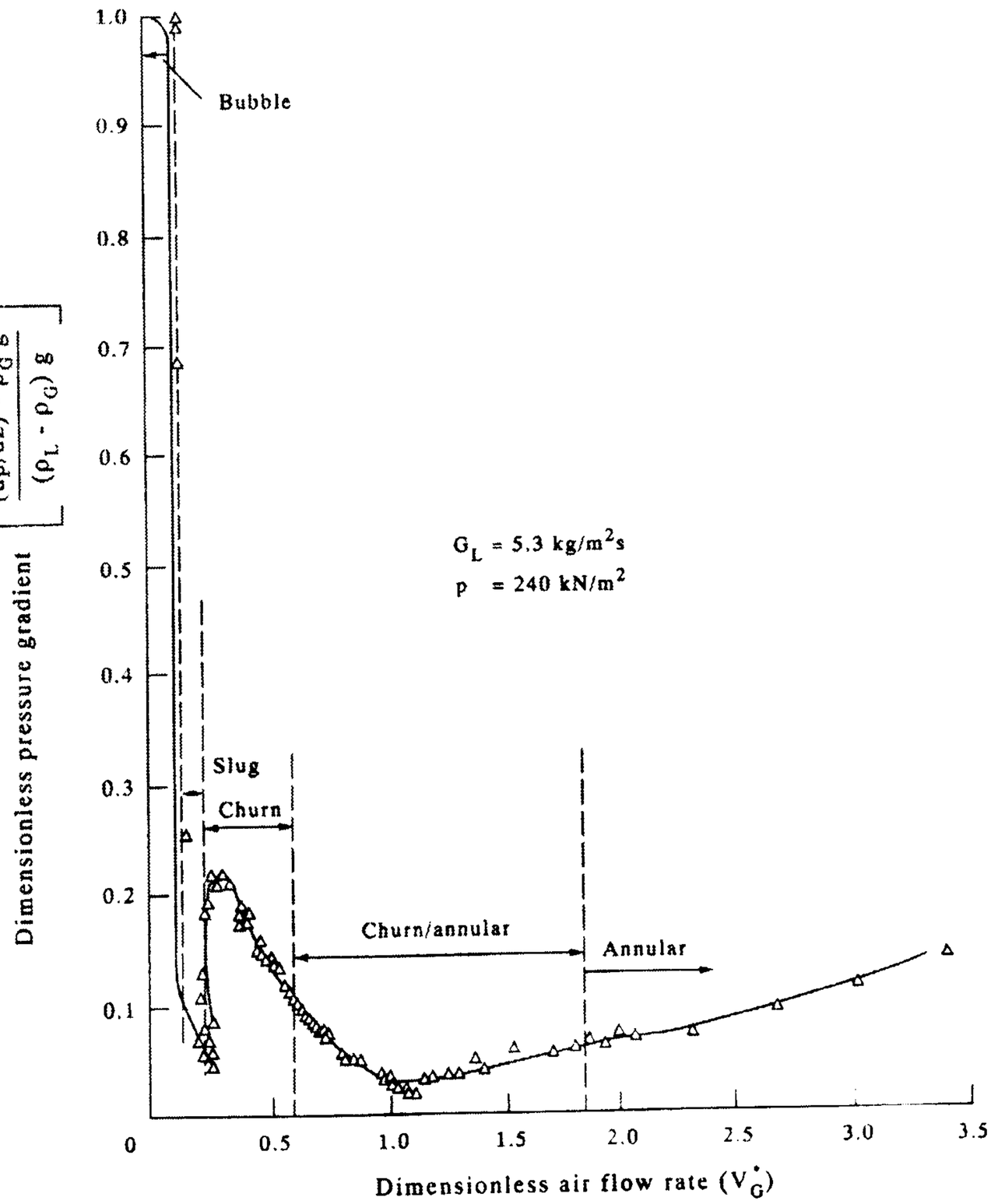


Fig.1 - 3: Variation of total pressure gradient with flow regime. Comparison of pressure gradient predictions with measurements for air-water flow (Owen, 1986).

As will be seen from **Fig.1 - 3**, an excursion in pressure gradient occurs at the slug/churn transition and, following this, the pressure gradient *decreases* with increasing gas flow rate. The pressure gradient reaches a minimum when $U_G^* \approx 1$. Owen designated two regimes, namely "churn" and "churn/annular" in the region following the pressure drop excursion, but it is probably better to define the churn flow regime as that in which the pressure gradient decreases with increasing gas flow rate.

Three types of explanation have been made for the slug/churn transition as follows:

(1) Entrance region effect. Taitel et al. (1980) suggested that churn flow was in fact just a manifestation of the development of slug flow (as mentioned above in the context of the experiments of Moissis and Griffis (1962)). However, experiments by Govan and Hewitt (1991) show that churn flow is a fully developed state in its own right and therefore this explanation is incorrect.

(2) Flooding in the Taylor bubble In this mechanism, the upwards gas velocity in the Taylor bubble is sufficient to cause "flooding" of the liquid film flowing around the outside of the bubble. Flooding occurs due to the formation of large waves on the film, which are then levitated by the gas flow. This leads to a destruction of slug flow and the onset of churn flow. This mechanism was first proposed by Nicklin and Davidson (1962) and was further investigated by McQuillan *et al.* (1985) who used a flooding correlation to close the model. Jayanti and Hewitt (1992) obtained better agreement with the observations of Owen (1986) (see **Fig.1 - 3**) by taking account of the effect of Taylor bubble length on flooding.

(3) Excessive aeration of liquid slug. In this mechanism, bubbles are entrained into the liquid slug at the point where the falling liquid film enters the slug. Some of these bubbles are re-entrained into the Taylor bubble, but many of them can be retained in the slug, increasing the void fraction until a critical value is reached, at which bubble coalescence leads to breakdown of the slug and a transition to churn flow. This

mechanism has been proposed by Mishima and Ishii (1984) and Brauner and Barnea (1986).

Qualitatively, the flooding mechanism is more consistent with the sudden transition in pressure gradient observed in results such as those shown in **Fig.1 - 3**. However, a more quantitative investigation of the alternative models is reported by Watson and Hewitt (1999). The results of some comparisons with the various models showed that the model of Jayanti and Hewitt (1992) is closest to predicting the correct trends. An important test of the phenomenological models for the transition is to study the effect of pressure. This has a significant effect on the flooding mechanism, but not on the other mechanisms.

1.3.5 Churn flow

In churn flow, visual observations (using axial view photography) confirm that there is a continuous gas core and that the liquid near the wall undergoes periodic flow reversals. These flow reversals were studied by Hewitt and Martin (1985) who used photochromic dye-tracing to show that upwards transport of liquid occurred by large (flooding-type) waves, between which the residual liquid layer reversed in flow direction until picked up by the next wave. It was possible to develop a model for this flow reversal as illustrated in **Fig.1 - 4**, and this was reasonably consistent with the observations.

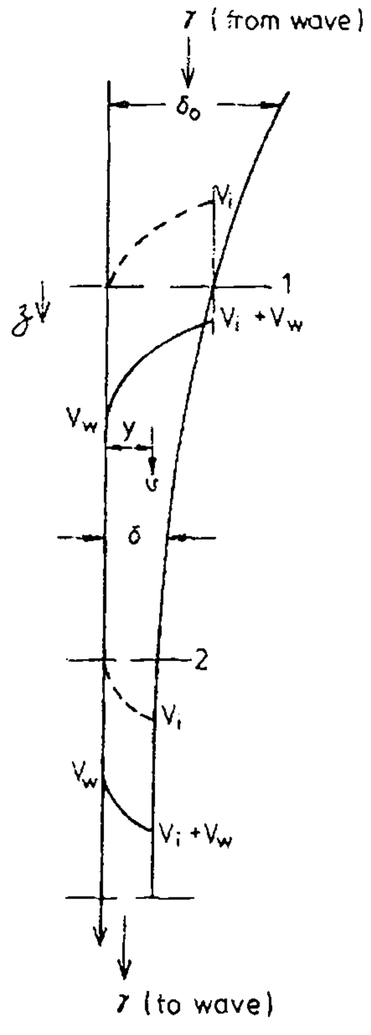


Fig.1 - 4: Flow reversal in the liquid film zone in churn flow (Hewitt *et al.*, 1985).

The mechanism of churn flow is further illustrated in **Fig.1 – 5**. Standing waves are formed at the point of liquid injection and these ultimately grow to a size at which the forces exerted on them by the gas phase leads to their levitation and transport along the channel. In between the waves. there is a falling film.

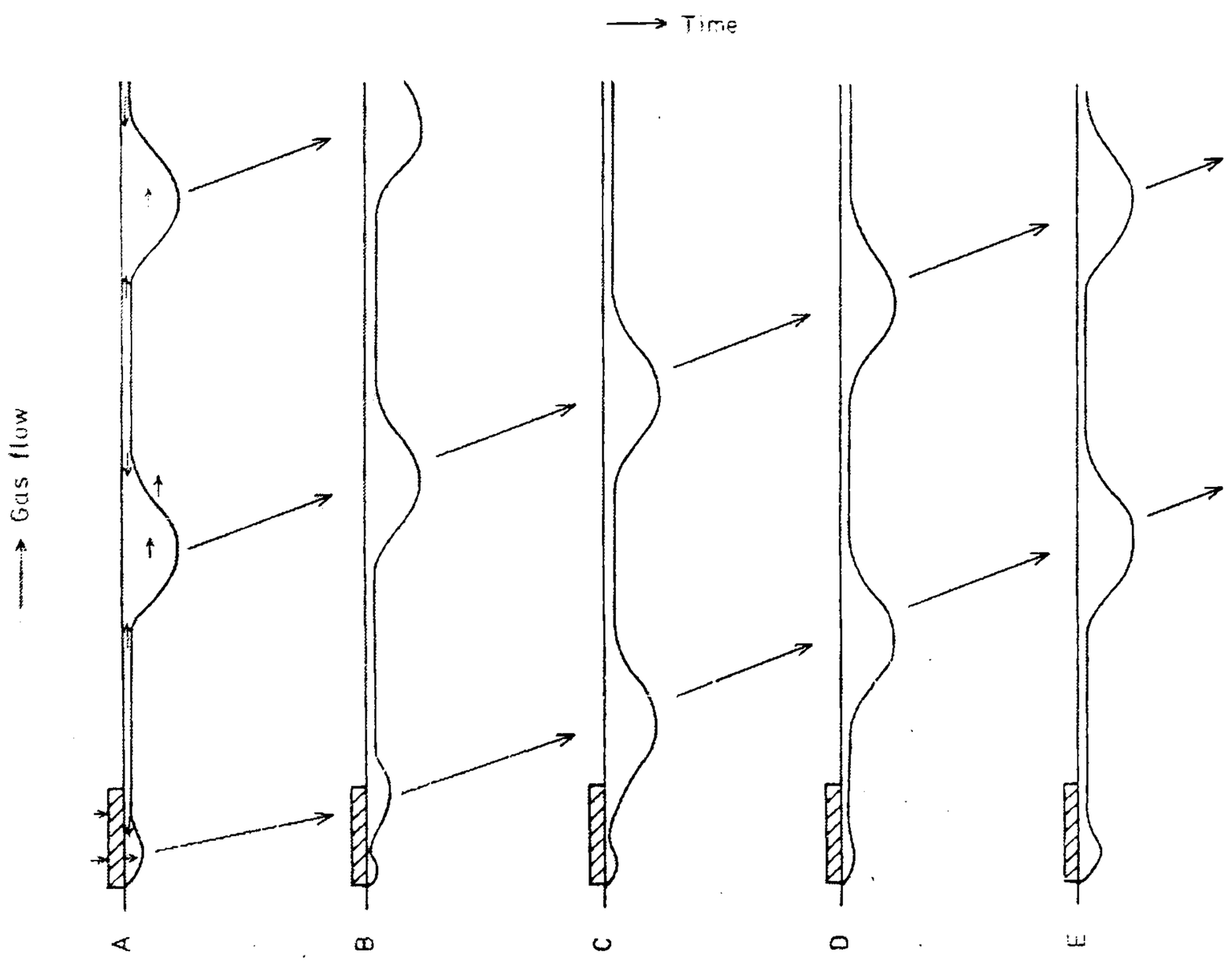


Fig.1 - 5: Repetitive wave formation and transport in churn flow (Hewitt *et al.*, 1985).

A model describing the interaction of the gas phase and the waves in churn flow is presented by Barbosa *et al.* (2001).

1.3.6 Churn/annular transition

As stated above, it is convenient to regard the churn/annular transition as occurring at approximately:

$$U_G^* \approx 1 \qquad \textbf{Eq.1 - 20}$$

and this is consistent with the minimum in the pressure gradient versus dimensionless gas flow rate data, as shown in **Fig.1 - 3**.

In modelling annular flow, an important parameter is the fraction of the liquid phase that is entrained as droplets at the churn/annular transition and this was investigated by Barbosa *et al.* (2002) whose data are illustrated in **Fig.1 - 6**. As will be seen, the entrained fraction reaches a minimum at approximately $U_G^* \approx 1$. Barbosa *et al.* presented a correlation for the entrained fraction at this situation, which can be used as a boundary value for annular flow modelling.

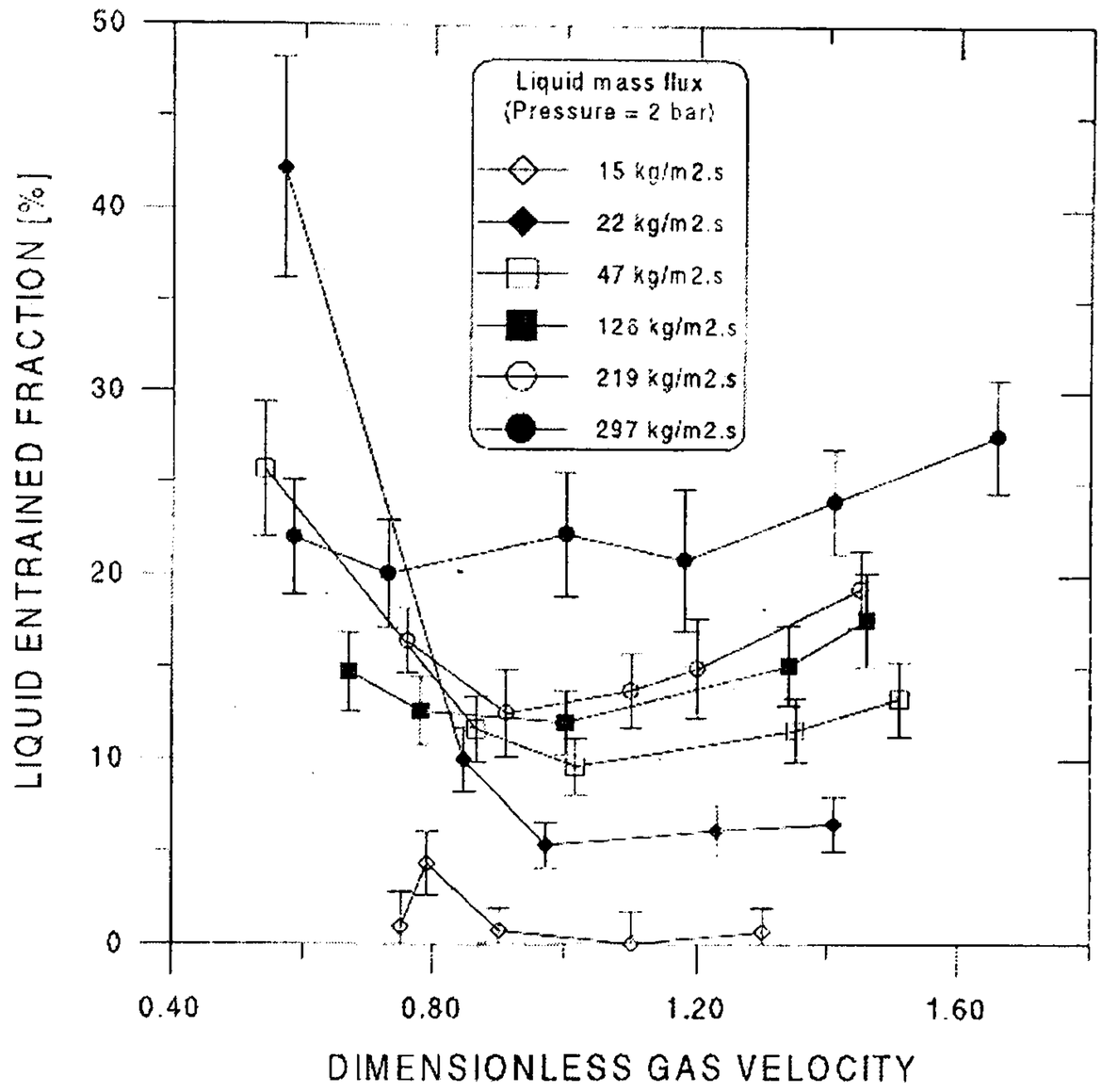


Fig.1 - 6: Data for liquid entrained fraction in the churn/annular transition region (Barbosa *et al.*, 2002).

1.3.7 Annular flow

A basic relationship in annular flow is the so-called *triangular relationship*, through which any one of the variables film thickness, pressure gradient (or interfacial shear stress) and film flow rate can be calculated from the knowledge of the other two. The normal procedure is to assume "thin film" conditions in which the wall shear stress (τ_0) is approximately equal to the interfacial shear stress (τ_i). The film is usually turbulent and development of the triangular relationship involves the implementation of turbulent eddy viscosity models in the region from the wall to the edge of the film. This can be done in a variety of ways, as discussed by Hewitt and

Hall-Taylor (1970). It is convenient to express the results of models in terms of a liquid film friction factor f_{LF} and the triangular relationship can then be written as follows:

$$\dot{M}_{LF} = \pi d \delta \sqrt{\frac{2\tau_0 \rho_L}{f_{LF}}} \qquad \textbf{Eq.1 - 21}$$

where $\dot{M}_{LF}$ is the film flow rate and δ the film thickness.

f_{LF} is related to a film Reynolds number which is defined as:

$$\mathrm{Re}_{LF} = \frac{4\dot{M}_{LF}}{\pi d \eta_L} \qquad \textbf{Eq.1 - 22}$$

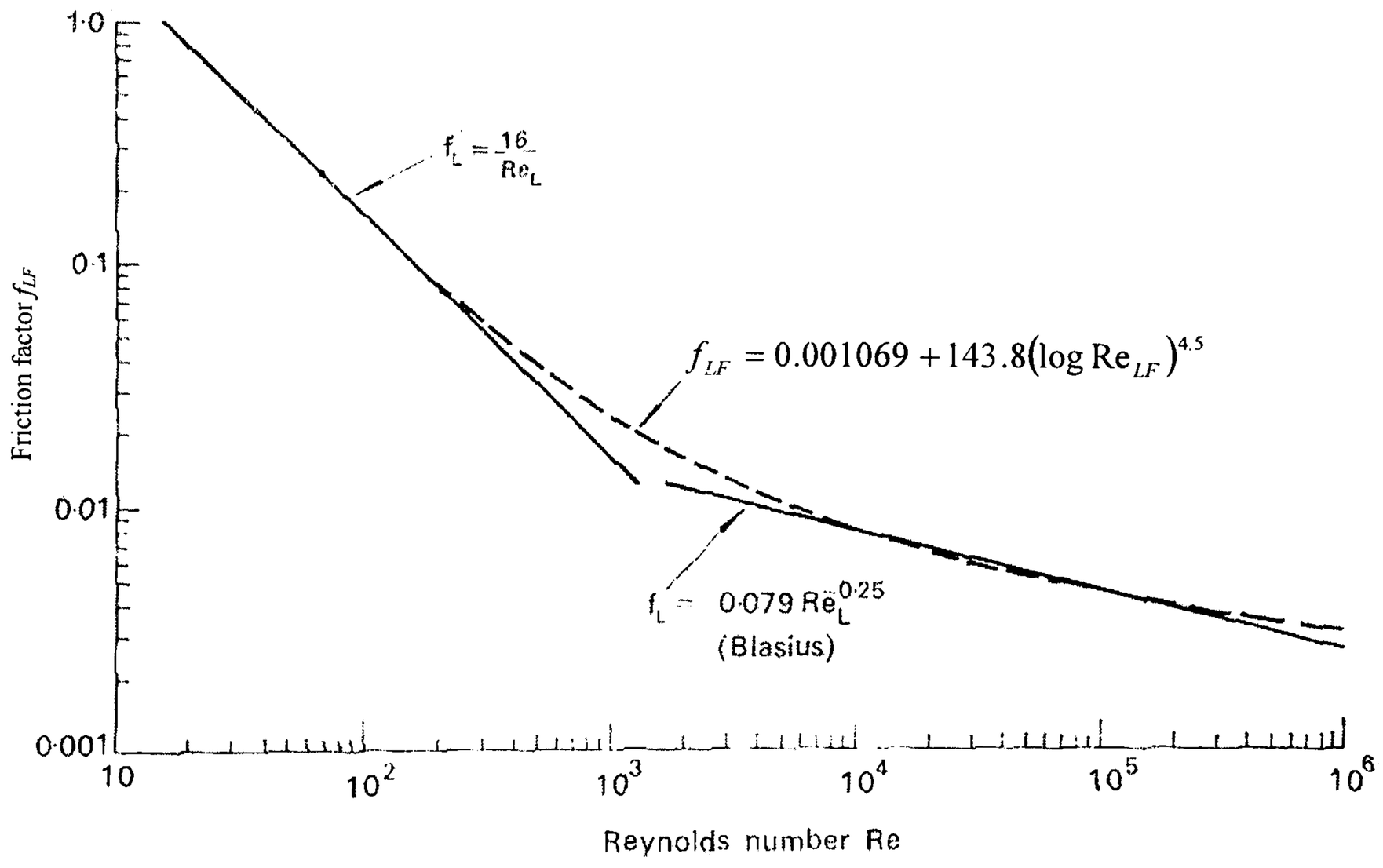


Fig.1 -7: Relationship between film friction factor and film Reynolds number for annular flow. Calculated by Hewitt and Hall-Taylor (1970) from the numerical integration results of Hewitt (1961).

Fig.1 - 8 shows comparisons between measured film flow rate data in adiabatic air-water flow with values calculated from corresponding data for film thickness and pressure gradient (shear stress). As will be seen, film flow rates calculated from the triangular relationship are in good agreement with the measured values. However, gross differences exist between the case where the liquid film is introduced uniformly around the wall of the (32mm diameter) pipe and the case where it is introduced as a centre jet. These differences persist even after nearly 170 tube diameters. The slow rate at which hydrodynamic equilibrium is reached is a crucial factor in annular flow.

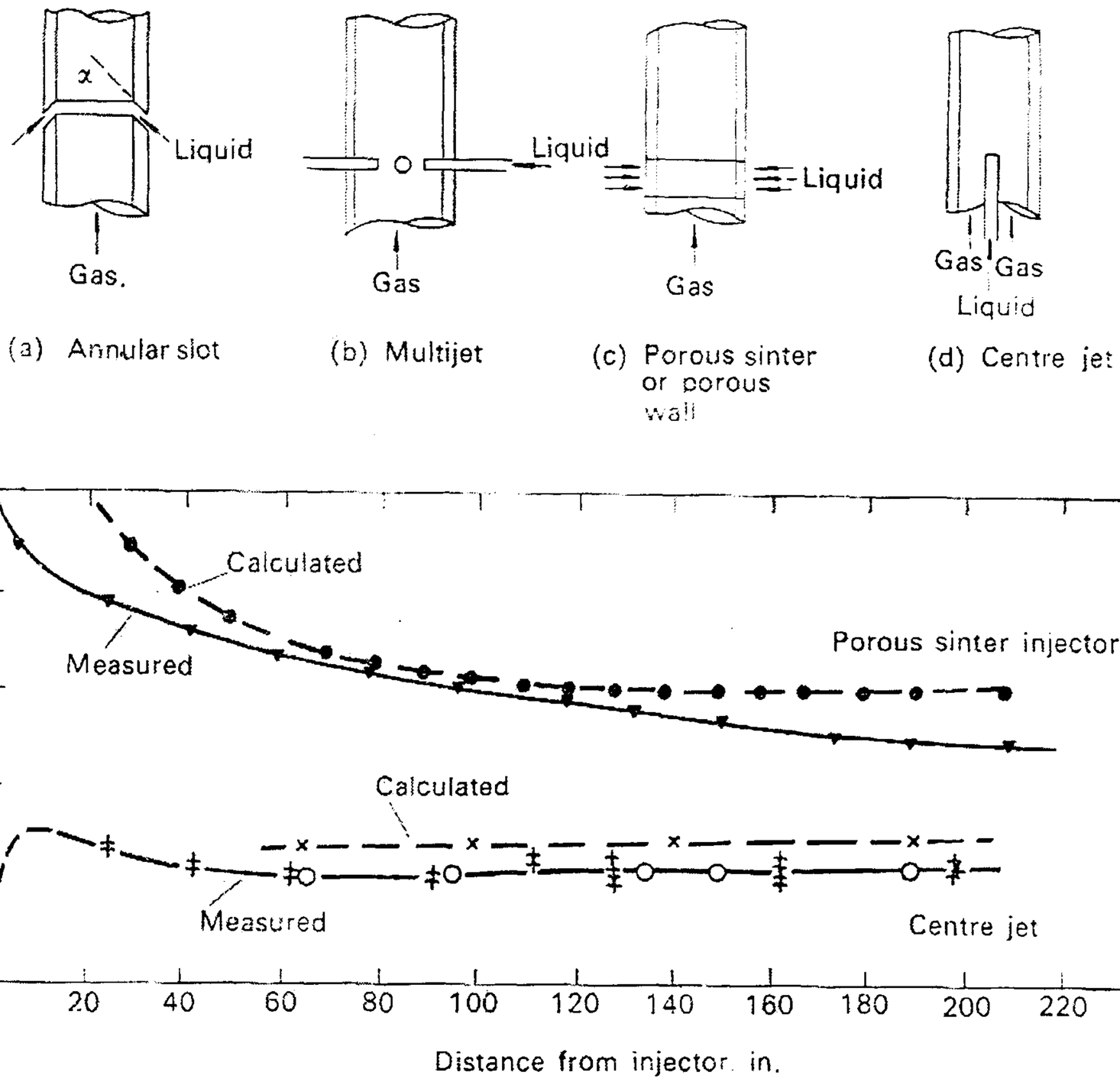


Fig.1 - 8: Comparison of triangular relationship with experimental data for film flow rate of Gill *et al.* (1963)

To provide a solution for film thickness and pressure gradient in an annular flow in which the film flow rate is known, a relationship is needed for interfacial shear stress, τ_i, which is assumed (in the thin film model) to be approximately equal to the wall

shear stress, τ_0. Owen (1986) expressed the interfacial shear stress in terms of an interfacial friction factor, f_i defined as follows:

$$f_i = \frac{2\tau_i}{\rho_m (u_{GC} - u_i)^2} \approx \frac{2\tau_i}{\rho_m U_G^2} \qquad \textbf{Eq.1 - 23}$$

where u_{GC} is the velocity of the gas core, u_i the interfacial velocity and ρ_m the mean density of the gas core given by:

$$\rho_m = \frac{\dot{M}_G + \dot{M}_{LE}}{\dot{M}_G / \rho_G + \dot{M}_{LE} / \rho_L} \qquad \textbf{Eq.1 - 24}$$

where $\dot{M}_{LE}$ is the entrained mass rate of flow (kg/s). Owen related f_i to interfacial roughness, e through the expression:

$$\sqrt{\frac{2}{f_i}} = \frac{1}{k_{TP}} \ln(\frac{r_i}{e}) + A_r + \frac{1}{k_{TP}} \left[\frac{2\delta}{r_0} \ln(\frac{r_0}{\delta}) - \frac{\delta}{r_0} - 1.5 \right] \approx \frac{1}{k_{TP}} \ln\left(\frac{r_0}{e}\right) + 8.5 - \frac{1.5}{k_{TP}}$$

Eq.1 - 25

where r_i and r_0 are the interfacial and wall radii and k_{TP} is the Von Karman constant. A_r is the Nikuradse roughness parameter which is equal to 8.5 for fully rough flows.

Owen (1986) examined data for velocity profile in annular flow with entrainment and showed that k_{TP} decreased with decreasing ratio of gas to core density. This relationship can be expressed by the equation:

$$k_{TP} = \exp\left[-1.9786 + 0.9381 \left(\frac{\rho_G U_G^2}{\rho_m u_{GC}^2} \right) \right] \approx \exp\left[-1.9786 + 0.9381 \left(\frac{\rho_G}{\rho_m} \right) \right]$$

Eq.1 - 26

To obtain f_i, the effective roughness, e needs to be determined and this is usually calculated on the basis of the empirically observed *geometrical similarity* in which

the roughness height is related to the film thickness. A simple form of this relationship (compatible with **Eq.1 - 23** to **Eq. 1 - 26** above) is the following form due to Wolf (1995):

$$\frac{e}{r_0} = 7.07\frac{\delta}{r_0} - 0.0088 \qquad \textbf{Eq.1 - 27}$$

The remaining key variable is the film flow rate (M_{LF}). M_{LF} is often expressed in terms of the *mass flux* corresponding to the film flow rate, namely $\dot{m}_{LF}$, which is simply $\dot{M}_{LF} / A$, where A is the channel cross sectional area. The value of $\dot{m}_{LF}$ may be calculated by integration of the equation:

$$\frac{d\dot{m}_{LF}}{dz} = \frac{4}{d}(D - E - \dot{q} / h_{LG}) \qquad \textbf{Eq.1 - 28}$$

where D and E are the rates of droplet deposition and droplet entrainment (kilograms per second per unit peripheral area), $\dot{q}$ is the heat flux and h_{LG} is the latent heat of vaporisation. Correlations for D and E are provided by Hewitt and Govan (1990). D is calculated from:

$$D = kC \qquad \textbf{Eq.1 - 29}$$

where C is the concentration (kg/m^3) of the droplets in the gas core calculated on a homogeneous basis as:

$$C = \frac{\dot{M}_{LE}}{\dot{M}_{LE} / \rho_L + \dot{M}_G / \rho_G} \qquad \textbf{Eq.1 - 30}$$

and where k is the deposition mass transfer coefficient (m/s), correlated as follows:

$$k\sqrt{\frac{\rho_G d}{\sigma}} = 0.18 \qquad \text{for} \qquad C / \rho_G \le 0.3$$

$$k\sqrt{\frac{\rho_G d}{\sigma}} = 0.83(C / \rho_G)^{-0.65} \qquad \text{for} \qquad C / \rho_G \ge 0.3 \qquad \textbf{Eq.1 - 31}$$

The entrainment rate E was correlated in the form:

$$E/\dot{m}_G = 5.75\times10^{-5}\left[\frac{d\rho_L}{\rho_G^2\sigma}(\dot{m}_{LF}-\dot{m}_{LFC})^2\right]^{0.316} \quad \text{for} \quad \dot{m}_{LF} \geq \dot{m}_{LFC} \qquad \textbf{Eq.1 - 32}$$

where:

$$\frac{\dot{m}_{LFC}d}{\eta_L} = \mathrm{Re}_{LFC} = \exp(5.8504 + 0.4249\frac{\eta_G}{\eta_L}\sqrt{\frac{\rho_L}{\rho_G}}) \qquad \textbf{Eq.1 - 33}$$

Comparisons of these expressions with experimental data for D and E showed a considerable scatter in the data, leading to the belief that there is scope for improvement of these relationships in the future.

There is some controversy about whether heat flux has a significant effect on entrainment rate. Milashenko *et al.* (1989) made measurements, which implied that there was a significant heat flux effect which they correlated as an additional entrainment due to heat flux as follows:

$$E_t = 5.53\times10^{-7}\dot{m}_{LF}\left[\frac{\dot{q}\rho_G}{\rho_L}\right]^{1.3} \qquad \textbf{Eq.1 - 34}$$

The component E_t was measured by determining the change in film flowrate occurring over a heated tube length. However, this kind of experiment can give misleading results since there is a change of quality, leading to a shift in the equilibrium value of film flow.

Fig.1 - 9 and **Fig.1 – 10** show predictions of adiabatic annular flow data using the above relationships. In **Fig.1 - 9**, pressure gradient data for fully developed annular flow (Owen, 1986) are compared with predictions from the above equations. The equations fit the data rather well at low liquid mass fluxes. The agreement is less good at higher mass fluxes though, in contrast to other models, the existence of a maximum and minimum in pressure gradients is predicted, reflecting the decrease in

k_{TP} as droplet concentration increases at high liquid mass fluxes. In **Fig.1 - 10**, the variation of film flow rate with distance, observed in experiments by Nigmatulin (1978) at 70 bar, is compared with the predictions. Rather encouraging agreement is obtained.

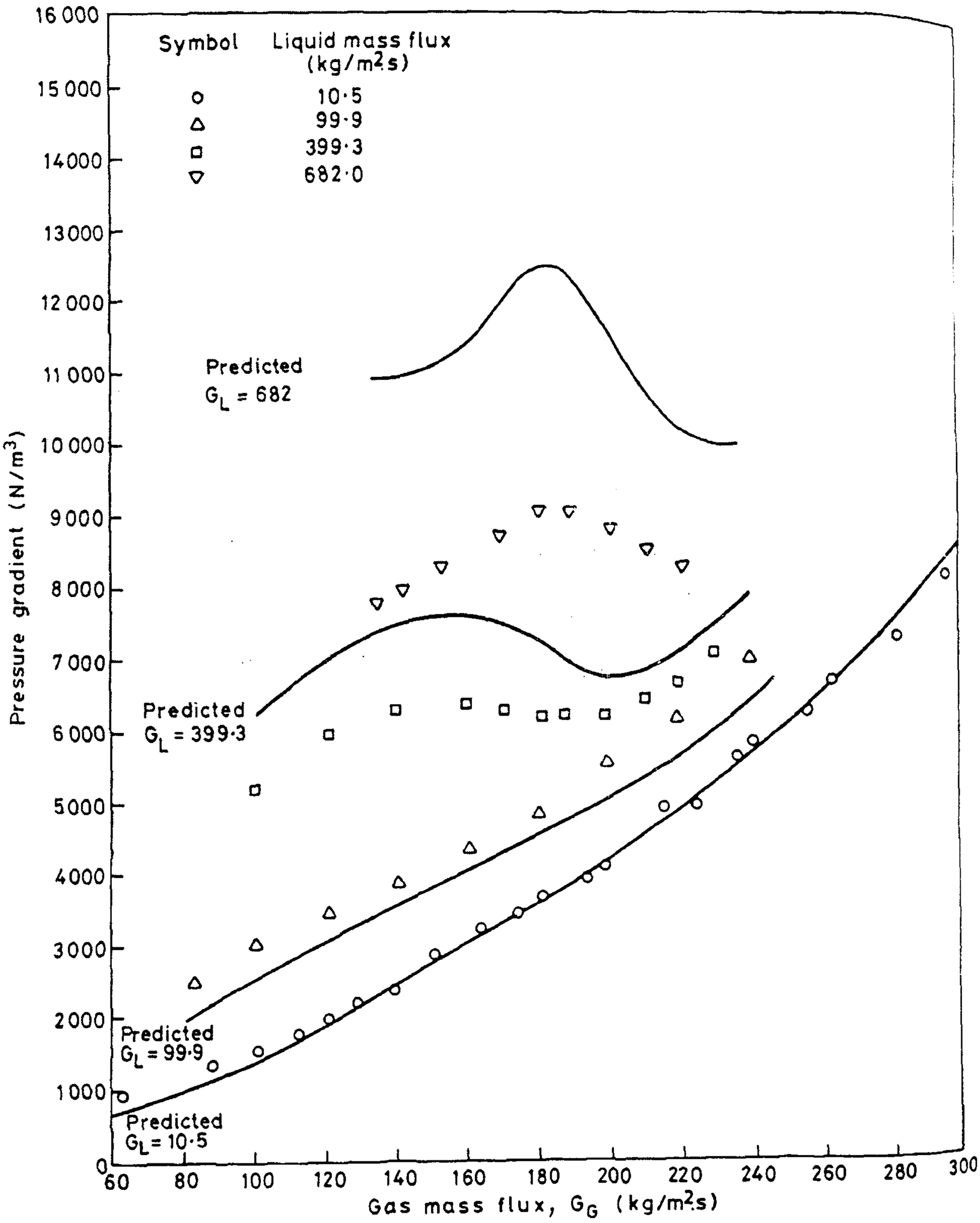


Fig.1 - 9: Comparison of pressure gradient predictions with measurements for air-water flow (Owen, 1986).

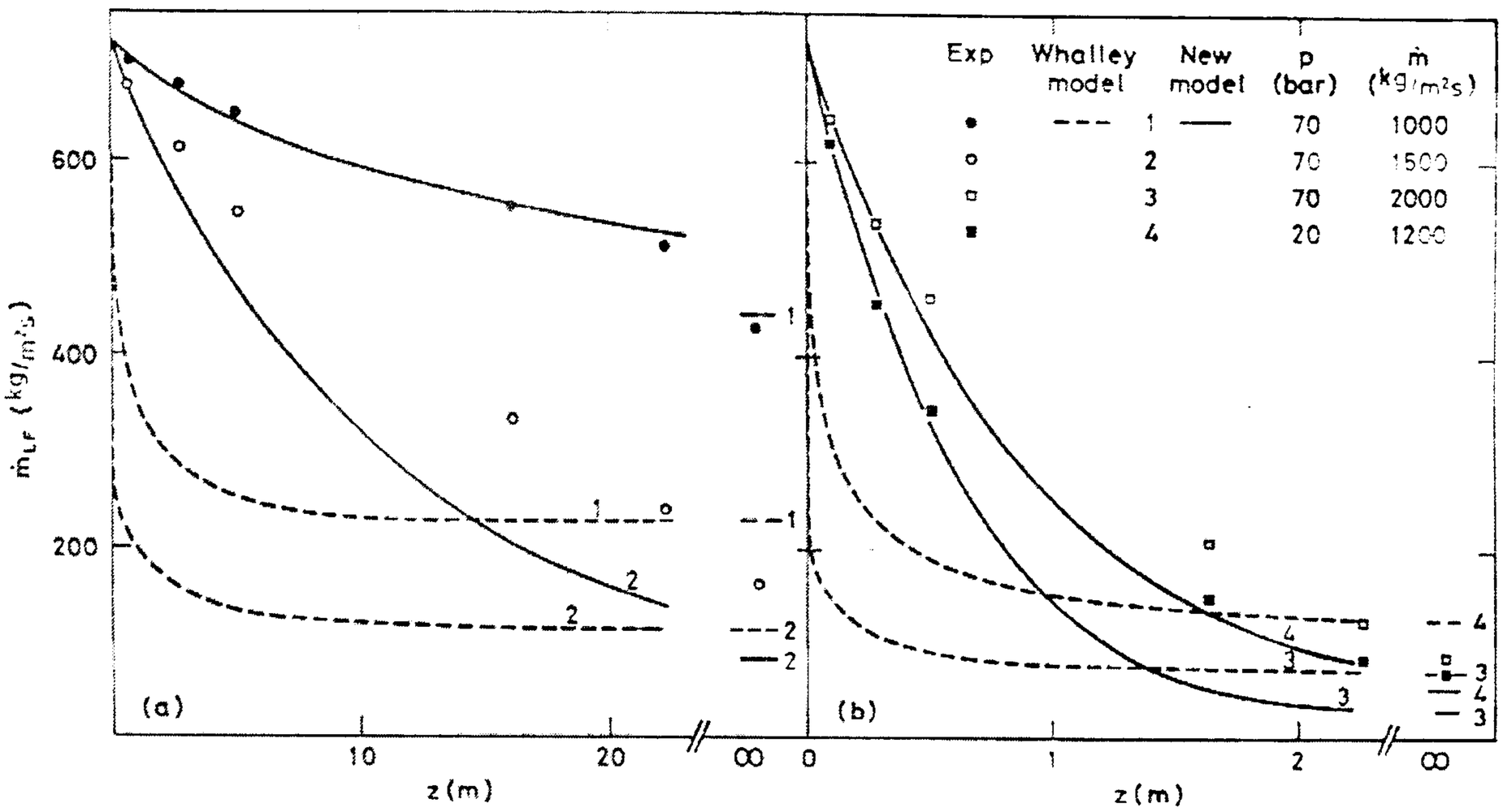


Fig.1 - 10 Comparison of film flow rates predicted by Hewitt and Govan (1990) with the experimental steam-water data of Nigmatulin (1978).

1.3.8 Annular/wispy annular transition

There is evidence (see below) that, in wispy annular flow, droplet concentration waves develop in the gas core. Thus, the transition between annular flow and wispy annular flow would correspond to the condition in which small perturbations in droplet concentration would grow and lead to the formation of such concentration waves. This hypothesis was investigated by Hawkes *et al.* (2001) who predicted conditions for concentration wave growth using linear stability analysis (LSA). Their results are compared with a transition line representing experimental data in **Fig.1 – 11**. Qualitative agreement is obtained. Further development of this model is described by Laforgia (2004)

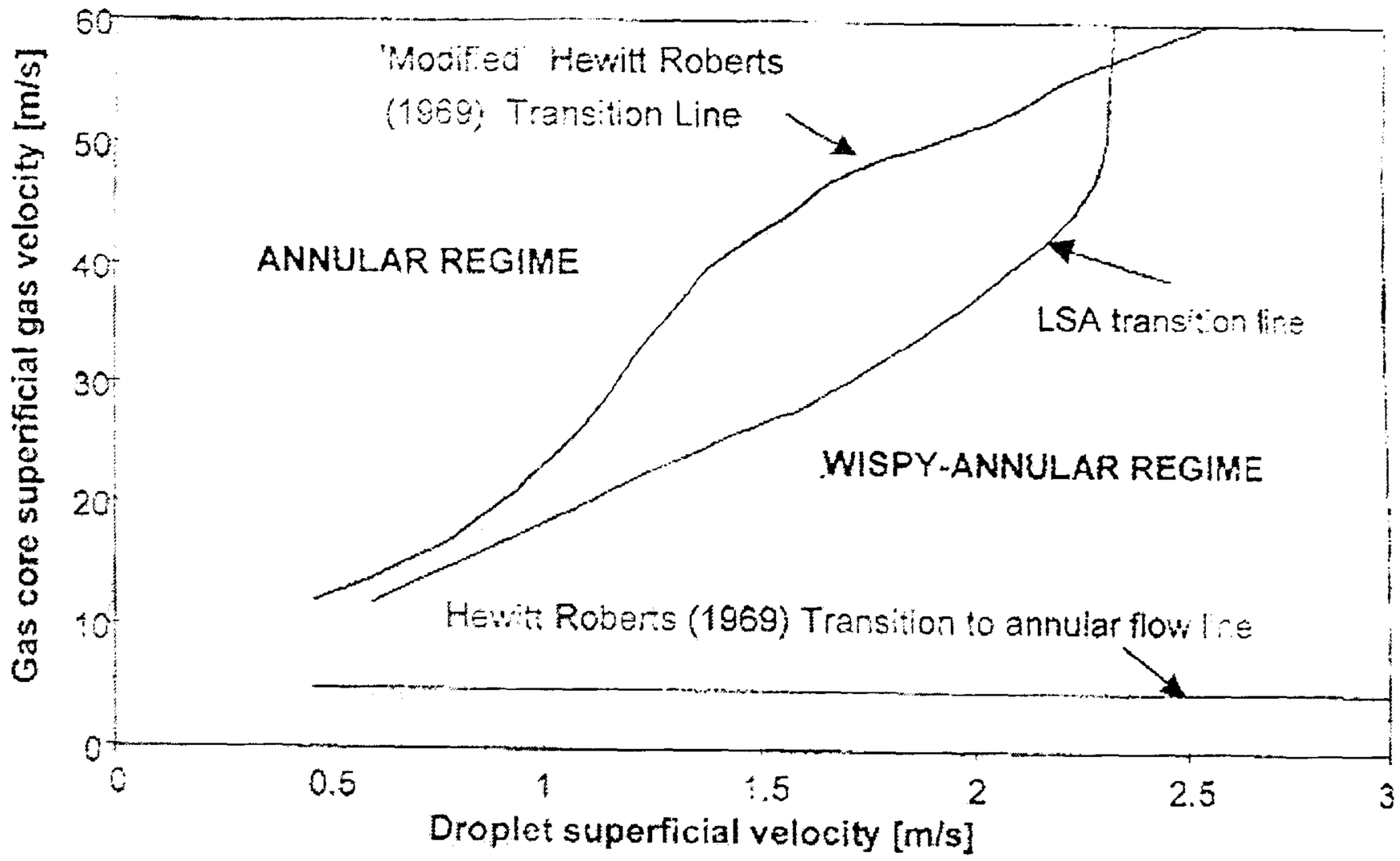


Fig.1 – 11: Comparison of predicted annular/wispy annular regime transition with transition line observed experimentally by Hewitt and Roberts (1969).

1.3.9 Wispy annular flow

Despite the fact that many applications lie within the wispy-annular flow region, detailed studies of this region are relatively rare. Recent work at Imperial College has attempted to address this deficiency, with detailed measurements being made of the characteristics of wispy annular flow. One such characteristic is the existence of large fluctuations in pressure gradient and **Fig.1 – 12** (Hawkes *et al., 2000*) shows how frequency spectra develop along the channel. Basically, two characteristics are observed, as showed in **Fig.1 – 13**: one of around 15-20 Hz, which probably corresponds to the disturbance waves on the surface of the film. The other frequency (of around 7 Hz) is hypothesised to correspond to the core concentration waves. Further evidence for this was obtained by Hawkes *et al.* (2000) by studying spectra from optical scattering. Both the disturbance waves and the core concentration waves strongly scatter a light beam passed through the channel and power spectral density information on scattering can be used to investigate the system. **Fig.1 – 14** shows the results of such an investigation. As with the pressure gradient data, two peaks are observed, but only one survives if the liquid film (and hence, also the disturbance waves) is removed upstream of the scattering device. This provides

convincing evidence that the core concentration waves are responsible for the lower frequency fluctuations.

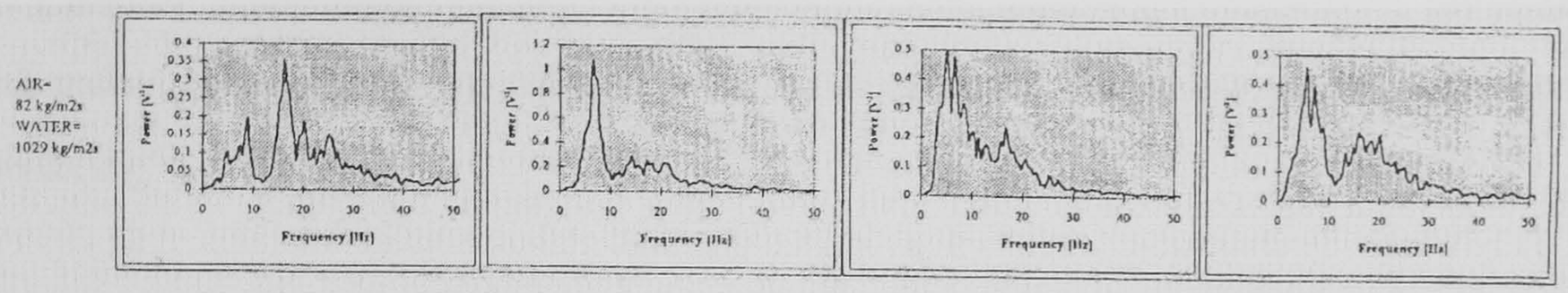


Fig.1 – 12: Development of frequency spectra for pressure gradient in air-water wispy annular flow (Hawkes *et al., 2000*).

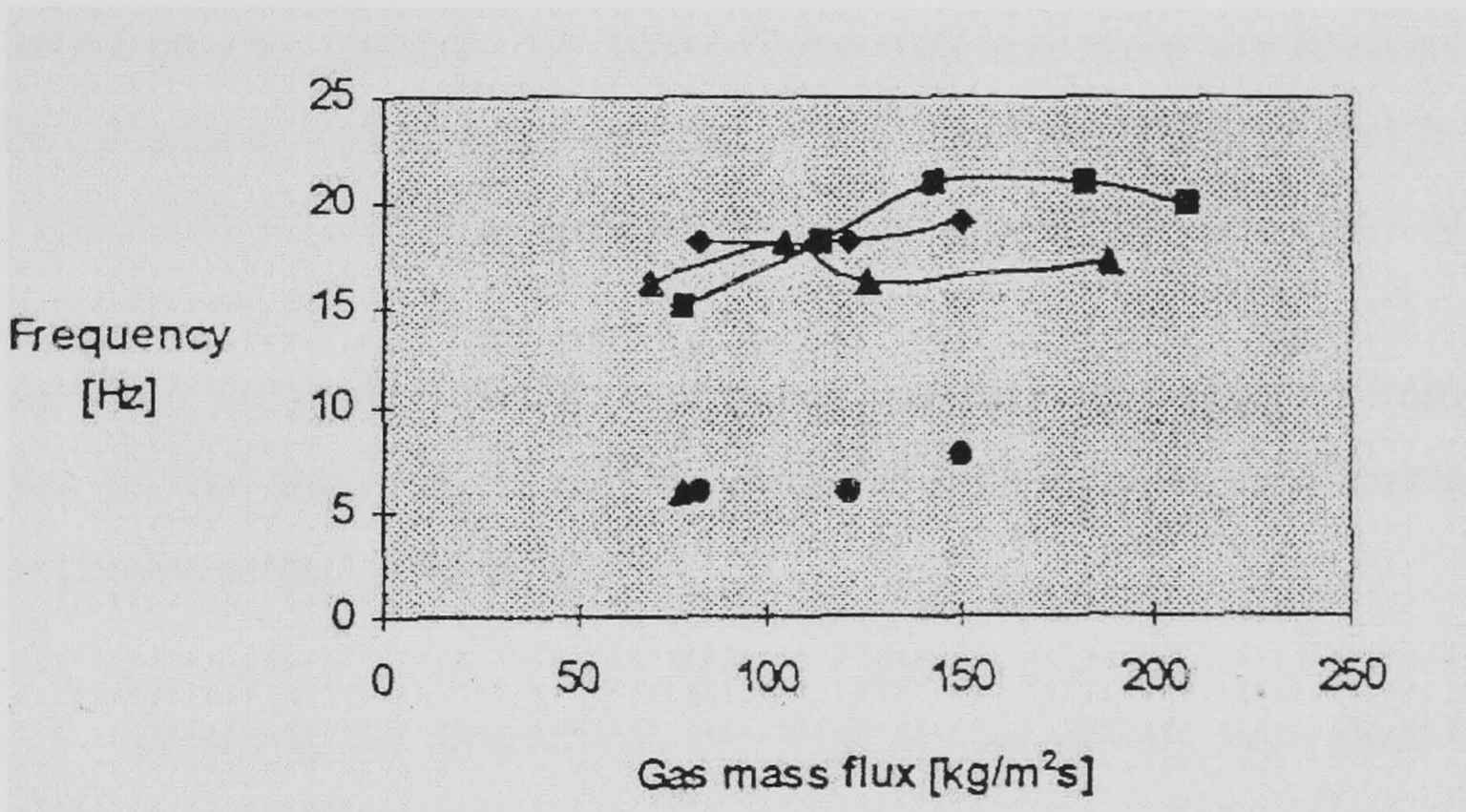


Fig.1 – 13: Peak frequencies in pressure gradient fluctuations in air-water wispy annular flow (Hawkes *et al., 2000*).

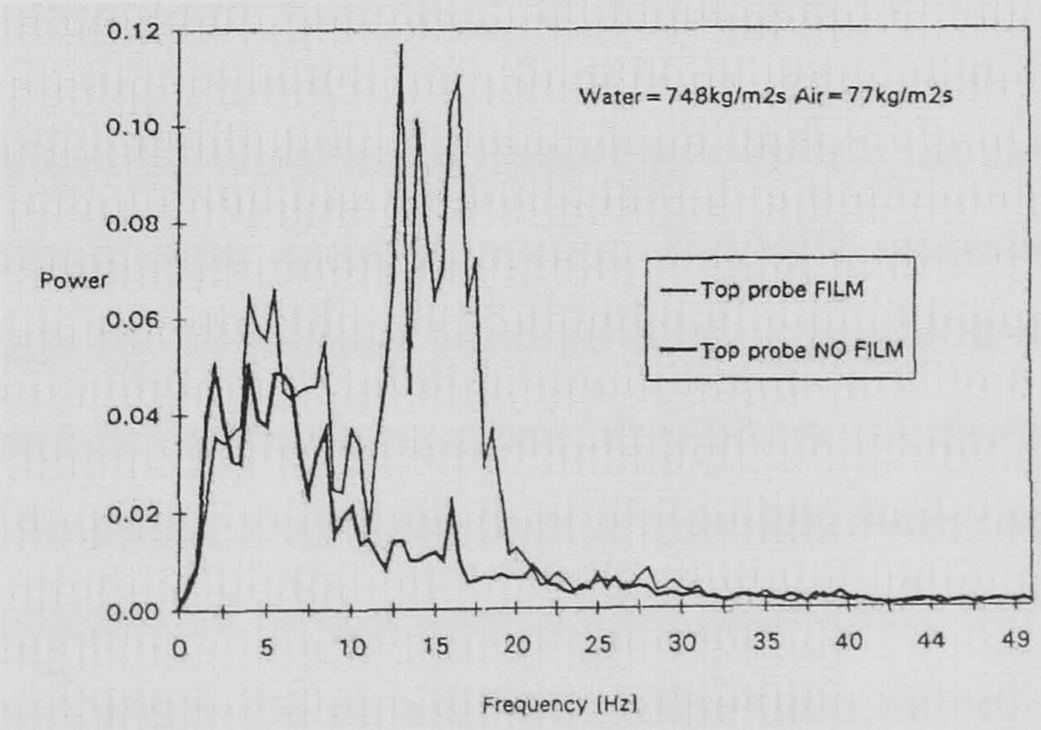


Fig.1 – 14: Power spectral density for optical scattering with and without the film removed upstream of the scattering device (Hawkes *et al., 2000*).

1.4 Structure of the thesis

Chapter 2 and 3 of this thesis deal with the first of the applications, namely multiphase flow metering.

In ***Chapter 2***, the state-of-the-art in multiphase flow metering is reviewed, revealing the main problem area, namely metering of streams with high gas content ("wet gas metering").

Chapter 3 describes the development of a potential solution to the wet gas metering problem, namely the ANUMET system (patented by Imperial College). Here, the liquid phase is separated to the wall and the triangular relationship (see Section 1.3.7 above) is invoked to calculate the liquid phase flow rate from the knowledge of liquid film thickness and pressure gradient. The flow is then remixed and fed to a venturi. The gas flow rate can be deduced from the pressure drop across the venturi.

In Chapters 4-7, the work related to well testing is presented. ***Chapter 4*** introduces the subject of well test analysis and Chapters 5-7 introduce the work carried out under the present project as follows:

Chapter 5 summarises the results from two MSc studies (jointly supervised by the present author) in which simple air-water experiments were carried out in a vertical tube. The Chapter also present a model for the simplest case, namely that of the pressure transients occurring following the trapping of a bubble flow in a vertical tube. This model showed good agreement with the experimental results.

Chapter 6 describes the evolution of a previously-developed code (GRAMP2) for the prediction of steady-state flows in wells. GRAMP2 embodies phenomenological prediction models for all regimes between single-phase flow and dispersed annular flow and is based on the models outlined in Section 1.3 above. However, the code was developed for simple fluid pairs (typically air and water) and was not, as it stood, suitable for prediction of typical hydrocarbon production flows (for example, gas-condensate flows) where the physical properties (and, indeed, the local phase flow rates) are a function of local pressure and temperature. In earlier work on GRAMP2, simplified physical property models ("black oil equations") had been used, but major

problems had been identified in applying these models to the complex case of two-phase flow in a long well. It was clear that more advanced physical property models were required and a major component of the present work was on linking the GRAMP2 code to a well-established commercial physical property package (Multiflash, produced by Infochem Ltd). The combined code (GRAMP2-Multiflash) was used to predict an example of steady-state well behaviours, with encouraging results.

Chapter 7 describes work towards the longer term objective of a fully-transient phenomenological model capable of predicting the transient flow in the well following well shut-down and the interaction between the transient flow in the well and that in the reservoir. Although the realisation of such an ambitious modelling framework is clearly beyond what can be achieved in a single doctoral project, two important steps were made towards it in the present work:

1. The most promising route for linking a transient phenomenological wellbore model to a reservoir model is through an Inflow Performance Relationship (IPR) which links the flow and the composition of fluid entering the well to the downhole pressure. This gives a boundary condition for the wellbore model. Work on IPR's was carried out in a DipIng project by Costantini (2005), which was jointly supervised by the present author. This work is described in Section 7.3.
2. Though the development of a transient two-phase reservoir-coupled wellbore model remains a longer-term aim, the case of a gas well (i.e. one in which the flow in the reservoir and in the well are in the form of single phase gas) is more readily analysed. Section 7.4 describes such an analysis, carried out as part of the present work.
3. In collaboration with Professor Jader Barbosa (University of Santa Catarina, Brazil), development work was pursued of the equations for a transient annular flow (Section 7.5). The resultant equations are presented in Appendix III.

In ***Chapter 8***, conclusions are drawn for the work described in this thesis and recommendations made for future work.

CHAPTER 2

State-of-the-art of Multiphase Flow Metering (MFM)

2.1 Summary

Over the last decade the development, evaluation and use of Multiphase Flow Metering (MFM) systems has been a major focus for the Oil & Gas industry worldwide. So far, many alternative metering systems have been developed, but none of them can be referred to as generally applicable or universally accurate. Both established and novel technologies suitable to measure the flow rates of gas, oil and water in a three-phase flow are reviewed and assessed within this chapter. Those technologies already implemented in the various commercial meters are then evaluated in terms of operational and economical advantages or shortcomings from an operator point of view. The lessons learned about the practical reliability, accuracy and use of the available technology are discussed. As operators now realise, incorporation of MFM's is an essential step in exploiting marginal fields. A new approach to flow assurance, deep water developments, downhole/seabed separation systems and wet gas fields is foreseen. This chapter suggests where the research to

develop the next generation of MFM devices will be focused in order to meet the as yet unsolved problems.

2.2 Brief history of MFM

The first commercial MFM's appeared about ten years ago, as a result of several multiphase metering research projects that took place in the early 1980's. Among those universities, research centres and oil companies that gave their contribution to the development of MFM's and that still are carrying out studies on the subject are: University of Tulsa (US), SINTEF (Norway), Imperial College (UK), National Engineering Laboratory (UK), CMR (Norway), BP, Total, Shell, ENI and Petrobras. The first tests of these prototype-MFM's were carried out by BP and Texaco. The driving force to develop MFM technology was the forecast decline of production from the major North Sea fields, accompanied by the necessity to tie back future smaller discoveries to existing infrastructure. Increasing gas and water fractions, inherent in a mature producing province, would create more unstable flow conditions in existing production facilities and require more flexible multiphase solutions.

Since the first field installations in 1992, MFM has become accepted in the field and is now being considered among the primary metering solutions for new field developments.

2.3 MFM applications

Within the oil and gas industry, it is generally recognised that MFM could lead to great benefits in terms of (Williams, 1994; Ribeiro, 1996; Thorn *et al.*, 1997):

2.3.1 Layout of production facilities

The use of MFM's reduces the hardware needed for onshore, offshore topside and offshore subsea applications. Of primary importance is the removal of a dedicated test separator for well testing applications. Utilising MFM (with its smaller "footprint") for topside applications minimises platform space and load requirements for well testing operations. Finally, costly well test lines can be omitted from the production facilities, which may be of vital importance for unmanned locations, deepwater developments and satellite fields.

2.3.2 Well testing

The conventional test separators are expensive and take a long time to monitor each well's performance because of the stabilised flow conditions required. This becomes particularly serious for deepwater developments, due to the exceptional length of the flowlines. In such cases, the production of individual wells connected to the same manifold may be monitored via a dedicated test line to avoid shutting down all the wells and testing them one by one (with considerable production loss). However, the expense of a separate flow line may be prohibitive, hence the advantages of having a MFM installed in the subsea manifold. Test separators have an accuracy of between ±5-10% (which nowadays is achievable via MFM's too), but require regular intervention by trained personnel and cannot provide continuous well monitoring. A further disadvantage of conventional well testing with conventional separators is that wells suffer from shutdown cycles related to well testing. Hence, wells that are tested on a regular basis usually require more frequent workovers to maintain their production rates.

Using MFM's for exploration well testing (Mus *et al.*, 2001) provides satisfactory flow measurements without separation of the phases. It is claimed that they can even be used to monitor the well during its clean up flow (traditionally, this flow information is lost as the well stream is not directed through the test separator). Added value is represented by improved control of the drawdown applied to the formation, the pressure transient and shortened flow periods

2.3.3 Reservoir management

MFM's provide real time, continuous data so that Operators can better characterise field and reservoir performance and react faster. Changes in gas-oil ratio or water cut can be detected and quantified immediately, whereas the traditional test separators only provide information on cumulative volumes at discrete points in time.

2.3.4 Production allocation

Any situation where production from different wells/fields owned by different Operators is commingled in the same pipeline for export to a common processing facility, requires allocation metering. Without MFM's, the production from each well

must flow through a test separator before commingling with the other produced streams.

2.3.5 Production monitoring

MFM's provide real time information on variations in the gas and liquid flow rates, so that well slugging effects or gas-lift problems may be detected as they occur. This allows production optimisation and extension of field life.

2.3.6 CAPEX and OPEX

When operators have to decide between a traditional approach to the production facilities and one including MFM's, they must compare the capital expenditure (CAPEX) and operating expenditure (OPEX) of both solutions. While it is relatively easy to estimate costs for hardware components, it is quite difficult to predict the OPEX. This is because the number of MFM applications worldwide is still relatively low and the operational history still very limited. In general, it is recognised that MFM CAPEX is significantly lower than that of conventional metering hardware, but Operators often underestimate the OPEX associated with MFM, especially for the commissioning phase and the first year of operation.

Typical CAPEX (Sheers and Noordhuis, 1999) for commercial MFM's are in the range of US$100-500,000, the actual cost varying according to the kind of application (onshore/offshore, topsides/subsea), the dimension of the metering tool (sizes from 2" to 10" in diameter) and the number of units ordered. Prices are likely to be lower whenever the competition increases, but they can rise very quickly in the case of tools that are claimed to cover special applications. A test separator may have an installed cost of US$1m-5m and require 25 to 60 instruments, depending on its complexity. The test lines may be omitted in some MFM installations. Carbon steel test flow lines of 4-6" in diameter cost approximately US$1.3m-3.6m per Km installed, so omitting them may lead to noticeable savings. It has been estimated (Douglas-Westwood, 2000-2004) that, for a subsea development 10 km from the host platform, using a subsea MFM could represent a 62% cost reduction through the elimination of test lines. In addition to this, MFM could improve the management of the system with a 6-9% gain in the value of the oil recovered.

Typical OPEX for test separators is in the range of US$350,000 per year. It has been estimated (Sheers and Noordhuis, 1999) that the OPEX for a MFM is likely to be 25% of the cost of the meter itself for the first year, then US$10-40,000 per year (for both onshore and topsides applications). We can therefore conclude that OPEX will be lower with a MFM than with a conventional test separator. It is hoped that after more operational experience is gained in the field, MFM's will require less maintenance after installation and therefore OPEX will be reduced.

2.3.7 Fiscal metering or custody transfer

Unfortunately, the current MFM's are not (and may never be) accurate enough to satisfy the metering requirements dictated by the Governments for taxation purposes (fiscal metering), although such an application would guarantee the future of MFM's. However, it is important to stress that, as indicated by the DTI (2003), the use of the phrase 'fiscal metering' does not necessarily imply any single expectation of the quality of the instrumentation to be installed. 'Fiscal' refers to the meter's service, not its quality. A fiscal meter is therefore any system, or element of that system, that is used to determine production rates that will ultimately generate revenue for the Government.

2.4 How accurate can MFM be?

To date, no International Regulation for MFM accuracy has been delivered, which makes it very difficult for an Operator to identify the scenarios where MFM can be implemented. However, the following levels of accuracy for multiphase measurements are generally agreed: ±5-10% for reservoir management, ±2-5% for production allocation and ±0.25-1% for fiscal metering.

Since the results from production measurements are implemented in the reservoir modelling or production optimisation processes, it is clear that the accuracy of such measurements will affect the prediction of ultimate recovery from a reservoir. More accurate measurements imply that this uncertainty can be reduced. It is also clear that different levels of uncertainty may be acceptable, depending on overall field reserves, oil price, production lifetime, etc. Hence, different levels of MFM accuracy may be tolerated, without necessarily being those indicated above. With the current MFM solutions, it is claimed to be possible to measure total liquid flow rate and gas flow

rate with a relative error of less than ±5-10%, and water cut with an absolute error lower than ±2% [Note: *Relative error = (measured – actual)/actual; Absolute error = (measured – actual)*]. However, it is important to remember that we are attempting to measure with MFM's the flow rates of oil, gas and water within a highly complex and unstable mixture. Hence, it may be optimistic to claim that the above ranges of accuracy apply to any flow regime and for any chemistry of the fluids.

Misunderstandings may occur when defining the level of uncertainty associated to MFM's, depending on which type of meter is used. For instance, if the required accuracy is referred to the measurement itself, then some devices, such as the venturi or others that use pressure drop for their measurement, often have a constant *absolute* error (i.e. the pressure drop is measured to a given number of mbar). In this case, we need to introduce the concept of "rangeability", which limits the minimum pressure drop that can be measured with a desired accuracy (the "low-side" limit) and so reduces its applicability (**Fig.2 – 1**).

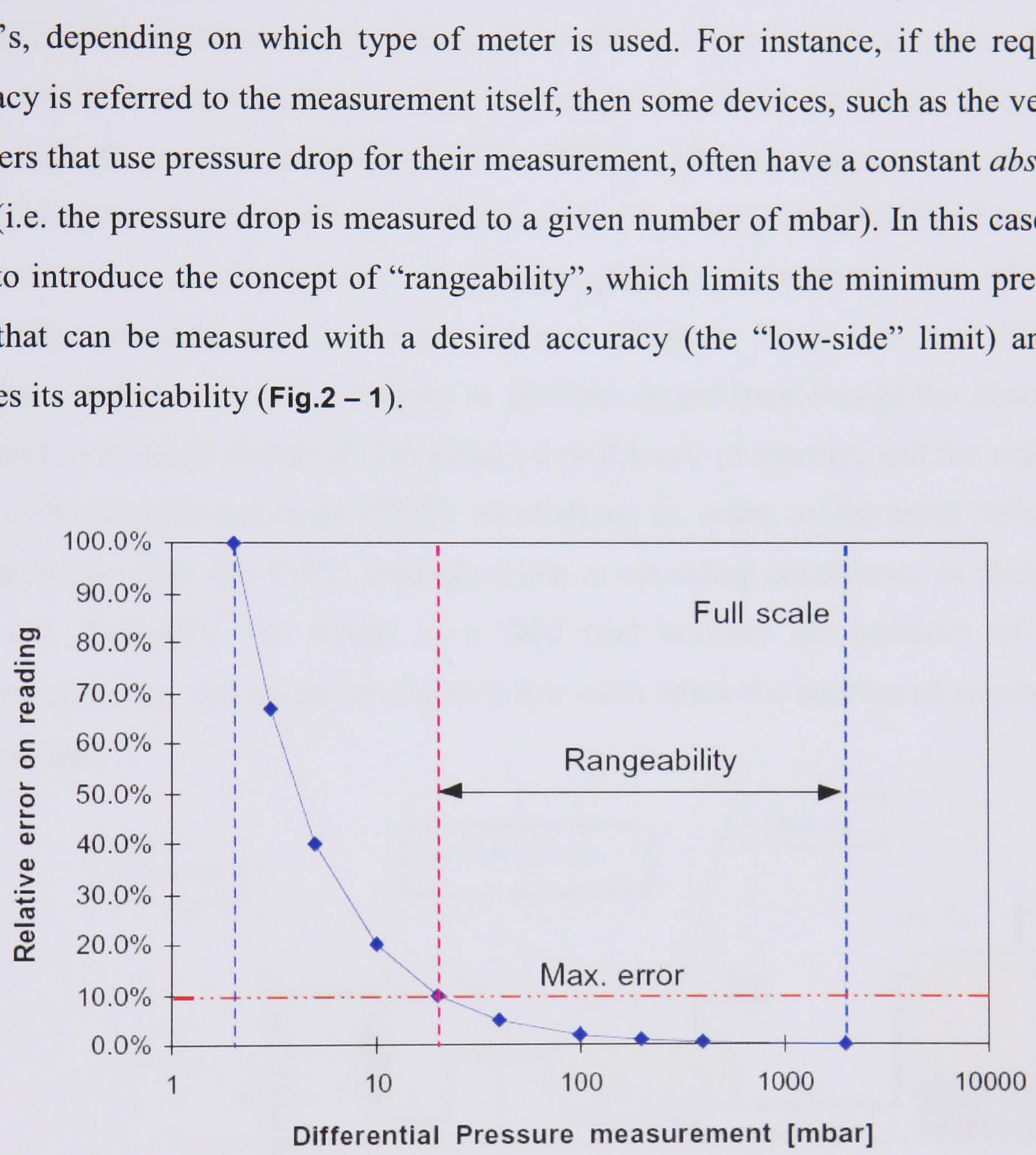


Fig.2 - 1: The concept of "rangeability" for differential pressure devices (Alimonti in Falcone *et al*, 2001).

Special attention must be paid to error propagation. Often, highly sophisticated models are established to achieve the requirements of a MFM, but the more complex the model, the more uncertain the measurement will be. If the measurement concept is to measure the phase fractions (which are interdependent) and the total mass velocity, the errors of the individual measurements are combined together and

propagated through to the final result. Thus, the overall error is always higher than that of the individual measurements. Due to the complex nature of multiphase flow modelling, tracking the error propagation through the algorithm can be extremely difficult, which is why MFM's may need to be characterised by experimental testing. There are two main steps in testing a MFM: a laboratory test followed by a field trial. The initial characterisation testing is carried out in specialised laboratories where three phase flows can be established. This testing is characterised by use of fluids with well known properties (e.g. water, air, synthetic oil or stabilised crude oil) and by controlled flow rates (corresponding to fixed gas and water fractions). This initial step defines the operational envelope of the MFM and the measurement errors. A lot of uncertainties are under control and others are completely avoided. Field tests are then required to identify potential operational problems. Compared with lab tests, field trials generally introduce more sources of error. These can be: different upstream conditions (small variations in facilities layout may change the history of the flow), real fluids instead of lab fluids of well know properties, and the need for Pressure/Volume/Temperature (PVT) correlations in order to reconcile reference measurements with the MFM readings taken at operating conditions, as shown in **Fig.2 - 2**. Typically, the results of a field trial indicate the presence of error compensation, i.e. the errors remain very low even when the sources of uncertainty are increased.

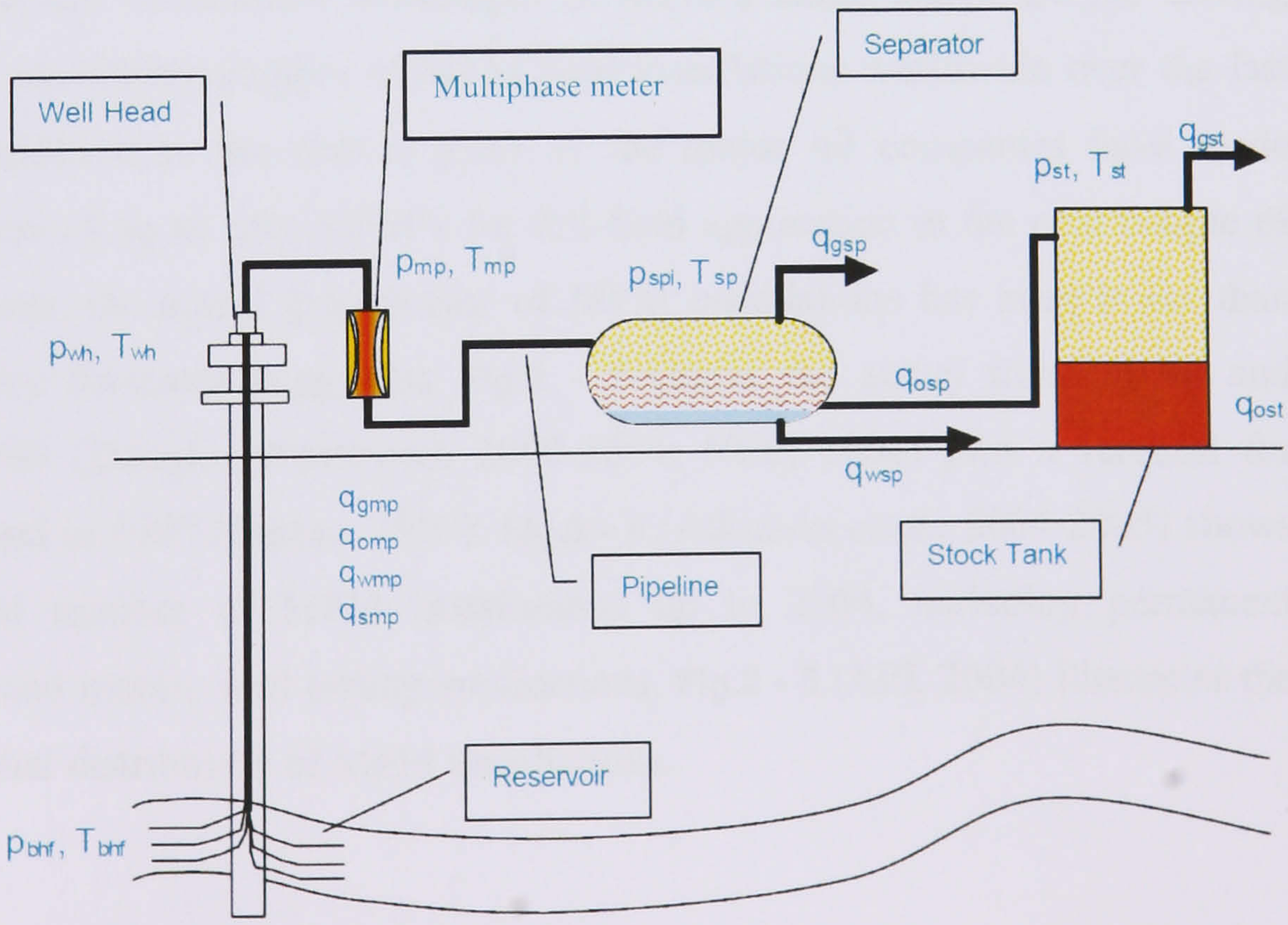


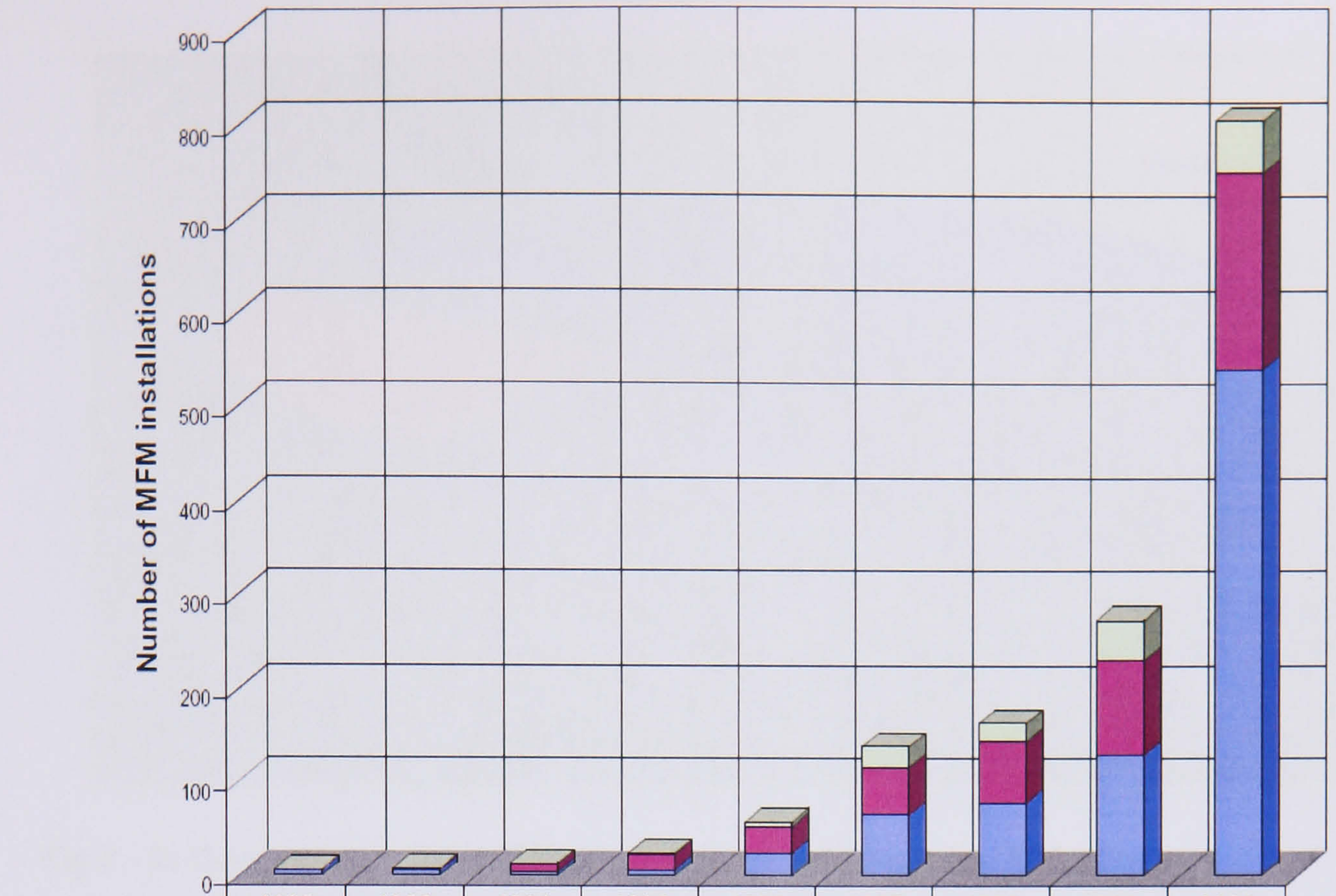
Fig.2 - 2: Schematic of a typical multiphase meter set-up (Pinguet *et al.*, 2005).

There are only a few field flow loops that allow controlled flow tests with real fluids, so that it is possible to characterise and calibrate the MFM simultaneously. The reference measurements are sufficiently accurate, but care must be taken when carrying out the tests (flow instabilities in the loop, possible malfunction of the test separator, etc.). Of course, the other possible field test is a real application in a producing field environment. In this case, the reference is usually taken to be the flow rates measured at a test separator. We must ask ourselves the questions, *"Just how accurate are the measurements at the test separator?"* and, *"Are the uncertainties in measurement for MFM and test separator comparable?"* These are crucial concerns when a meter has to be calibrated or characterised.

In fact, from error theory, it is clear that in order to characterise and calibrate a meter "A", a more accurate meter "B" should be used as to establish whether meter "A" can perform as accurately as the reference meter "B". Otherwise, an option would be to use whatever reference meter "B" is available (even if not sufficiently accurate for calibration purposes) and record a large enough number of measurements to calibrate meter "A" simply by statistical analysis of its performance against the reference meter "B". In theory, a MFM could even be calibrated against another MFM.

2.5 MFM installations worldwide

The technical and economical advantages of MFM's stated above are the driving force for the increasing number of MFM field installations worldwide over the last decade. In addition to the above, some of the major oil companies have made multiple orders of up to fifty MFM's for full-field application in the next couple of years. However, the actual growth rate of MFM installations has been lower than initial industry forecasts suggested. **Fig.2 - 3** shows the actual trend up to and including 1999 (Douglas-Westwood, 2000-2004; NEL, 2001) plus a forecast for 2000 published in 1997 (Hatton, 1997). **Fig.2 - 4** (Atkinson *et al.*, 2004-2005) shows the estimated number of MFM installations up to 2004, including permanent installations and mobile well testing applications. **Fig.2 - 5** (API, 2004) illustrates the current regional distribution of MFM installations.



	1992	1993	1994	1995	1996	1997	1998	1999	2000
Offshore subsea	0	0	0	1	5	22	20	43	55
Offshore topside	1	2	10	17	29	52	66	103	210
Onshore	5	5	3	6	24	65	78	129	542

Fig.2 - 3: Growth rate of MFM installations.

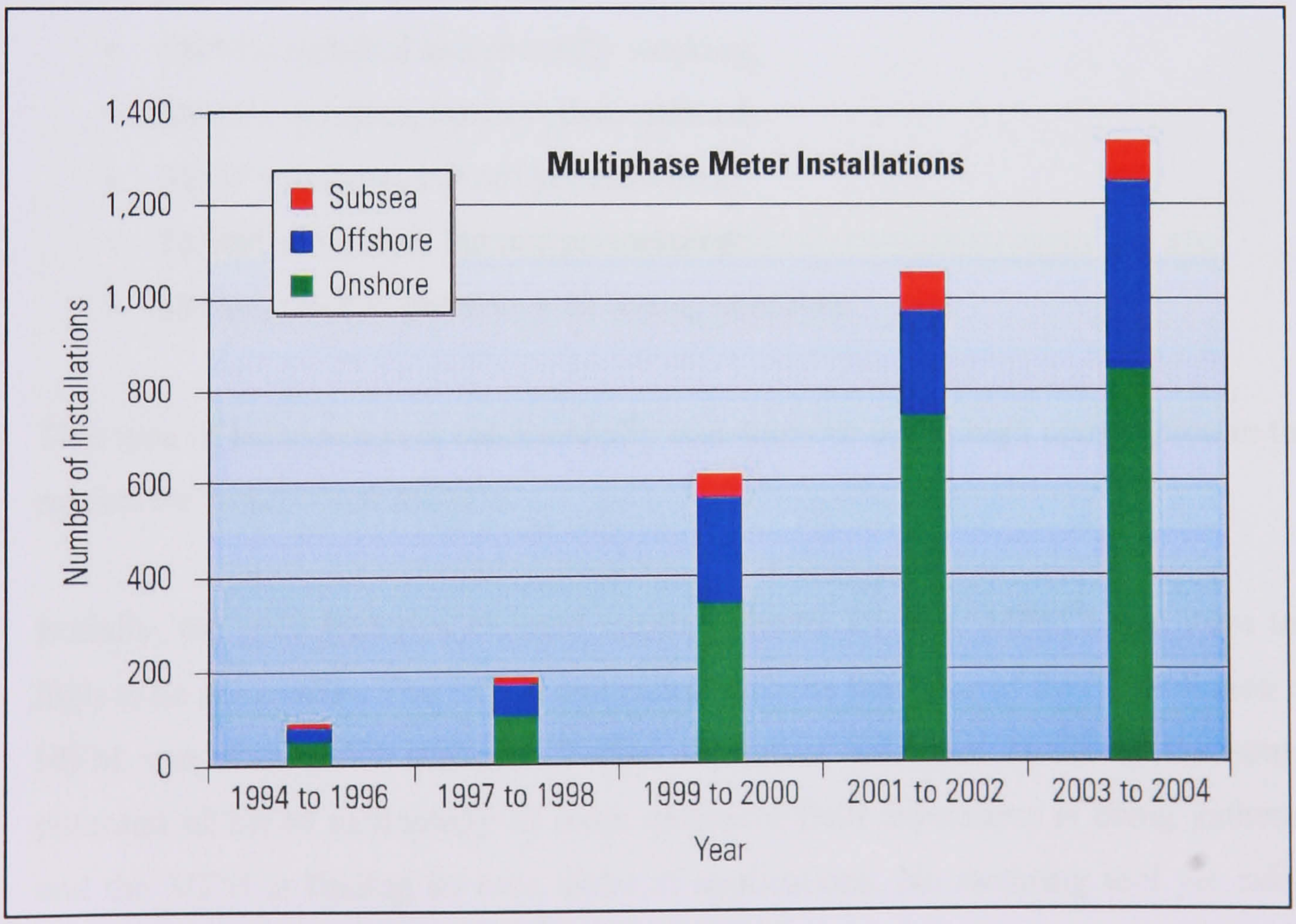


Fig.2 - 4: Estimated number of MFM installations up to 2004, including permanent installations and mobile well testing applications (Atkinson *et al.*, 2004-2005).

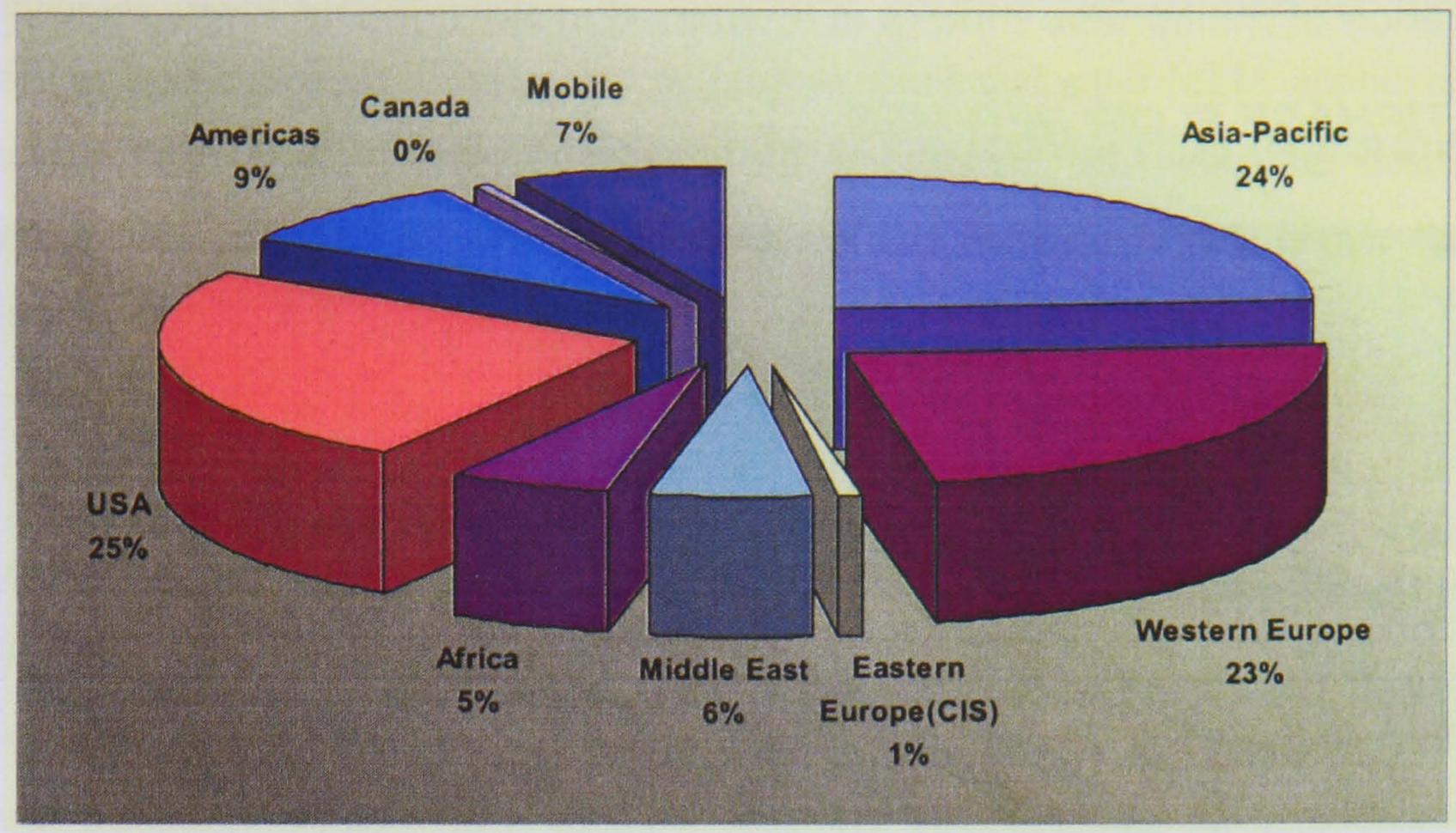


Fig.2 - 5: Current regional distribution of MFM installations (API, 2004).

However, it remains difficult to establish accurate figures, as it is necessary to distinguish between:

- MFM's installed and currently working;
- MFM's installed, but now discontinued;
- MFM's ordered, but not yet delivered;
- MFM's delivered, but not yet installed;
- MFM's used as portable well testing solutions.

This type of information is commercially sensitive due to the high competition in the market for commercial MFM's.

Initially, the manufacturers claimed accuracy levels for their MFM's that were too high to be achievable. The OPEX associated with the first year of field installation of MFM was also underestimated. Today, Operators are more aware of the actual potential of MFM technology as more extensive field experience is being gathered and the MFM is finding its own niche of applications. No metering tool yet exists that can to cope with the complete fraction range of each component and the full range of flow patterns. However, Operators now realise that there are already several

BRL LONG N. UNIV

commercial MFM's from which an acceptable solution can be selected for a particular application. It is important to keep in mind that each MFM application should be carefully engineered before field installation, otherwise the desired metering performance may not be achieved and the resultant OPEX higher than expected.

2.6 Fundamentals of MFM technologies

Basically, there are two approaches to measuring the flow rates of a three-phase flow. In the first, parameters of the flow are measured which are functions of the three flow rates. Thus, for instance, a pressure drop across a venturi, the attenuation of a gamma beam and the impedance of the mixture can be determined and relationships established between these measurements and the flow rates of the respective phases, three independent measurements being required to establish the three flows. There is no way that such relationships can be theoretically predicted and, therefore, they must be established by calibration. Unfortunately, it is not usually possible to calibrate over the full range of conditions over which the measurement technology is to be applied and this approach is not always a productive one. The calibration methodology can often be enhanced using techniques such as neural networks, which can identify the functional interrelationships to a higher order of accuracy. However, though useful, such techniques cannot overcome the fundamental problem, namely that the calibrations (or "training" in neural network parlance) only apply over the range of conditions in which they are carried out. Change the conditions and the established functions become invalid!

The second approach involves measuring the basic parameters of phase velocities and phase cross sectional fractions (holdups) or quantities that can be unequivocally related to these. In order to measure the volume flows (and hence the mass flows) of three components (oil, water and gas) in a pipe, three mean velocities and three phase cross sections need to be established. Thus, five measurements are needed (three velocities and two phase fractions – the third phase fraction is obtained by difference between unity and the sum of the two measured ones). This formidable measurement requirement can be reduced, of course, by separation or homogenisation. By separating the phases, the need for cross sectional holdup measurements disappears

and the three volume flows can be established by conventional single phase metering technology. However, separation is expensive and, in any case, difficult to achieve in many cases. The measurement requirement can also be reduced to three if the velocities are equalised by homogenising the mixture. This is a much more economic option and is at the heart of some commercial flowmeters. However, the range over which satisfactory homogenisation can be achieved is always limited (it is less feasible, for instance, at very high gas fractions where a large proportion of the liquid phase is at the wall).

Thus, both approaches to metering suffer from fundamental drawbacks and it is for this reason that no completely satisfactory metering methodology has been achieved so far. It is important, however, to recognise that these difficulties stem from fundamental problems within the constituent measuring technologies. Here, we briefly review the status and problems of some of these technologies and highlight those that have been used most widely:

2.6.1 Dual energy gamma densitometry

Dual energy gamma densitometry uses a gamma source (or sources) with different energies, it is possible to determine the holdups of the three phases and these measurements can be coupled with velocity measurements to yield the required phase flow rates. Problems involved with this technique include shielding, source decay, averaging over the cross section, fundamental statistical inaccuracies, limitations in detection equipment, effects of changing water salinity and the normal problems of operating sophisticated electronics for subsea applications.

Fig.2 - 6, **Fig.2 - 7** and **Fig.2 - 8** show the absolute error in phase fraction measurement in a two-phase flow system of air-water, air-oil and water oil, respectively. The calculations are based on a 4'' diameter pipe section made of Perspex material, with single-energy gamma-ray beams passing through pipe walls of 12.7mm of thickness. The sources and energy levels used in this example are those commonly adopted in commercial MFM's: Americium 241 (17.8 and 59.5 KeV), Barium 133 (31, 81 and 356 KeV) and Caesium 137 (33 and 661 KeV). Assuming that all sources can provide the same initial intensity I_0 = 5,000 counts/s, it is possible to calculate the

intensity I of a single-energy gamma-ray beam transmitted through the Perspex conduit in which there are two static or flowing phases as:

$$I = I_0 \exp\left(-\gamma_{wall} x_{wall} - \gamma_1 x_1 - \gamma_2 x_2\right) \qquad \textbf{Eq.2 - 1}$$

where:

γ_1 and γ_2 are the linear attenuation coefficients of phase 1 and phase 2, respectively;

x_1 and x_2 are the thicknesses of phase 1 and phase 2, respectively;

γ_{wall} is the linear attenuation coefficient of the conduit;

x_{wall} is the thickness of the conduit.

The absolute error in phase fractions is given by (Pan, 1996):

$$\delta\varepsilon_{1,2} = \pm \frac{1}{(\gamma_1 - \gamma_2) D \sqrt{Ct}} \qquad \textbf{Eq.2 - 2}$$

where:

D is the internal diameter of the pipe;

C is the transmitted count rate;

t is the counting time.

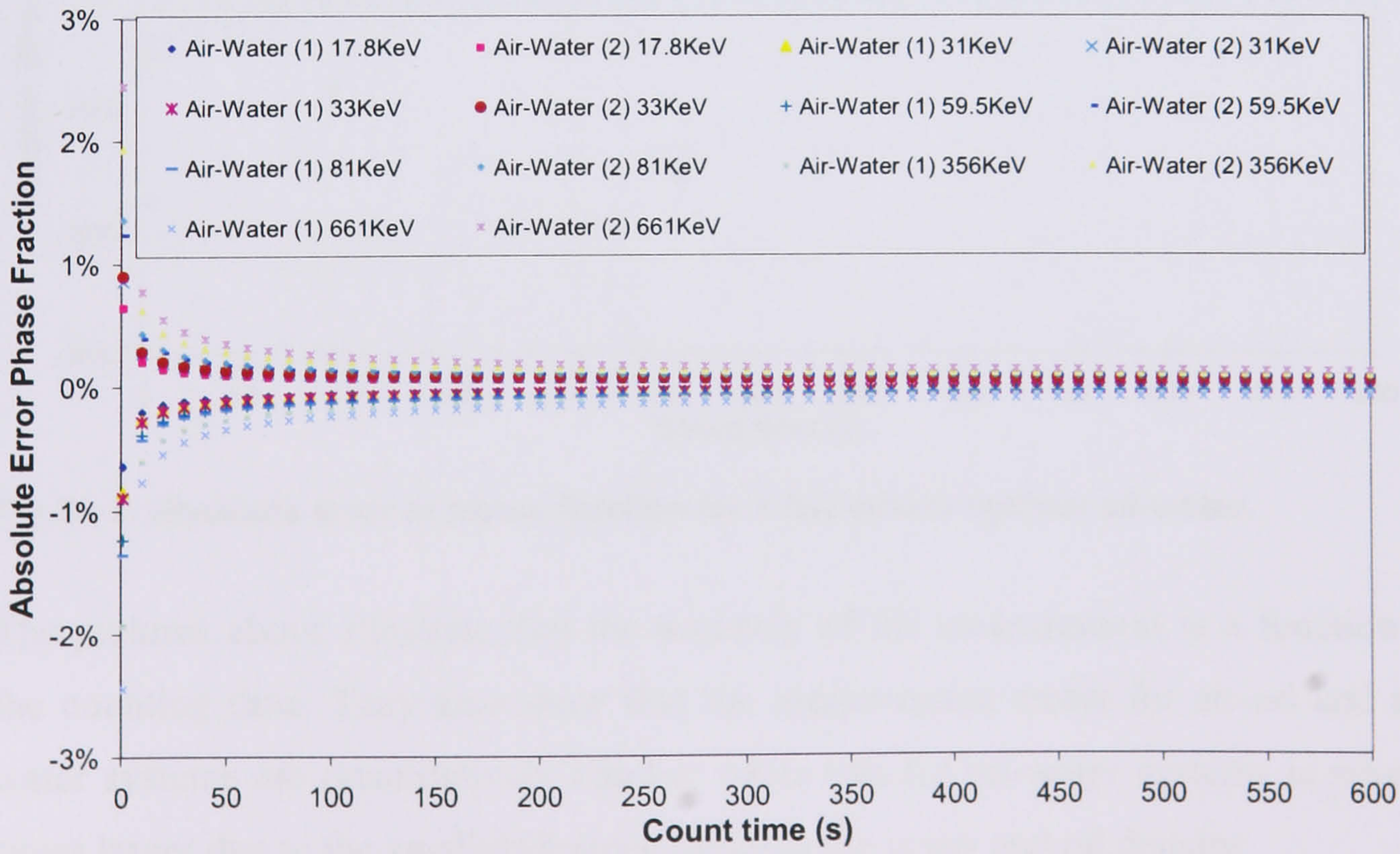


Fig.2 - 6: Absolute error in phase fraction for a two-phase system air-water.

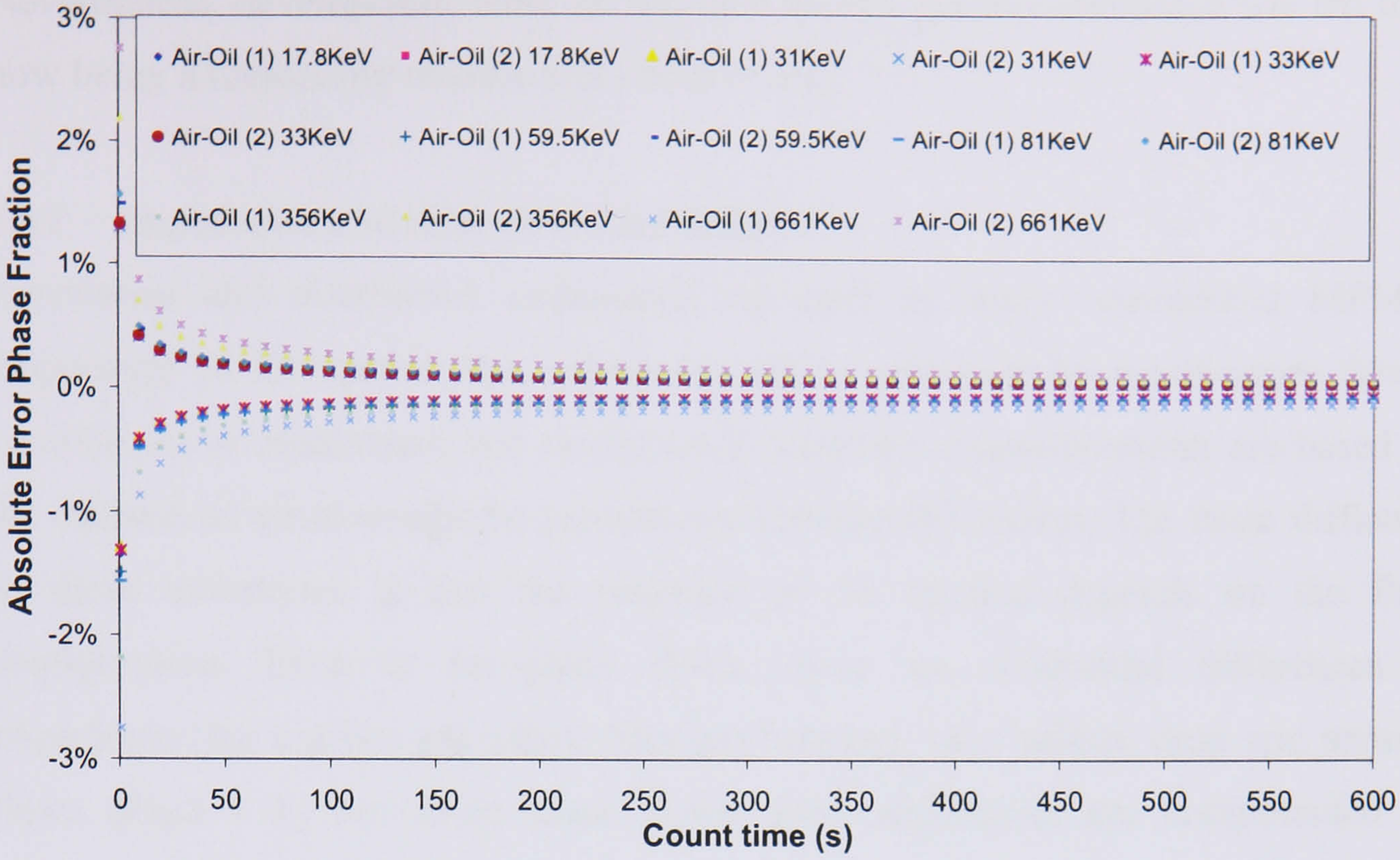


Fig.2 - 7: Absolute error in phase fraction for a two-phase system air-oil.

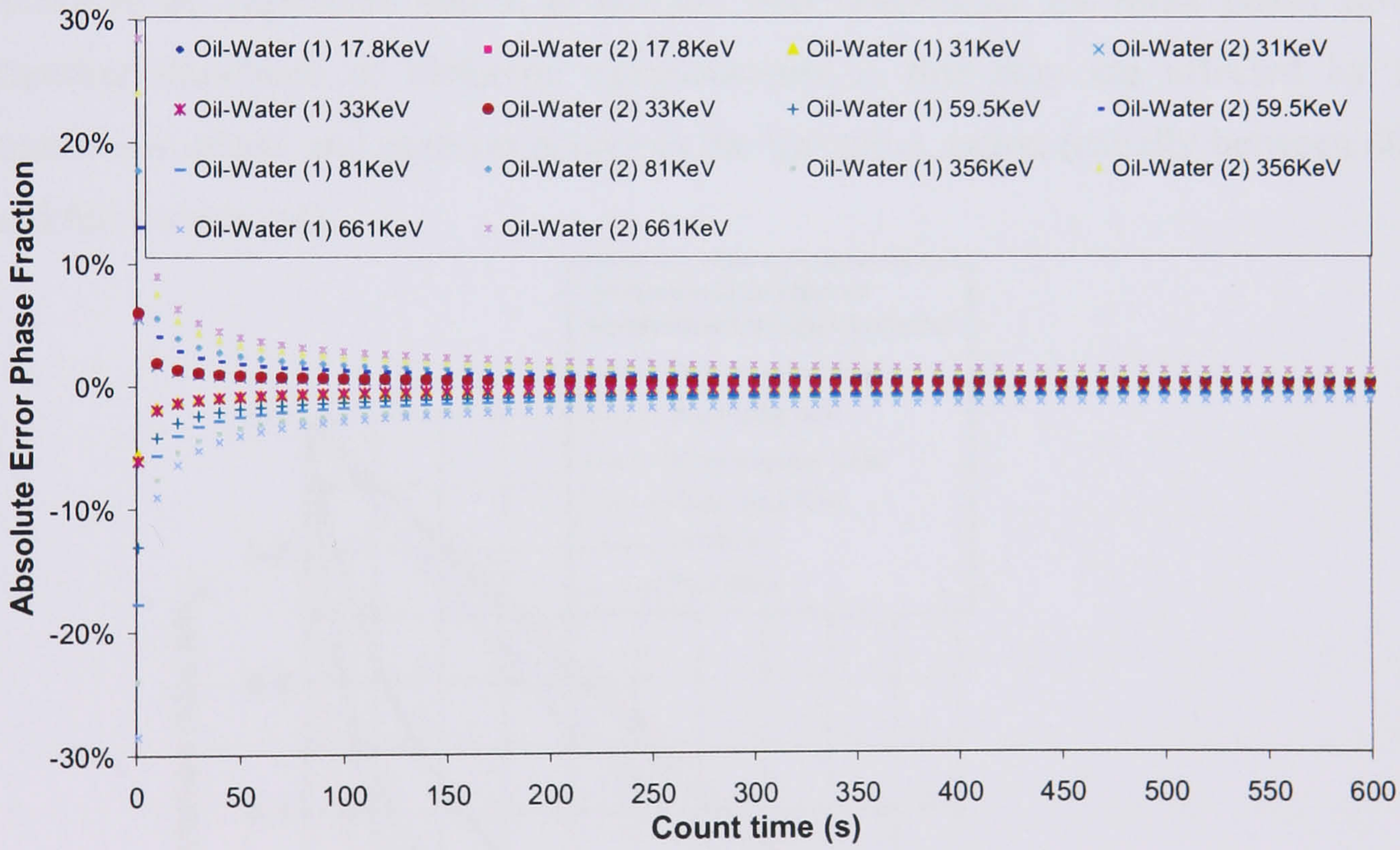


Fig.2 - 8: Absolute error in phase fraction for a two-phase system oil-water.

The pictures above illustrate that the accuracy of the measurement is a function of the counting time. They also show that the measurement errors for air-oil and air-water systems are quantitatively similar, while that for oil-water systems is several times larger due to the small difference between the water and oil density.

Nevertheless, development work on the dual energy gamma technique has led to it now being a reasonably reliable and effective one.

2.6.2 Impedance and microwave techniques

Impedance and microwave techniques are used in many commercial MFM's. Depending on the system, the impedance will be governed by conductance (water continuous) or capacitance (oil continuous). Microwave measurements are based on the contrast of electromagnetic permittivity between the phases. The basic difficulty in these techniques is that the response of the method depends on the flow configuration. Even in two-phase flows, there are substantial differences in impedance (for a given gas phase fraction) between, say, bubble, drop and annular flows (**Fig.2 - 9**). For three phase flows, these difficulties are compounded by presence of the third phase. Despite the success claimed, the general applicability of such devices must be considered questionable. It may be possible to achieve improvements in the impedance method by using tomography techniques, but this is likely to be expensive and it is not yet well established for three phase flows. Another drawback of dielectric measurements is that they are affected by the continuous phase and perform poorly in the inversion region (usually between 40% and 60% water cut).

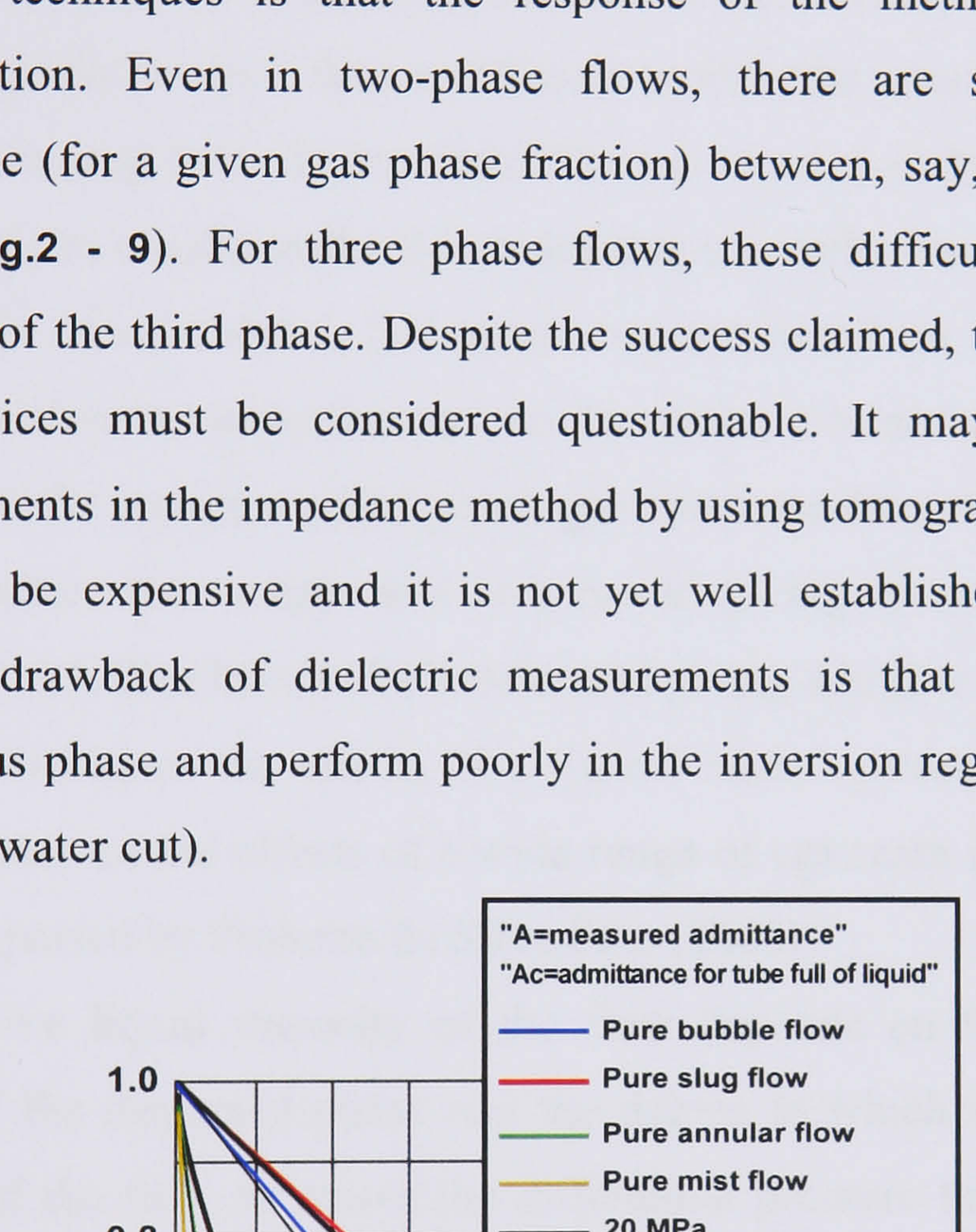


Fig.2 - 9: Effects of flow regime and void fraction on theoretical response (Bouman *et al.*, 1974).

2.6.3 Differential pressure devices

Differential pressure devices are commonly used in single phase and multiphase flow measurements. The device most commonly used for multiphase flows is the venturi, but other devices such as V-cones, orifices or chokes are sometimes used.

Generally speaking, the response of such devices for multiphase flows depends on the upstream flow conditions. Indeed, at Imperial College, attempts have recently been made to use these upstream effects as a basis for a flowmeter. If the flow is fully homogenised, then the pressure difference would be given by the homogeneous flow model. If, on the other hand, the flow remains fully separated (in annular flow, say) through the venturi, then a different model (the separated flow model) applies. The pressure drop for truly separated flows is lower than that for homogenised flows. It is possible to condition the flow such that it is either separated of homogenised as it enters the venturi and a flowmeter concept based on the different response for these two situations seemed attractive. However, it turned out that the case with flow separated at the entrance could give higher pressure drops than the homogenised one. This is because the venturi acts as a mixer, giving re-entrainment of the liquid as droplets, which then have to be accelerated giving a higher pressure drop.

Fig.2 - 10 illustrates the effects of a typical insert upstream of a venturi. Extensive measurements on the effects of a wide range of upstream inserts on venturi pressure drop are reported by Pinheiro da Silva Fiho (2000).

The effective liquid viscosity of the flow depends on the continuous phase, the fraction of the dispersed phase and the degree to which they are mixed. Increased viscosity of the flow increases the differential pressure through the meter and may affect the calculation of the velocity of the flow.

There are no general relationships for differential pressure across venturis and other devices in multiphase flow. The best approach is to attempt to get as close as possible to a homogeneous flow; homogenisation is most effective at low gas volume flow fractions and least effective at high gas fractions (typically above 0.9). Recent work at Imperial College has concentrated on developing better homogenisation schemes for this high gas fraction region.

It is sometimes helpful to measure also the pressure recovery in the diverging region after the venturi throat. The recovery is a strong function of the phase fraction and this fact can be used as an input to multiphase measurement. However, the point made above about calibration also applies in this case; there are no generic

relationships and creating calibrations which cover all conceivable cases is usually impracticable.

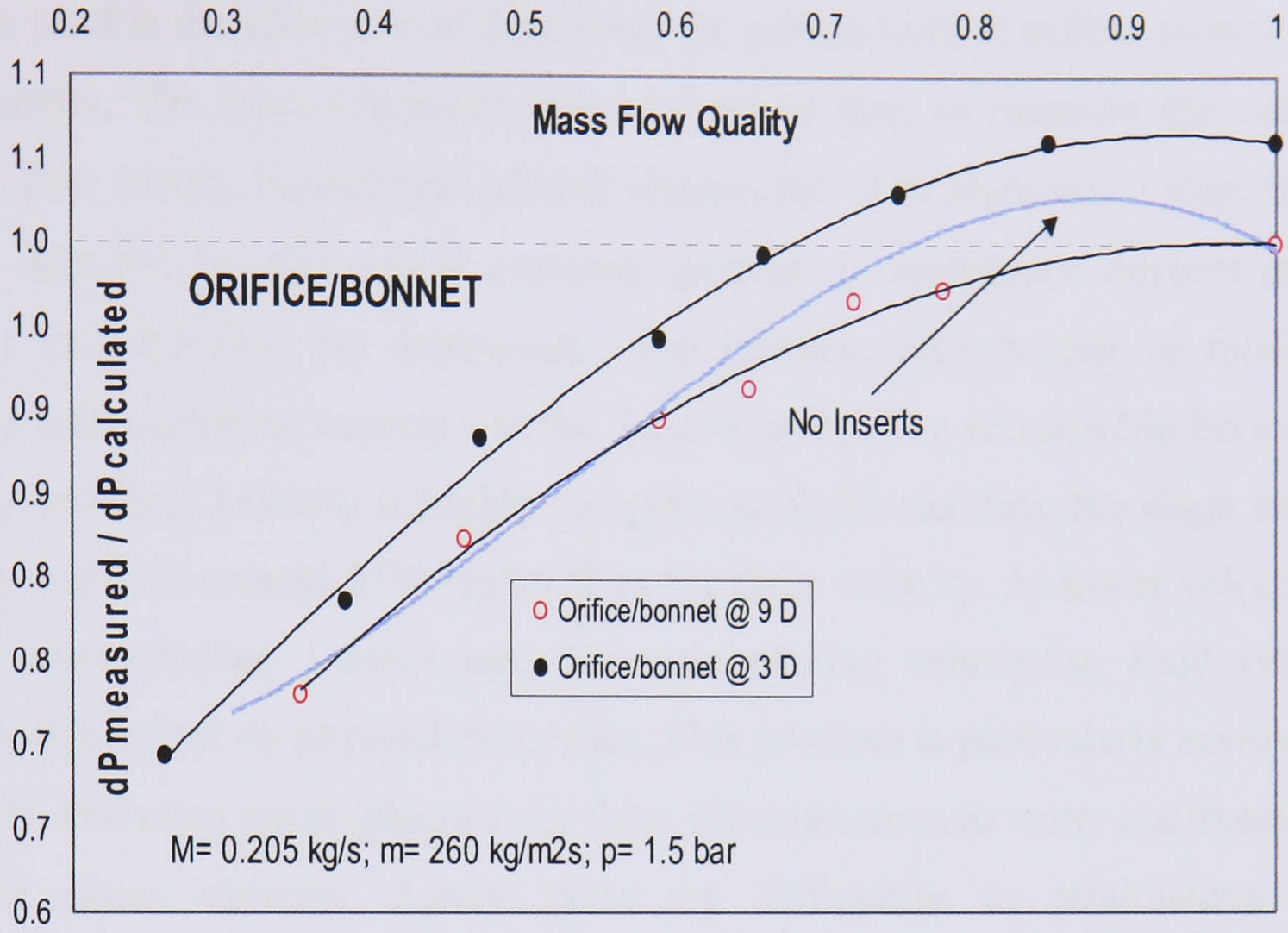


Fig.2 - 10: Effects of Orifice/bonnet inserts upstream of a venturi. Data compared with pressure drop calculated for the homogeneous model (Pinheiro, 2000).

2.6.4 Cross correlation

Cross correlation between signals obtained at two positions along a pipe is used in a number of MFM's. Thus, the peak in the cross correlation function between the two measurements represents the "time of flight" of a flow feature between the two measurement positions. The cross correlation principle is illustrated in **Fig.2 - 11**.

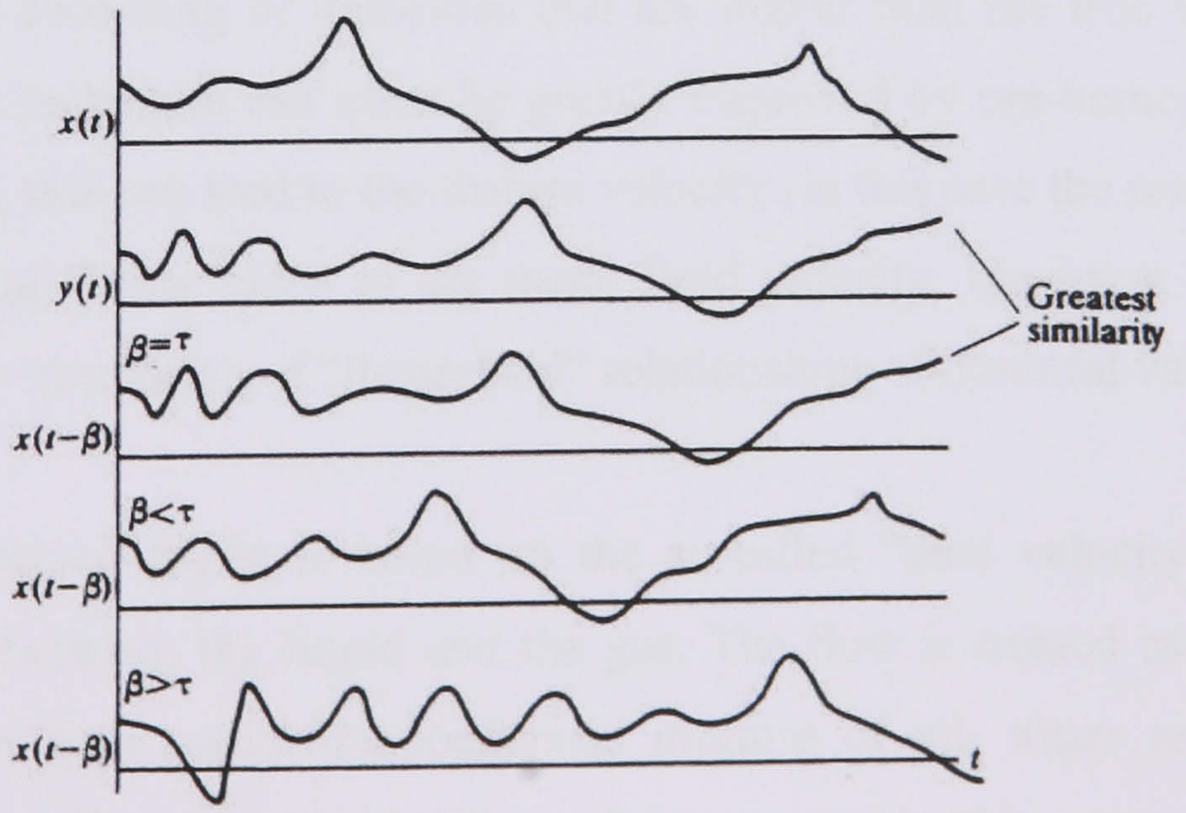


Fig.2 - 11: Cross correlation principle.

Measurement techniques to which this methodology can be applied include differential pressure, impedance, gamma attenuation and acoustic transmission. Although the cross correlation method has the advantage of directly measuring a velocity (and is therefore not as dependant on calibration), it suffers from a number of problems. The most important one of these is that, to measure the velocity, a distinct flow feature is required. Almost always, this flow feature is a slug. Slugs are readily detected by differential pressure, gamma or impedance devices and their velocity can therefore be determined. The problem here is that of relating this velocity with sufficient accuracy to the fluid velocity. The relationship between slug velocity and fluid velocity is highly complex; at high velocities, the slugs travel at a velocity which is around 25% higher than the fluid velocity. At lower velocities, the ratio is much higher. Furthermore, the ratio of slug velocity to fluid velocity is strongly dependent on physical properties. This problem is particularly severe around the phase inversion point (changeover from oil continuous to water continuous flows) in three phase systems. Again, there are difficulties in establishing general relationships and the requirement for calibration is not avoided after all! This may present a fundamental limitation as mentioned above.

Another problem affecting the relationship between slug velocity and fluid velocity is that of slug velocity fluctuations. If slugs pass through restrictions, then the flow is slowed down during the time of passage of the slug because of the higher resistance to flow in the liquid (slug) zone. Pressure builds up in the upstream region and, following the release of this pressure excess gives rise to acceleration of the upstream slugs and to the recording of velocities that are higher than the true velocity. The cross correlation technique can often be greatly improved by pre-homogenisation of the flow. Ideally, this can lead to the feature velocity (in this case the residuum of the homogenised slug) being close to the mean fluid velocity, obviating the need for calibration or the invocation of "theoretical" relationships of doubtful validity.

A currently marketed MFM is based on the so-called "dual velocity" method to handle slippage between the liquid and the gas. The flow is treated as a two-phase mixture made of a) a pseudo-homogeneous mixture of oil, water and small gas bubbles, and b) a free phase consisting of larger gas bubbles travelling with a velocity significantly higher than that of a). The flow rates are calculated by cross-

correlation from two pairs of electrodes: one large pair, sensitive to the signals generated by large gas bubbles, and one small pair, sensitive to the signals generated by small gas bubbles. However, this method requires the presence of some variation in bubble size. It can therefore show limitations when applied at very low or very high GVF's.

2.7 Novel MFM technologies

The above brief discussion illustrates why a generic solution to the MFM problem has proved so elusive. However, adequate solutions are emerging for specific applications. If regular calibration is feasible over the full range of conditions, then many alternative metering schemes could be made to work; in this case, it is probably best to go for relatively cheap technologies and to use methods such as neural network processing to deduce the flow rates. To date, flow pattern identification techniques based on neural networks have been applied to conductance probes, differential pressures and gamma densitometers. The main advantage of artificial neural networks is that they are not based on pre-defined rules (as for conventional signal processing techniques), but rather "learn" from the experience on training data sets. This feature makes neural networks able to cope with the non-linear nature of multiphase flows and achieve high accuracy. However, as mentioned above, these intelligent systems may fail to reproduce the reality as soon as they are asked to work outside the range of conditions over which they have been calibrated. A possible solution to this is the implementation of a fuzzy logic approach. Briefly, independent sets of results from different types of measurements (or physical models) are each interpreted via neural networks. Then, on the basis of the reliability of each physical and neural network model with regard to a particular flow configuration, the most accurate solution is selected via a kind of decisional tree. It has been shown that such integrated solutions tend to be more accurate than those derived from a single neural network model (Alimonti and Bilardo, 2001).

Volume fraction measurements using techniques such as X-ray absorption (Morton *et al.*, 1998) or capacitance tomography (Ismail *et al.*, 2005; Gamio *et al.*, 2004), microwave techniques (Bentolila and Constant, 2005), grab or isokinetic sampling)

are already undergoing noticeable improvements and could provide the flow rates of the phases when combined with independent velocity measurements.

Infrared water cut meters are commercially available. They aim at measuring the volumetric proportion of oil in a mixture of petroleum and water by passing a beam of infrared light through the stream, which is absorbed by oil but not water.
Infrared spectroscopy is the measurement of the wavelength and intensity of the absorption of infrared light by a sample. This infrared light can excite molecular vibrations to higher energy levels (in other words, the protons of the light can pass energy to the electrons of the sample. The electrons though can only change their energy level if the input energy imparted by the photons is sufficient for an electron to move up to the next energy level for the atom). The wavelengths of infrared absorption bands are characteristic of specific types of chemical bonds. If the sample is a hydrocarbon, the infrared light can be absorbed by the hydrogen-carbon bonds of the atomic structure of hydrocarbons. The light absorbed would fall within a "sample" band of the infrared spectrum. Thus, once the energy band for a specific problem has been selected, it is possible to choose the "sample" band; in fact a somewhat larger band is chosen so as to account for possible variations in the strength of the signal, caused by humidity, condensation, and even dust. This extended band is called the "reference" band. At that point, the difference between sample and reference signal strengths is taken as proportional to the concentration of hydrocarbons contained in the path length.
One commercial meter measures simultaneously in four infrared wavelengths bands. These additional frequencies are claimed to allow extension of the range of applicability of this optical technology to low water cut levels and reducing the effects of gas presence.

Alternatively, new “stand-alone” technologies are also under development. Some can be highly complex, difficult to achieve and may imply safety considerations, such as Nuclear Magnetic Resonance (NMR) (Ong *et al.*, 2004) and Pulsed Neutron Acivation (PNA) (Hall *et al.*, 1997). However, these are the only methods based on direct measurement of individual component velocities and fractions. This means that, if available, NMR and PNA meter technology could satisfy the requirements for fiscal metering and hence guarantee the future of MFM. Cheaper “stand-alone”

technologies are pressure pulse (Gudmundsson and Celius, 1999; Gudmundsson *et al.*, 2001) and acoustic noise interpretation (Piantanida *et al.,* 1998). A new multiphase flow meter, which is based on advanced software processing of passive acoustic energy patterns, has recently entered the commercial arena. This meter uses either existing construction details (such as a choke valve or similar) or a simple flow conditioner as a signal generator with a sensor attached to the surface. As the well flow passes through, acoustic energy signals are generated which correlate to the flow rates and composition of the medium. Although very attractive in terms of field applicability, these techniques could offer only limited operating ranges.

2.8 Review of commercial MFM's

A critical review of the MFM solutions currently available in the market is far from being an easy task. Most MFM research projects are now driven by the oil and gas industry and usually end up with a patented solution. Thus, scientific and commercial interests often tend to overlap in a sector of the oil and gas market where competition is intense. MFM manufacturers have to act quickly in order to secure the implementation of a particular technology before their rivals. This results in a very limited amount of published information on the performance of the various MFM's. Unless Operators are ready to pay non-negligible sums to gain access to the results of independent MFM assessments carried out at well-established labs, they are usually offered "black-box" packages where very little is unveiled about the technical principles behind the MFM's.

One way to overcome such problems is for the Operators to establish a more open dialogue among themselves, in order to exchange past MFM experiences so that the same mistakes are not made twice. This is crucial in the pre-engineering phase of a project. The MFM market is a dynamic reality, with new solutions entering the field every year, new alliances being signed and new Joint Industrial Projects being carried out. In such a scenario, the younger, smaller manufacturing companies will struggle to capture their slice of the MFM market, unless they can offer particularly reliable solutions at low cost. In an ideal world, Operators should have some "MFM Reference Guidelines" to help them select the most appropriate device for a particular application from amongst the thirty or more MFM's currently available

(including those still under development). When choosing a MFM, Operators should give particular consideration to:

Level of confidence in a particular technique. This is entirely up to the Operator, based on its in-house expertise and liaisons with MFM specialists or Academia.

Safety and environmental issues. For some applications, MFM's that use nuclear sources must be discarded.

Intrusiveness of the measurement. Whenever wax, scale or asphaltene deposition is likely, intrusive devices are clearly not the best solution. Intrusiveness also is a safety issue.

High Gas Void Fraction (GVF) fields. It is common understanding that the majority of the MFM show larger error for Gas Volume Fraction (GVF) >90%.

Operating range to be covered. As already mentioned, no metering tool exists which is able to cope with the entire range of GVF, flow rate, pressure, water cut and flow patterns. Hence, it is fundamental to accurately identify the window of conditions to be covered by the tool.

Tool size available. Most manufacturers claim that they can deliver tools between 2" and 10-12" in diameter with the same level of metering accuracy. However, due to the highly unpredictable nature of multiphase flow it is very dangerous to upscale small diameter results without performing dedicated tests on large diameter tools. The main limitation is that there are no large diameter facilities worldwide able to guarantee the same kinds of test accuracy as those already possible with small diameter flow loops.

Level of calibration needed over field life. Although manufacturers tend to say that their products do not need further calibration after the factory calibration, we have already illustrated the dangers of not accounting for the dependence of MFM's performance on the range of conditions (upstream conditions, fluid properties, etc.) over which they have been certified.

Costs (CAPEX and OPEX). This may seems an obvious statement, but Operators still tend not to see the long-term advantages associated to MFM installations. In addition, MFM manufacturers tend to hide the real order of magnitude of OPEX costs.

Level of assistance provided by the manufacturers. Although, when buying MFM's, Operators will also buy other services from the manufacturers, including the training of the in-situ personnel, it is very important to guarantee some long-term technical assistance and co-operation, in the case of failure of malfunction of any part of the system.

Previous marinisation experience. For subsea installation, previous marinisation experience is obviously a plus for the manufacturers.

Vertical or horizontal installation. Some MFM's must be installed vertically, some others horizontally. For a particular layout of flowlines, one option can be better than the other.

"Stand-alone" MFM's versus integrated packages. Some manufacturers have now started to offer MFM's as part of a larger package of integrated solutions for reservoir management and production optimisation. The Operators have to evaluate whether they prefer such solutions or rather separate components.

Table 2 - 1 presents a list of the current commercial MFM's, divided into "traditional" MFM's (GVF<95-98%), high GVF MFM's (WGM's, GVF>95-98%) and Downhole MFM's (DMFM's). **Table 2 - 2, Table 2 - 3, Table 2 - 4** and **Table 2- 5** present possible ways to classify the current commercial MFM's based on their features. Those meters that are still under development have not been included (e.g. JNOC, IFP, University of Manchester, Imperial College, Robert Gordon University/QuantX). Also omitted are those MFM solutions that need to be integrated with other techniques in order to provide the three flow rates (e.g. pressure pulse, virtual metering). The tables are based on the main characterising features of a MFM that often determine the choice by an Operator.

MFM's	WGM's	DMFM's
Roxar-MPFM	Roxar-WGM	QuantX
Schlumberger/Framo-Vx	Schlumberger/Framo-Vx	Weatherford/CIDRA
Flowsys/FMC-TopFlow	Petrotech-Smartvent	Schlumberger
Jiskoot-MIXMETER		
TEA Sistemi-Lyra	TEA Sistemi-VEGA	
Agar-MPFM	Agar-MPFM 400 loop	
Red Eye-REMMS	Red Eye-REMMS (?)	
Abbon-Flow Master	Abbon-Flow Master	
Haimo-MPFM	Haimo-MPFM	
ESMER	ESMER (e.g. + V-cone)	
Kvaerner-DUET	Kvaerner-CCM	
Kvaerner-CCM		
Accuflow	Accuflow	
Daniel/Emerson-MEGRA	Solartron/Emerson-Dualstream II	
Hydralift-Wellcomp		

Table 2 - 1: Current commercial MFM's, WGM's and DMFM's

Flow conditioning /Homogenisation	Leave-as-it-is	In-line separation	Isokinetic sampling
Roxar-WGM	Roxar-MPFM	Agar	TEA Sistemi-VEGA
Jiskoot-MIXMETER	Schlumberger/Framo-Vx	Wellcomp	
TEA Sistemi-Lyra	Flowsys/FMC-TopFlow	Accuflow	
Daniel/Emerson-Dualstream II	Daniel/Emerson-MEGRA (for GVF<25%)	Daniel/Emerson-MEGRA (for GVF>25%)	
	Abbon-Flow Master	Red Eye-REMMS	
ESMER (+ V-cone)	ESMER	Haimo-MPFM	
	Petrotech-Smartvent		
	Kvaerner-DUET	Kvaerner-CCM	

Table 2 - 2: Current commercial MFM's with/without flow conditioning

Gamma source	No Gamma source
Roxar-MPFM	Roxar-WGM
Jiskoot-MIXMETER	Red Eye-REMMS
Daniel/Emerson-MEGRA	Daniel/Emerson-Dualstream II
Kvaerner-DUET	Kvaerner-CCM
Haimo-MPFM	Agar
Schlumberger/Framo-Vx	Wellcomp
TEA Sistemi-Lyra	TEA Sistemi-LYRA (for WC>30%)
	TEA Sistemi-VEGA
	Flowsys/FMC-TopFlow
	Petrotech-Smartvent
	Abbon-Flow Master
	ESMER
	Accuflow

Table 2 - 3: Current commercial MFM's with/without gamma ray source

Intrusive	Non-intrusive(*)
Roxar-WGM	Roxar-MPFM
Jiskoot-MIXMETER	Schlumberger/Framo-Vx
TEA Sistemi-VEGA	TEA Sistemi-LYRA
Kvaerner-CCM	Kvaerner-DUET
Daniel/Emerson-Dualstream II	Daniel/Emerson-MEGRA
Haimo-MPFM (flow conditioning vessel)	Petrotech-Smartvent
Accuflow	Flowsys/FMC-TopFlow
Red Eye-REMMS	Abbon-Flow Master
Agar	ESMER
Wellcomp	

Table 2 - 4: Current commercial MFM's intrusive/non-intrusive

(*) venturi's are not regarded as intrusive devices

X-correlation	No X-correlation
Roxar-MPFM	Roxar-WGM
Kvaerner-DUET	Kvaerner-CCM
Haimo-MPFM (flow conditioning vessel)	TEA Sistemi-LYRA
Flowsys/FMC-TopFlow	Schlumberger/Framo-Vx
	Daniel/Emerson-MEGRA
	Petrotech-Smartvent
	Daniel/Emerson-Dualstream II
	Abbon-Flow Master
	ESMER
	Accuflow
	Red Eye-REMMS
	Agar
	Wellcomp
	TEA Sistemi-VEGA
	Jiskoot-MIXMETER

Table 2- 5: Current commercial MFM's with/without cross-correlation

2.9 The future of MFM

In times of low oil price, Operators tend to focus their efforts on the short-term rather than the long-term investment. Hence, "young" technologies such as MFM, not yet 100% proven in the field, tend to be classified as too risky and therefore temporarily neglected. This probably contributed to slower uptake of MFM between 1999 and 2000. With the oil price stable at around US$28 per barrel or as high as US$90 per barrel, the MFM market resumes its exponential trend. Since the cycles of the oil and gas industry are notoriously difficult to predict, it may be ambitious to attempt a five-year or ten-year MFM look-ahead. The future of MFM depends very much on how it will fit with other technologies toward global field wide solutions, as well as on whether relevant scientific contributions will become mature for technical applications. Nonetheless, it is possible to address some MFM goals for the new Millennium:

2.9.1 Better accuracy, repeatability, and reliability

Thanks to the increasing demand of MFM's for field installations, performing dedicated tests should become more frequent, thus allowing the MFM's manufacturers to gain a better understanding of the strengths and weaknesses of their devices and lead them to improve their technologies. The operating ranges of each particular solution would become clearer to the Operators, who would then be able to look at the MFM market and pick the most appropriate options for their applications.

2.9.2 Clamp-on solutions for topsides and seabed applications

Retrofitting existing installations is one of the main issues to be faced by MFM. Subsea manifolds where MFM options were not taken into account at the time of the design may need major intervention to accept any of the current MFM's, with associated production loss. Remote onshore fields too would benefit from clamp-on MFM's to be easily moved from one flow line to another, without having to flange-connect the tool or to periodically rent a portable MFM.

2.9.3 International Regulation on MFM accuracy requirements

Although MFM technology is now recognised and accepted by the oil and gas industry, it still lacks universally approved guidelines on how to select, test, validate and certificate a MFM, which unfortunately creates lots of misunderstandings among the MFM community (manufacturers, Operators and Governmental bodies). Still absent are international regulations indicating which level of accuracy MFM's must satisfy for each particular application, in order for the Operators not to break the Law. In some cases, MFM may be the only viable technical and economic solution to the development of a new field. We recognise that MFM's cannot always achieve the same performance as single-phase meters. However, in the North Sea as well as in the other major producer countries, the only available legislation on metering requirements still requires a stream to be measured with single-phase metering accuracy (which obviously implies separation of the phases). To date, relevant efforts in this direction have been made by the Norwegian Society for Oil and Gas Measurement and the Norwegian Society of Chartered Technical and Scientific Professionals (NFOGM, 2005), the Department of Trade and Industry (DTI, 2002 and 2003), the American Petroleum Institute (API, 2004) and the Alaska Oil & Gas

Conservation Commission (AOGCC, 2004), who have tried to standardise definition, classification, qualification procedure and implementation of MFM.

2.9.4 Flow assurance via integration of technologies

Marginal and deepwater fields will only be commercialised if costs are kept to a minimum, so there is a tendency to develop them via subsea tiebacks to existing host facilities when possible. Use of MFM avoids the need for a dedicated test line and also allows metering of the produced stream before it is commingled with production from other fields. The advantages of MFM can be combined with other technologies that also contribute to guarantee the feasibility of a deepwater or marginal field development:

Subsea/downhole separation removes excess water from the produced stream before it is lifted to surface. There are several subsea separation systems in various stages of development: Baker Centrilift's DOWS, Doris Engineering' DIPSIS and Kvaerner's H-SEP. In addition to removing the water from the produced oil-water stream, the systems must re-inject the water downhole into a suitable formation. The major advantages of knocking out water downhole are improved vertical lift to the surface that will improve well productivity (and increase oil recovery via increased sweep efficiency), reducing the processing load on the topside facilities and allowing simpler flowline networks without to be used. As the separated water is re-injected downhole, subsea separation reduces multiphase flow problems by providing less severe slugging and reducing the risk of hydrate formation and corrosion. Subsea separation is performed at higher pressures than on surface which is more efficient, providing lower flow viscosity, larger density difference between phases, less likelihood to form unstable emulsions and keeps asphaltenes dissolved in the oil stream. Thus, many flow assurance issues will be eased by the introduction of subsea separation and benefits the application of MFM in this environment. By coupling a MFM to a downhole separation system we can monitor changes in the performance of the well(s) both at the production and injection zones and optimise separation efficiency.

Subsea/downhole MFM is easier because of lower GVF, lower potential for hydrate, scale or asphaltene formation, and higher density contrast between oil and water.

Downhole MFM would appear to be best suited for "intelligent wells", where streams from different producing intervals need monitoring. Downhole MFM also allows continuous optimisation of artificial lift systems (electrical submersible pumps and gas lift) via a real-time detection of any well performance change (Aspelund *et al.,* 1996). At present, there are three commercial downhole MFM's available on the market. One is based on fibre-optic measurements of pressure, temperature and holdup (Kragas *et al.,* 2003). However, it is currently limited to two-phase (oil and water) systems. Another is a combination of a conventional venturi plus a gamma-ray densitometer with a low active source (Webster *et al.,* 2004). The densitometer must be placed at a strategic position downstream of the venturi where it can be assumed that the phases are well mixed and slip is eliminated. However, the point at which the homogeneous mixture will start separating again is not the same for all flow conditions and this may have an impact on the overall performance of this downhole metering solution. The third commercial downhole MFM, which is to be installed during the completion phase of the well, uses a venturi, with the addition of a permanent pressure and temperature gauge above or below the main meter carrier, to estimate the water fraction. This meter is produced by QuantX, a 50/50 joint venture between the Expro Group and Baker Hughes.

In the future, it may be possible to achieve satisfactory metering accuracy so that, when combined with seabed multiphase pumping, topside metering will be redundant.

Multiphase pumping (Leporcher, 2000) is used to boost production to the delivery point. It can be applied without any phase separation or after seabed/downhole separation to knock out water from the main hydrocarbon stream.

There are numerous ways to combine the above technologies to optimise a particular field development. For example, several wells from the same field could be metered separately (i.e. no need for test lines) then have their production gathered at the same manifold and, from there, boosted to the delivery point with a multiphase pump. Alternatively, a downhole MFM could be used, followed by downhole separation and then a multiphase pump on the seabed to boost the resultant production to the delivery point. Each development scenario will vary according to the number of wells, the number of fields commingled together, the produced fluid properties and the distance from the delivery point. The only real drawback to all of this new

subsea/downhole technology is the lack of operational history and the concerns over reliability in the field.

2.9.5 Integrated solutions to optimise field recovery

An integrated monitoring and metering approach that allows a better management of producing fields helps improvement in the recovery from oil and gas reservoirs. From a "flow rate measurement" point of view, it is fundamental to obtain continuous information from each producing well or producing layer in the reservoir. A "distributed" metering approach allows a real-time diagnosis of wells health, since changes in wells operating parameters could indicate deposition of wax, scale or asphaltene, changes in the fluid properties, water break-through. This information can then be integrated with stock tank measurements and reservoir modelling, and interpreted via nodal analysis to verify the chosen production strategy for the field. Research carried out at "La Sapienza" University, Rome, on the use of wellhead choke valves to monitor and predict well performance (**Fig.2 - 12**) has lead to promising results, especially when the system is integrated with MFM's or test separators.

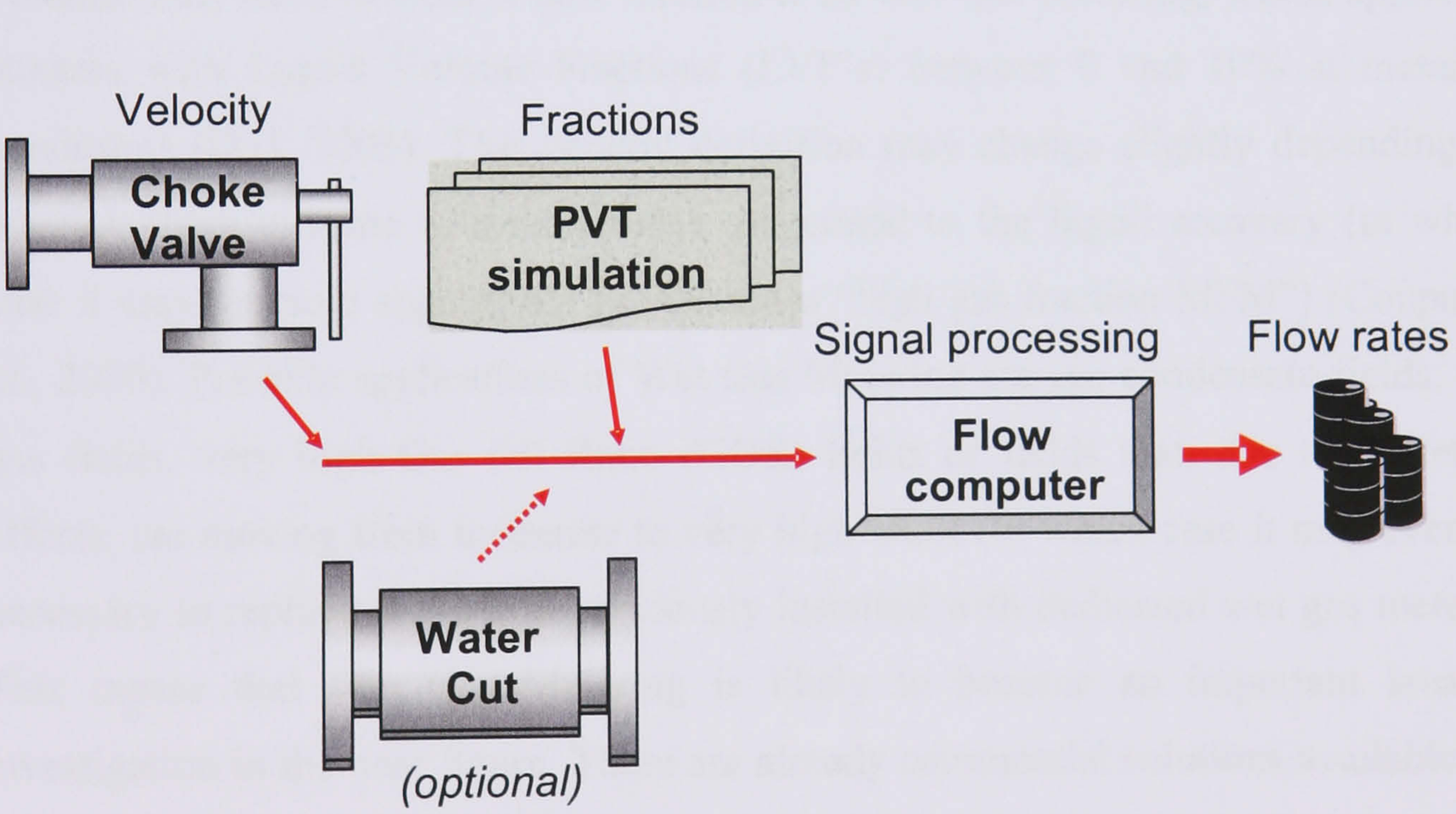


Fig.2 - 12: The use of wellhead choke valves to monitor and predict well performance (Alimonti *et al.*, 2001).

The integrated monitoring and metering approach is usually referred to as "virtual metering" (Rasmussen, 2004). This is a supplement or back-up to multiphase flow meters. It is designed to provide estimates of multiphase flow rates, based on

extensive databases of production data recorded continuously from distributed sensors along the production system. Virtual metering can be defined as a mathematical model of the underlying multiphase flow processes taking place in a given production system, which extracts information from available data and includes automatic controllers that adjust the control variable as and when necessary. The use of virtual metering for production optimisation purposes is increasing, although it cannot be considered as a substitute for physical multiphase flow measurements.

Such a field-wide monitoring & metering approach, from downhole to stock tank, gives a real-time picture of what is happening in the reservoir and therefore provides the best support to reservoir simulation (Gjerstad, 2000).

2.9.6 Wet gas metering

There seems to be a point where MFM and gas metering cross their path. The MFM operational envelope is unlikely to exceed GVF's above 90%. Similarly, gas metering systems are unlikely to operate accurately with liquid content of 1% in volume. This leads to what is now referred to as Wet Gas Metering, which applies to streams with Liquid Volume Fractions (LVF's) between 0 and 10% at metering conditions (DTI, 2003). This general definition may change slightly depending on whether there is some economic value associated to the liquid recovery (in which case it may be more appropriate to talk about "high gas fraction MFM") (Couput *et al.,* 2000). Possible applications of Wet Gas Metering are gas condensate fields, wet gas fields, very high Gas Oil Ratio (GOR) fields or fields that, due to depletion effects, are moving from moderate to very high GOR (in which case it may even be necessary to replace any MFM previously installed with dedicated wet gas meters). This means that Wet Gas Metering is likely to become an important area of investigation in the near future. There are already commercial solutions available for wet gas metering. Although partial separation, isokinetic sampling, vortex meters and ultrasonic meters may offer satisfactory results in some cases, the oil and gas industry seems to favour venturi meters, since they have already been used in the past specifically for such applications. The subject of Wet Gas Metering will be discussed in more detail in Chapter 3.

2.10 Conclusions

After more than twenty years of dedicated research and more than a decade of field trials, MFM has now become an established discipline within the Oil & Gas Industry. Although, to date, a generic solution to MFM does not exist, adequate methodologies are available for specific applications. The quality of the results achievable with existing commercial MFM solutions is dependent on the quality of the work that Operators undertake in the pre-engineering phase of an MFM application. Throughout this period, an open dialogue with the MFM manufacturers is crucial.

Though MFM technology has now been widely applied in hydrocarbon recovery systems, there are still unresolved questions regarding the accuracy and range of applicability of commercial meters. There is a tendency to forget some of the basic limitations, as exemplified here by the cases of gamma densitometry and venturi meters. Even in the case of straight pipe flows, the structure and local behaviour of multiphase flows is still, in all but the simplest cases, poorly understood and certainly not predictable. Small wonder then that the developing flows through the complex geometries which occur in many metering systems are not captured by the simplified models used to interpret meter outputs. Perhaps the real surprise is that, even after discounting the sales hyperbole common in this field, the meters work even as well as they do. There is a long way to go in this field and the user should realise that MFM's are one piece of the optimised production system jigsaw.

With respect to deepwater and marginal fields developments, there is an anticipated increase in demand for accurate MFM solutions in the years to come. In order for MFM to meet these expectations, more technical/scientific contributions will be needed, and more proactive communication between the Oil & Gas Industry and Governmental organisations worldwide needs to be established.

CHAPTER 3

Wet Gas Metering and ANUMET

3.1 Summary

Wet gas metering is rapidly establishing itself as a special problem area within the more general area of multiphase flow metering. In fact, while attempts are being made across the Oil and Gas Industry to define the boundaries between humid gas, gas-condensate and high GVF (gas volume fraction) multiphase systems, a few commercial wet gas meters are already available for specific field applications.

A major interest of Imperial College has been the development of metering schemes for three-phase (oil-gas-water) flows in oil-field production systems. Imperial College has already developed a flow meter (MIXMETER) (Hewitt *et al.,* 1997), which performs satisfactorily in the range of gas volume fractions of 0 to 90%. Imperial College has therefore been recently developing a new concept (ANUMET), which shows some promise for measuring two-phase flows at much higher gas volume fractions.

The technical description of the ANUMET wet gas meter is outlined in this chapter. Preliminary experiments on this new metering concept have been carried out with air-water flows in a 32 mm diameter tube in the LOTUS (LongTUbeSystem) facility at Imperial College. Encouraging results have been obtained and they are presented here.

3.2 Introduction

World natural gas consumption grew by 3.3% in 2004, compared with a 10-year average of 2.3%. Gas production rose in every region except North America (BP Review, 2005). International trade in natural gas increased by 9% in 2004 (BP Review, 2005). Pipeline shipments rose by more than 10% (BP Review, 2005). Compared with oil fields, gas fields tend to be more environment-friendly because of lower carbon dioxide emissions and a cleaner combustion. However, the production of gas is, in most cases, associated with the production of liquid hydrocarbons (that form in the reservoir, in the wellbore and at surface as pressure and temperature drop), free formation water and condensed vapour. This is why, from a metering point of view, the techniques normally implemented for dry gas metering cannot be always applied.

Now that operators have become aware of the potential benefits in using multiphase flow meters for metering the produced streams of oil fields, in terms of cost savings, production optimization, field monitoring and reservoir management (*see Chapter 2*), it is almost straightforward to extend the same considerations to wet gas and gas condensate fields. However, before generalising the problem of multiphase flow metering and deciding which techniques can be applied for the case of wet gas metering, it is necessary to first define "wet gas".

3.2.1 Definition of wet gas and wet gas metering issues

To date, several definitions of wet gas have been proposed within the Oil and Gas industry, all of them equally important in covering the full range of possible stream compositions, operating pressures and temperatures, and flow regimes. Wet gas metering, in fact, may apply to gas condensate fields, high GOR fields and wet gases. Accordingly to the definition given in the SPE monograph volume 20 (Whitson and Brule', 2000) and as illustrated in **Fig.3 - 1**, a reservoir fluid is classified as dry gas when the reservoir temperature is greater than the cricondertherm and surface/transport conditions are outside the two-phase envelope; as wet gas when the reservoir temperature is greater than the cricondertherm but the surface conditions are in the two-phase region; as gas condensate when the reservoir temperature is less than the

cricondertherm and greater than the critical temperature; and as an oil (volatile or black oil) when the reservoir temperature is less than the mixture critical temperature.

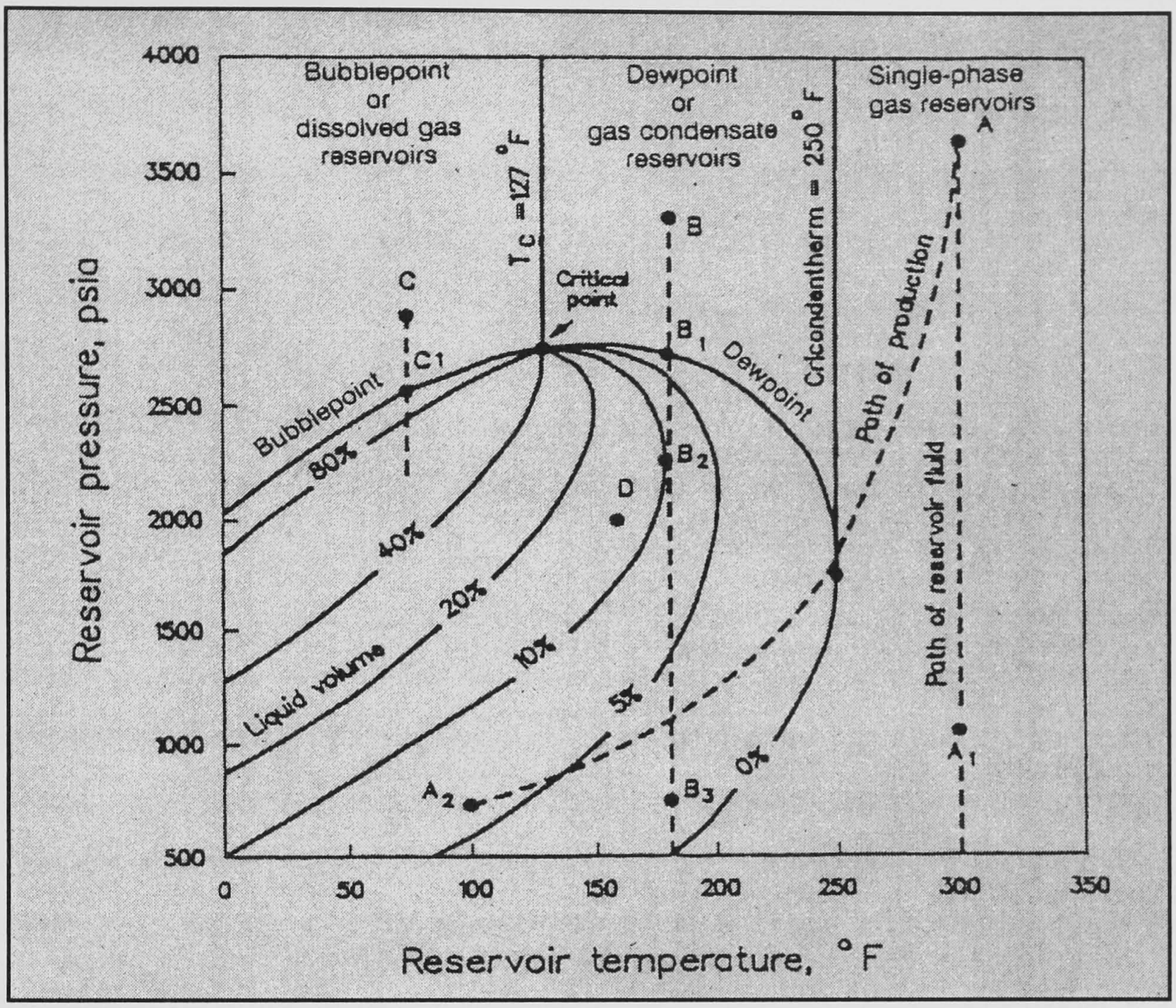


Fig.3 - 1: Classification of reservoir fluids (Whitson and Brule', 2000).

In 2002, the DTI (2002) issued Guidelines where wet gas was taken to mean a two-phase flowing liquid with the LVF in the region of 5-10%. The DTI (2003) later modified the same Guidelines providing a more general definition of wet gas as that of a stream with LVF's between 0 and 10% at metering conditions. Following this definition, wet gas metering can be seen as the top boundary of multiphase flow metering (oils with high gas volume fractions) and the bottom boundary of gas metering (gases with high liquid volume fractions). This implies that by pushing either multiphase flow metering or gas metering to their extremes, wet gas metering solutions could, in theory, be found. However, due to the complexity and peculiarity of wet gas flows, wet gas metering may necessitate a dedicated effort.

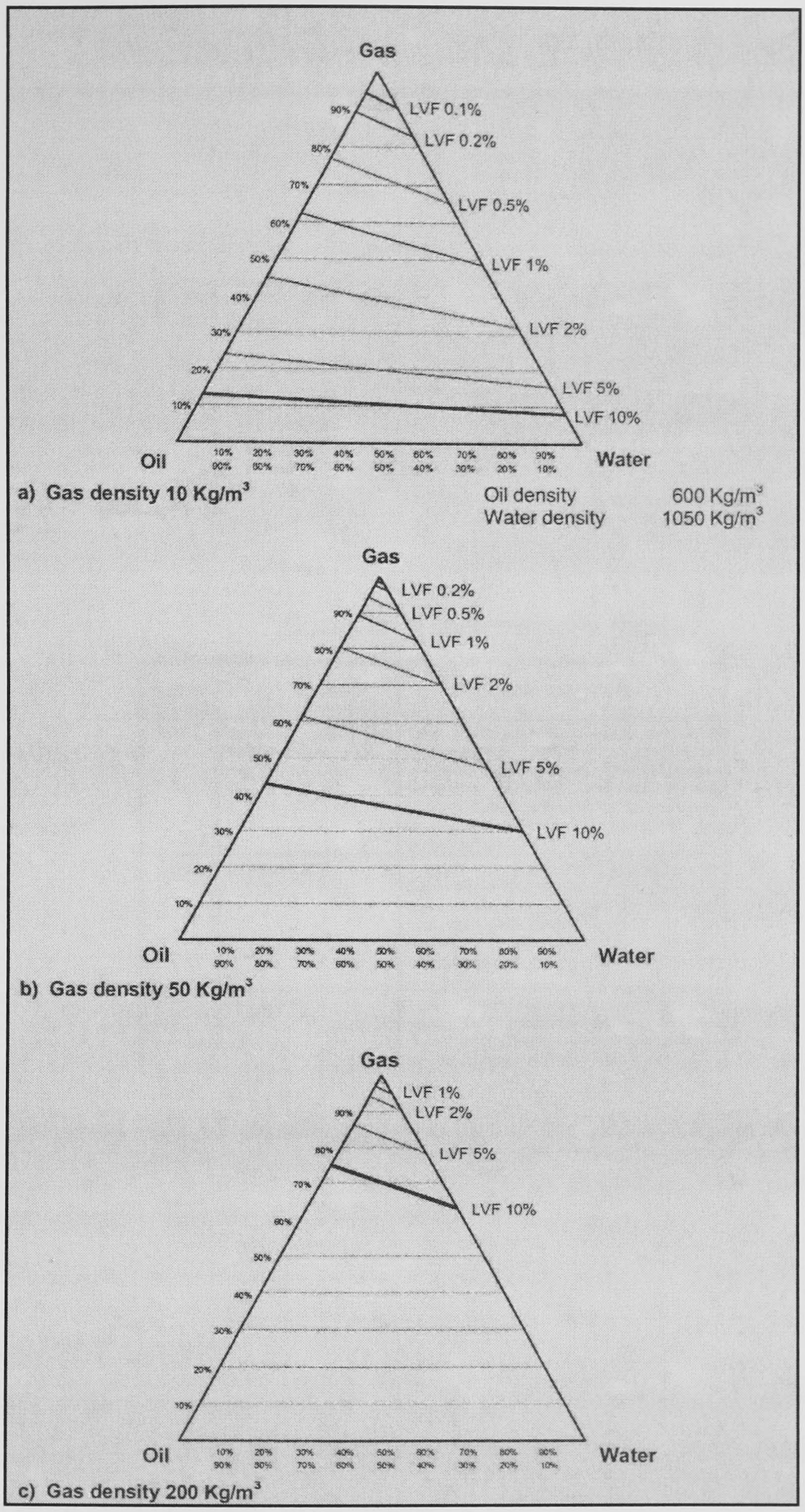
The occurrence of slip between the liquid and the gas, the difficulties in predicting the transition between flow regimes in horizontal as well as in vertical currents, and the uncertainties related to the PVT characterization of gas condensate fields are among the problems still associated with wet gas metering. In addition to the above, the liquid phase of wet gas streams may be a combination of hydrocarbons and water, in which case wet gas metering becomes a problem in three-phases and the oil/water inversion point may have a big impact on the multiphase flow correlations used to calculate pressure drops and boundaries between flow regimes. Finally, solids may also be present in the stream, so that the problem of wet gas metering extends to four phases.

The importance of working in mass fractions rather than volume fractions when characterising wet gas fields has been highlighted in the literature (Couput *et al.*, 2000; Jamieson, 2001). The operator may be interested in metering wet gas streams for a variety of reasons: thus, the main focus may be economics and/or reservoir management, on allocation issues, on metering the produced gas only or on metering both the liquid and the gas. Depending on the specific requirement (or requirements), different metering accuracies may be required and thus different wet gas metering solutions sought. For this reason, multiphase mass fraction triangles have been produced for different fluids densities, showing the possible percentages of gas, oil and water in a wet gas stream (**Fig.3 - 2**). Also, in order to account for the joint effects of flow regime, operating pressure and temperature, and liquid content of the gas, a revised classification for wet gas, based on the Lockhart-Martinelli parameter*, has been recently presented (**Fig.3 - 3**).

From the above brief description of wet gas, it is possible to infer that a unique metering solution for all gas condensate, high GOR and wet gas fields, based on the technologies available to date and able to satisfy every requirement in the wish list of operators, may not exist. Some wet gas meters have already been developed and made commercially available (see Chapter 2) and some manufacturers are extending the range of applicability of their "traditional" MFM's to cover field cases at high GVF's.

---

* The Lockhart-Martinelli parameter X is given as the square root of the ratio of the pressure gradients for the liquid and for the gas phases flowing alone in the pipe.



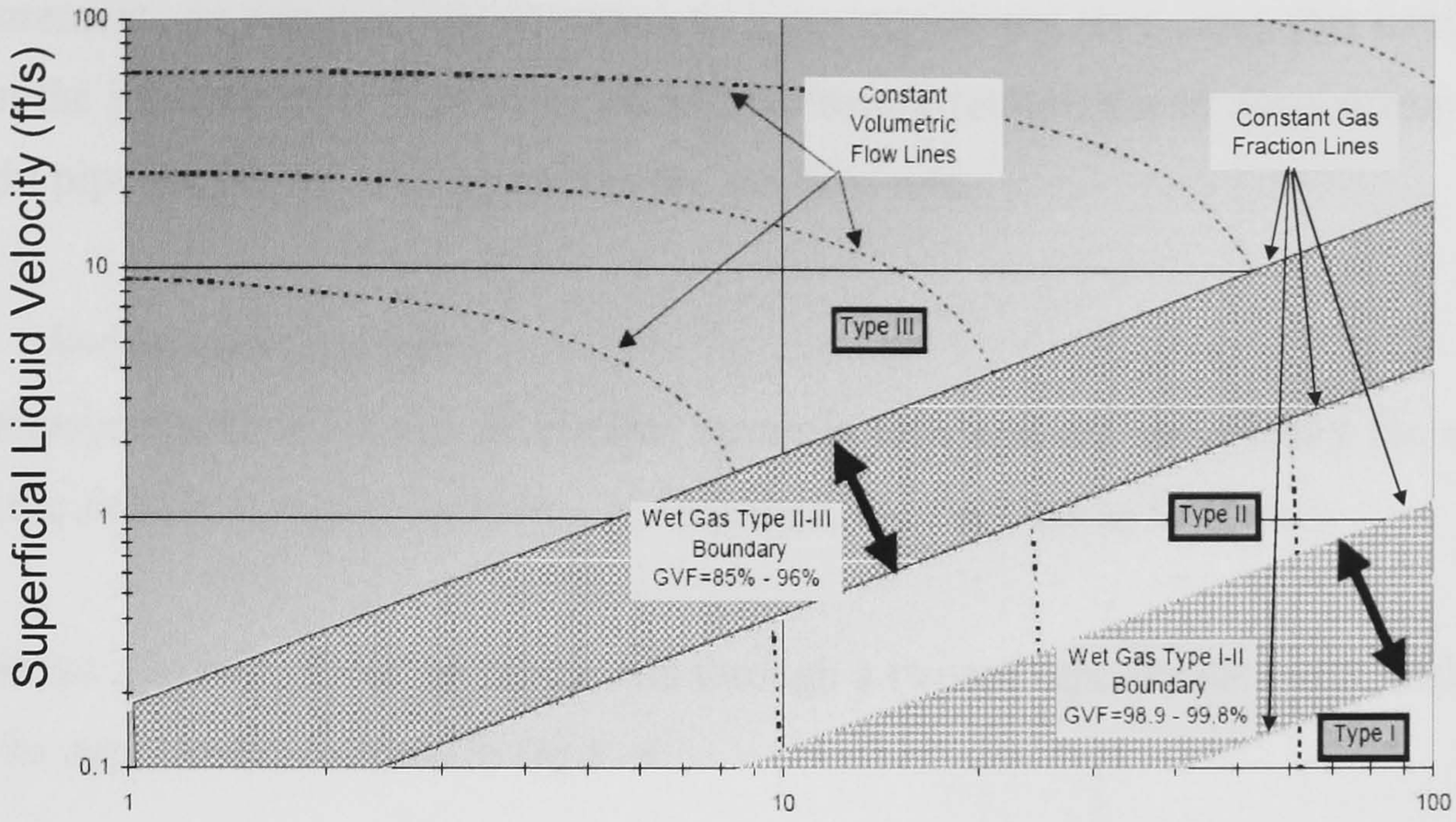
a) Gas density 10 Kg/m^3

Oil density 600 Kg/m^3
Water density 1050 Kg/m^3

b) Gas density 50 Kg/m^3

c) Gas density 200 Kg/m^3

Fig.3 - 2: Multiphase mass fraction triangles showing liquid volume fraction lines at three gas densities (Jamieson, 2001).



Type of Wet Gas	Lockhart-Martinelli Number	Typical Applications
Type 1	Equal or less than 0.025	Type 1 wet gas measurement represents measurement systems at production wellheads, unprocessed gas pipelines, separators, allocation points, and well test facilities. Liquid measurement is necessary to make correction for improved gas measurements.
Type 2	0.025 to 0.30	Type 2 wet gas-metering systems cover higher liquid flow ranges so that the users often require more accurate gas and liquid flow rates. Applications include the flow stream at the production wellhead, commingled flow line, or well test applications.
Type 3	Above 0.30	Type 3 meter must make an oil, gas and water rate determination at relatively high GVF > 80% or X≥0.3. Typical application is gas condensate wells and gas lift wells.

Fig.3 - 3: A proposed map for classifying a wet gas stream, on the basis of superficial velocity for gas and liquid (Mehdizadeh and Marrelli, 2002). Three types of "wet gas" have been defined on the basis of the superficial velocity of gas/liquid, GVF and Lockhart Martinelli parameter (Mehdizadeh and Williamson, 2004).

3.3 The ANUMET system

The ANUMET system was conceived as a follow up from previous work on multiphase flow metering carried out at Imperial College. In particular, several Ph.D. thesis and one DIC thesis (Wolf, 1995; Hawkes, 1996; Machado, 1997; Watson, 1999; Pinheiro, 2000) had already been written on the validation of various methods and instruments for the measurement of key parameters in vertical upward gas-liquid flow.

The concept behind the ANUMET meter is that of deducing the liquid flow rate from measurements on annular flow in a straight pipe section and then using this liquid flow rate in the interpretation of pressure drop data from a venturi placed downstream of the straight pipe section in order to deduce the gas flow rate.

3.3.1 Technical description

The measurements are made in vertical upwards flow and are specifically for annular flow, the dominant regime involved. In sequence, the steps are as follows:

1. The annular flow flows up a tube and through a twisted tape device (with "fish tails" at its upper end) as shown in **Fig.3 - 4**.

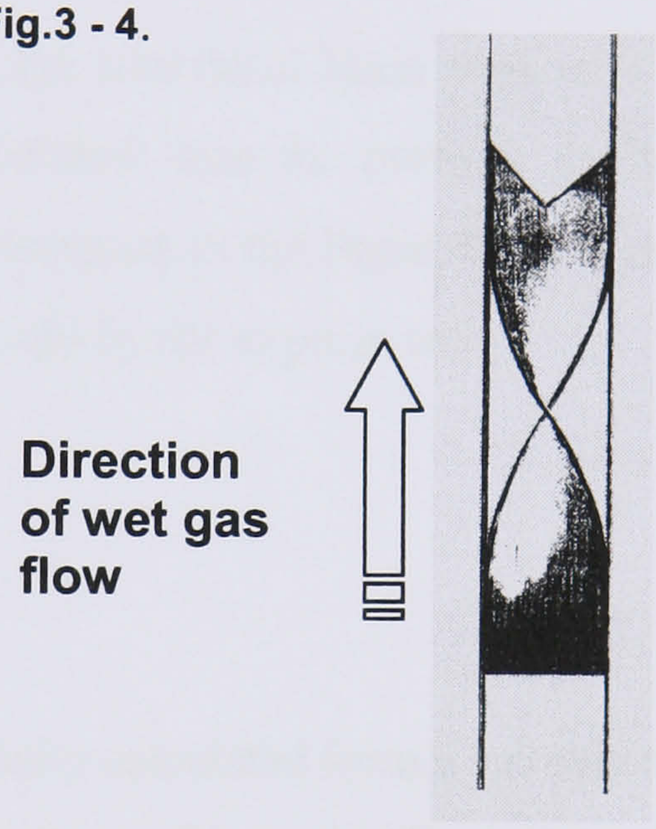


Fig.3 - 4: Twisted tape with "fish tail" end for separation of liquid drops in annular flow.

2. Downstream of the twisted tape device, nearly all the liquid phase has been separated into the annular film on the tube wall. It continues to flow as an annular film in a straight pipe section downstream of the swirl device. Of course, re-entrainment of the droplets will occur but this process is relatively slow (Pinheiro, 2000) and there is an opportunity of making measurements in this region immediately downstream of the swirler in order to determine the liquid flow rate in the film and hence the total liquid flow rate if all the liquid has been separated. The liquid flow rate is determined by measuring the liquid film thickness (δ) and the pressure gradient (dp/dz) along the straight pipe section. The pressure gradient can be measured using standard

transducer systems (taking care to avoid problems of ambiguity of the line fluid) and the film thickness can be measured by a variety of techniques. In the validation tests at Imperial College, gamma densitometry and conductance probes were used to measure the film thickness, but viable alternatives might be ultrasonic or fluorescence, depending on the system. The liquid film flow rate M_{LF} is obtained from the "triangular relationship" (see Section 1.3.7) which has the form (Hewitt and Hall-Taylor, 1970; Hewitt, 1982]:

$$\dot{M}_{LF} = fn[\delta, (dp/dz)] \qquad \textbf{Eq.3 - 1}$$

Basically, in this relationship, the interfacial shear stress and wall shear stress (often approximately equal) are calculated from the pressure gradient and the local shear stress τ (often approximately constant in the liquid film) is related to the gradient of liquid velocity in the film (du_L/dy) by the expression:

$$\tau = \mu_{eff}\left(\frac{du_L}{dy}\right) \qquad \textbf{Eq.3 - 2}$$

where μ_{eff} is the effective viscosity calculated from a suitable turbulence model. **Eq.3 - 2** is integrated to give the velocity profile in the film, which, in turn, is integrated to give the total liquid flow rate. Early experiments at Harwell (Gill *et al.,* 1964), in which all three quantities ($\dot{M}_{LF}, \delta$ and (dp/dz)) were measured, showed that the triangular relationship fitted the data remarkably well. Thus, the film flow rate can be determined from measurements of film thickness and pressure gradient. The comparisons obtained by Gill *et al.* are shown in **Fig.3 - 5**, expressed in terms of a non-dimensional film flow rate W^+, which is defined as follows:

$$W^+ = \frac{\dot{M}_{LF}}{\pi D \eta_L} \qquad \textbf{Eq.3 - 3}$$

where D is the tube diameter and η_L the liquid viscosity. An assumption of the method is that ($\dot{M}_{LF} \approx \dot{M}_L$).

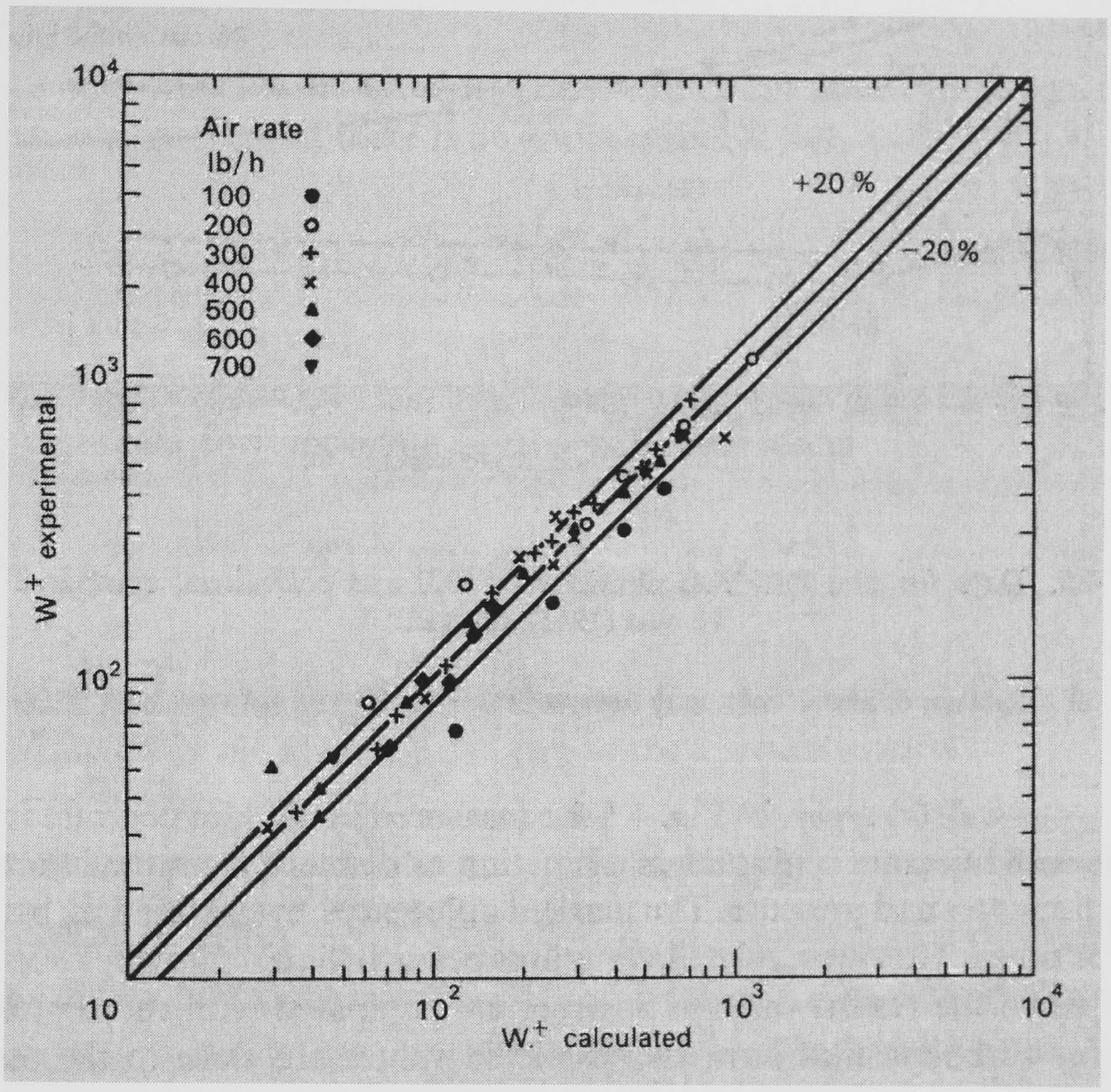


Fig.3 - 5: Comparison between experimental and calculated (from the "triangular relationship") dimensionless film flow rates (Gill *et al.* 1964).

Measurements by Hills *et al*. (1996) indicated very efficient removal of the droplets by the device shown in **Fig.3 - 4**, with less than 5% of the liquid remaining as droplets after the device. Measurements at Imperial College (Pinheiro, 2000) confirmed that good separation was possible under some circumstances, though the separation was less favourable at higher gas velocities as illustrated in **Fig.3 - 6**. The development of improved separation devices could be an area for further development. Nevertheless, there are significant regions in which the separation is better than 90%.

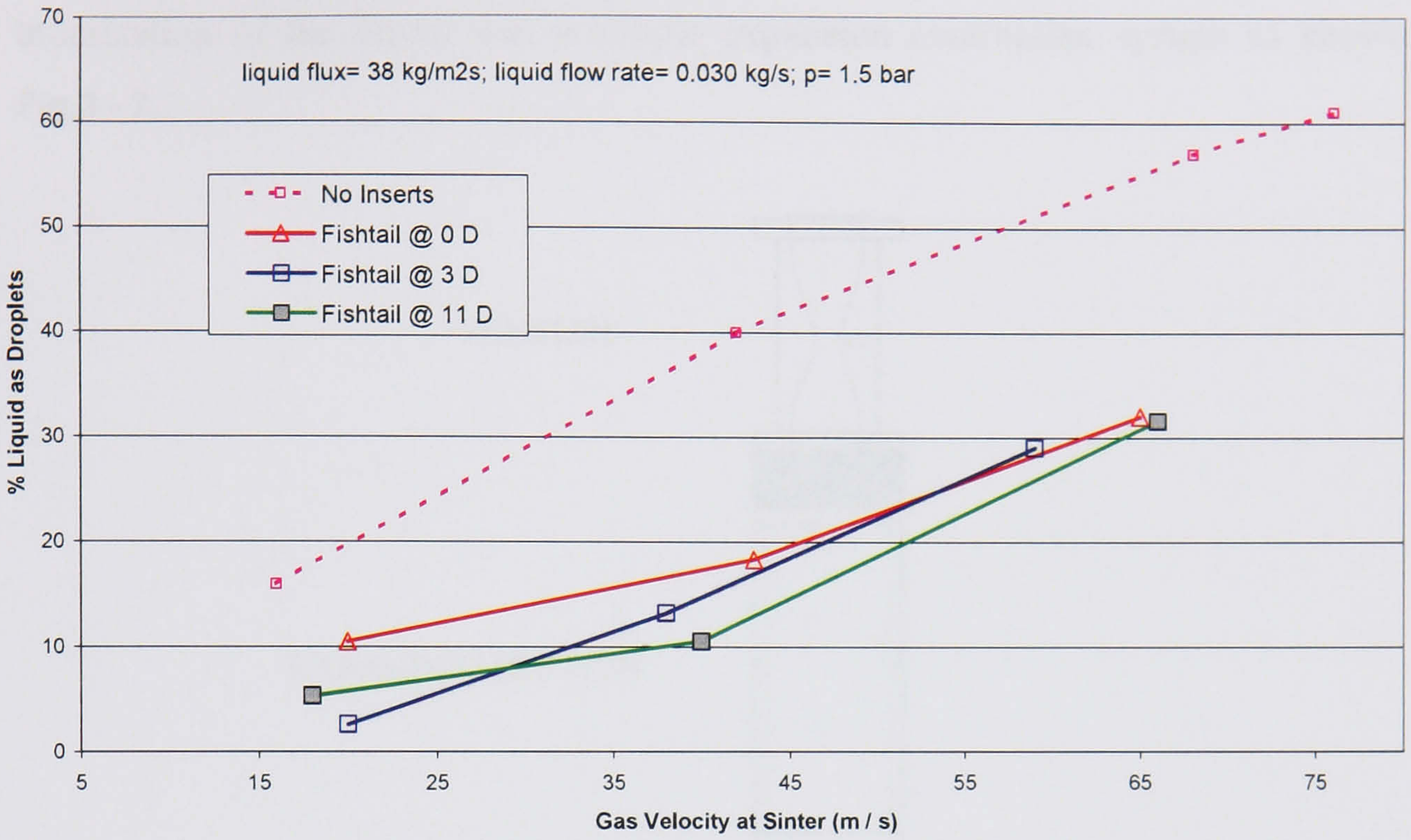


Fig.3 - 6: Droplet separation by a "fish-tail" twisted tape device (Pinheiro, 2000).

3. Following the straight pipe section in which the film thickness and pressure gradient are measured, (leading to an evaluation of $\dot{M}_L$), the next step is to re-entrain all of the droplets into the gas stream before passing this stream into a venturi (step 4.). The objective is to homogenise the gas and the liquid. Experiments carried out during the development of the MIXMETER flow meter, with parallel development of the mixing devices, led to a device which gave satisfactory homogenisation of the flow over a gas volume flow fraction range of 0-90%. For higher gas fractions, it is not possible to maintain such mixing and a large fraction of the liquid phase flows on the surface of the mixer and on the channel wall downstream of the mixer. This fact was demonstrated in experiments carried out at Imperial College by Machado (1997), which indicated that, with the MIXMETER mixer, the in-situ liquid fraction downstream of the mixer was very much larger than the purely mixed value for liquid volume fractions less than around 5-10%. This led to a search for mixing devices, which can more satisfactorily homogenise the flow in this low liquid fraction, high

gas fraction region. This work was continued by Pinheiro (2000). A wide range of homogenising devices was studied and it was found that the device that gave the best atomisation of the liquid was a simple expansion contraction system as shown in **Fig.3 - 7**.

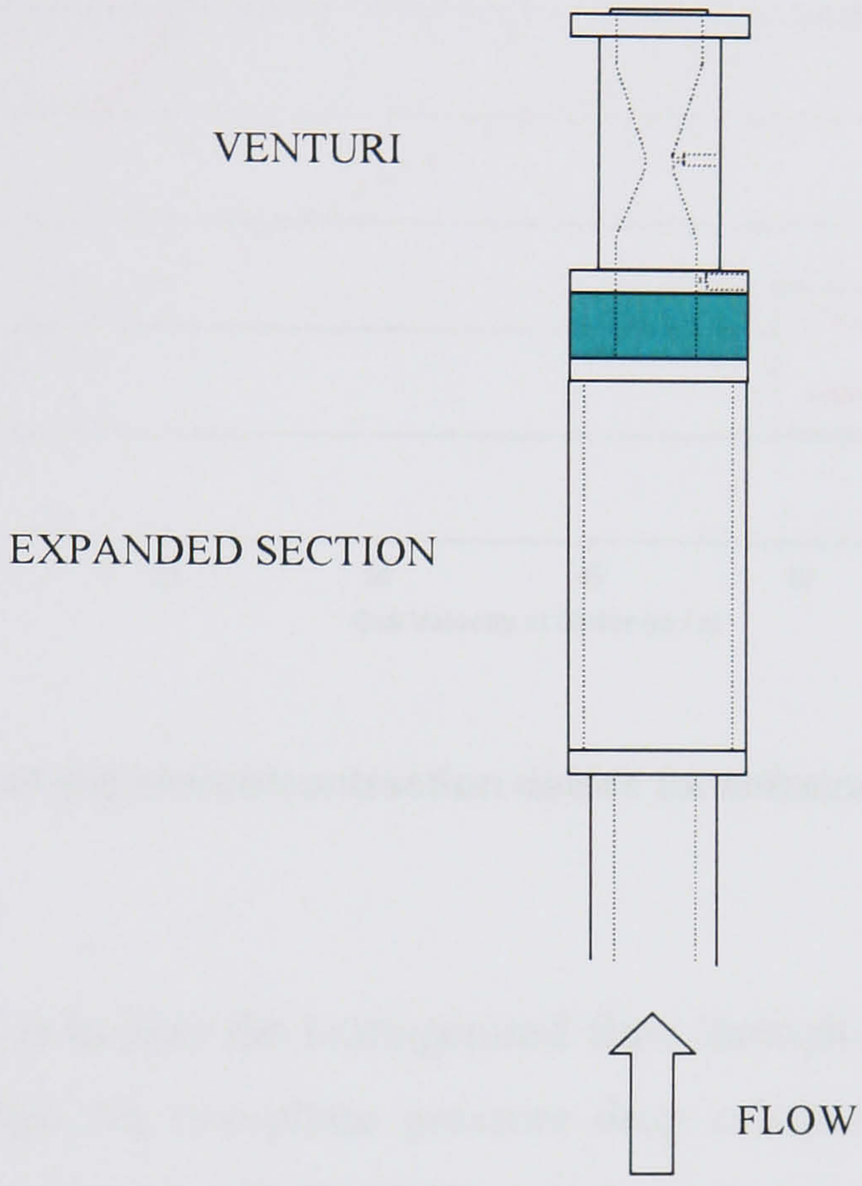


Fig.3 - 7: Expansion / contraction device.

Measurements of liquid film flow rates downstream of this device indicated a large increase in the fraction entrained compared to measurements in the absence of the device as illustrated in **Fig.3 - 8**. Although the device does not give complete entrainment, it certainly increases the entrained fraction to over 70% over a wide range of gas velocities as seen.

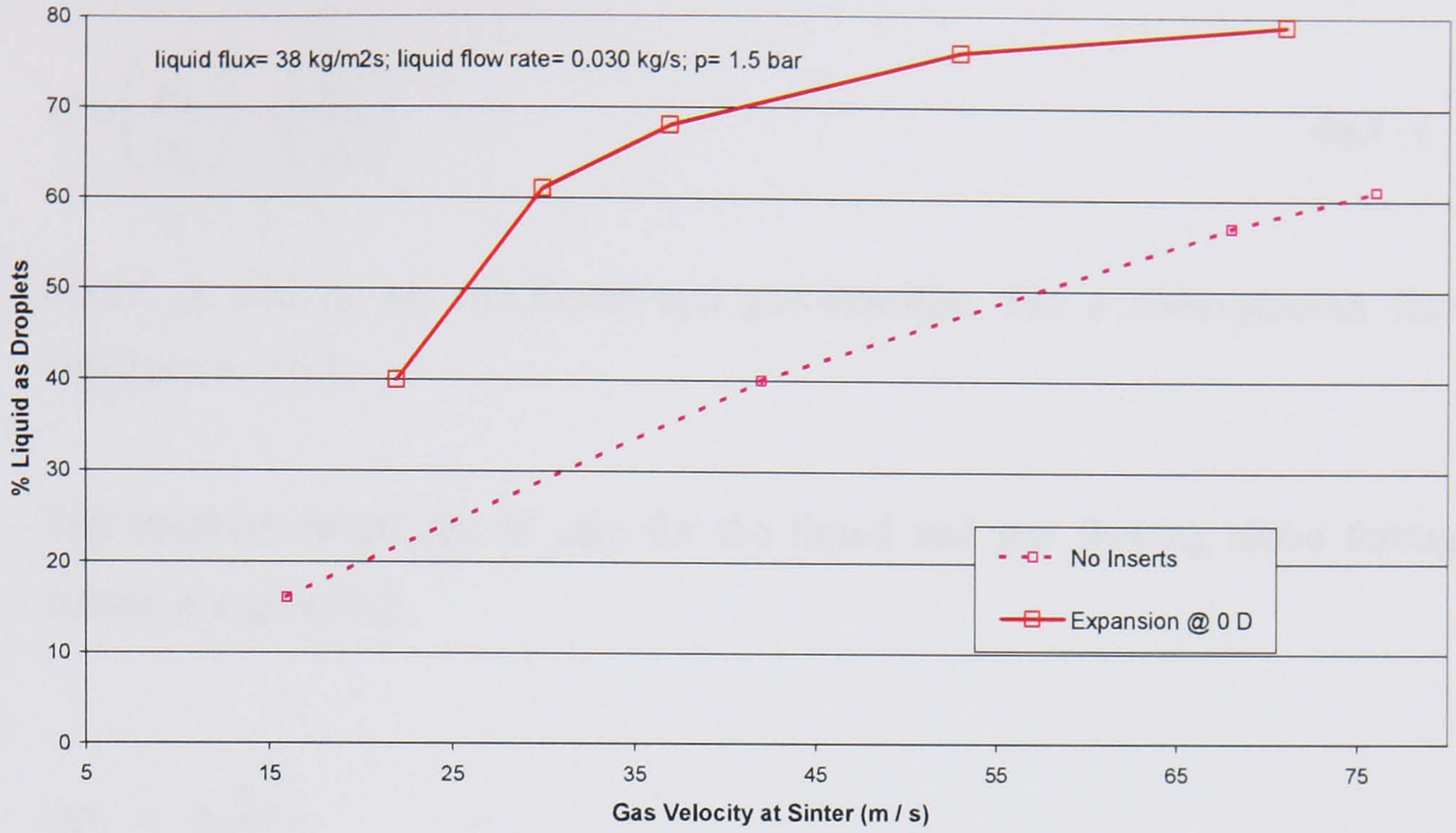


Fig.3 - 8: Effect of expansion/contraction device on entrained fraction (Pinheiro, 2000).

4. The final stage is to pass the homogenised flow through a venturi. The most widely used relationships for two-phase pressure drop calculations in venturi meters are perhaps those of Chisolm (DTI, 2003), which relate the two-phase pressure drop Δp to the pressure drops Δp_L or Δp_G for the liquid and gas phase respectively flowing alone through the device. These relationships can be written as:

$$\frac{\Delta p}{\Delta p_L} = 1 + \frac{C}{X} + \frac{1}{X^2}$$

$$\frac{\Delta p}{\Delta p_G} = 1 + CX + X^2$$

Eq.3 - 4

where X is the Lockhart-Martinelli parameter defined as follows:

$$X = \sqrt{\frac{\Delta p_L}{\Delta p_G}}$$

Eq.3 - 5

A widely-used relationship for C is as follows:

$$C = \left(\frac{\rho_L}{\rho_G}\right)^n + \left(\frac{\rho_G}{\rho_L}\right)^n \qquad \textbf{Eq.3 - 6}$$

where ρ_L and ρ_G are the liquid and gas densities. For a homogeneous flow, the exponent n is 0.5.

The pressure drops Δp_L or Δp_G for the liquid and gas flowing alone through the venturi are given by:

$$\Delta p_L = -k\frac{\dot{m}_L^2}{2\rho_L}$$

$$\Delta p_G = -k\frac{\dot{m}_G^2}{2\rho_G} \qquad \textbf{Eq.3 - 7}$$

where m_L and m_G are the liquid and the gas mass fluxes respectively.

The venturi loss coefficient k is given by:

$$k = \frac{1-\left(\frac{D_2}{D_1}\right)^4}{C_D{}^2\left(\frac{D_2}{D_1}\right)^4} \qquad \textbf{Eq.3 - 8}$$

where C_D is the discharge coefficient (usually taken as 0.984 for a venturi with flow at high Reynolds numbers) and D_2 and D_1 are the throat diameter and the upstream diameter respectively.

Combining equations **Eq.3 - 5** and **Eq.3 - 7** leads to the following expression for the Lockhart-Martinelli parameter:

$$X = \frac{\dot{m}_L}{\dot{m}_G}\left(\frac{\rho_G}{\rho_L}\right)^{\frac{1}{2}} \qquad \textbf{Eq.3 - 9}$$

Combining the above equations leads to a quadratic expression for the gas flow rate as follows:

$$a\dot{m}_G^2 + b\dot{m}_G + c = 0 \qquad \textbf{Eq.3 - 10}$$

where:

$$a = 1$$

$$b = C\dot{m}_L\sqrt{\frac{\rho_G}{\rho_L}} \qquad \textbf{Eq.3 - 11}$$

$$c = \left(1 + \frac{2\rho_L \Delta p}{k\dot{m}_L^2}\right)\frac{\rho_G}{\rho_L}\dot{m}_L^2$$

Of course, **Eq.3 - 10** is a quadratic equation, which has two solutions for $\dot{m}_G$. However, one of the solutions is usually negative and therefore unphysical.

For n=0.5, the Chisolm equation above [**Eq. 3 – 4**] gives the same results as the general equation for a homogeneous two-phase gas-liquid flow written as:

$$\Delta p = -k\frac{(\dot{m}_L + \dot{m}_G)^2}{2\rho_H} \qquad \textbf{Eq.3 - 12}$$

where ρ_H is the mixture density given by, in terms of quality x:

$$\rho_H = \frac{\rho_L \rho_G}{(1-x)\rho_G + x\rho_L} \qquad \textbf{Eq.3 - 13}$$

Pinheiro da Silva Filho (2000) studied the performance of the expansion/contraction device placed upstream of a venturi and his results are illustrated in **Fig.3 - 9** where the ratio of the measured pressure drop to that calculated from the homogeneous theory is shown as a function of mass flow quality (fraction by mass of the gas phase in the total flow) for a constant total mass flow. As will be seen, this form of homogenisation device does, indeed, lead to a much closer agreement with the homogeneous model than that obtained in the absence of the device ("No inserts").

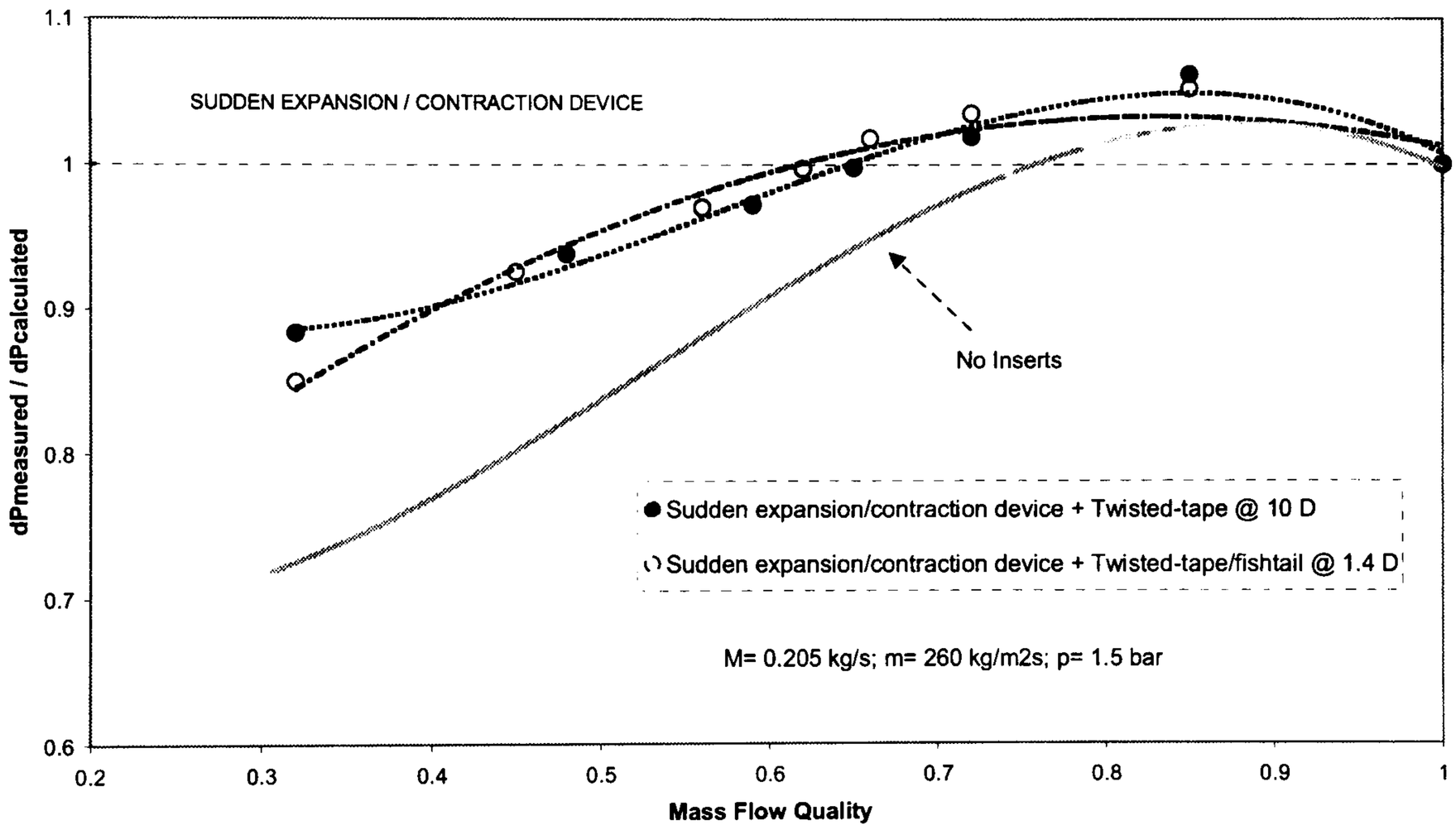


Fig.3 - 9: Comparison of venturi pressure drop measured with venturi downstream of expansion/contraction device with that calculated from the homogeneous model (Pinheiro, 2000).

Fig.3 – 10 below summarises the ANUMET metering strategy as explained above.

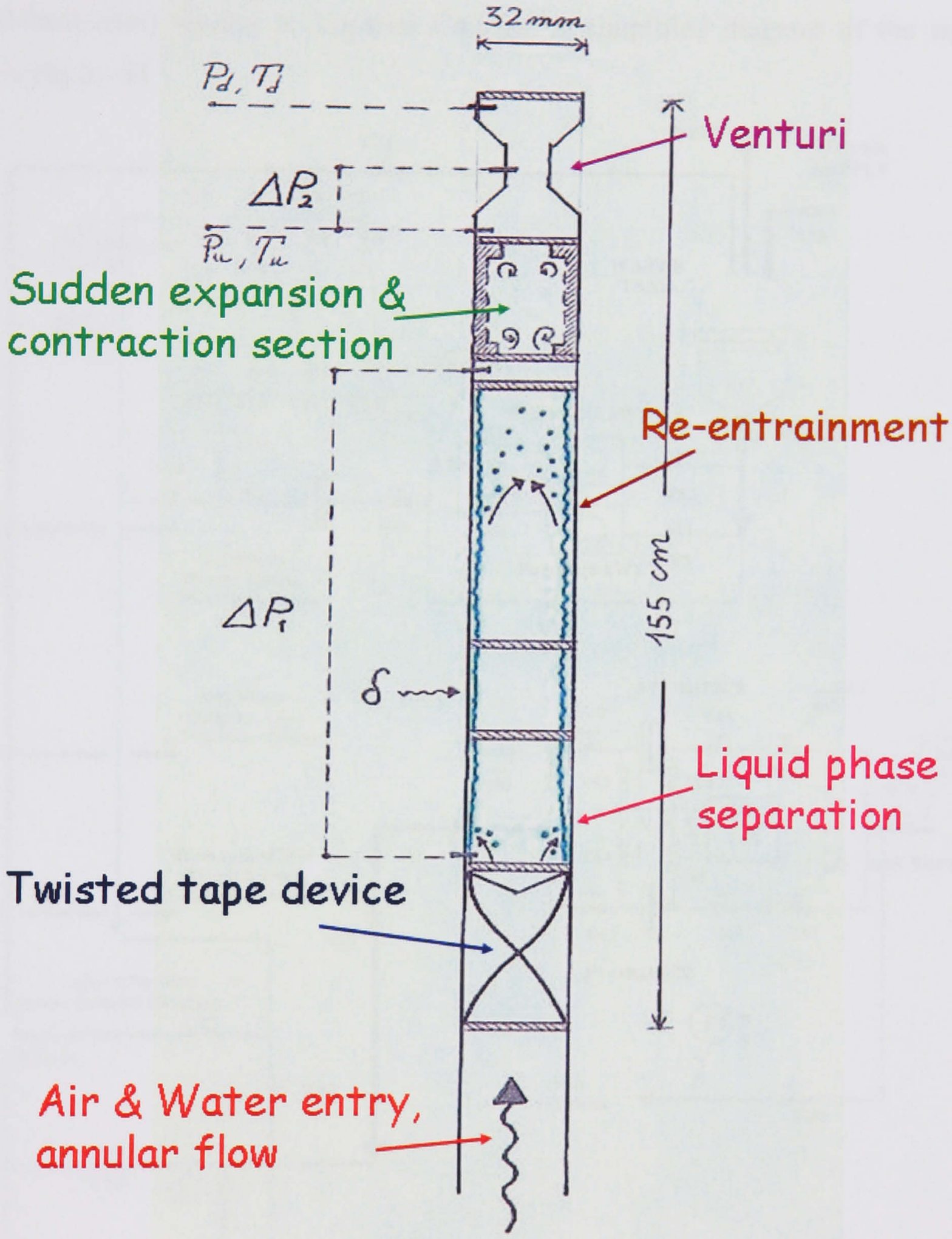


Fig.3 - 10: ANUMET metering concept.

3.4 Experimental equipment and test procedure

3.4.1 The LOTUS rig

The experiments described in this paper were carried out in the LOTUS (LongTUbeSystem) facility at Imperial College. A simplified diagram of the rig is shown in **Fig.3 – 11**.

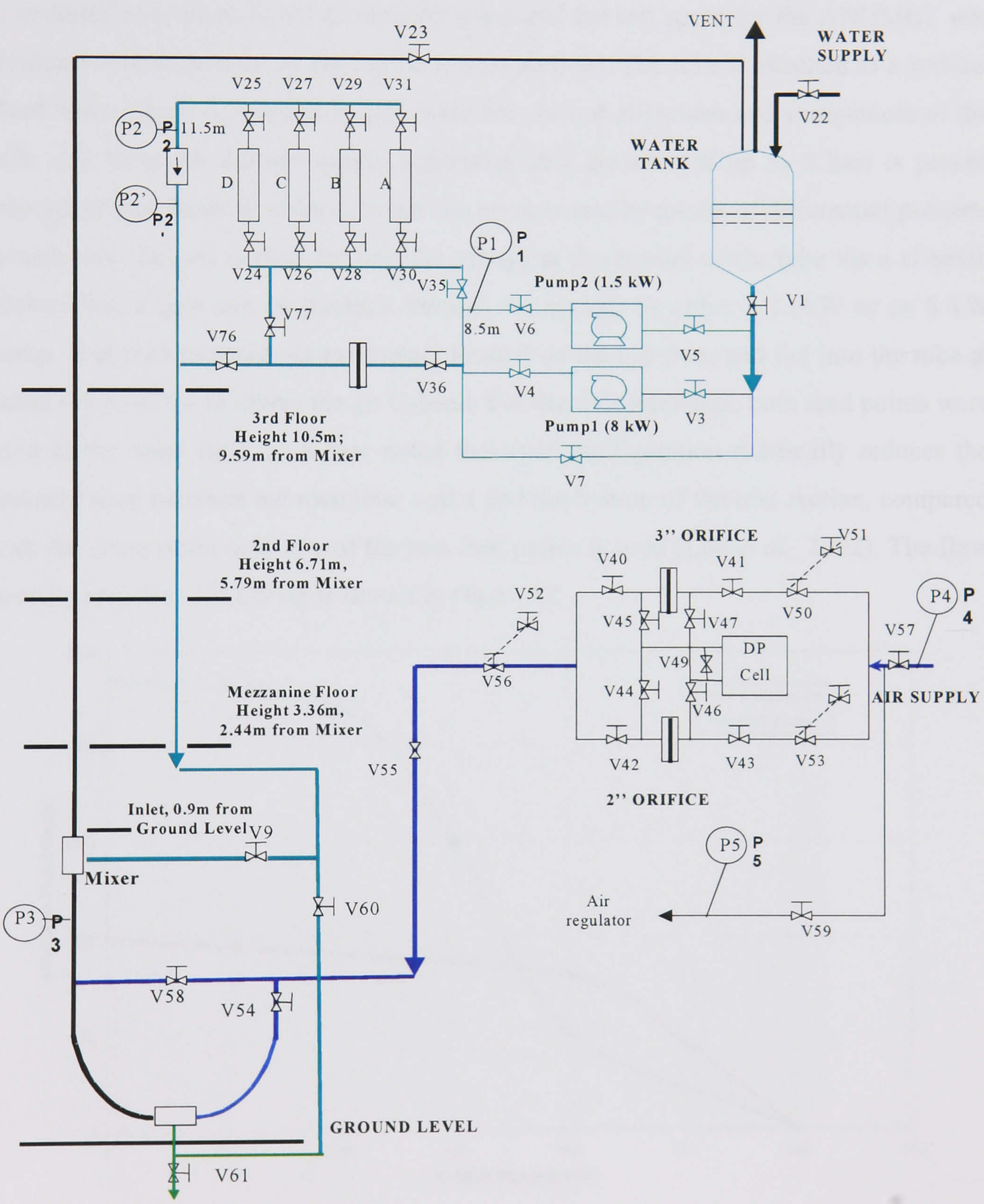


Fig.3 - 11: The LOTUS rig.

LOTUS is a vertical two-phase air-water system that was originally built at the Harwell Laboratory of the UKAEA in the early nineteen-sixties. It was relocated to the pilot plant area of the Chemical Engineering Department of Imperial College in 1992. It consists of a long vertical, 31.8mm (1.25 inch) copper tube, originally of around 19m active length at Harwell but now with a shorter active length of 10.8m. The vertical tube is mounted over three floors of the pilot plant and the test spool for the ANUMET was arranged almost entirely on the top floor (test section). The tube is attached to a vertical fixed beam, carefully aligned to guarantee the vertical alignment and straightness of the tube. Air from the college supply (operating at a pressure of up to 6 bar) is passed through orifice plates in order to meter the air flow rate by means of differential pressure transducers. The air is then fed into the system at the bottom of the tube via a U-bend. Water from a tank can be pumped through the system by either a 1.5kW or an 8 kW pump. It is then metered via rotameters located on the top floor and fed into the tube at either 0.9 m or 5.4 m above the air U-bend. For these experiments, both feed points were used at the same time, as it was noted that such configuration drastically reduces the pressure drop between the rotameter outlet and the bottom of the text section, compared with the cases when only one of the two feed points is used (Lao *et al.*, 2002). The flow envelope for the LOTUS rig is shown in **Fig.3 – 12**.

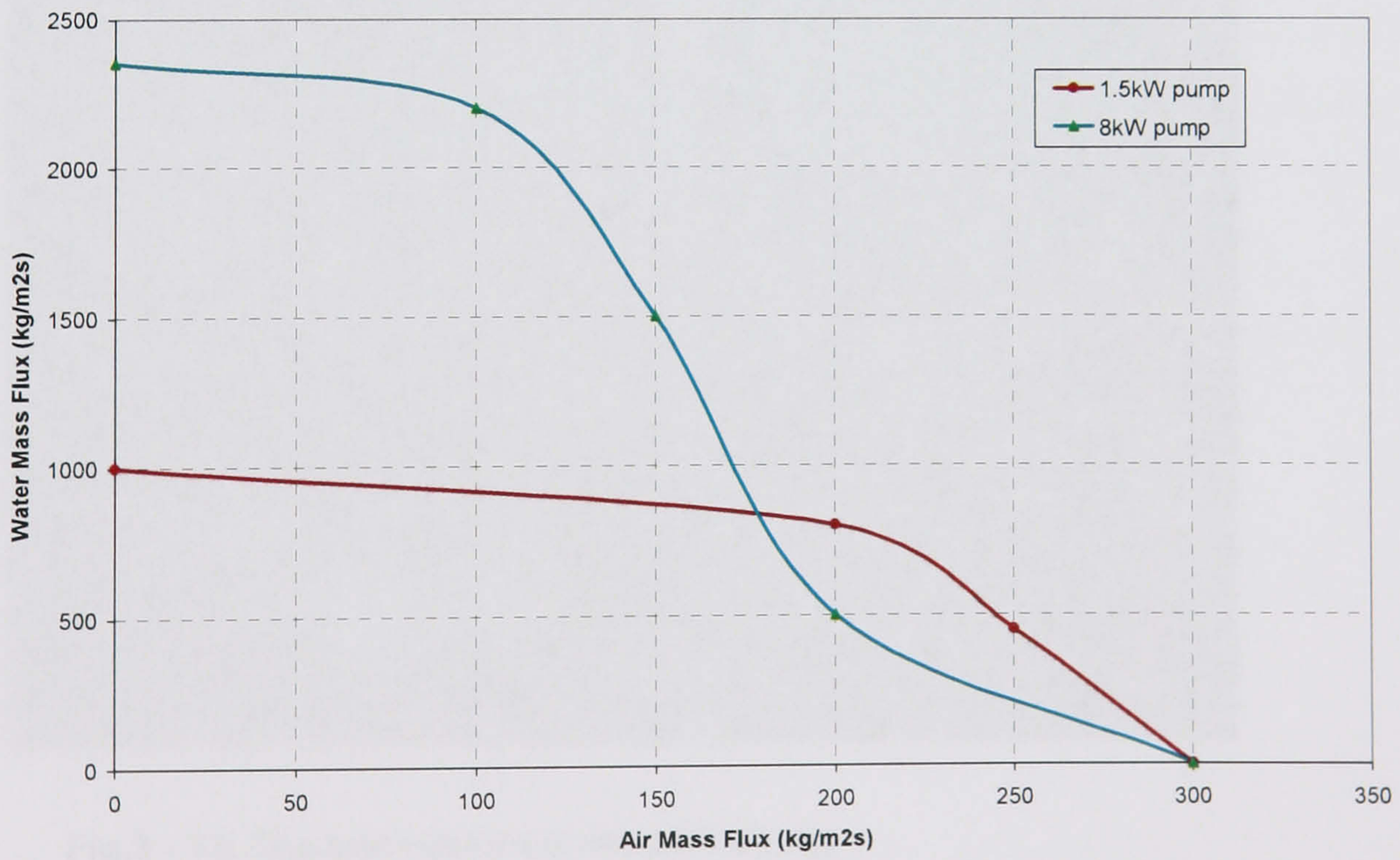


Fig.3 - 12: Flow envelope for the LOTUS rig.

3.4.2 The experimental set up

A picture of the test section as built on the third floor of the LOTUS rig is showed in **Fig.3 – 13**.

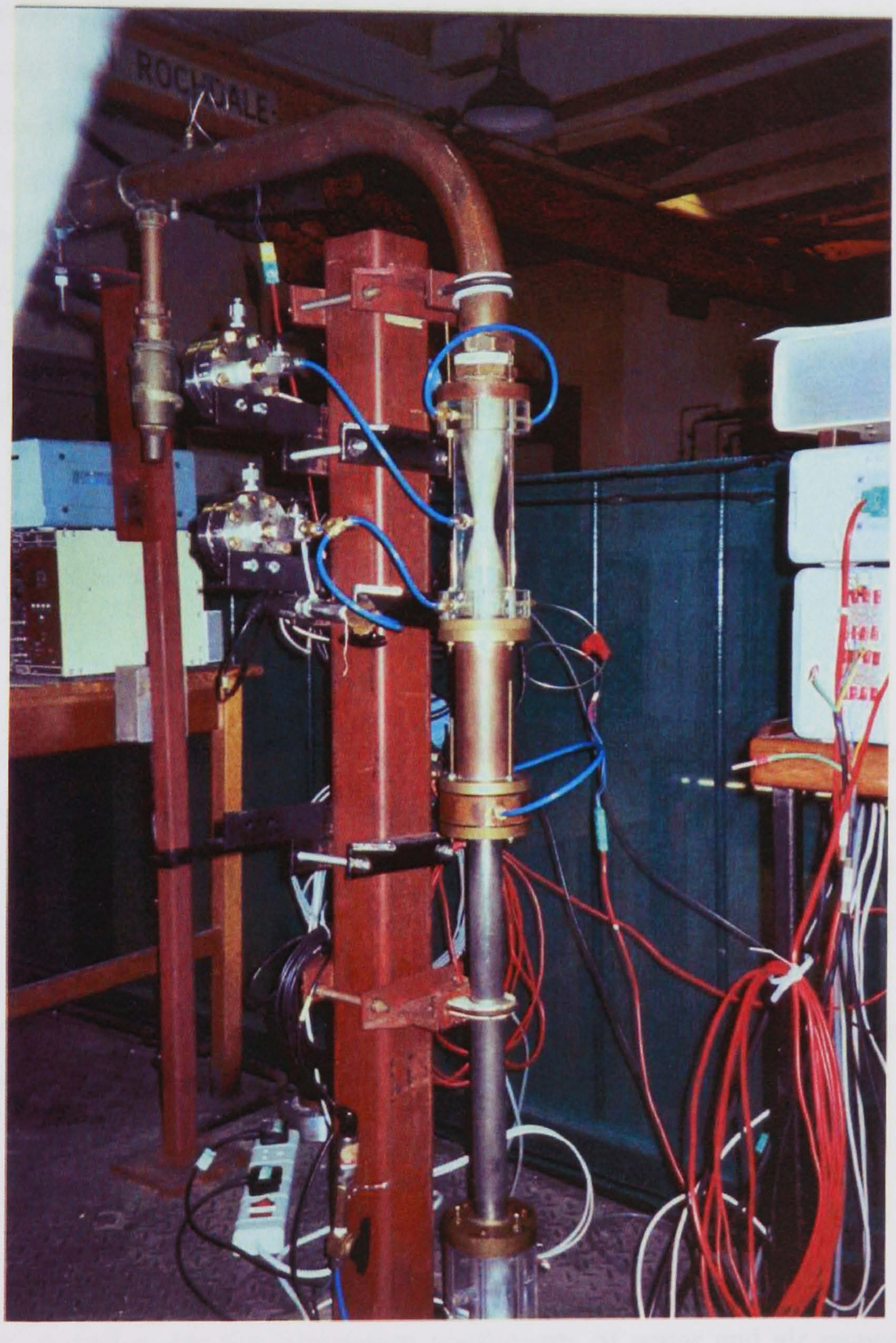


Fig.3 - 13: The test section in the LOTUS rig.

Calculation of the liquid mass flux. The location for the liquid-film thickness measurements was chosen on the basis of the results previously obtained by Pinheiro da Silva Filho (2000) and summarised in **Fig.3 – 6**. Although the point of minimum entrained fraction (i.e. the point that corresponds to the peak of the film thickness) increases with increasing air flow rate and decreases with increasing water flow rate, an optimal location was considered to be that at approximately ten diameters downstream the outlet of the swirler.

For the majority of the experiments described here, the film thickness was measured using a 45milliCurie Americium 241 gamma source with a scintillation crystal detection system linked via an amplifier to a computer counting system reading the radiation count at frequencies set by the user. The 59.5 keV energy window was chosen for these experiments. The film thickness was calculated as follows:

$$\delta = \frac{D}{2} \frac{\ln \frac{I}{I_a}}{\ln \frac{I_w}{I_a}} \qquad \textbf{Eq.3 - 14}$$

where D is the internal diameter of the pipe, I_a and I_w are the intensities of the transmitted photons when the pipe is filled with air and water respectively, and I is the intensity of the transmitted photons with the two-phase air-water stream flowing in the pipe. It must be noted that the ratio between the calibration values of air and water is very important because it affects the ability of the photons to 'see' the difference between a pipe full of air and a pipe full of water (Mareuge, 2000). This ratio can be written as:

$$\frac{I_a}{I_w} = e^{(\gamma_w - \gamma_a)D} \qquad \textbf{Eq.3 - 15}$$

where γ_w and γ_a are the attenuation coefficients of water and air respectively. For the 59.5 keV energy and for the water and air densities encountered during the experiments presented here, the ratio between the calibration values of air and water was about 1.9.

Two sets of experiments were carried out with conductance probes in place of the gamma densitometry system. The geometry of the probes used for these experiments and the calibration procedure carried out with the Americium 241 source are described by Lao (2003). As a result of the calibration, the liquid-film thickness was expressed as a function of the normalized output voltage, V^*, given by:

$$V^* = \frac{(V - V_0)}{(V_s - V_0)}, \qquad \textbf{Eq.3 - 16}$$

where V is the output voltage measured during the two-phase experiments, V_s is the output voltage when the pipe is filled with water and V_0 is the output voltage when the pipe is filled with air.

The pressure drop to be used, together with the liquid-film thickness, in the triangular relationship described in **Eq.3 - 1** was measured over a straight length of 77 cm, from the outlet of the swirler to the inlet of the expansion contraction device.

Calculation of the gas mass flux. A venturi meter, 20 cm long and with a throat-to-upstream diameter ratio (β) of 0.493, was placed immediately downstream of the expansion contraction section. A differential pressure transducer was used to measure the pressure drop between the inlet and the throat of the venturi, while two absolute pressure transducers were used to measure the inlet and outlet pressure. The inlet and outlet temperatures were also recorded. The inlet pressure and inlet temperature were used to calculate the inlet fluid properties, while the outlet pressure was measured to allow the investigation of the relationship between the total pressure loss across the venturi and the liquid fraction (these data have not been analysed in the present project).

Test matrix. The water mass flux was varied between 103 and 770 kg/m^2 s, and for each water mass flux the air mass flux was varied between approximately 30 and 200 kg/m^2 s. This corresponded to gas volume fractions between 96 and 99.7% (calculated with the assumption of homogeneous flow).

A check was made to confirm that the flow was in annular regime and not in churn regime (flow reversal of the falling film). The annular regime is likely to exist if (Hewitt and Wallis, 1963):

$$U_G^* = U_G \sqrt{\frac{\rho_G}{gD(\rho_L - \rho_G)}} \succ 1 \qquad \textbf{Eq.3 - 17}$$

where U_G is the gas superficial velocity. All of the current tests lay in the region $U_G^* > 1$. At very low liquid film flow rate ($\dot{m}_{LF}$), liquid entrainment does not occur. Of course, there would be no need to use a swirl device to move liquid back into the film in this case. The value of film flow rate ($\dot{m}_{LFC}$) at which entrainment starts is given by (Govan *et al.*, 1988):

$$\dot{m}_{LF} \leq \dot{m}_{LFC} \longrightarrow E = 0$$

$$\dot{m}_{LFC} = \frac{\eta_L}{D} \exp(5.8504 + 0.4249 \frac{\eta_G}{\eta_L} \sqrt{\frac{\rho_L}{\rho_G}}) \qquad \textbf{Eq.3 - 18}$$

where η_L and η_G are the liquid and gas viscosities and E stands for entrainment. For all of the tests reported here, the flows were such that significant entrainment upstream of the swirl device would be expected.

3.5 Results

The results presented here were obtained from six experimental campaigns. The data collected during the experiments are presented in Appendix I. A reasonable number of experimental points were collected and a critical review of the results is presented below, in an attempt to differentiate between the effects due to limitations of the instrumentation available in the LOTUS rig, the effects due to the main assumptions behind the ANUMET concept and also the intrinsic difficulties associated with wet gas metering.

Liquid mass flux. The liquid mass fluxes calculated from the film thickness and pressure gradient in the straight pipe section are compared with the rig input values in **Fig.3 – 14**. **Fig.3 – 15** shows the relative error of liquid mass flux.

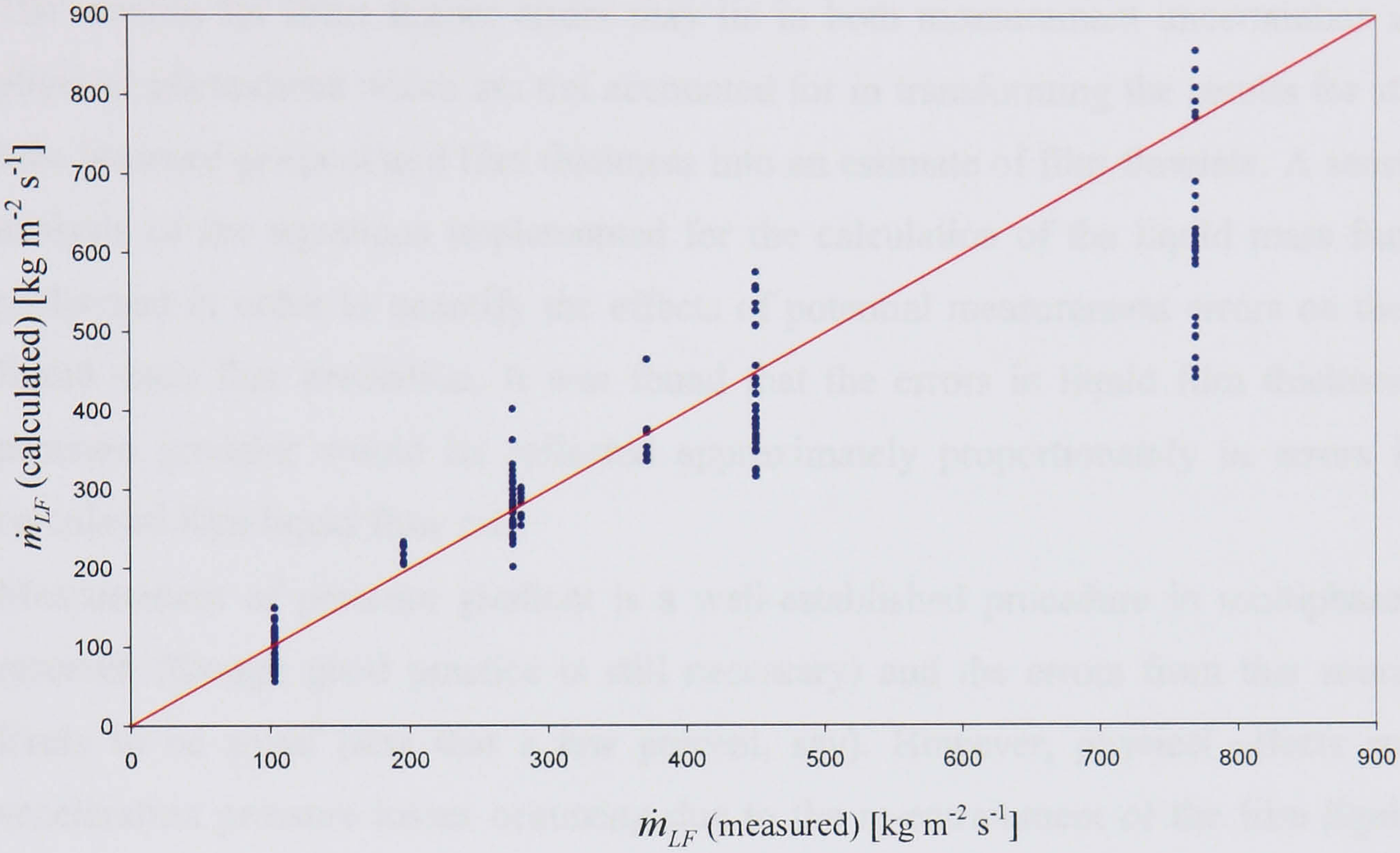


Fig.3 - 14: Calculated vs. measured liquid mass flux.

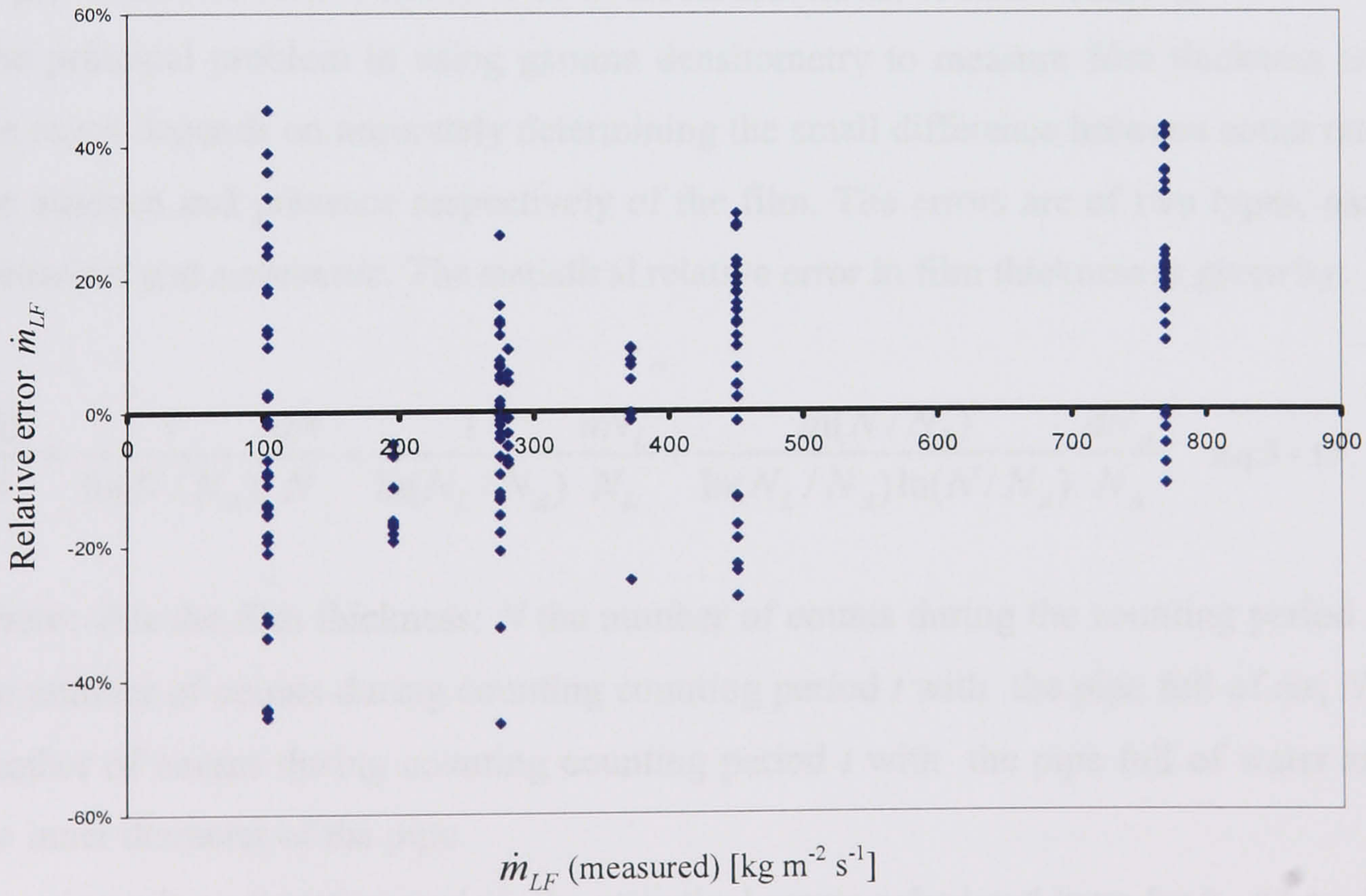


Fig.3 - 15: Relative error of liquid mass flux (Measured-Calculated)/Measured.

Though the results are qualitatively encouraging, it has to be recognised that the accuracy in liquid flow estimation is significantly worse than the $\pm 20\%$ expected from the early results on the triangular relationship illustrated in **Fig.3 – 5.**

The reasons for these higher errors may lie in both measurement uncertainties and in physical phenomena which are not accounted for in transforming the results for straight tube pressure gradient and film thickness into an estimate of film flowrate. A sensitivity analysis of the equations implemented for the calculation of the liquid mass flux was performed in order to quantify the effects of potential measurement errors on the final liquid mass flux prediction. It was found that the errors in liquid film thickness and pressure gradient would be reflected approximately proportionately in errors in the calculated film liquid flow rate.

Measurement of pressure gradient is a well-established procedure in multiphase flow research (though good practice is still necessary) and the errors from this source are likely to be small (less that a few percent, say). However, physical effects such as acceleration pressure losses occurring due to the re-entrainment of the film liquid and residual effects of the swirl may occur and need to be further quantified. However, the largest source of error is likely to be in the measurement of film thickness.

The principal problem in using gamma densitometry to measure film thickness is that the result depends on accurately determining the small difference between count rates in the absence and presence respectively of the film. The errors are of two types, namely *statistical* and *systematic*. The statistical relative error in film thickness is given by:

$$\frac{d\delta}{\delta} = \frac{1}{\ln(N/N_A)}\frac{dN}{N} - \frac{1}{\ln(N_L/N_A)}\frac{dN_L}{N_L} + \frac{\ln(N/N_L)}{\ln(N_L/N_A)\ln(N/N_A)}\frac{dN_A}{N_A} \qquad \textbf{Eq.3 - 19}$$

where: δ is the film thickness; N the number of counts during the counting period t ,N_A the number of counts during counting counting period t with the pipe full of air, N_L the number of counts during counting counting period t with the pipe full of water and D the inner diameter of the pipe.

By using a long counting period, the statistical errors calculated from **Eq.3 - 19** could be reduced to a few percent. However, a more serious source of error was the systematic

effects of drift in the basic count rate due to time variations in the electronics and investigations revealed that these errors could be the cause of the errors revealed in **Fig.3 – 14** and **Fig.3 – 15**. This is clearly an area in which further development is required. Improvements in the stability of the electronics, in calibration and in optimisation of the choice of radioactive source would be expected to yield the required precision. Thus, there is no reason to believe that adequate accuracy could not be achieved in a developed system.

Gas mass flux. Gas mass fluxes were calculated from the input liquid flow rate and the measured upstream-to-throat pressure drop in the venturi using the methodology described above. The results were corrected for compressibility effects using the standard compressibility factor given by EN ISO 5167-1:1995. The values calculated with and without correction for compressibility effects are compared with the input values in **Fig.3 – 16** and **Fig.3 – 17**, respectively. The agreement between measured and calculated values, as shown in **Fig.3 – 16**, is rather encouraging.

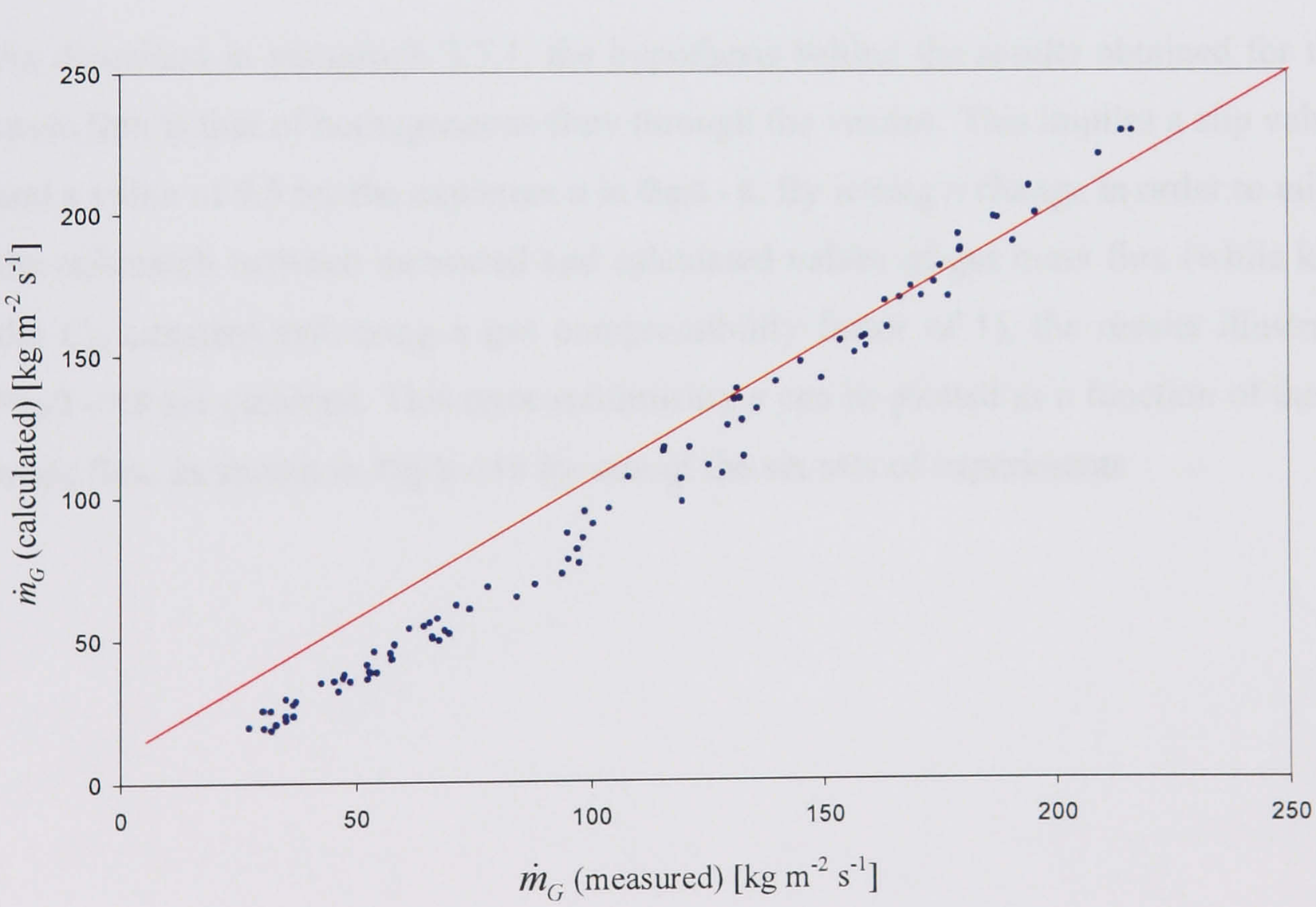


Fig.3 - 16: Calculated vs. measured gas mass flux (with correction for compressibility effects).

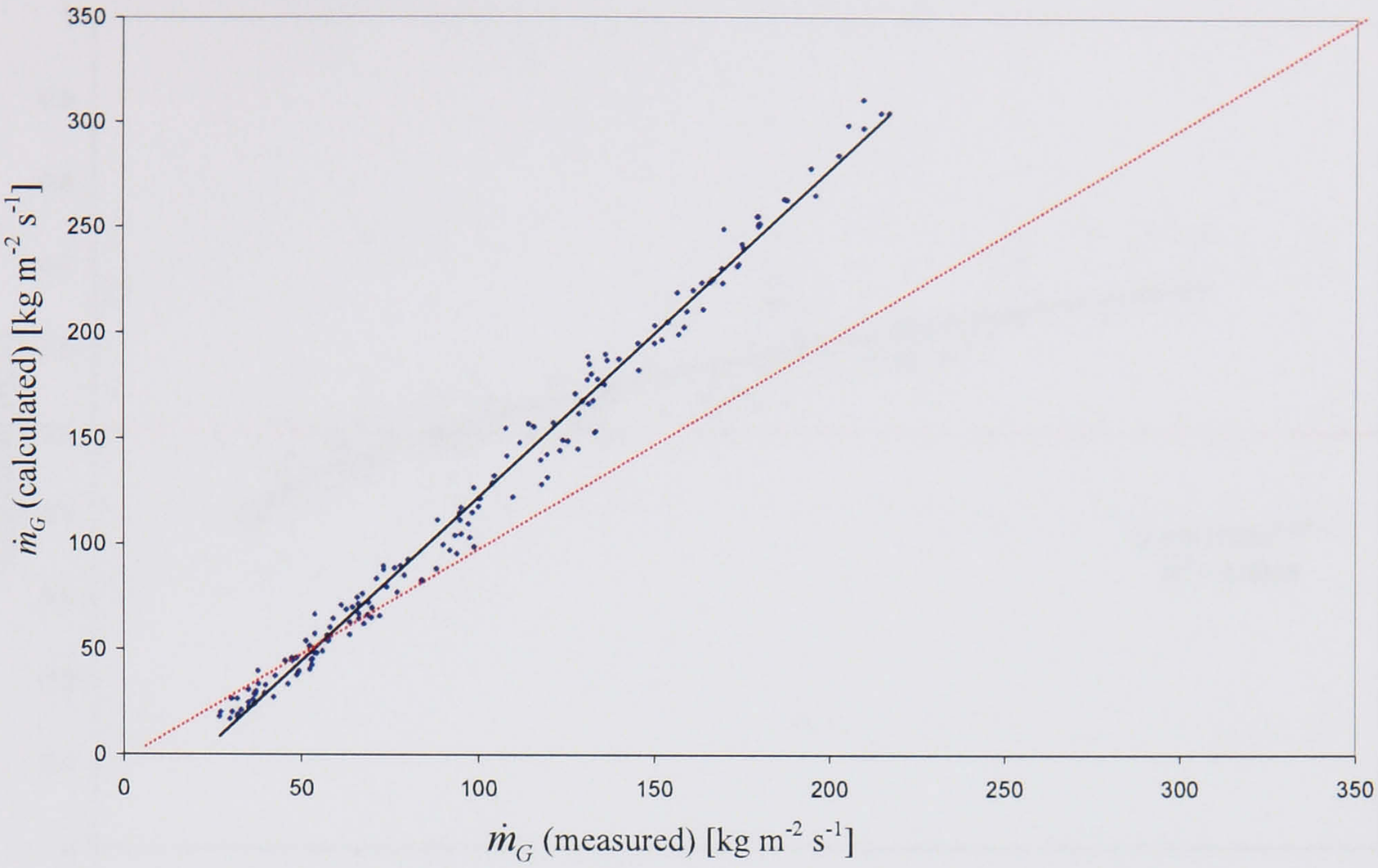


Fig.3 - 17: Calculated vs. measured gas mass flux (without correction for compressibility effects).

As described in paragraph 3.3.1, the hypothesis behind the results obtained for the gas mass flux is that of homogeneous flow through the venturi. This implies a slip value of 1 and a value of 0.5 for the exponent n in **Eq.3 - 6**. By letting n change in order to minimise the mismatch between measured and calculated values of gas mass flux (while keeping the C_D constant and using a gas compressibility factor of 1), the results illustrated in **Fig.3 – 18** are obtained. This error-minimising n can be plotted as a function of the liquid mass flux, as shown in **Fig.3 – 19** for one of the six sets of experiments

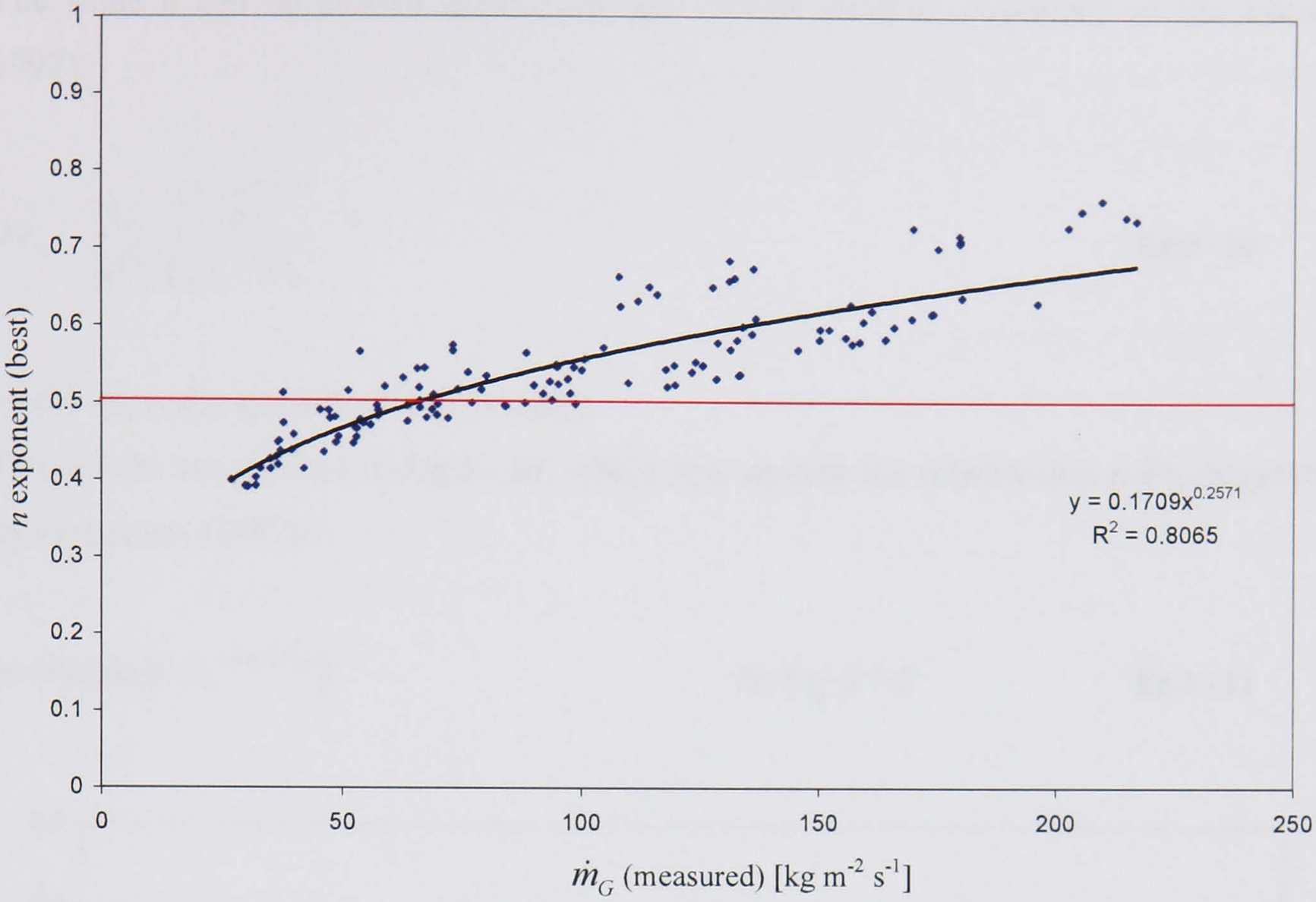


Fig.3 – 18: Error-minimising *n* exponent vs. measured gas mass flux.

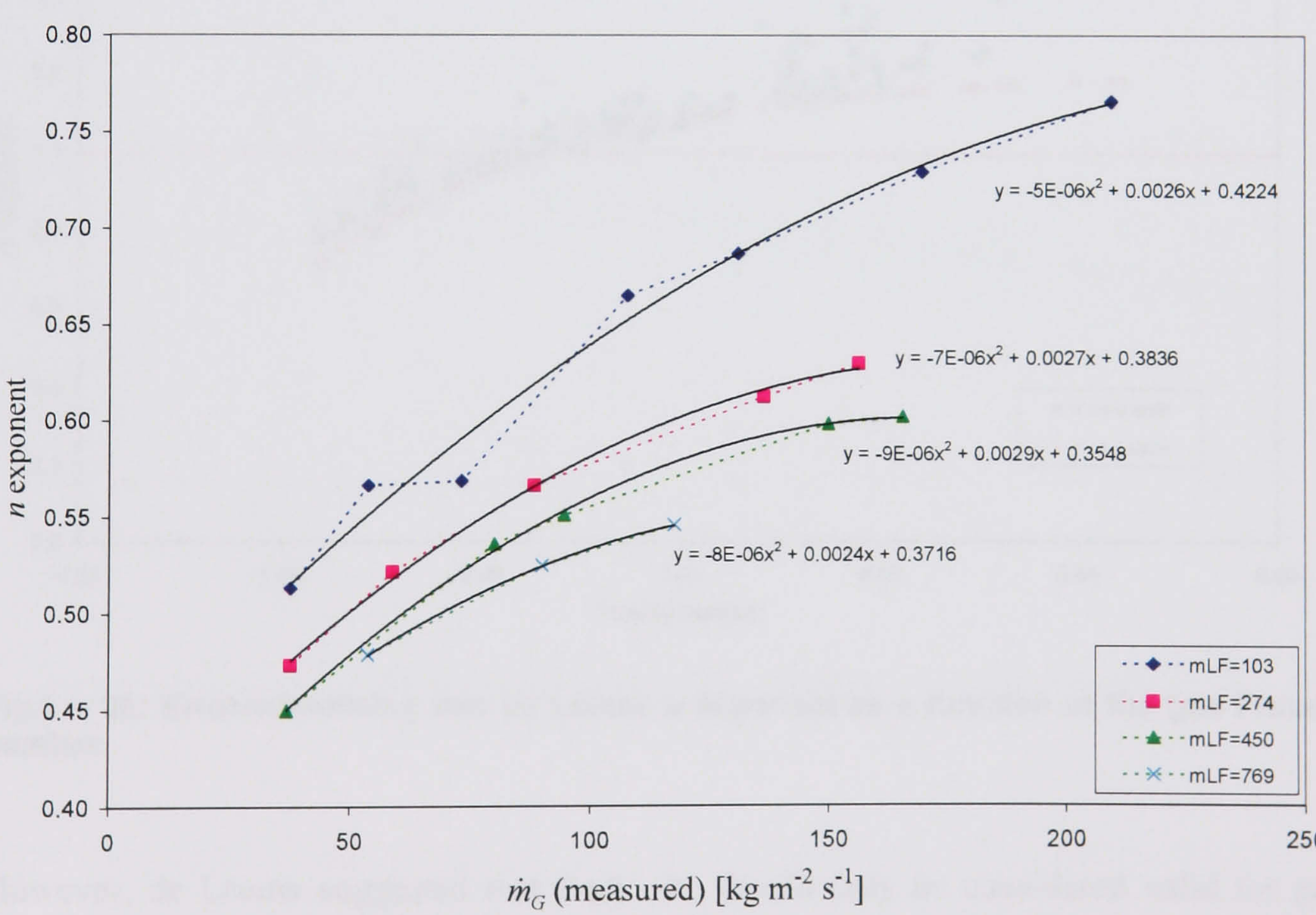


Fig.3 – 19: Error minimising *n* exponent vs. measured gas mass flux, plotted for one of the six sets of experiments.

The same n can be plotted against the gas Froude number, expressed as (de Leeuw, 1997):

$$Fr_g = \frac{v_{sg}}{gD_1}\sqrt{\frac{\rho_G}{\rho_L - \rho_G}} \qquad \textbf{Eq.3 - 20}$$

where v_{sg} is the gas superficial velocity.

The results are showed in **Fig.3 - 20**, which also reports the relationship n-Fr_g suggested by de Leuuw (1997):

$$n = 0.606\left(1 - e^{-0.746 Fr_g}\right) \qquad \text{for } \mathrm{Fr_g} \geq 1.5 \qquad \textbf{Eq.3 - 21}$$

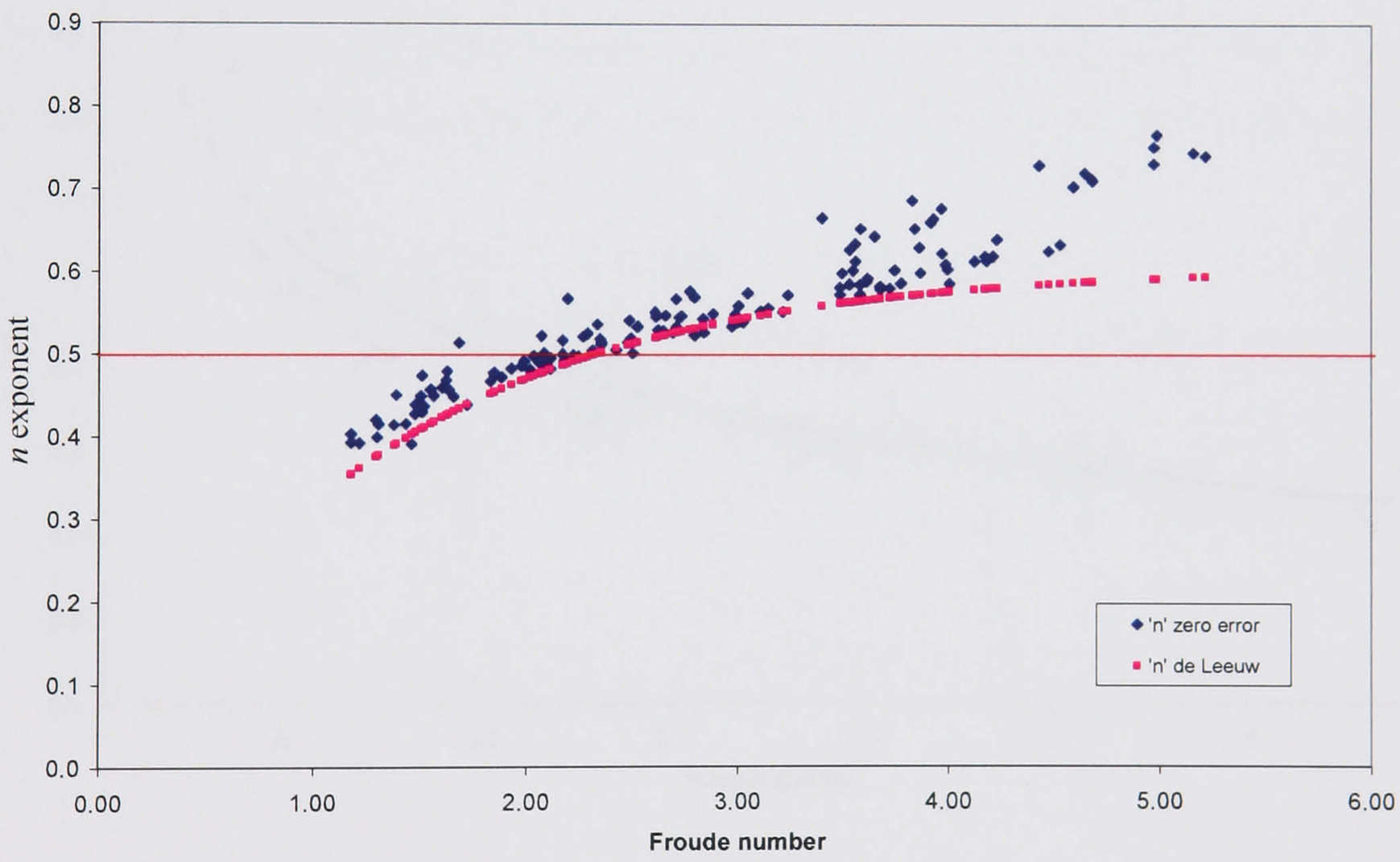


Fig.3 – 20: Error-minimising and de Leeuw *n* exponent as a function of the gas Froude number.

However, de Leeuw suggested that **Eq.3 - 21** should only be considered valid for gas densities above 17 kg/m^3 (up to the liquid density), gas Froude numbers above 0.5 and Lockhart-Martinelli parameters up to 0.3. The results presented by de Leeuw were

obtained from experiments at pressures ranging between 15 and 90 bars, whereas the experiments on the ANUMET concept, described in this chapter, were carried out at much lower pressures (less than 6 bars). The Lockhart-Martinelli parameter ranged between 0.0013 and 0.0286 for the experiments.

The behaviour of the venturi discharge coefficient, C_D, was also investigated. The C_D was let to vary in order to minimise the error between measured and calculated gas mass flux, while leaving n constant (n=0.5) and using a gas compressibility factor of 1. **Fig.3 - 21** shows a dependency of the error-minimising C_D on the stream quality, while a constant C_D equal to 0.984 was assumed in the calculations presented here.

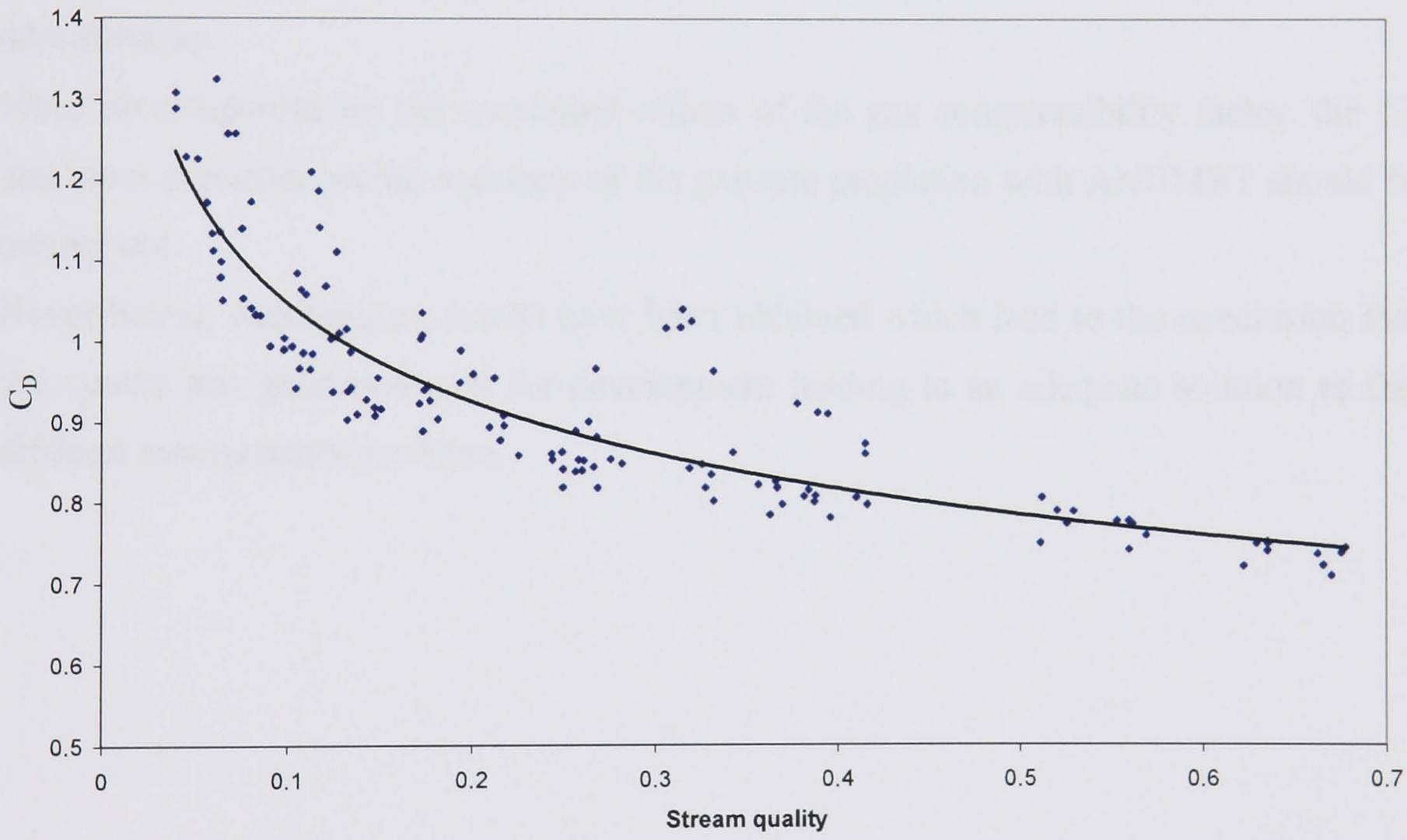


Fig.3 – 21: Error-minimising venturi discharge coefficient vs. stream quality.

Fig.3 - 16 to **Fig.3 - 21** show that the gas compressibility factor, the C_D and the n exponent all play an important role in determining the accuracy of the results. It would be interesting to perform a sensitivity analysis (using Monte Carlo techniques, for instance)

to assess what combinations of these three parameter have the highest impact on the results.

3.6 Conclusions

The metering concept presented in this Chapter introduces a novel approach to wet gas metering. In fact, although the individual devices used in ANUMET and the basic equations applied for annular flow and for homogeneous flow have been known to the oil and gas community for some decades now, the novelty lies in the way they have been combined towards a wet gas metering solution.

The limitations of the ANUMET concept, at its present stage of development, have been identified. They mainly relate to the instrumentation chosen for the measurements and in particular to the method used for film thickness measurement, namely gamma densitometry.

More investigations on the combined effects of the gas compressibility factor, the C_D and the n exponent on the accuracy of the gas rate prediction with ANUMET should be carried out.

Nevertheless, encouraging results have been obtained which lead to the conclusion that the system has good potential for development leading to an adequate solution to this difficult measurement problem.

CHAPTER 4

Introduction to Well Test Analysis

4.1 Introduction

Well test analysis aims to provide a description of hydrocarbon reservoirs in dynamic conditions, as a supplement to static geological and well log data. The information that can be inferred from a well test includes the reservoir deliverability, properties and size. In particular, a well test attempts to determine the reservoir *kh* (or permeability-thickness product), the initial reservoir pressure and the reservoir boundaries and heterogeneities. At the same time, the reservoir fluids can be sampled so that their PVT properties can be determined in the laboratory. Information on the near-wellbore area can also be analysed to assess whether the reservoir productivity is dominated by wellbore phenomena or by the reservoir properties. All this information can help examine, improve and forecast reservoir performance. In this Chapter, an introduction to the well testing methodology is provided; the textbooks by Horne (1990) and Bourdet (2002) give further details.

During a well test, a transient pressure response is created by a change in production (or injection) rate. The flow rate is usually measured at surface while the pressure is recorded downhole. It is assumed that, prior to production, a constant and uniform initial pressure p_i exists across the reservoir. During the flowing period, the drawdown pressure response Δp is defined as:

$$\Delta p = p_i - p(t) \qquad \textbf{Eq.4 - 1}$$

When the well is shut-in, the build-up pressure response Δp is expressed as a function of the last flowing pressure $p(\Delta t=0)$:

$$\Delta p = p(t) - p(\Delta t = 0) \qquad \textbf{Eq.4 - 2}$$

The pressure response for both drawdown and build-up is analysed versus the elapsed time Δt since the start of the period (time of opening or shut-in).

Fig.4 - 1 shows a drawdown and build-up test sequence.

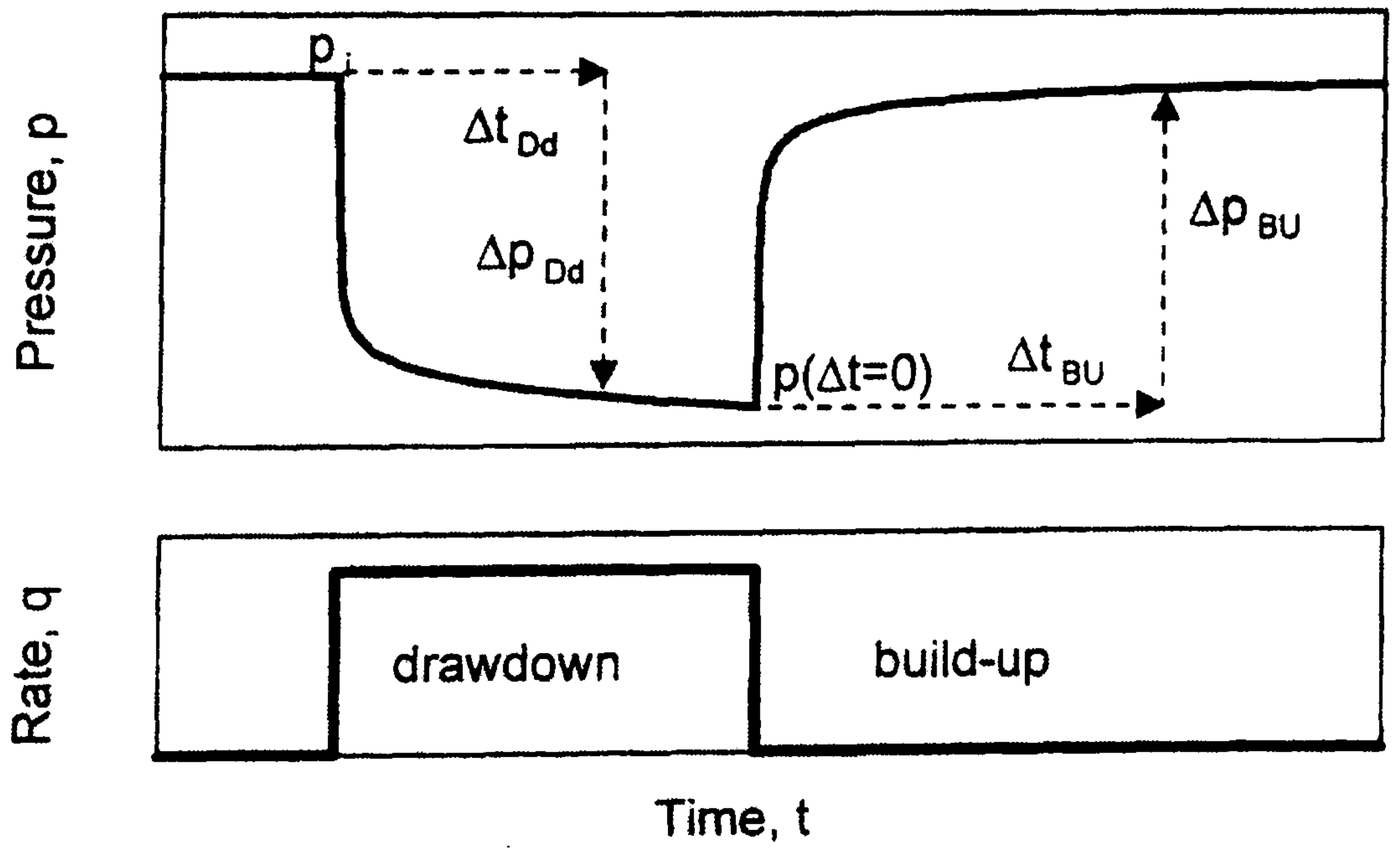


Fig.4 - 1: Drawdown and build-up test sequence (Bourdet, 2002).

During a drawdown test, the well is assumed to be flowing at a constant rate while the flowing bottomhole pressure is recorded for the analysis. In practice, it is very difficult to keep the well conditions static and stable for the duration of the test, therefore the analysis of drawdown tests can often be inaccurate.

A build-up test begins when the well is shut-in after it has been producing long enough to establish a stabilised pressure distribution. During the shut-in period, the well rate at the surface is zero.

The interpretation of transient well testing is based on the so-called diffusivity equation. This is a differential equation for transient flow of a fluid through in a porous medium, resulting from a combination of Darcy's law, the principle of conservation of mass and a law describing the behaviour of the fluid inside the porous medium. The diffusivity equation, in radial coordinates and for a single-phase fluid, can be written as (in SI units) (Chierici, 1989):

$$\frac{1}{r}\frac{\partial}{\partial r}\left(\frac{k}{\eta}\rho r\frac{\partial P}{\partial r}\right)=\rho\phi c_t\frac{\partial P}{\partial t} \qquad \textbf{Eq.4 - 3}$$

where

P = pressure

r = radial position

φ = rock porosity

c_t = total compressibility (formation + fluid)

t = time

η= fluid viscosity

k = rock permeability

ρ = fluid density

As φ, k, c_t, ρ and η are functions of pressure, the above is a non-linear differential partial equation. The linearised form of the diffusivity equation is:

$$\frac{\partial^2 P}{\partial r^2}+\frac{1}{r}\frac{\partial P}{\partial r}=\frac{\phi\eta c_t}{k}\frac{\partial P}{\partial t} \qquad \textbf{Eq.4 - 4}$$

where the following assumptions are made:

- Homogeneous and isotropic porous medium
- Uniform thickness

- Single phase flow
- Laminar flow
- Rock and fluid properties independent of pressure

For gases, the governing partial differential equation becomes unavoidably non-linear, due to the gas compressibility being highly dependent on pressure. The gas viscosity also varies with pressure. To linearise the diffusivity equation for gases, the real gas pseudo-pressure was introduced (Al-Hussein *et al.,* 1966):

$$m(P) = 2\int_{P_{ref}}^{P} \frac{P}{\eta(P)z(P)}dP \qquad \textbf{Eq.4 - 5}$$

where:

P_{ref} = arbitrary base pressure

z = gas deviation factor

The pressure dependence of permeability is ignored (i.e., the reservoir is assumed insensitive to stress).

The radial diffusivity equation for compressible fluids can therefore be written as:

$$\frac{\partial^2 m(P)}{\partial r^2} + \frac{1}{r}\frac{\partial m(P)}{\partial r} = \frac{\phi\eta c_t}{k}\frac{\partial m(P)}{\partial t} \qquad \textbf{Eq.4 - 6}$$

For the specific case of gas-condensate reservoirs (discussed in detail in the following paragraph), the diffusivity equation is further linearised by introducing a two-phase pseudo-pressure (Raghavan, 1986):

$$m(P) = \int_{P_{ref}}^{P}\left(\frac{k_{rg}}{\eta_g B_g} + \frac{k_{ro}}{\eta_o B_o}\right)dP \qquad \textbf{Eq.4 - 7}$$

where:

B_o, B_g = formation volume factors of oil and gas, respectively

k_{ro}, k_{rg} = relative permeability of oil and gas*, respectively

η_o, η_g = viscosity of oil and gas, respectively

To obtain a unique solution to the diffusivity equation, it is necessary to specify one initial condition (because of the first derivative, with respect to time) and two boundary conditions (because of the second-order derivative, with respect to radius of investigation). In well test analysis, the boundary conditions at the wellbore (either a constant-pressure or constant-rate well) and at the external radius (infinite-acting reservoir or no-flow or constant-pressure outer boundary) are specified (Ertekin *et al.*, 2001). In most transient pressure analysis techniques, the so-called constant-terminal-rate solution to the diffusivity equation is considered, where the well is assumed to be flowing at a constant flow rate.

Specialised scale plots, based on dimensionless pressure and time (which are linear functions of actual pressure and time), are used to identify typical flow regimes and late-time boundary effects. The pressure type-curves are usually accompanied by the derivative type curves, which represent the time derivative of pressure. These specialised plots are usually in a log-log scale. By comparing the log-log data plot with a set of theoretical curves, the model that best describes the observed pressure response is defined.

4.2 Well test analysis in gas condensate and volatile oil reservoirs

Pressure transient analysis is a well established reservoir evaluation method. However, much of the pressure data recorded during a well test may be dominated by wellbore effects that can mask reservoir characteristics and lead to erroneous well test interpretations. This is particularly true when the well production rate is controlled at surface and more than one phase is flowing. These effects, which are transient in nature, include phase change, flow reversal, and re-entry of the heavier phase into the producing zone (Qasem *et al.*, 2001; Al-Afaleg and Giliani, 2001).

---

* The *relative permeability* is defined as the permeability of the medium to one phase in the presence of the other phase, divided by the *absolute permeability* (K).

Wellbore storage is due to the expansion or compression of the fluids in the wellbore. Immediately after a change in flow rate, such as after the start of a drawdown test or after shut-in, the influx from the reservoir and the wellhead flow rate will be different. This is due to the expansion or compression of the fluids in the wellbore as a consequence of the changing pressure.

The effect of wellbore storage on pressure tests is illustrated in **Fig.4 – 2**, where:

Q_{sf} = rate at the sand face

Q_{wh} = rate at the wellhead

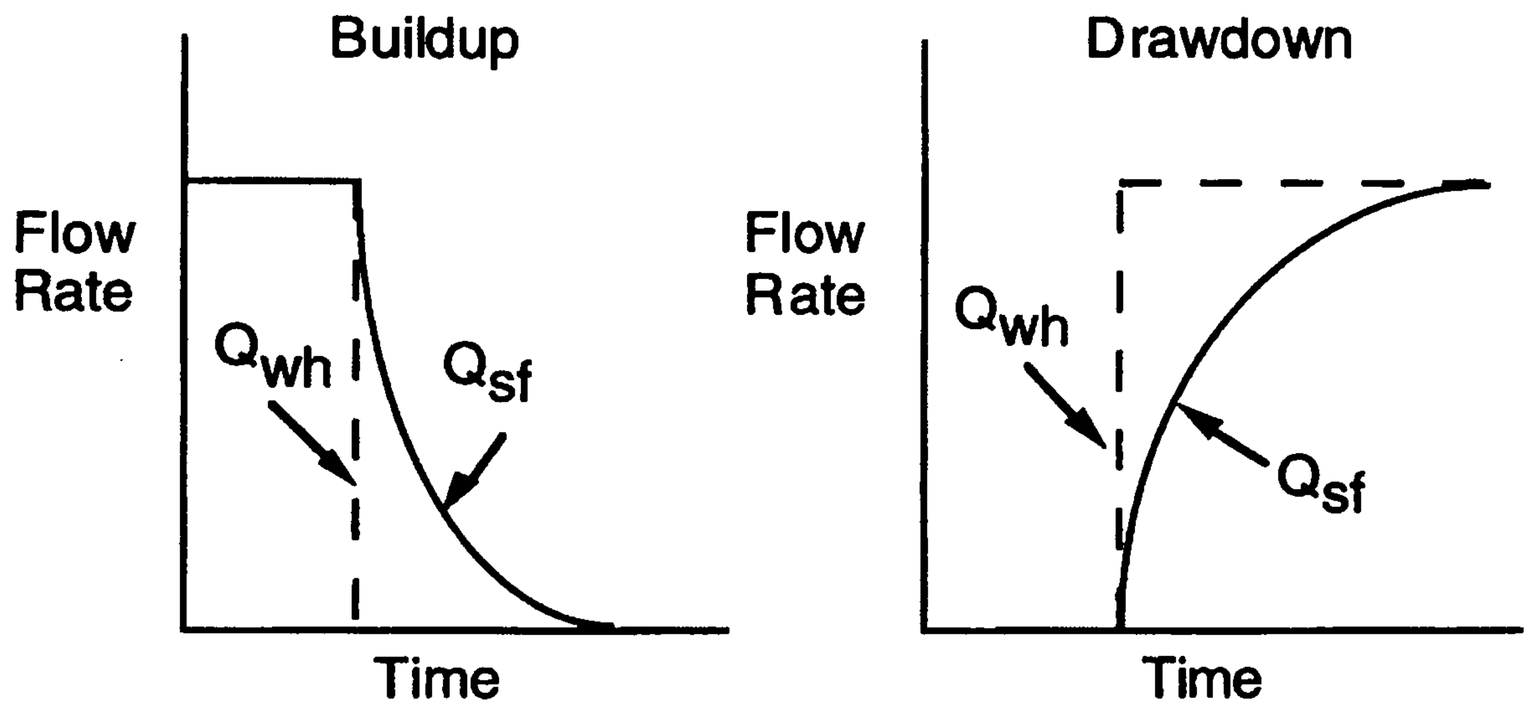


Fig.4 - 2: Effect of wellbore storage on pressure tests (Zimmerman, 1998-1999).

The wellbore storage coefficient is the volume of fluid that the wellbore itself will produce due to a unit drop in pressure. Wellbore phase redistribution (WPR) (Gringarten *et al.,* 2000) may cause an increase in the wellbore storage coefficient in both drawdowns and build-ups. Phase change, on the other hand, casuses the wellbore storage coefficient to decrease during build-ups and to increase during drawdowns. While the impact of phase change on the pressure behaviour is usually limited to early times, WPR may dominate a well test for several hours. When WPR occurs, derivative shapes can be easily be misinterpreted as being due to double porosity, partial penetration or composite behaviour.

Typical derivative shapes due to WPR are shown in **Fig.4 - 3**, where curve 5 is typical of situations where the denser phase is re-injected into the formation.

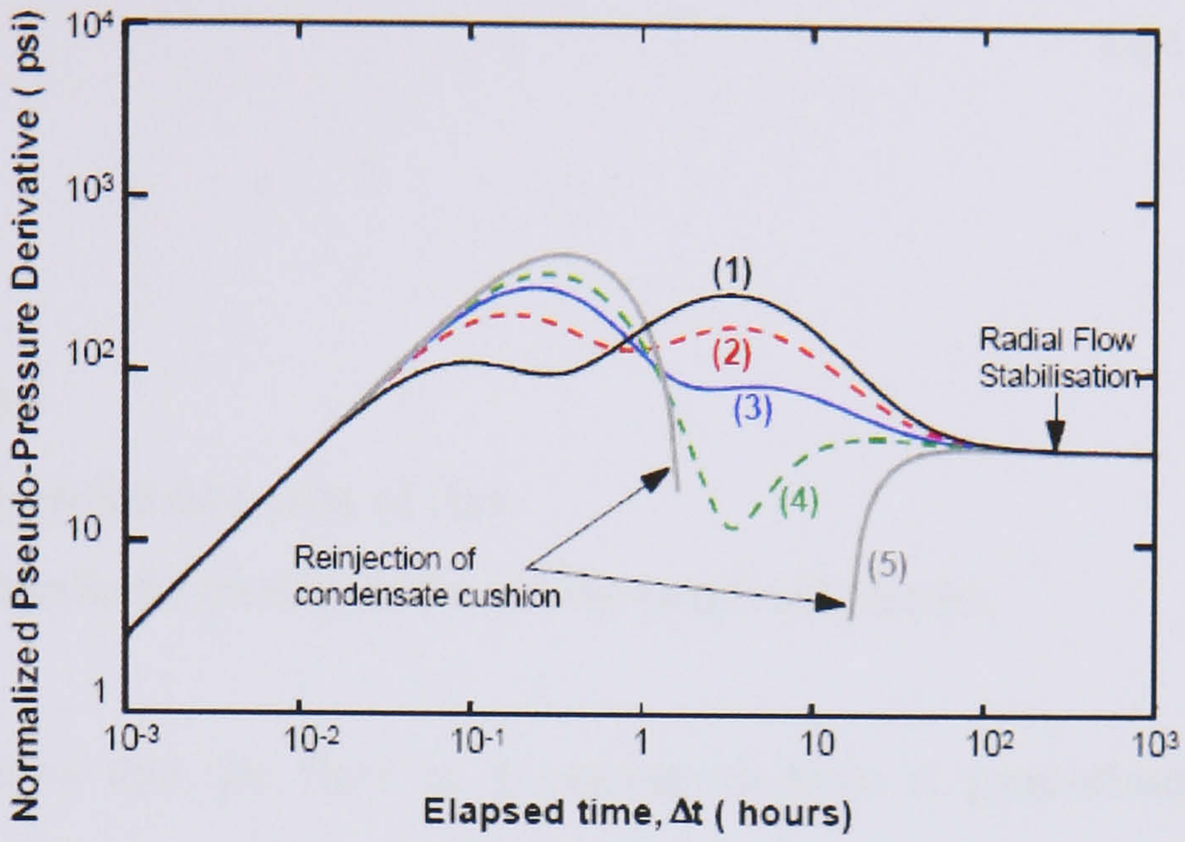


Fig.4 - 3: Log-log derivative plots, increasing wellbore storage due to phase redistribution in the wellbore (Gringarten et al., 2000). The normalised pseudo-pressure is: $nm(P) = \left(\frac{\mu z}{P}\right)_{P_{ref}} \int_{P_{ref}}^{P} \frac{P}{\eta(P) z(P)} dP$

It has been found (Gringarten *et al.,* 2000) that, as the pressure drops in a gas condensate reservoir, three zones may form around the well, each of them with different liquid and gas saturations and mobility: an outer zone, away from the well, with the initial liquid condensate saturation; an intermediate zone, nearer the well, with increased liquid saturation and decreased gas mobility ("condensate banking"); an inner zone, in the immediate vicinity of the well, where the liquid saturation reaches a critical value and the gas relative permeability increases, so that both gas and liquid can flow and much of the gas mobility lost from the condensate banking can be recovered. This latter zone, closest to the well, can be difficult to identify from well tests because of the wellbore effects mentioned above.

Ultimately, the overall gas well productivity is dictated by a combination of capillary number effects and non-Darcy effects (Bozorgzadeh and Gringarten, 2005). The capillary number represents the relative effect of viscous forces and surface tension

acting across an interface between a liquid and a gas, or between two immiscible liquids. It is defined as:

$$N_c = \frac{\eta_g v_g}{\sigma} \qquad \textbf{Eq.4 - 8}$$

where:

η_g = gas viscosity

v_g = gas velocity in the direction of flow

σ = surface or interfacial tension between the two fluid phases.

Darcy's law states that the flow in a porous medium is proportional to pressure gradient and inversely proportional to viscosity. At higher flow rates, inertial effects become important and there are significant variations from Darcy's law. Non-Darcy effects are captured by the Forchheimer equation, which adds an extra velocity-dependent term in Darcy's law. For radial flow, Forchheimer's equation can be written as:

$$\frac{dP}{dr} = \frac{\eta}{K} v + \beta \rho v^2 \qquad \textbf{Eq.4 - 9}$$

where:

v = fluid velocity

η = fluid viscosity

K = absolute permeability of the porous medium

ρ = fluid density

β = coefficient of inertial resistance, which has the dimension of $(\text{length})^{-1}$

The non-Darcy component in the equation above is negligible at low flow velocities and is generally omitted for liquid flow. However, for a given pressure drawdown, the gas velocity is at least an order of magnitude greater than the liquid velocity, due to the low viscosity of the gas, and the non-Darcy component must therefore be included in equations describing the flow of a real gas through a porous medium (Dake, 1978).

At high gas rates, capillary forces decrease, which result in an improvement of the gas relative permeability under near-wellbore flow conditions. Under the same conditions, pressure gradients in both the gas and the liquid phase are large and the interfacial tension between them is low, which causes a decrease in the saturation of the residual phase. On the other hand, high gas rates cause non-Darcy effects that reduce the well productivity.

Fig.4 - 4 and **Fig.4 - 5** show the capillary number effects on liquid saturation and gas relative permeability in the near-wellbore region.

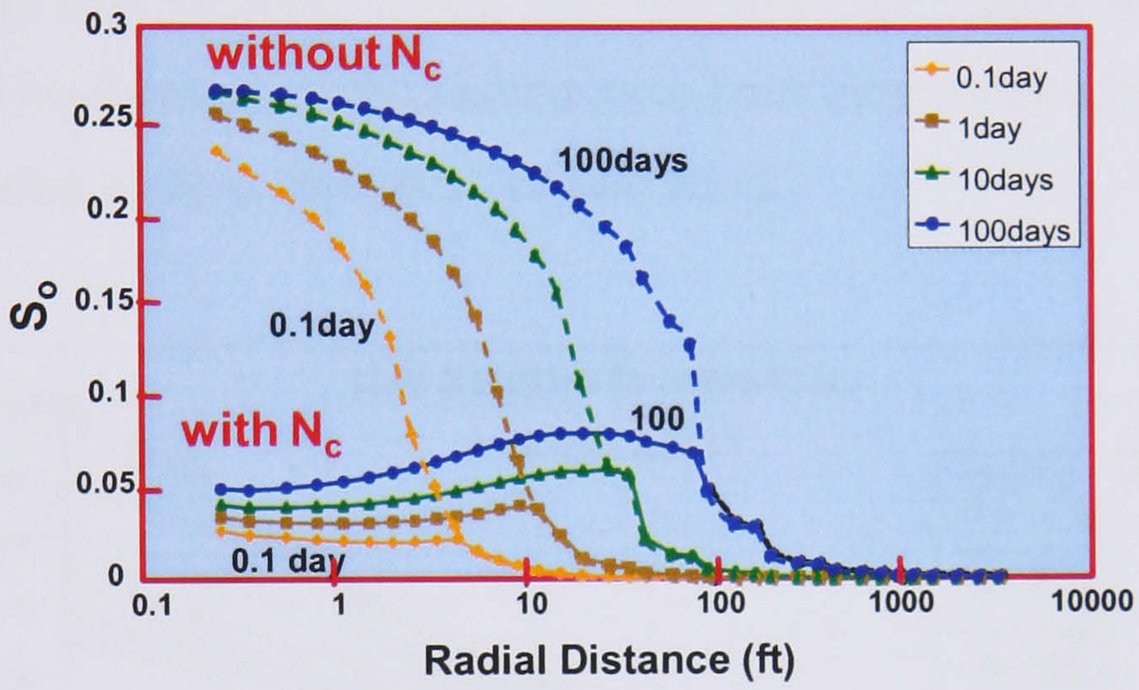


Fig.4 - 4: Decrease in near-wellbore liquid saturation below the dew point due to capillary number effects (JIP Annual Report Phase II, 2005).

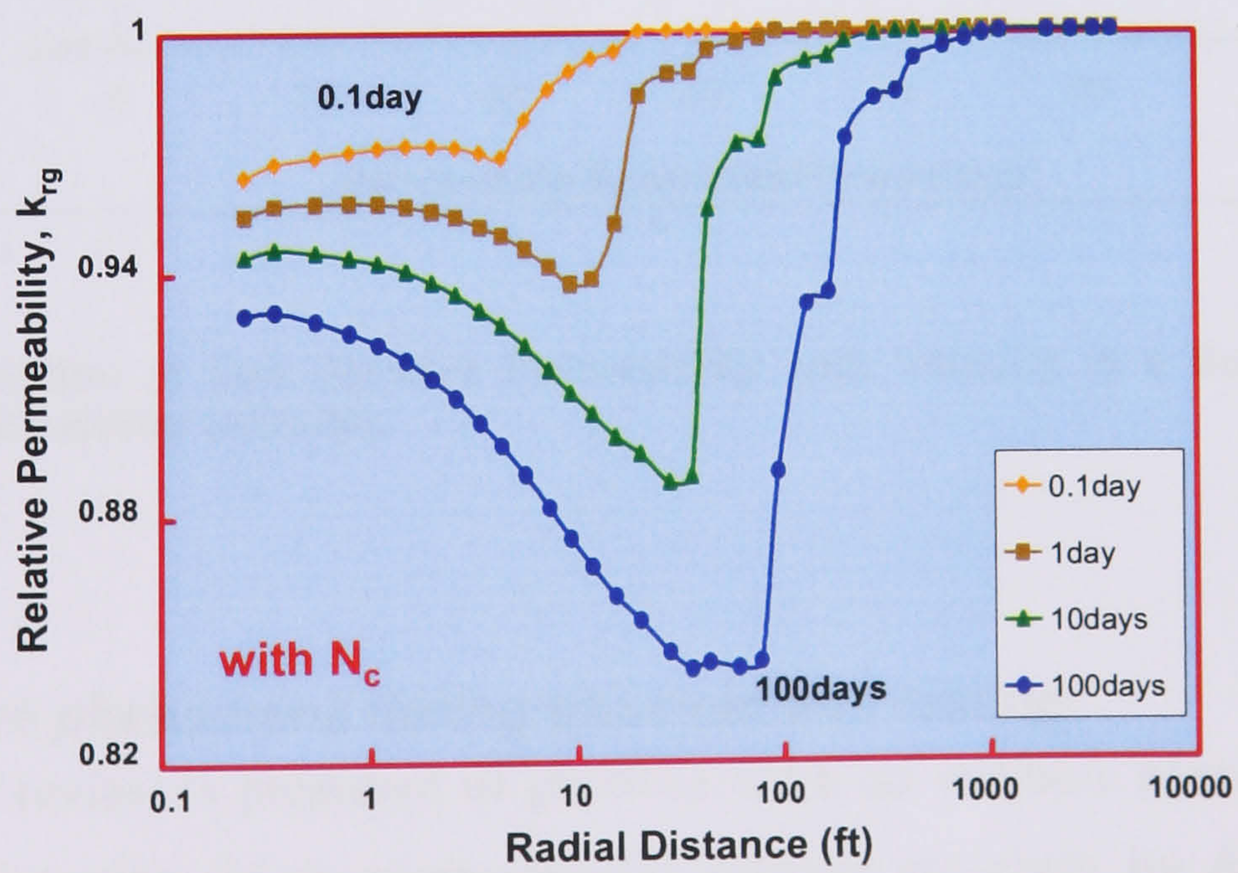


Fig.4 - 5: Increase in near-wellbore gas relative permeability below the dew point due to capillary number effects (JIP Annual Report Phase II, 2005).

The flow of gas and condensate in reservoirs has also been studied in a laboratory at Heriot-Watt University since 1986, investigating several recovery processes including pressure depletion, gravity drainage and water encroachment. Three core test rigs, which include in-situ saturation monitoring using X-rays and allow both steady and unsteady state relative permeability tests, have been designed, commissioned and evaluated. Specific experimental procedures for testing gas and condensate fluids have been developed. Theoretical and numerical models, based on mechanistic approaches, have been developed to interpret and generalise the results. Heriot-Watt demonstrated for the first time in 1994 that the relative permeabilities of gas-condensate in the near wellbore region may improve significantly by increasing the rate (**Fig.4 - 6**). The developed relationships have been incorporated in major reservoir simulators including Eclipse 300, and VIP Landmark.

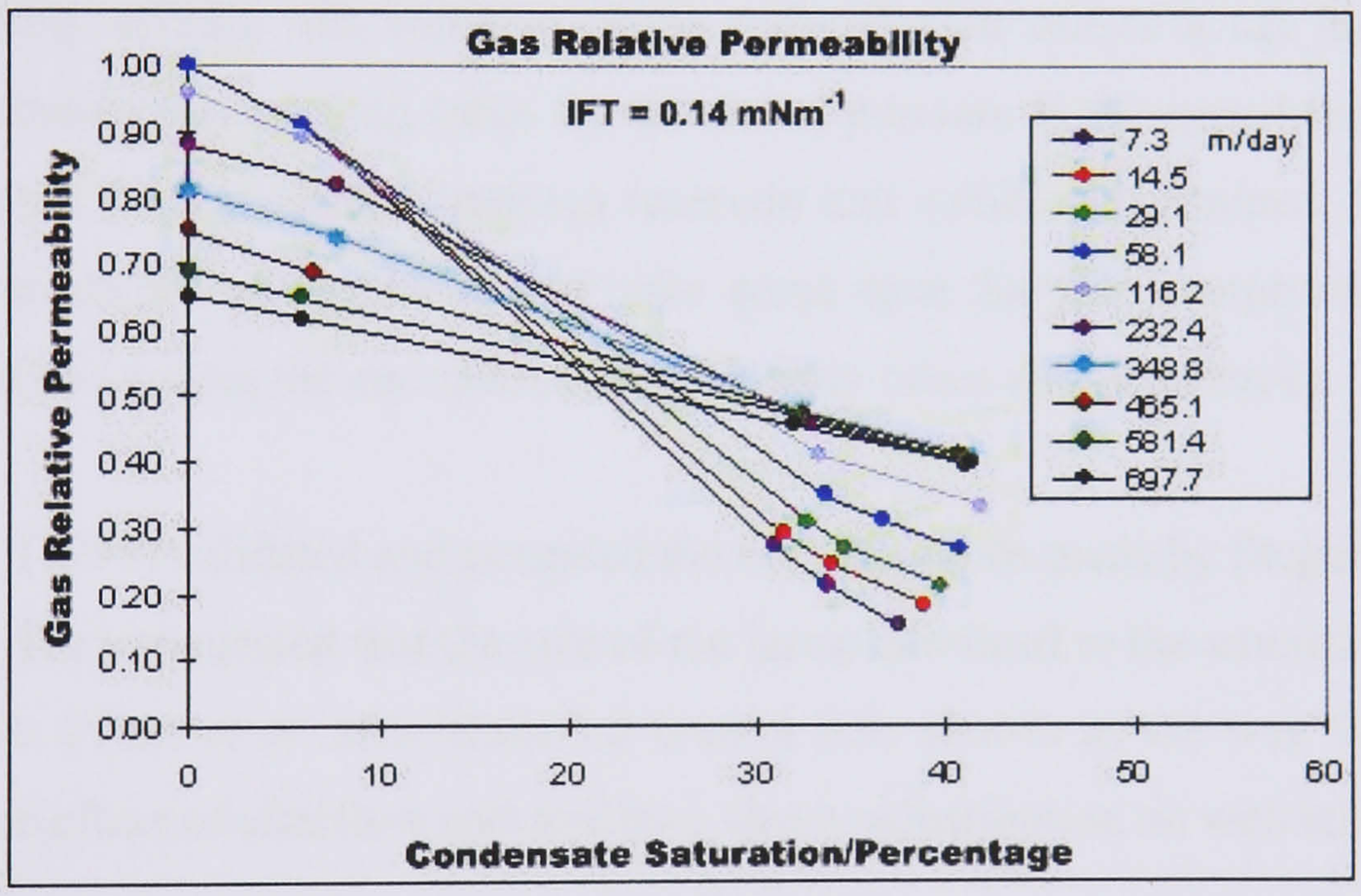


Fig.4 - 6: Variation of Gas Relative Permeability with Velocity in a Sandstone Core (Heriot-Watt University website).

4.3 Wellbore phenomena during transient well testing

Here, a brief review is presented of previous work on wellbore phenomena during transient well testing. More comprehensive reviews are given by Ali (2004) and Akemu (2001). Pressure transients in a wellbore imply transient multiphase flows, opposite the producing reservoir zones and higher up in the tubing. Gravity, friction

and acceleration effects play an important role in this scenario, as they determine the pressure profile and the flow regime in the well. To date, there has been limited research into wellbore phenomena during well testing. Initial research has focused on empirical models to identify and match wellbore phase redistribution. However, these models do not account for the underlying physical mechanisms causing wellbore phase redistribution. More recently, robust mechanistic modelling of multiphase flows has been proposed to characterise wellbore phenomena.

Stegemeier and Matthews (1958) were the first to provide a physical explanation for the anomalous pressure hump observed in build-up data from South Texas and Louisiana fields. When a two-phase (liquid and gas) fluid is flowing in a well and the well is shut in at surface, the denser phase will start travelling toward the bottom of the well while the lighter phase will have a tendency to rise to surface. Due to compressibility effects, this wellbore phase redistribution causes a net increase of wellbore pressure. In build-up tests, the increased pressure is dissipated through the formation until the equilibrium between reservoir and wellbore is attained. However, in low permeability reservoirs, it may take some time for this overpressure to be relieved and this causes the anomalous hump at early times after the shut-in.

Pitzer *et al.* (1959) validated and extended the considerations made by Stegemeier and Matthews. They suggested that the size of the hump is related to the amount of gas in the wellbore. Pitzer *et al.* also identified bottom hole shut-in as the way forward to eliminate the effect of afterflow and wellbore phase redistribution on well test data.

Fair (1979) was the first to propose a mathematical model for phase redistribution in well testing. He treated wellbore phase redistribution as a wellbore storage effect, which was incorporated into a new solution of the diffusivity equation. An exponential function was used to express the pressure change caused by a change in wellbore phase storage between two constant values, C_{aD} and C_D. At early times, the pressure response is the same as that of a well with constant storage coefficient C_{aD}. After a transition period, when the wellbore storage coefficient can increase or decrease, the well is characterised by a constant wellbore storage coefficient C_D higher than C_{aD}. For this reason, Fair's model is known as an increasing wellbore storage model. Fair found that the exponential form was suitable to represent phase

redistribution in a gas-lifted oil well, but suggested that further validation was necessary against meaningful experimental data.

Thompson *et al.* (1984) produced a detailed study of Fair's wellbore phase redistribution solution. They showed that Fair's model could yield non-unique and widely varying estimates of formation parameters. Thompson *et al.* established conditions under which build-up data could be analysed with Fair's drawdown type curves They defined a methodology to determine when it can be assumed that wellbore storage effects have terminated and radial flow analysis can be performed.

Winterfeld (1986) was the first to attempt a rigorous modelling of multiphase flow in the wellbore to investigate wellbore phenomena during build ups. Winterfeld simulated a pressure build-up test in a multiphase system consisting of a wellbore and a reservoir. Wellbore flow was assumed to be governed by conservation of mass and momentum, reservoir flow by conservation of mass and Darcy's law. Finite-difference versions of the flow equations were solved on a discretised system. Counter-current two-phase flow in the wellbore during shut-in was allowed by the use of semi-empirical expressions to account for phase-to-phase viscous forces. The single-phase example presented by Winterfeld illustrated the wellbore storage and wellbore fluid inertia shortly after shut-in. The two-phase examples illustrated phase redistribution and the hump caused by phase segregation.

Based on the approach by Winterfield (1986), Almehaideb *et al.* (1989) proposed a fully implicit technique for the coupling of wellbore and reservoir flow equations. They used an isothermal, three phase black-oil model for the flow in the wellbore. In order to account for slippage between liquid and gas phase, they adopted a separated flow model. Almehaideb *et al.* showed that the so-called two-fluid model for multiphase flow in wells was able reproduce a pressure hump in the build-up curve. This model treats the general case of modelling each phase or component as a separate fluid with its own set of governing balance equations. In general, each phase has its own velocity, temperature and pressure. The velocity difference, as in the separated flow, is induced by density differences. The temperature difference between the phases is fundamentally induced by the time lag of energy transfer between the phases at the interface as thermal equilibrium is reached. They concluded that a two-

phase flow model, simpler than the two-fluid model, is unable to reproduce the pressure hump.

Rushing and Lee (1989) developed an automated history matching technique to analyse pressure buid-up data affected by wellbore phase redistribution. The method, based on the type curve analysis, was based on a Gauss-Newton least squares procedure to match observed field pressures with those predicted by Fair's phase segregation method. Rushing *et al.* thus reduced the non-uniqueness problem associated with Fair's manual type curve fitting.

Olarewaju and Lee (1989) and Olarewaju (1990) proposed the use of pressure derivatives, defined as the slope of the pressure with respect to the logarithm of time (Bourdet *et al.,* 1984), to identify phase redistribution distortion when it is not apparent from the pressure plot. This technique requires that good test data exist beyond the start of infinite-acting radial flow. Olarewaju concluded that phase redistribution causes a V-shaped depression in the pressure derivative plot. They noted that, even though double porosity systems have a similar V-shaped depression, phase redistribution is usually associated with the bell-shaped wellbore storage distortion.

Hasan and Kabir (1992) developed a mechanistic wellbore model based on the physics of bubble migration. Hasan and Kabir coupled a numerical wellbore model with an analytical reservoir model and applied Duhamel's principle to account for continually decreasing afterflow from the reservoir after shut-in. Their conclusion was that the anomalous increase or decrease in pressure in a well shut in at surface may be explained by the preferential upward movement of the gas phase.

Hasan and Kabir (1993) later proposed a simple physical model of the wellbore, consisting of liquid and a small pocket of segregated gas at the top. The model well cannot receive any fluid from the reservoir during shut-in, but back flow from the wellbore into the reservoir is permitted to relieve the excess pressure generated by rising bubbles. Hasan and Kabir studied the velocity of a single bubble of gas rising through the liquid column. An approximate analytical solution of the model justified Fair's empirical exponential model for early times. This simplified model showed that

bubble migration causes an increase in wellbore pressure similar to that observed in a well during phase redistribution.

Mattar and Santo (1992) and Mattar and Zaoral (1992) proposed the use of the Primary Pressure Derivative (PPD), which is defined as the slope of the pressure-time curve on Cartesian coordinates, to differentiate between wellbore-dominated effects and reservoir effects. They showed that, when increasing PPD is observed, that portion of the pressure response is affected by wellbore dynamics and not reservoir characteristics.

Hegeman *et al.* (1991) modified the technique of Fair. By applying an increasing/decreasing wellbore storage model, they concluded that, in some cases, a sharper (than exponential) changing-storage pressure function was required. They proposed the error function as a different form of changing-storage transition, with a sharper, more abrupt transition period. Hegeman *et al.* used a wellbore storage coefficient at early times greater that that at late times to match field data. The Hegeman *et al.* model is therefore known as a decreasing wellbore storage model.

Xiao *et al.* (1994) developed a simple mechanistic model to predict the effect that transient two-phase flow (oil and gas) has on pressure build-up data. The aim was to explain why some field data appeared to follow the Hegeman *et al.* model while other data followed the Fair model. Xiao *et al.* assumed single-phase flow of oil in the reservoir in order to couple the reservoir and the wellbore via a convolution integral (Duhamel's principle). However, they allowed for injection of gas at the bottom hole to simulate the effects of two-phase flow at the sand face. Xiao *et al.* adopted an isothermal, black-oil model throughout and handled the effects of interphase mass transfer by including a variable bubble-point pressure option. The drift-flux model was used as mechanistic wellbore model. Xiao *et al.* showed that build-up test in multiphase flow wells can present either an increase or a decrease of wellbore storage coefficient, as a consequence of phase segregation and gas compression. If the magnitude of afterflow from the reservoir into the wellbore is small after the end of phase segregation, then the latter will be the dominating factor and the pressure build-up data will show an increasing wellbore storage coefficient. On the other hand, if the afterflow is still large after phase segregation, the gas column will be compressed due

to afterflow and the pressure build-up data will show a decreasing wellbore storage coefficient.

Vasquez-Cruz and Camacho-Velasquez (1996) introduced a new method of analysis for well tests with insufficient duration to reach radial flow conditions. Their approach was based on an approximation of the general solutions of changing wellbore storage previously presented by Fair and Hegeman *et al.*. This new approach proved to be independent of the type of function used to model the changing wellbore storage (i.e. exponential or error function) and of its behaviour (i.e. increasing or increasing storage). Vasquez-Cruz and Camacho-Velasquez stated that their method was an improving alternative to the type-curve matching technique for the analysis of the early time pressure data affected by changing wellbore storage. However, the validity of the results was limited to homogeneous reservoirs with radial flow conditions and this method was not recommended for high-permeability reservoirs with light fluids produced at high rates.

Al-Haddad *et al.* (1997) investigated gas cooling effects on pressure transient testing with surface shut-in in gas wells. They demonstrated the effect of gas cooling, in combination with gas compression, on the pressure derivative curves. This could lead to continuing effects of wellbore storage being interpreted as radial flow and boundary effects in the reservoir.

Gringarten *et al.* (2000) showed that phase redistribution can occur in either build-up or drawdown tests and dominate the entire duration of a test. By comparing drawdown and build-up tests for a gas condensate well in the North Sea, they showed that the degree to which phase redistribution affects a well test depends on the rate. No simulation of the dynamic behaviour of the fluid within the well was carried out.

Following Mattar and Santo (1992) and Mattar and Zaoral (1992), Qasem *et al.* (2001) reported the problems encountered with the Bourdet derivative method and the PPD method in detecting low degrees of wellbore phase redistribution. They proposed the use of the derivative of PPD on log-log scale plots. They also proposed the use of anomaly separation techniques from exploration geophysics to enhance the effect of wellbore phase redistribution on PPD plot.

Al-Afaleg and Giliani (2001) presented field examples from high-permeability oil reservoirs to demonstrate the effect of fluid segregation on recorded build-up data. Depending on the position of the downhole pressure gauge, fluid gradient changes between the gauge and the tested reservoir zone may significantly distort the recorded pressure. Al-Afaleg and Giliani illustrated a field case where downhole shut-in proved to be non-effective in removing phase segregation effects. The distortion of the recorded pressure was shown to depend on reservoir permeability and water or gas cut.

Fairuzov *et al.* (2002) presented a lumped-parameter model of transient two-phase gas/liquid flow in a wellbore. The model was based on a simplified two-phase flow model that assumes thermal equilibrium between the phases but allows mechanical non-equilibrium. A numerical algorithm for coupling the wellbore model with a reservoir model (the convolution integral) was proposed, based on the secant method. Calculations were carried out to determine the behaviour of the wellbore flow during a pressure build-up test. The results indicated that a slip-flow model can be used to provide a reasonable assessment of the wellbore effect on pressure build-up data.

Two MSc projects (Ali, 2004 and Al-Darmaki, 2005) were carried out as part of the present project and supervised jointly by the present author, in which experiments were performed on geometries simulating the reservoir/wellbore interaction. This work, and an associated analytical study, is summarised in Chapter 5.

4.4 Conclusions

This chapter has introduced the subject of well test analysis, with a specific focus on the phenomena that occur in the wellbore, particularly at high gas fraction. It is clear that an understanding of the transient multiphase flow in the wellbore is of crucial importance in the interpretation of well test data – and also, of course, in the interpretation of a whole range of transients occurring in field operations. Chapters 5, 6 and 7 describe the work that was done as part of the present project in pursuit of such an understanding.

CHAPTER 5

Experimental studies simulating well testing and their interpretation

5.1 Background

It is clear from the previous work on well test analysis, described in Chapter 4, that the complex multiphase behaviour in the wellbore is crucial to this analysis. In order to gain some insights into this process, two MSc projects were carried out, jointly supervised by the present author, in which the wellbore flows were simulated using the LOTUS facility at Imperial College. These experimental studies are summarised in Section 5.2 below. In one of the MSc projects, pressure changes following simple isolation of the tube simulating the wellbore were studied over a wide range of flow regimes. These measurements will provide a data base with which predictions obtained at later stages of the project (of which the work described in this thesis forms a part) can be validated. However, a simple model was derived for the specific (and quite important) case of bubbly flow. This model is described in Section 5.3; it shows encouraging agreement with the experiments.

5.2 Experimental studies simulating well testing

The two experimental studies were carried out on the Imperial College LOTUS facility. This facility was also used for the flow metering studies discussed in Chapter 3 and a description of the facility is given in that chapter (see **Fig. 3 - 11**).

In the first MSc study, Ali (2004) carried out experiments to investigate the effects of wellbore phase redistribution (WPR) and phase re-injection on pressure build-up data. Single-phase and two-phase flow tests were conducted with air and water. The LOTUS test layout was designed to emulate a reservoir connected, via a resistance, to the base of a flowing well. The "reservoir" was recreated by a pressurised vessel, while the "well" was simulated by a 10.8m long, 32mm diameter vertical pipe (i.e. the main LOTUS test section). The "well" was flowed at controlled rates to mimic those encountered in gas condensate reservoirs. After steady-state conditions had been attained, the "well" was shut-in at the top of the rig (i.e. at the surface) and the associated transient phenomena monitored via distributed measurements of pressure, temperature, liquid hold-up and wall shear stress. Pressure build-up data were interpreted using established well test analysis techniques. Ali's experiments provided a qualitative and quantitative understanding of the effects of gas rates, liquid rates and rising gas bubbles on WPR and phase re-injection. WPR was found to have a higher effect than water flow rate on WPR. This was most probably due to annular flow being the predominant flow regime for the experiments. Phase re-injection was successfully simulated. The lower the "reservoir" pressure, the higher the liquid re-injection, an analogue to low-permeability reservoirs. For a closed system, WPR was shown to take place. Rising gas causes an increase in bottomhole pressure. Further details of this study are given in the thesis of Ali (2004) and in an SPE paper (Ali *et al.*, 2005); the present author was a co-author of this paper and a copy of it is appended to this thesis for reference.

Though the results of the experiments in the first study were revealing, they are complex as they reflect the real well situation. To obtain results in which the phase redistribution in the well is studied independently of the interactions with the reservoir, a further MSc project (Al-Darmaki, 2005) was carried out, in which the LOTUS tube was isolated at both the top and the bottom at the same time. The test section was again the LOTUS 10.8m long, 32mm internal diameter vertical tube. A

two-phase flow was set up with known air and water flow rates. The pressure distribution and void fraction were measured for the steady-state flow and the flow subsequently shut down by simultaneously closing valves at the top and at the bottom of the test section. Pressure distribution was measured during the transient following shut-in and for the steady-state final condition in which there was a liquid-filled zone at the bottom of the test section and a gas-filled zone at the top.

Although the Al-Darmaki experiments covered a wide range of conditions (up to and including annular flow), a substantial number of tests were conducted in the bubble flow regime and can thus be analysed by a simple model, based on the one-dimensional model for bubbly flow presented in Section 1.3. Such a model was developed and implemented, and compared with the experimental data.

In what follows, Section 5.3 describes the model, Section 5.4 briefly presents comparisons between the model and the Al-Darmaki experiments and, finally, Section 5.5 draws some conclusions from the exercise.

5.3 A model for transient bubbly flow

In the bubbly flow model described here, the simplifying assumptions made are as follows:

- That the pressure changes occurring in the well are due entirely to gravity effects. Thus, pressure changes due to friction and acceleration are neglected. This is often a reasonable assumption for bubble flow.
- That the gas phase obeys the perfect gas law. Again, this is a reasonable assumption for the low pressure range covered in the Al-Darmaki experiments. It would not, of course, be reasonable for the high pressure conditions applying in many wells.
- That the mass of the bubbles remains constant along the channel – i.e. that no bubble break-up of coalescence occurs. This is consistent with some experimental findings. However, the bubble diameter may change as the pressure, and hence the gas density, changes.

- That the flow is one-dimensional in that the phase velocities and phase fractions remain constant over a given cross section. This means that the flow can then be considered in terms of the one-dimensional models pioneered by Wallis (1969) and described in Section 1.3.

In what follows, the steady state case will be considered first and then aspects of the transient following shut- in will be considered.

5.3.1 Well with bubbly flow in steady-state

Let us assume that we form a bubble flow at the tube entrance in which the superficial velocity of the liquid is U_L and the superficial velocity of the gas is U_{G0}. It is assumed that the superficial velocity of the liquid remains constant over the whole length of the tube and that the superficial velocity of the gas is given by:

$$U_G = U_{G0} p_0 / p \qquad \textbf{Eq.5 - 1}$$

where p_0 is the pressure at the bottom of the tube and p is the pressure at a distance z from the bottom. We may define a drift flux j_{GL} which is the flux of gas moving through a plane passing along the tube at the total superficial velocity (U_G+U_L). Classically (see Section 1.3) this is given by the mass balance:

$$j_{GL} = U_G(1-\varepsilon_G) - U_L \varepsilon_G \qquad \textbf{Eq.5 - 2}$$

where ε_G is the void fraction, and by the physical relationship:

$$j_{GL} = \varepsilon_G u_\infty (1-\varepsilon_G)^n \qquad \textbf{Eq.5 - 3}$$

where u_∞ is the rise velocity of the bubble in an infinite fluid (assumed to be 0.24 m/s for a typical air-water flow) and n is and empirical constant with a typical value of 2. If we make the assumption that the second term on the RHS of the above equation is close to unity (which it will tend to at lower void fractions), then we have:

$$j_{GL} \approx \varepsilon_G u_\infty \qquad \textbf{Eq.5 - 4}$$

and combining this with the mass balance equation it follows that:

$$\varepsilon_G = \frac{U_G}{(u_\infty + U_G + U_L)} \qquad \textbf{Eq.5 - 5}$$

The gravitational pressure gradient is given by:

$$-\frac{dp}{dz} = g[\varepsilon_G \rho_G + (1 - \varepsilon_G \rho_L)] \qquad \textbf{Eq.5 - 6}$$

where ρ_G and ρ_L are the gas and liquid density, respectively. Thus:

$$-\frac{\frac{dp}{dz} + \rho_L g}{(\rho_G g - \rho_L g)} = \varepsilon_G = \frac{U_G}{u_\infty + U_G + U_L} = \frac{\frac{U_{G0} p_0}{p}}{u_\infty + \frac{U_{G0} p_0}{p} + U_L} \qquad \textbf{Eq.5 - 7}$$

Noting that:

$$\rho_G = \frac{p}{RT} \qquad \textbf{Eq.5 - 8}$$

and rearranging, we have:

$$-\frac{dp}{dz} = \frac{g\frac{U_{G0} p_0 p}{RT} + (u_\infty + U_L)\rho_L g p}{(u_\infty + U_L)p + U_{G0} p_0} = \frac{(a+b)p}{cp+d} \qquad \textbf{Eq.5 - 9}$$

where:

$$a = g\frac{U_{G0} p_0}{RT} \qquad \textbf{Eq.5 - 10}$$

$$b = (u_\infty + U_L)\rho_L g \qquad \textbf{Eq.5 - 11}$$

$$c = (u_\infty + U_L) \qquad \textbf{Eq.5 - 12}$$

$$d = U_{G0} p_0 \qquad \textbf{Eq.5 - 13}$$

Integrating, we have:

$$\int_{p_0}^{p}\frac{(cp+d)dp}{(a+b)p}=\int_{0}^{z}dz=z=e(p_0-p)+h\log\left(\frac{p_0}{p}\right) \qquad \textbf{Eq.5 - 14}$$

where:

$$e=\frac{c}{(a+b)} \qquad \textbf{Eq.5 - 15}$$

$$h=\frac{d}{(a+b)} \qquad \textbf{Eq.5 - 16}$$

5.3.2 Situation after shut-in

After shut-in, the gas passes to the top of the tube and the liquid falls to the bottom. We can determine the total volume of gas in the tube (V_{GT}) from the integral:

$$V_{GT}=\frac{\pi d^2}{4}\int_{0}^{L}\varepsilon_G dz \qquad \textbf{Eq.5 - 17}$$

Where d is the tube diameter, L the tube length and ε_G the local void fraction. Similarly, the mass of gas in the tube (M_{GT}) after shut-in is given by the integral:

$$M_{GT}=\frac{\pi d^2}{4}\int_{0}^{L}\varepsilon_G\rho_G dz \qquad \textbf{Eq.5 - 18}$$

The pressure p_G in the final gas volume at the top of the tube is given by the ideal gas law as:

$$p_G=\frac{RTM_{GT}}{V_{GT}} \qquad \textbf{Eq.5 - 19}$$

The length (L_{liq}) of the liquid column collected at the bottom of the tube is given by:

$$L_{liq} = \frac{L - V_{GT}}{\frac{\pi d^2}{4}} \qquad \textbf{Eq.5 - 20}$$

Thus, the final bottom pressure in the tube (p_S) is:

$$p_S = \rho_L g L_{liq} + p_G \qquad \textbf{Eq.5 - 21}$$

The time for completion of the shut-in transient is simply $\frac{L_{liq}}{u_\infty}$.

5.3.3 Implementation

The model was implemented using an EXCEL spreadsheet. The first step was to calculate z for a series of values of p descending in small fixed intervals (Δp) from an initial value p_0. The range chosen was such that the calculated z values encompassed the actual tube length L. This gave the steady-state pressure distribution. The local values of ε_G were calculated and the integrals **Eq.5 – 17** and **Eq.5 - 18** evaluated numerically by the expressions:

$$V_{GT} = \frac{\pi d^2}{4}\int_0^L \varepsilon_G dz = \frac{\pi d^2}{4}\sum_{n=1}^{n} \bar{\varepsilon}_G \Delta z \qquad \textbf{Eq.5 - 22}$$

$$M_{GT} = \frac{\pi d^2}{4}\int_0^L \varepsilon_G \rho_G dz = \frac{\pi d^2}{4}\sum_{n=1}^{n} \bar{\varepsilon}_G \rho_G \Delta z \qquad \textbf{Eq.5 - 23}$$

where $\bar{\varepsilon}_G$ is the mean void fraction in the element Δz corresponding to a change of pressure Δp.

5.4 Comparison with the experiments of Al-Darmaki

Comparisons between the data obtained for bubbly flow by Al-Darmaki (2005) and the model described in Section 5.3 are shown in **Fig.5 – 1** and **Fig.5 – 2** (more extensive comparisons are given in the thesis by Al-Darmaki, 2005). **Fig.5 – 1** shows the experimental and predicted pressure distributions for the steady-state flow and for the situation after the flow was shut down. Good agreement is shown between

prediction and experiments. An interesting result is that the pressure rises after shut-in. This is due to the fact that the gas, initially at the bottom of the tube (which rises to the top after shut-in) has a higher density and the net result is to increase the supernatant gas pressure.

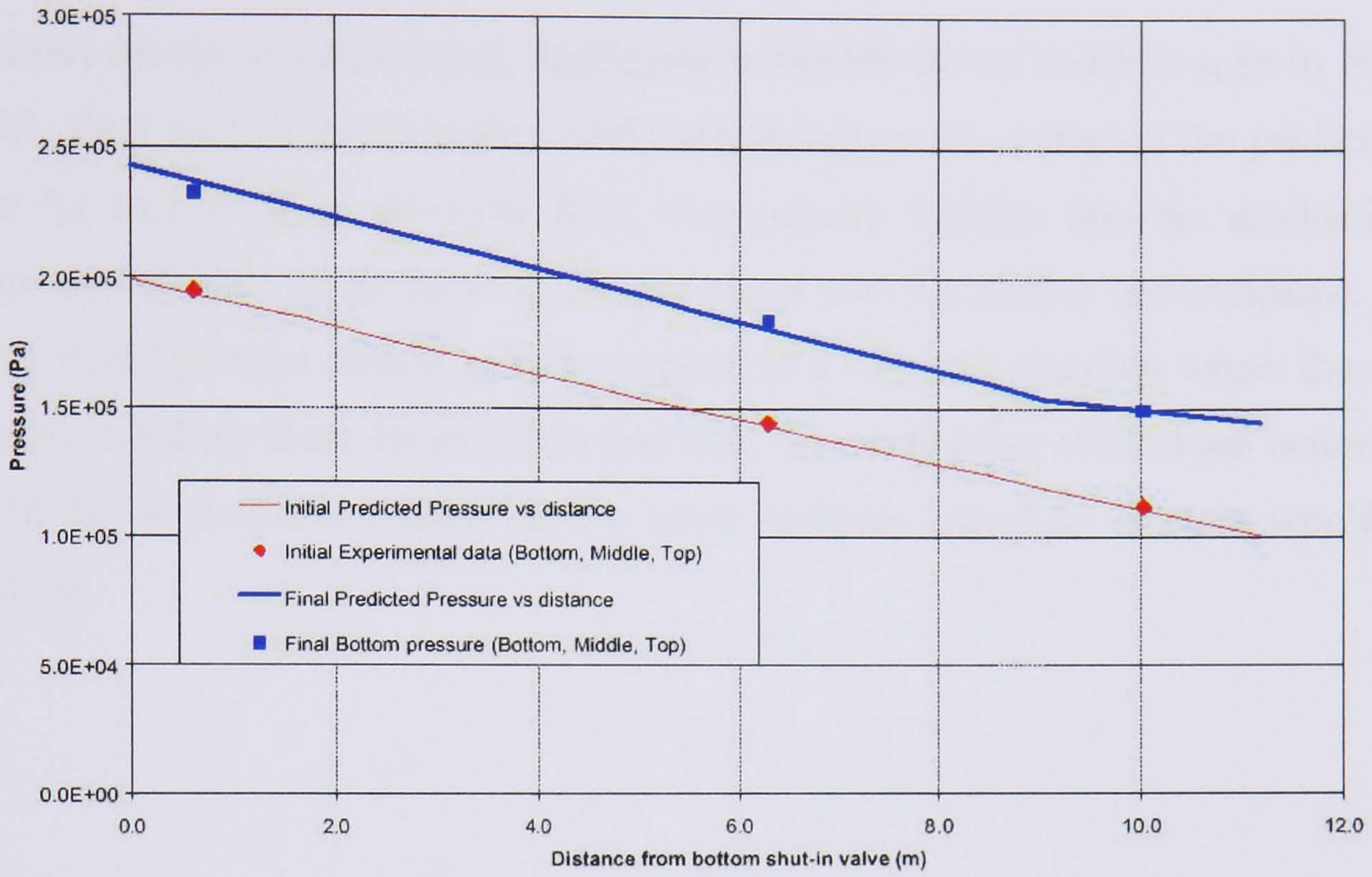


Fig.5 – 1: Comparison of predicted and observed pressure distributions during steady-state flow (in red) and after shut-in (in blue) (Al-Darmaki, 2005).

Fig.5 – 2 shows comparisons of the time taken after shut-in to reach the steady-state. Again, good agreement is obtained between the experiments and the predictions.

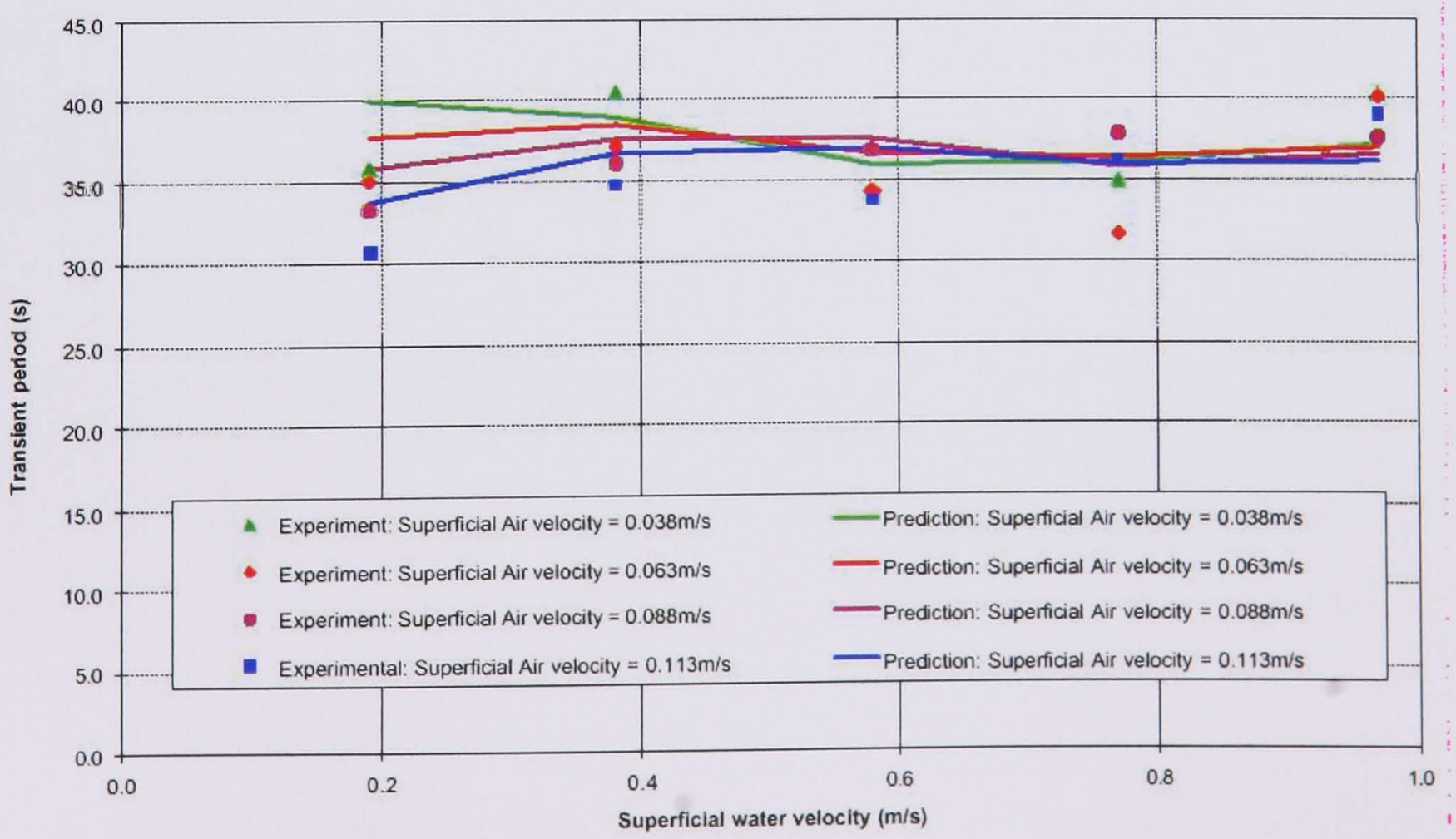


Fig.5 – 2: Comparison of predicted and observed times to reach steady-state after shut-in (Al-Darmaki, 2005).

5.5 Conclusions

The simple experiments carried out on the LOTUS facility gave very useful insights into wellbore behaviour and reservoir/wellbore interactions. They also provide a useful and well-defined data set against which models can be validated.

A simple model was developed, applicable to bubbly flows, and it is seen to fit the bubbly flow data of Al-Darmaki (2005) surprisingly well. Although the predictions were for shut-in of an air-water flow, they provide insights into the mechanisms which are valuable, as do the simple experiments with which they are compared. The model could perhaps occasionally be applied in a real well situation where the well remains in bubbly flow. However, in this case, the assumption of ideal gas behaviour would be of doubtful validity and a more complex equation of state would be required.

CHAPTER 6

Wellbore modelling as an aid to Well Test Analysis for Gas Condensate Reservoirs: GRAMP2

6.1 Introduction

This chapter deals with the modelling of flows in vertical pipes and its application to the prediction of well performance at high gas content. It describes the evolution of a previously-developed code (GRAMP2) for the prediction of steady-state flows in wells. The aim of wellbore modelling as an aid to well test analysis is to develop a methodology for predicting pressure changes along the well.

6.2 Background to GRAMP2

GRAMP2 is a flow pattern based wellbore modelling code for the solution of one-dimensional two phase flow. GRAMP2 embodies the phenomenological prediction models described in Section 1.3 for all regimes between single-phase and dispersed annular flow.

The original version of GRAMP, conceived for air-water annular flow calculations, was written by Neil Hawkes at Imperial College between 1994 and 1996. In its initial

version, the code was unable to handle sub-annular flow regimes, which were dealt with by using Friedel's two-phase pressure drop correlation.

During his Ph.D. work at Imperial College, Jader Barbosa wrote MULTIGRAMP. This was essentially GRAMP extended to deal with binary and multicomponent mixtures, by taking into account mixture effects in both fluid flow and heat transfer.

In 2001, a more refined treatment of the sub-annular flow patterns was implemented by Jader Barbosa, together with a black-oil fluid characterisation.

Another modification to the code was made by Jader Barbosa in 2004. GRAMP2 now integrates the energy equation together with the momentum equation. This means that it is now no longer required to assume an *a priori* temperature profile along the wellbore.

The aim of the work presented in this thesis was to use two-phase flow modelling (GRAMP2) for the investigation of WPR effects in well test analysis (described in Chapter 4). However, the modelling of WPR effects requires transient multiphase flow modelling, where counter-current flow, phase re-injection into the reservoir and afterflow from the reservoir can occur. This is arguably the most complicated case to handle in wellbore modelling and implies a dynamic link to the reservoir equations. Thus, it was decided to approach the problem in steps, starting from the available steady-state version of GRAMP2.

6.3 Enhancements to the code: compositional PVT characterisation

During the work presented in this thesis, a fully compositional characterisation of the fluids was added to the existing steady-state version of GRAMP2 as an alternative to the black-oil characterisation.

Within the group working on the JIP on Well Test Analysis for Gas Condensate and Volatile Oil Reservoirs, the reservoir engineering team was using the compositional numerical simulator Eclipse300 for the modelling of the reservoir. Eclipse300 is a product by GeoQuest, linked to another GeoQuest software package, PVTi, for the initial compositional fluids characterisation. The grid blocks in an Eclipse 300 reservoir model are initialised with the PVT characterisation made in PVTi. Once the reservoir simulation is started, the change of fluids properties with time (and pressure)

is simulated within Eclipse300 itself, by means of the same Equation of State (EoS) and flash calculations as in PVTi.

Thus, two alternatives were initially considered to make GRAMP2 work in compositional mode and link it to the results obtained by the reservoir engineering group using Eclipse300:

- Build an interface between GRAMP2 and PVTi.
- Implement in GRAMP2 the same EoS and flash calculations as in PVTi/Eclipse300.

6.6.1 Building an interface between GRAMP2 and PVTi

PVTi is a commercial software package which is usually not sold by Geoquest as a stand-alone PVT simulator but rather as part of the Eclipse suite. Eclipse is arguably the market leader of reservoir simulation software packages in the oil and gas business, therefore GeoQuest are very concerned about the confidentiality of the code. PVTi is not the market leader of PVT simulation packages but is a "must have" for those who want to run Eclipse300. PVTi was not conceived as a tool for code developers and no straightforward interface with external codes is provided by GeoQuest. Thus, it was concluded that an interface between GRAMP2 and PVTi was not the best way forward for the purpose of this Ph.D. work.

6.6.2 Implementing EoS and flash calculations in GRAMP2

In this approach, the main concern was the consistency between the EoS to be implemented in GRAMP2 and that incorporated in PVTi.

The workflow PVTi – Eclipse300 – GRAMP2 was to be as follows:

1. Perform an initial fluid characterisation with PVTi.

2. Initialise Eclipse300 with that PVT characterisation and let it run for the required number of time steps (till the time step corresponding to the beginning of the well test, for instance).

3. Stop Eclipse300 and extract z_i, x_i, y_i (mole fraction of component i in mixture, liquid phase and vapour phase) from the results of the reservoir simulation.

4. Convert Q_o^{sc}, Q_g^{sc} (measured wellhead liquid and gas flow rates, reported at standard conditions) in mass flow rates, and assume that the total mass flow rate remains constant along the wellbore (steady-state conditions):

$$\dot{M}_{TOT}^{SC} = Q_o^{sc}\rho_0^{sc} + Q_g^{sc}\rho_g^{sc} = const = \dot{M}_{TOT}(P,T) \qquad \textbf{Eq.6 - 1}$$

where ρ_o^{sc}, ρ_g^{sc} (the oil and gas densities at standard conditions) can be obtained by performing a flash of the initial x_i, y_i at standard conditions (see point 10 below).

5. Calculate the gas mass fraction, x, and the gas and liquid mass flow rates, $\dot{M}_g, \dot{M}_o$, at bottom hole conditions using the relationships below:

$$\begin{cases} x(P,T) = \dfrac{\sum_{i=1}^{Nc} y_i * \sum_{j=1}^{Nc} y_j M_{w,j}}{\sum_{i=1}^{Nc} x_i * \sum_{j=1}^{Nc} x_j M_{w,j} + \sum_{i=1}^{Nc} y_i * \sum_{j=1}^{Nc} y_j M_{w,j}} \\ \dot{M}_g + \dot{M}_o = \dot{M}_{TOT} \\ \dfrac{\dot{M}_g}{\dot{M}_g + \dot{M}_o} = x(P,T) \end{cases} \qquad \textbf{Eq.6 - 2}$$

In this case, $P = P_{bh}$ (bottomhole pressure) and $T = T_{res}$ (reservoir temperature). An initial guess must be taken for the bottomhole pressure, P_{bh} to initiate the bottom-up calculations in GRAMP2. This could be the P_{bh} predicted by Eclipse300 at the final time step, for instance. The following can be obtained:

$$x(P_{bh}, T_{res}), \dot{M}_g(P_{bh}, T_{res}), \dot{M}_o(P_{bh}, T_{res})$$

6. Call a subroutine with the EoS to calculate the density of oil and gas at bottomhole conditions:

$$\rho_g(P_{bh}, T_{res}), \rho_o(P_{bh}, T_{res})$$

An example of the Peng-Robinson EoS implemented in FORTRAN is reported by Assael *et al.* (1996):

SUBROUTINE PR

```
&(T,P,IP,IS,X,TC,PC,OMEG,Y1,Y2,Y3,Y4,BK,D,H,S,FUG)
C
C    The subroutine calculates the following thermodynamic properties
C    of mixtures, as a function of temperature, T in [K], and pressure,
C    P in [PA]:
C         1) Molar Density                (D)  in [MOL/M3]
C         2) Molar Enthalpy               (H)  in [J/MOL]
C         3) Molar Entropy                (S)  in [J/MOL/K]
C         4) Partial Fugacity Coefficient (FUG) in [-]
C    based on the Peng & Robinson EoS
C
C    - Enthalpy and Entropy are arbitrary assumed to be equal to zero
C      at 273.15 K and 0.1013 MPA.
C    - Perfect-gas properties are calculated from perfect-gas Heat
C      Capacities as: CP=W1+W2*T+W3*(T**2)+W4*(T**3) in [J/MOL/K]
C      where W1=Sum(Xi*Y1i) etc.
C    - Two Switches are required from the subroutine:
C      IP = Phase specification switch (Liquid=1, Vapour=2)
C      IS = Number of components in mixture (Pure fluid=1)
C    - Other data required for each component (I) are:
C      mole fraction X (-), critical temperature, TC in [K], critical
C      pressure in [PA], and acentric factor, OMEG.
C    - Binary interaction parameters BK(I,J) must also be specified.
C
      INTEGER I,J,IS,IP
      DOUBLE PRECISION BT,AS(10),R,TC(IS),PC(IS),FM(10),OMEG(IS),
     &ALP(10),T,A(10),P,B(10),X(IS),AAT,AT,DT,BIP,BK(IS,IS),Z,F,
     &F1,H,D,S,W1,W2,W3,W4,Y1(IS),Y2(IS),Y3(IS),Y4(IS),PGH,T0,PGS,
     &DH,DS,XAAT,FILN,FUG(IS)
      DATA R,T0,P0/8.314,273.15,0.101325D+6/
C
C     Parameters calculation AT,BT,CT,DT &  AST,ALP
C
      BT=0.
      DO 100 I=1,IS
      AS(I)=0.45724*R*R*TC(I)*TC(I)/PC(I)
      FM(I)=0.37464+1.54226*OMEG(I)-0.26992*(OMEG(I)**2)
      ALP(I)=(1.+FM(I)*(1.-(T/TC(I))**.5))**2
      A(I)=0.45724*ALP(I)*(P/PC(I))/((T/TC(I))**2)
      B(I)=0.0778*(P/PC(I))/(T/TC(I))
```

```
100 BT=BT+X(I)*B(I)
    AAT=0.
    AT=0.
    DT=0.
    DO 200 I=1,IS
    DO 200 J=1,IS
    BIP=(1.-BK(I,J))
    AAT=AAT+X(I)*X(J)*BIP*((AS(I)*AS(J)*ALP(I)*ALP(J))**.5)
    AT=AT+X(I)*X(J)*BIP*((A(I)*A(J))**.5)
200 DT=DT+X(I)*X(J)*FM(J)*BIP*((AS(I)*ALP(I)*AS(J)*(T/TC(J)))**.5)
C
C    Density Calculation
C
    IF (IP.EQ.1) Z=0.01
    IF (IP.EQ.2) Z=0.8
300 F=(Z**3)-(1.-BT)*Z*Z+(AT-3.*(BT**2)-2.*BT)*Z-(AT*BT-BT*BT-BT**3)
    F1=(3.*Z*Z)-(2.*Z*(1.-BT))+(AT-3.*(BT**2)-2.*BT)
    H=F/F1
    Z=Z-H
    IF (DABS(H/Z).LE.0.0001) GOTO 400
    GOTO 300
400 D=P/(Z*R*T)
C
C    Perfect-gas Enthalpy & Entropy
C
    W1=0.
    W2=0.
    W3=0.
    W4=0.
    DO 500 I=1,IS
    W1=W1+X(I)*Y1(I)
    W2=W2+X(I)*Y2(I)
    W3=W3+X(I)*Y3(I)
500 W4=W4+X(I)*Y4(I)
    PGH=W1*(T-T0)+W2*((T**2)-(T0**2))/2.+W3*((T**3)-(T0**3))/3.
   &+W4*((T**4)-(T0**4))/4.
    PGS=W1*DLOG(T/T0)+W2*(T-T0)+W3*((T**2)-(T0**2))/2.
   &+W4*((T**3)-(T0**3))/3.-R*DLOG(P/P0)
C
C    Molar Enthalpy & Entropy
C
    DH=1.-Z+(AT/(2.828*BT))*(1.+DT/AAT)*DLOG((Z+2.414*BT)/
   &(Z-0.414*BT))
    H=(PGH-R*T*DH)
    DS=DLOG(Z-BT)-(BT*DT/(2.828*AT*AAT))*DLOG((Z+2.414*BT)/
   &(Z-0.414*BT))
    S=PGS+(R*DS)
C
C    Partial Fugacities
C
    DO 700 I=1,IS
    XAAT=0.
    DO 800 J=1,IS
    BIP=(1.-BK(I,J))
800 XAAT=XAAT+X(J)*BIP*((AS(I)*AS(J)*ALP(I)*ALP(J))**.5)
    FILN=(B(I)*(Z-1.)/BT)-DLOG(Z-BT)+ (AT/(2.828*BT))*((B(I)/BT)-
   &(2.*XAAT/AAT))*DLOG((Z+2.414*BT)/(Z-0.414*BT))
700 FUG(I)=DEXP(FILN)
    RETURN
    END
```

The Peng-Robinson subroutine above is a two-parameter EoS while the EoS selected by the reservoir engineering team in PVTi/E300 was the three-parameter EoS. The so-called volume shift correction can be introduced to obtain the three-parameter EoS (Søreide et al., Report RE 88-8):

$$V_{mol,g}^{PR3} = V_{mol,g}^{PR2} - \sum_{i=1}^{Nc} y_i c_i$$

$$V_{mol,o}^{PR3} = V_{mol,o}^{PR2} - \sum_{i=1}^{Nc} x_i c_i \qquad \textbf{Eq.6 - 3}$$

$$c_i = S_i b_i$$

$$b_i = \Omega_b R \frac{T_{c_i}}{P_{c_i}}$$

where S_i are the dimensionless shift parameters and Ω_b is a constant. For $T=T_{res}$, the S_i can be directly exported from PVTi/E300, but for temperatures other than T_{res} a temperature-dependent correlation should be used.

7. Calculate the liquid and gas viscosities. The method selected by the reservoir engineering team in PVTi/E300 was the Lorentz-Bray-Clark (Lorentz *et al.* 1964).

8. Calculate the surface tension. The method selected by the reservoir engineering team in PVTi/E300 was the Macleod-Sudgen (Reid *et al.,* 1977). The surface tension σ is calculated as follows:

$$\sigma^{\frac{1}{4}} = \sum_{i=1}^{Nc} [P_i]\left(\rho_{mol,o,i} x_i - \rho_{mol,g,i} y_i\right) \qquad \textbf{Eq.6 - 4}$$

where P_i are the components parachors, which can be exported from PVTi/E300, and $\rho_{mol,o,i}, \rho_{mol,g,i}$ are the liquid and gas molar densities for the ith component (at the given P and T), respectively.

9. With this initial data set of gas and liquid properties at bottom hole conditions, GRAMP2 can initiate the flow calculations along the tubing.

GRAMP2 will identify the flow regime and calculate the ΔP for the first length step. It will then work out the P and T downstream of the first integration step of the GRAMP2 flow calculations:

$$P_2 = P_1 \pm \Delta P$$
$$T_2 = T_1 \pm \Delta T \qquad \textbf{Eq.6 - 5}$$

where, for the first length step, P_1 and T_1 are the bottom hole pressure and the reservoir temperature, respectively. A linear gradient approximation for the temperature was originally adopted in GRAMP2, prior to the developments that will be described in the next paragraph.

10. With the new P and T, perform flash calculations to work out the new x_i, y_i under thermodynamic equilibrium. First, an initial guess must be assigned to the equilibrium constants (K-values) of each component. This can be done by using Wilson's formula below:

$$K_i = \frac{\exp\left[5.37(1-\omega_i)\left(1-\frac{1}{T_{r_i}}\right)\right]}{P_{r_i}} \qquad \textbf{Eq.6 - 6}$$

where the ω_i (acentric factor), P_r (reduced pressure) and T_r (reduced temperature) that can be exported from PVTi/E300. In this formula, T is in ^{0}R and P is in psia.

Then the following flash equation is solved for the vapour fraction, α:

$$g(\alpha) = \sum_{i=1}^{Nc} \frac{z_i(K_i - 1)}{1 + \alpha(K_i - 1)} = 0 \qquad \textbf{Eq.6 - 7}$$

The above equation can be solved with Newton-Raphson (Ahmed, 2001):

a) Assume $\alpha = 0.5$ or $\alpha = \frac{A}{A-B}$, where:

$$\begin{cases} A = \sum_{i=1}^{Nc} \left[z_i \left(K_i - 1 \right) \right] \\ B = \sum_{i=1}^{Nc} \left[z_i \left(K_i - 1 \right) / K_i \right] \end{cases} \qquad \textbf{Eq.6 - 8}$$

b) Calculate $g(\alpha)$

c) If $g(\alpha) \leq 10^{-5}$ then the initial guess for α is correct → go to f)

d) If $g(\alpha) \succ 10^{-5}$ then calculate a new value for α as:

$$\alpha^{NEW} = \alpha^{OLD} - \frac{g(\alpha)}{g'(\alpha)} \qquad \textbf{Eq.6 - 9}$$

where

$$g'(\alpha) = -\sum_{i=1}^{Nc} \frac{z_i (K_i - 1)^2}{\left[\alpha (K_i - 1) + 1 \right]^2} \qquad \textbf{Eq.6 - 10}$$

e) Calculate x_i, y_i :

$$\begin{cases} x_i = \dfrac{z_i}{1 + \alpha (K_i - 1)} \\ y_i = \dfrac{K_i z_i}{1 + \alpha (K_i - 1)} \end{cases} \qquad \textbf{Eq.6 - 11}$$

f) Call the Peng-Robinson subroutine to calculate the fugacities of each component in the liquid and vapour phase. For a thermodynamic system to be in equilibrium, it is required that the fugacities in the liquid and vapour phase must be equal for each component. Thus, if:

$$\sum_{i=1}^{Nc} \left(\frac{f_{l,i}}{f_{v,i}} - 1 \right)^2 \leq \xi \qquad \textbf{Eq.6 - 12}$$

then the x_i, y_i calculated at step f) are OK and can be used as the new x_i, y_i for the next length step of the GRAMP2 flow calculations.

g) If:

$$\sum_{i=1}^{Nc}\left(\frac{f_{l,i}}{f_{v,i}}-1\right)^2 \succ \xi \qquad \textbf{Eq.6 - 13}$$

then assume new values for the K_i and start again from step a). The new K_i can be assigned as follows:

$$K_i^{NEW} = K_i^{OLD}\left(\frac{f_{l,i}}{f_{v,i}}\right) \qquad \textbf{Eq.6 - 14}$$

11. We now have P_2 and T_2 from step 9), $\rho_g(P_2,T_2), \rho_o(P_2,T_2)$ from the last iteration of step 10)-g), the gas and liquid viscosity and the surface tension from steps 7) and 8). We can calculate $x(P_2,T_2), \dot{M}_g(P_2,T_2), \dot{M}_o(P_2,T_2)$ from step 5), and therefore initiate the next integration step of the GRAMP2 flow calculations for the next well length section.

The implementation of the Peng-Robinson EoS, as shown above, solves the cubic equation for the Z-factor with the Newton-Raphson method by taking an initial guess for Z. Convergence problems could arise in some circumstances, especially near the critical point. Flash calculations solved for the molar fraction of vapour, as shown above, may also imply convergence problems.

Thus, the problem of implementing robust PVT calculations in FORTRAN for integration with GRAMP2 appeared to be non-trivial. This could have caused delays to and fallen beyond the scope of this Ph.D. work. This option for making GRAMP2 work in compositional mode was therefore discarded.

As the initial two alternatives to the problem had both been discarded, a third option was considered to make GRAMP2 work in compositional mode:

- Build an interface between GRAMP2 and Multiflash (a PVT software package developed by Infochem Computer Services Ltd)

6.6.3 Building an interface between GRAMP2 and Multiflash

It later emerged that Multiflash was a more suitable candidate for this specific application, due to the following reasons:

- Multiflash is written in FORTRAN 77/95 (the language of GRAMP2).
- For PC's, Multiflash is available as a Dynamic Link Library (DLL). The Multiflash modules can be exported from the DLL and imported in other software in a very flexible manner.
- Imperial College had already had positive experience using Multiflash for previous research work. The ongoing working relationship between Infochem and Imperial College was likely to guarantee a more direct involvement of Infochem during the implementation of the interface with GRAMP2, with obvious advantages to the work.

Multiflash is a comprehensive and flexible system that returns the thermo-physical properties of pure substances and mixtures and carries out phase and chemical equilibrium calculations for fluid and solid phases. Multiflash consists of a number of distinct software modules that may be used individually or together. These modules are: databanks; databank access software; pure component property evaluation; binary interaction parameter handling; mixture models for thermodynamic properties; mixture models for transport properties; phase equilibrium calculations; and chemical equilibrium calculations.

The Peng-Robinson three-parameter EoS, the Lorentz-Bray-Clark method for viscosity calculations and the Macleod-Sudgen method for surface tension calculations are all available in Multiflash. Although there is no 100% guarantee that they are implemented exactly in the same way as in PVTi, it is debatable whether PVTi performs better than Multiflash. Having also considered that the ultimate applicability of the compositional version of GRAMP2 would not be limited to the purpose of the JIP on Well Test Analysis, where PVTi is adopted, it was concluded

that building a FORTRAN interface between GRAMP2 and Multiflash was going to be the most robust option.

6.4 Enhancements to the code: temperature calculation

During the work presented in this thesis, a new way of calculating the temperature at every integration step was implemented, thus allowing for the elimination of the linear gradient approximation originally adopted in GRAMP2. As a consequence of the integration of GRAMP2 with compositional PVT calculations, it is possible to write the temperature as a function of the pressure and the composition of the stream. Multiflash allows performing flashes where the variable temperature is adjusted to satisfy a constraint, which can be the gas fraction, for a given pressure. This kind of problem may not have a unique solution. However, in steady-state flow calculations, starting from known temperature and pressure at bottomhole conditions and using very small steps for the integration, it is unlikely that these flashes will cause instability. The following paragraph will show how the new temperature calculations were implemented within the compositional version of GRAMP2.

6.5 GRAMP2: new (compositional) version

The GRAMP2 code was modified to solve the energy equation together with the momentum equation, with the local pressure and the local quality as the dependent variables. For the specific case of annular flow, the mass conservation equation is also added to the integration. The local flow patterns are evaluated at each integration step and a specific set of closure relationships are embedded into the conservation equations, depending on the flow pattern. A detailed description of the flow patter based models implemented in GRAMP2 can be found in the original report written by Barbosa and Hewitt (2001).

The one-dimensional, steady-state momentum conservation equation for two-phase gas-liquid flow can be written in terms of the total pressure gradient, $\frac{dp}{dz}$:

$$-\frac{dp}{dz} = -\frac{p}{A}\left(\frac{dA}{dz}\right) - \left.\frac{dp}{dz}\right|_f - \left.\frac{dp}{dz}\right|_g - \left.\frac{dp}{dz}\right|_a \qquad \textbf{Eq.6 - 15}$$

where the subscripts *f, g*, and *a* denote the individual contributions due to friction, gravity and flow acceleration, respectively.

The first term on the right hand side of the above relationship is due to a change in cross-sectional area and reduces to zero for flows in channels of constant cross-sectional area.

The frictional contribution is calculated as a function of the flow pattern (bubble, slug, churn or annular) identified, taking into account phenomenological aspects of the distribution of the phases in the channel.

The gravitational contribution is given by:

$$-\left.\frac{dp}{dz}\right|_g = [(1-\varepsilon_G)\rho_L + \varepsilon_G\rho_G]g\sin\theta \qquad \textbf{Eq.6 - 16}$$

where ε_G is the void fraction, ρ_L and ρ_G are the liquid and gas density, respectively, and θ is the deviation from the vertical axis.

The acceleration contribution is given by:

$$-\left.\frac{dp}{dz}\right|_a = \frac{1}{A}\frac{d}{dz}\left[\frac{G^2 x_G{}^2 A}{\rho_G\varepsilon_G} + \frac{G^2(1-x_G)^2 A}{\rho_L(1-\varepsilon_G)}\right] \qquad \textbf{Eq.6 - 17}$$

which, for a constant total mass flux, can be expanded as follows to account for axial variations of gas mass fraction, ε_G, ρ_L and ρ_G :

$$-\left.\frac{dp}{dz}\right|_a = G^2\left[\frac{x_G{}^2}{\rho_G\varepsilon_G} + \frac{(1-x_G)^2}{\rho_L(1-\varepsilon_G)}\right]\frac{dA}{dz} + G^2\frac{dx_G}{dz}\left[\frac{2x_G}{\rho_G\varepsilon} - \frac{2(1-x_G)}{\rho_L(1-\varepsilon_G)}\right]$$
$$-G^2\frac{d\rho_G}{dz}\left(\frac{x_G{}^2}{\rho_G^2\varepsilon_G}\right) - G^2\frac{d\rho_L}{dz}\left[\frac{(1-x_G)^2}{\rho_L^2(1-\varepsilon_G)}\right] + G^2\frac{d\varepsilon_G}{dz}\left[\frac{(1-x_G)^2}{\rho_L(1-\varepsilon_G)^2} - \frac{x_G{}^2}{\rho_G\varepsilon_G{}^2}\right]$$

Eq.6 - 18

The energy equation is derived from the first law of thermodynamics, which states that the rate of change of energy of a fluid particle is equal to the net rate of heat exchanged by the control volume plus the net rate of work done on the particle by external forces. The energy of a fluid can be defined as the sum of internal (thermal)

energy, kinetic energy and gravitational potential energy. Thus, the energy conservation equation for two-phase gas-liquid flow, with the assumption of thermodynamic equilibrium, can be written as:

$$\frac{d}{dz}x_G = \frac{1}{h_{LG}}\left\{\frac{4}{d_T}\frac{\dot{q}}{G} - x_G\frac{dh_G}{dz} - (1-x_G)\frac{dh_L}{dz} - g - \frac{G^2}{2}\frac{d}{dz}\left[\frac{x_G^3}{\rho_G^2\varepsilon_G^2} + \frac{(1-x_G)^3}{\rho_L^2(1-\varepsilon_G)^2}\right]\right\}$$

Eq.6 - 19

where h_G and h_L are the gas and liquid enthalpy, respectively, d_T is the wellbore diameter, $h_{LG} = h_G - h_L$, and $\dot{q} = U(T - T_{out})$ is heat flux between formation and wellbore, proportional to a global heat transfer coefficient U to account for the heat transfer resistances inside and outside the tube.

The mass conservation equation for annular flow can be written as:

$$G = G_{LE} + G_G + G_{LF}$$ **Eq.6 - 20**

where G_{LE}, G_G and G_{LF} are the mass fluxes of entrained liquid droplets, gas in the core and liquid in the film, respectively.

In terms of phase mass fractions, the above relationship becomes:

$$1 = x_{LE} + x_G + x_{LF}$$ **Eq.6 - 21**

where x_{LE} and x_{LF} are the fractions of liquid entrained and liquid in the film, respectively.

Introducing the fraction of liquid flow entrained as droplets in the gas core, e_F:

$$e_F = \frac{G_{LE}}{G_{LE} + G_{LF}} = \frac{x_{LE}}{x_{LE} + x_{LF}}$$ **Eq.6 - 22**

Using the conservation equation for the mass fraction:

$$\frac{d}{dz}x_{LE} = \frac{4}{d_T G}(E - D) \qquad \textbf{Eq.6 - 23}$$

(with D and E are deposition and entrainment mass flow rates of droplets per unit perimeter area) and considering that:

$$\frac{d}{dz}x_{LE} + \frac{d}{dz}x_{LF} + \frac{d}{dz}x_G = 0, \qquad \textbf{Eq.6 - 24}$$

it is possible to derive an equation for the entrained fraction as a function of distance:

$$\frac{de_F}{dz} = \frac{1}{(1-x_G)}\left[\frac{4}{d_T G}(E-D) + e_F\frac{dx_G}{dz}\right] \qquad \textbf{Eq.6 - 25}$$

By arranging the energy and momentum equations with P and x_G as independent variables, a linear system of equations is obtained:

$$\begin{cases} a\dfrac{dp}{dz} + b\dfrac{dx_G}{dz} = c \\ d\dfrac{dp}{dz} + e\dfrac{dx_G}{dz} = f \end{cases} \qquad \textbf{Eq.6 - 26}$$

where the coefficients are as follows:

$$a = 1 + EK13 \qquad \textbf{Eq.6 - 27}$$

$$b = (EK4 + EK5\ VK1) + EK9(EK7 + EK5\ VK2) + EK11(EK6 + EK5\ VK3) \qquad \textbf{Eq.6 - 28}$$

$$c = -\left.\frac{dp}{dz}\right|_f - \left.\frac{dp}{dz}\right|_g \qquad \textbf{Eq.6 - 29}$$

$$d = EK19 + (1 - x_G)EK20 + x_G EK22 \qquad \textbf{Eq.6 - 30}$$

$$e = h_{LG} + EK18 + (1 - x_G)EK21 + x_G EK23 \qquad \textbf{Eq.6 - 31}$$

$$f = \frac{4\dot{q}}{d_T G} - g \qquad \textbf{Eq.6 - 32}$$

where

$$EK23 = \left(\frac{\partial h_G}{\partial T} \frac{\partial T}{\partial x_G} + \frac{\partial h_G}{\partial x_G} \right)$$ **Eq.6 - 33**

$$EK22 = \left(\frac{\partial h_G}{\partial p} + \frac{\partial h_G}{\partial T} \frac{\partial T}{\partial p} \right)$$ **Eq.6 - 34**

$$EK21 = \left(\frac{\partial h_L}{\partial T} \frac{\partial T}{\partial x_G} + \frac{\partial h_L}{\partial x_G} \right)$$ **Eq.6 - 35**

$$EK20 = \left(\frac{\partial h_L}{\partial p} + \frac{\partial h_L}{\partial T} \frac{\partial T}{\partial p} \right)$$ **Eq.6 - 36**

$$EK19 = EK10\left(EK16 + VK3\,EK15\right) + EK8\left(EK17 + VK2\,EK15\right)$$ **Eq.6 - 37**

$$EK18 = \left(EK14 + EK15VK1\right) + EK11\left(EK16 + VK3\,EK15\right) + EK9\left(EK17 + VK2\,EK15\right)$$ **Eq.6 - 38**

$$EK17 = -G^2 \frac{\left(1 - x_G\right)^3}{\rho_L^3 \left(1 - \varepsilon_G\right)^2}$$ **Eq.6 - 39**

$$EK16 = -G^2 \frac{x_G^3}{\rho_G^3 \varepsilon_G^2}$$ **Eq.6 - 40**

$$EK15 = G^2 \left[\frac{\left(1 - x_G\right)^3}{\rho_L^2 \left(1 - \varepsilon_G\right)^3} - \frac{x_G^3}{\rho_G^2 \varepsilon_G^3} \right]$$ **Eq.6 - 41**

$$EK14 = \frac{3}{2} G^2 \left[\frac{x_G^2}{\rho_G^2 \varepsilon_G^2} + \frac{\left(1 - x_G\right)^2}{\rho_L^2 \left(1 - \varepsilon_G\right)^2} \right]$$ **Eq.6 - 42**

$$EK13 = EK8\left(EK7 + VK2\,EK5\right) + EK10\left(EK6 + VK3\,EK5\right)$$ **Eq.6 - 43**

$$EK12 = \left(EK4 + EK5\ VK1\right) + EK9\left(EK7 + VK2\,EK5\right) + EK11\left(EK6 + VK3\,EK5\right)$$ **Eq.6 - 44**

$$EK11 = \left(\frac{\partial \rho_G}{\partial T} \frac{\partial T}{\partial x_G} + \frac{\partial \rho_G}{\partial x_G} \right)$$ **Eq.6 - 45**

$$EK10 = \left(\frac{\partial \rho_G}{\partial p} + \frac{\partial \rho_G}{\partial T} \frac{\partial T}{\partial p} \right)$$ **Eq.6 - 46**

$$EK9 = \left(\frac{\partial \rho_L}{\partial T} \frac{\partial T}{\partial x_G} + \frac{\partial \rho_L}{\partial x_G} \right)$$ **Eq.6 - 47**

$$EK8 = \left(\frac{\partial \rho_L}{\partial p} + \frac{\partial \rho_L}{\partial T} \frac{\partial T}{\partial p} \right)$$ **Eq.6 - 48**

$$EK7 = -G^2 \frac{(1 - x_G)^2}{\rho_L^2 (1 - \varepsilon_G)}$$ **Eq.6 - 49**

$$EK6 = -G^2 \frac{x_G^2}{\rho_G^2 \varepsilon_G}$$ **Eq.6 - 50**

$$EK5 = G^2 \left[\frac{(1 - x_G)^2}{\rho_L (1 - \varepsilon_G)^2} - \frac{x_G^2}{\rho_G \varepsilon_G^2} \right]$$ **Eq.6 - 51**

$$EK4 = 2G^2 \left[\frac{x_G}{\rho_G \varepsilon_G} + \frac{(1 - x_G)}{\rho_L (1 - \varepsilon_G)} \right]$$ **Eq.6 - 52**

The solution of the linear system above is:

$$\begin{cases} \dfrac{dx_G}{dz} = \dfrac{cd - af}{bd - ae} \\ \dfrac{dP}{dz} = \dfrac{cd}{da} - \dfrac{bd}{da} \dfrac{(cd - af)}{(bd - ae)} \end{cases}$$ **Eq.6 - 53**

In GRAMP2, the above equations are integrated along the wellbore (Runge-Kutta integration of the 4th order - Barbosa and Hewitt, 2001) to determine the local quality and pressure. However, closure relationships are required to close the system. While x_G, ρ_L, ρ_G, h_G and h_L are obtained from flashes at given pressure and temperature, $\left.\frac{dp}{dz}\right|_f$ and ε_G are obtained from relationships specific to the flow pattern identified. $\frac{d\varepsilon_G}{dz}$ is derived from the derivation of a universal (i.e. valid for all flow regimes) drift-flux relationship (Collier and Thome, 1994):

$$\varepsilon_G = \frac{1}{C_0 \left[1 + \frac{\rho_G}{\rho_L} \frac{(1 - x_G)}{x_G} \right] + \frac{\rho_G}{G x_G} \bar{u}_{Gj}}$$ **Eq.6 - 54**

where:

$$C_0 = 1.13$$ **Eq.6 - 55**

$$\bar{u}_{Gj} = 1.41\left[\sigma g \frac{(\rho_L - \rho_G)}{\rho_L^2}\right]^{1/4} \qquad \textbf{Eq.6 - 56}$$

The gradient $\frac{d\varepsilon_G}{dz}$ can be written as:

$$\frac{d\varepsilon_G}{dz} = VK1\frac{dx_G}{dz} + VK2\frac{d\rho_L}{dz} + VK3\frac{d\rho_G}{dz} \qquad \textbf{Eq.6 - 57}$$

where:

$$VK1 = \frac{A3 + C_0(A6 + A7)}{A0} \qquad \textbf{Eq.6 - 58}$$

$$VK2 = \frac{1}{A0}\left[C_0 A5 - A2\frac{C1}{B0}(B2 - B1)\right] \qquad \textbf{Eq.6 - 59}$$

$$VK3 = \frac{1}{A0}\left[\frac{C1}{B0}A2B2 - (A1 + C_0 A4)\right] \qquad \textbf{Eq.6 - 60}$$

$$A1 = \frac{\bar{u}_{Gj}}{Gx_G} \qquad \textbf{Eq.6 - 61}$$

$$A2 = \frac{\rho_G}{Gx_G} \qquad \textbf{Eq.6 - 62}$$

$$A3 = \frac{\rho_G \bar{u}_{Gj}}{Gx_G^2} \qquad \textbf{Eq.6 - 63}$$

$$A4 = \frac{(1 - x_G)}{\rho_L x_G} \qquad \textbf{Eq.6 - 64}$$

$$A5 = \frac{\rho_G(1 - x_G)}{\rho_L^2 x_G} \qquad \textbf{Eq.6 - 65}$$

$$A6 = \frac{\rho_G(1 - x_G)}{\rho_L x_G^2} \qquad \textbf{Eq.6 - 66}$$

$$A7 = \frac{\rho_G}{\rho_L x_G} \qquad \textbf{Eq.6 - 67}$$

$$A0 = \left[C_0 \left(1 + \frac{\rho_G (1 - x_G)}{\rho_L x_G} \right) + \frac{\rho_G \overline{u}_{Gj}}{G x_G} \right]^2 \qquad \textbf{Eq.6 - 68}$$

$$B1 = 2\sigma g \frac{(\rho_L - \rho_G)}{\rho_L^3} \qquad \textbf{Eq.6 - 69}$$

$$B2 = \frac{\sigma g}{\rho_L^2} \qquad \textbf{Eq.6 - 70}$$

$$B0 = 4 \left[\sigma g \frac{(\rho_L - \rho_G)}{\rho_L^2} \right]^{3/4} \qquad \textbf{Eq.6 - 71}$$

The remaining information required to close the above linear system of equations are the gradients of ρ_L, ρ_G, h_G and h_L. For ρ_L it is possible to write:

$$\frac{d\rho_L}{dz} = \frac{\partial \rho_L}{\partial P} \frac{dP}{dz} + \frac{\partial \rho_L}{\partial T} \frac{dT}{dz} + \sum_i^{Nc} \frac{\partial \rho_L}{\partial x_i} \frac{dx_i}{dz} \qquad \textbf{Eq.6 - 72}$$

and using the relationships:

$$T = T(P, x_1, x_2, ..., x_N) \qquad \textbf{Eq.6 - 73}$$

we obtain:

$$\frac{d\rho_L}{dz} = \left(\frac{\partial \rho_L}{\partial P} + \frac{\partial \rho_L}{\partial T} \frac{\partial T}{\partial P} \right) \frac{dP}{dz} + \sum_i^{Nc} \left(\frac{\partial \rho_L}{\partial T} \frac{\partial T}{\partial x_i} + \frac{\partial \rho_L}{\partial x_i} \right) \frac{dx_i}{dz} \qquad \textbf{Eq.6 - 74}$$

Introducing a relationship between molar fractions x_i and gas mass fraction x_G, we can write:

$$\frac{d\rho_L}{dz} = \left(\frac{\partial \rho_L}{\partial P} + \frac{\partial \rho_L}{\partial T} \frac{\partial T}{\partial P} \right) \frac{dP}{dz} + \sum_i^{Nc} \left(\frac{\partial \rho_L}{\partial T} \frac{\partial T}{\partial x_i} + \frac{\partial \rho_L}{\partial x_i} \right) \frac{dx_i}{dx_G} \frac{dx_G}{dz} \qquad \textbf{Eq.6 - 75}$$

or:

$$\frac{d\rho_L}{dz} = \left(\frac{\partial \rho_L}{\partial P} + \frac{\partial \rho_L}{\partial T} \frac{\partial T}{\partial P} \right) \frac{dP}{dz} + \left(\frac{\partial \rho_L}{\partial T} \frac{\partial T}{\partial x_G} + \frac{d\rho_L}{dx_G} \right) \frac{dx_G}{dz} \qquad \textbf{Eq.6 - 76}$$

Analogue relationships can be written for the gradients of ρ_G, h_G and h_L.

The gradients of the thermodynamic properties of gas and liquid w.r.t. P, T and x_G can be obtained from flash calculations performed with Multiflash. For the specific case of the density, though, these gradients are not directly calculated by Multiflash. However, knowing that:

$$\rho_L = \frac{M_L}{V_L}, \qquad \textbf{Eq.6 - 77}$$

the gradients of phase density w.r.t. the independent variable θ (which are not directly calculated by Multiflash) can be obtained as follows:

$$\begin{cases} \dfrac{\partial \rho_L}{\partial \theta} = \dfrac{1}{V_L}\dfrac{\partial M_L}{\partial \theta} - \dfrac{M_L}{V_L^2}\dfrac{\partial V_L}{\partial \theta} \\ M_L = \sum_i x_i M_i \\ \dfrac{\partial M_L}{\partial \theta} = \sum_i M_i \dfrac{\partial x_i}{\partial \theta} \end{cases} \qquad \textbf{Eq.6 - 78}$$

where V is the liquid volume.

The simplified sequence followed by GRAMP2 for one integration step, based on the system of energy and momentum equations (plus the mass conservation equation for annular flow), is:

- Identification of the flow pattern.
- Calculation of $\left.\dfrac{dp}{dz}\right|_f$ and ε_G from relationships specific to the flow pattern identified.
- Calculation of thermodynamic properties of gas and liquid phases, together with their gradients w.r.t. P, T and x_G (with Multiflash).
- Calculation of parameters EK4 to EK23.
- Runge-Kutta integration to calculate $\dfrac{dp}{dz}$ and x_G (plus e_F for annular flow).

- Updating of P (from previous value of P and $\frac{dp}{dz}$) and T (from new P and from new x_G, with Multiflash) for the following integration step.

In annular flow, the liquid flows as a film along the pipe wall, with some droplets entrained in the gas core. The following assumptions are made:

- Steady-state flow;
- One-dimensional flow;
- Film thickness uniform around the perimeter of the pipe;
- Mechanical equilibrium, i.e., constant pressure across an entire pipe section;
- Homogeneous flow in the core, i.e. no slippage between gas and entrained droplets.
- Thermodynamic equilibrium.

For the specific case of annular flow, the workflow of GRAMP2 is as illustrated in **Fig.6 – 1** below:

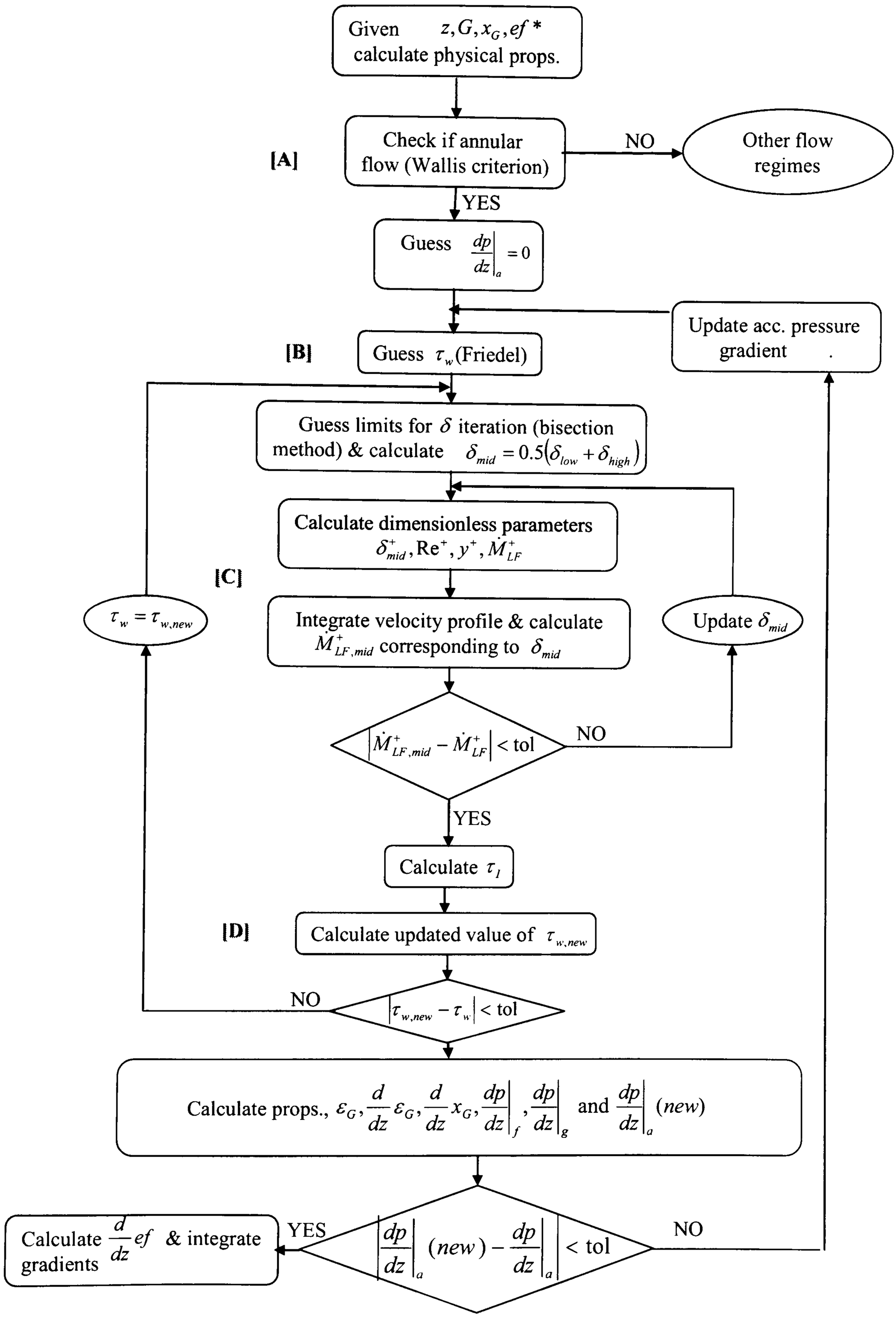


Fig.6 - 1: Workflow of GRAMP2 for annular flow regime.

With reference to **Fig.6 - 1**:

[A] The most commonly used criterion is that by Hewitt and Wallis (1963), based on the flooding correlation:

$$\sqrt{U_{GS}^*} + \sqrt{U_{LS}^*} \approx 1 \qquad \textbf{Eq.6 - 79}$$

with zero liquid down flow, i.e., $U_{LS}^* = 0$.

[B] The wall shear stress is initially guessed as:

$$\tau_w = \frac{d_T}{4}\left.\frac{dp}{dz}\right|_f \qquad \textbf{Eq.6 - 80}$$

where

$$-\left.\frac{dp}{dz}\right|_f = \phi_{LO}^2 \left.\frac{dp}{dz}\right|_{f,LO} \qquad \textbf{Eq.6 - 81}$$

ϕ_{LO}^2 is the "all liquid" two-phase multiplier and $\left.\frac{dp}{dz}\right|_{f,LO}$ is the frictional pressure drop for an equivalent single phase flow in which all the flow is assumed to be liquid. The method by Friedel (1979) is used here to calculate ϕ_{LO}^2.

[C] The "triangular relationship" (Hewitt, 1961) relates the liquid film flow rate, the liquid film thickness δ and the wall shear stress. If two of these parameters are known, the third can be determined.

The local shear stress τ (often approximately constant in the liquid film) is related to the gradient of liquid velocity in the film ($\frac{du_L}{dy}$) by the expression:

$$\tau = \eta_{eff}\left(\frac{du_L}{dy}\right) \qquad \textbf{Eq.6 - 82}$$

where η_{eff} is the effective viscosity calculated from a suitable turbulence model. The equation above is integrated to give the velocity profile in the film, which, in turn, is integrated to give the total liquid flow rate.

The local liquid film thickness, averaged along the perimeter of the cross sectional area, can be determined by matching the known value of the film flow rate at a certain distance with the integral of a hypothetical velocity profile across the film.

Several velocity profiles have been suggested in the literature. The Double Velocity Profile (DVP) proposed by Jensen (1987) is used in GRAMP2, as explained in the original GRAMP report by Barbosa and Hewitt (2001).

The dimensionless liquid film flow rate is defined as:

$$\dot{M}_{LF}^{+} \equiv \frac{\dot{M}_{LF}}{\pi d_T \eta_L} = \int_0^{\delta^+} u_{LF}^{+} \left(1 - \frac{y^+}{\mathrm{Re}^+}\right) dy^+ , \qquad \textbf{Eq.6 - 83}$$

where y^+ and δ^+ are the dimensionless co-ordinate with origin at the wall and the dimensionless film thickness, respectively. These are given by:

$$y^+ = \frac{\rho_L u^* y}{\eta_L} \qquad \textbf{Eq.6 - 84}$$

and

$$\delta^+ = \frac{\rho_L u^* \delta}{\eta_L} . \qquad \textbf{Eq.6 - 85}$$

Re^+ is the dimensionless pipe radius:

$$\mathrm{Re}^{+} = \frac{\rho_L u^{*} d_T}{2\eta_L}. \qquad \textbf{Eq.6 - 86}$$

u_{LF}^{+} is the dimensionless liquid film velocity:

$$u_{LF}^{+} = \frac{u_{LF}}{u^{*}} \qquad \textbf{Eq.6 - 87}$$

where u^{*} is the friction velocity:

$$u^{*} = \sqrt{\frac{\tau_w}{\rho_L}}. \qquad \textbf{Eq.6 - 88}$$

The von Kármán or Universal Velocity Profile (UVP) is given by:

$$u_{LF}^{*} = \begin{cases} y^{+} & \text{for } y^{+} \le 5 \\ -3.05 + 5\ln\left(y^{+}\right) & \text{for } 5 < y^{+} \le 30 \\ 5.46 + 2.5\ln\left(y^{+}\right) & \text{for } y^{+} > 30 \end{cases} \qquad \textbf{Eq.6 - 89}$$

Integration of the equations above provides the following relationships for the dimensionless liquid film flow rate:

$$\dot{M}_{LF}^{+} = \begin{cases} \frac{1}{2}\delta^{+^2} - \frac{1}{3}\delta^{+^3}; & \text{for } \delta^{+} \le 5 \\ 12.51 - 8.05\delta^{+} + 5\delta^{+}\ln\left(\delta^{+}\right) + \\ \qquad \frac{1}{\mathrm{Re}^{+}}\left[65.8 - 2.78\delta^{+} - 2.5\delta^{+^2}\ln\left(\delta^{+}\right)\right]; & \text{for } 5 < \delta^{+} \le 30 \\ -63.9 + 3\delta^{+} + 2.5\delta^{+}\ln\left(\delta^{+}\right) + \\ \qquad \frac{1}{\mathrm{Re}^{+}}\left[649.5 - 2.125\delta^{+^2} - 1.25\delta^{+^2}\ln\left(\delta^{+}\right)\right]; & \text{for } \delta^{+} > 30 \end{cases}$$

Eq.6 - 90

The DVP uses the UVP up to $y^+ = \delta^+/2$ and an inverted reflection of the UVP for $\delta^+/2 \le y^+ \le \delta^+$. In terms of the liquid film flow rate the DVP is given by:

$$\dot{M}_{LF}^{+} = \begin{cases} \dfrac{1}{2}\delta^{+^2} - \dfrac{1}{3}\delta^{+^3}; & \text{for } \delta^+ \le 10 \\ -3.05\delta^+ + 5\delta^+ \ln\left(\dfrac{\delta^+}{2}\right) + & \\ \dfrac{1}{\mathrm{Re}^+}\left[17.22 - 22.26\delta^+ + 0.594\delta^{+^2} - 2.5\delta^{+^2}\ln\left(\dfrac{\delta^+}{2}\right)\right]; & \text{for } 10 < \delta^+ \le 60 \\ 5.5\delta^+ + 2.5\delta^+ \ln\left(\dfrac{\delta^+}{2}\right) + & \\ \dfrac{1}{\mathrm{Re}^+}\left[1146 - 63.9\delta^+ - 3.688\delta^{+^2} - 1.25\delta^{+^2}\ln\left(\dfrac{\delta^+}{2}\right)\right]; & \text{for } \delta^+ > 60 \end{cases}$$

Eq.6 - 91

[D] The wall shear stress is calculated as:

$$\tau_w = \frac{R^2 - R_i^2}{2R}\left[\left(\rho_L - \rho_C\right)g - \left.\frac{dp}{dz}\right|_a + \frac{2R^2\tau_I}{R_i\left(R^2 - R_i^2\right)}\right] \qquad \textbf{Eq.6 - 92}$$

where ρ_C is the homogeneous core density, defined as:

$$\frac{1}{\rho_C} = \frac{\hat{x}_C}{\rho_G} + \frac{\left(1 - \hat{x}_C\right)}{\rho_L} \qquad \textbf{Eq.6 - 93}$$

with a homogeneous core quality $\hat{x}_C$ defined as:

$$\hat{x}_C \equiv \frac{G_G}{G_G + G_{LE}} = \frac{x_G}{x_G\left(1 - e_F\right) + e_F} \qquad \textbf{Eq.6 - 94}$$

and:

$$R = \frac{d_T}{2}, \qquad \textbf{Eq.6 - 95}$$

$$R_i = R - \delta. \qquad \textbf{Eq.6 - 96}$$

The interfacial shear stress, τ_I, is given by a correlation due to Wallis (1969):

$$\tau_I = \frac{1}{2}(\rho_G + C)V_{GC}^2 f_I \qquad \textbf{Eq.6 - 97}$$

where C is the concentration of droplets in the core

$$C = \frac{G_{LE}}{\frac{G_G}{\rho_G} + \frac{G_{LE}}{\rho_L}}, \qquad \textbf{Eq.6 - 98}$$

V_{GC} is the homogeneous core velocity

$$V_{GC} = \frac{G_G}{\rho_G} + \frac{G_{LE}}{\rho_L}, \qquad \textbf{Eq.6 - 99}$$

f_I is the modified Fanning friction factor,

$$f_I = f_{GC}\left[1 + 360\frac{\delta}{d_T}\right] \qquad \textbf{Eq.6 - 100}$$

with

$$f_{GC} = 0.079\,\mathrm{Re}_{GC}^{-0.25} \qquad \textbf{Eq.6 - 101}$$

and

$$\mathrm{Re}_{GC} = \frac{(G_G + G_{LE})d_T}{\eta_G} \qquad \textbf{Eq.6 - 102}$$

6.6 Steady-state simulations using the new version of GRAMP2

The new version of GRAMP2, as described above, was tested under steady-state conditions against one set of field data representative of a gas condensate field in the North Sea.

The PVT input data were extracted from the PVT characterisation previously carried out by Bozorgzadeh (Bozorgzadeh and Gringarten, 2004 and 2005) using PVTi. These input data were used in Multiflash to build a fluid property model for the gas condensate field under study, to be linked to GRAMP2. No further match or optimisation of the PVT data set, other than what had been previously performed in PVTi by Bozorgzadeh (Bozorgzadeh and Gringarten, 2004 and 2005), was carried out as part of the work presented here.

Table 6 – 1 shows the fluid composition adopted in the Multiflash model.

Well stream composition	Mole %
CO2	1.8
N2	0.83
C1	79.16
C2	6.83
C3	3.2
IC4	0.49
NC4	1.19
IC5	0.37
NC5	0.54
C6	0.68
C7+	4.91

Table 6 – 1: Well stream composition as implemented in Multiflash (Bozorgzadeh and Gringarten, 2004)

Table 6 – 2 summarises the input data fed to GRAMP2 for the wellbore simulations. It must be pointed out that, under its present status of development, GRAMP2 cannot deal with deviated wells. Thus, even though the well selected for this preliminary test is not vertical, it has been assumed so for the purpose of the simulation exercise presented in this work. Also, due to time constraints and to the quality of the production data that were available to the present author for the selected field, the value of flowing bottomhole pressure (used as input to the wellbore simulations) had to be guessed for the particular pair of liquid and gas flow rate selected. In fact, the production rates available were daily allocated figures rather than instantaneous values. The values of liquid flow rate and gas flow rate were taken for a particular day when a well test had been carried out. The flowing bottomhole pressure showed in **Table 6 – 2** was obtained by averaging the stabilised pressures at the end of each drawdown period during the well test for that day.

INPUT PARAMETERS		
Gas Flow Rate	52970	Mscf/d
Liquid Flow Rate	3120	bbl/d
Flowing Bottomhole Pressure	241	bar
Flowing Bottomhole Temperature	408	K
Tube diameter	0.2158	m
Tube Length	4800	m
Inlet Entrained Fraction (annular flow)	0.7	
Overall Heat Transfer Coefficient (*)	17.02	W/m2.K
Geothermal Gradient (*)	-0.025	K/m
Reservoir Temperature	408	K

(*) typical values

Table 6 – 2: Input data fed to GRAMP2

For a full validation of this new version of GRAMP2 it is recommended that, in the future, the code is tested against more datasets. These could be represented by either a synthetic case or another field case for which, however, the wells must be vertical and accurate field measurements of wellhead P and T, bottomhole P and T, surface flow rates and, possibly, P and T gradients along the well must be available. Unfortunately, due to time constraints, it was not possible, under the work described in this thesis, to perform analyses other than that presented here.

6.6.1 Results of simulations

The output of the simulation run performed with GRAMP2 using the input data of **Table 6 – 1** and **Table 6- 2** are shown in **Fig.6 – 2** to **Fig.6 – 7**.

All parameters are reported as a function of the distance from bottomhole, with the liquid and the gas flowing towards the wellhead.

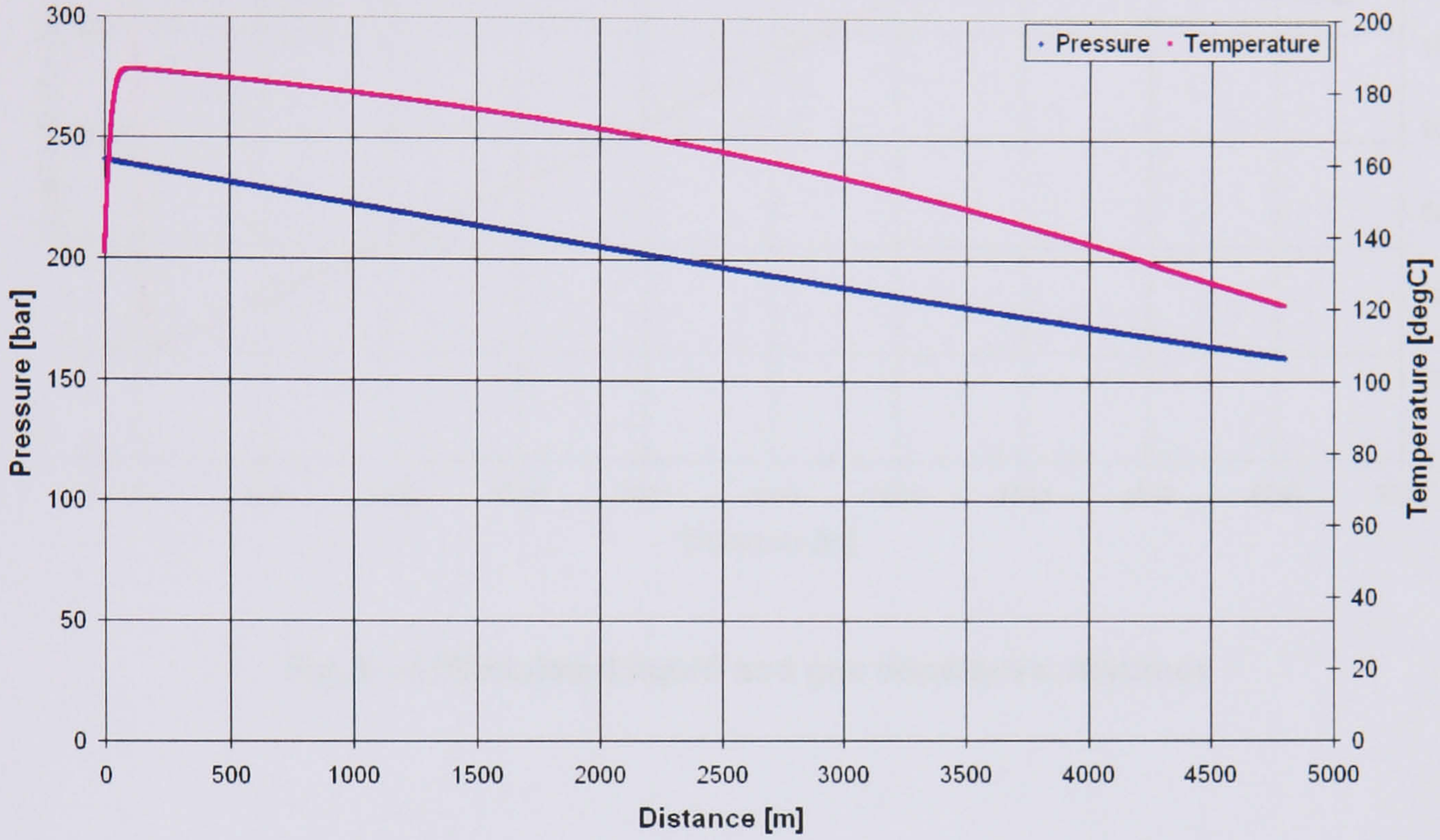


Fig. 6 – 2: Simulated pressure and temperature vs. distance

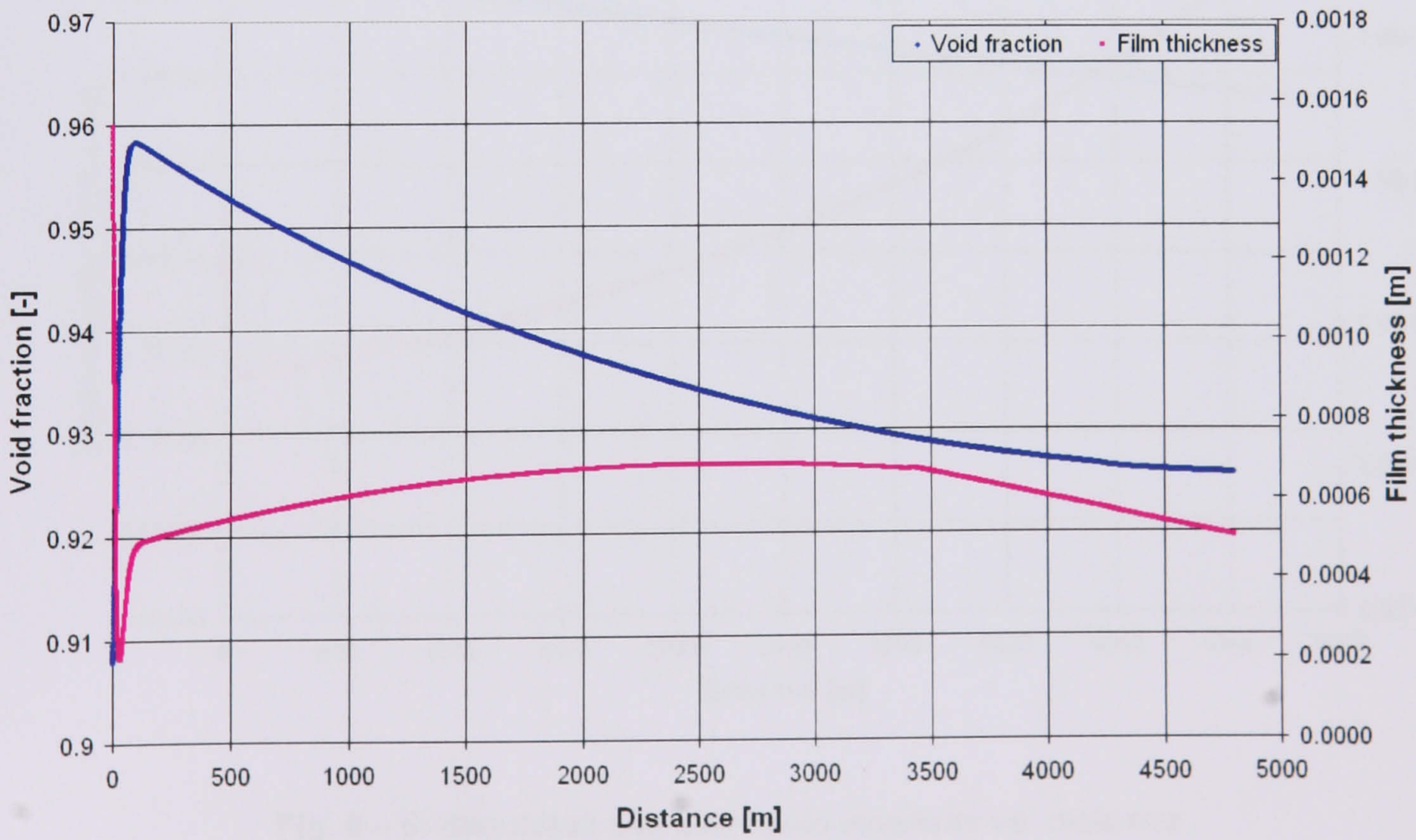


Fig. 6 – 3: Simulated void fraction and film thickness vs. distance

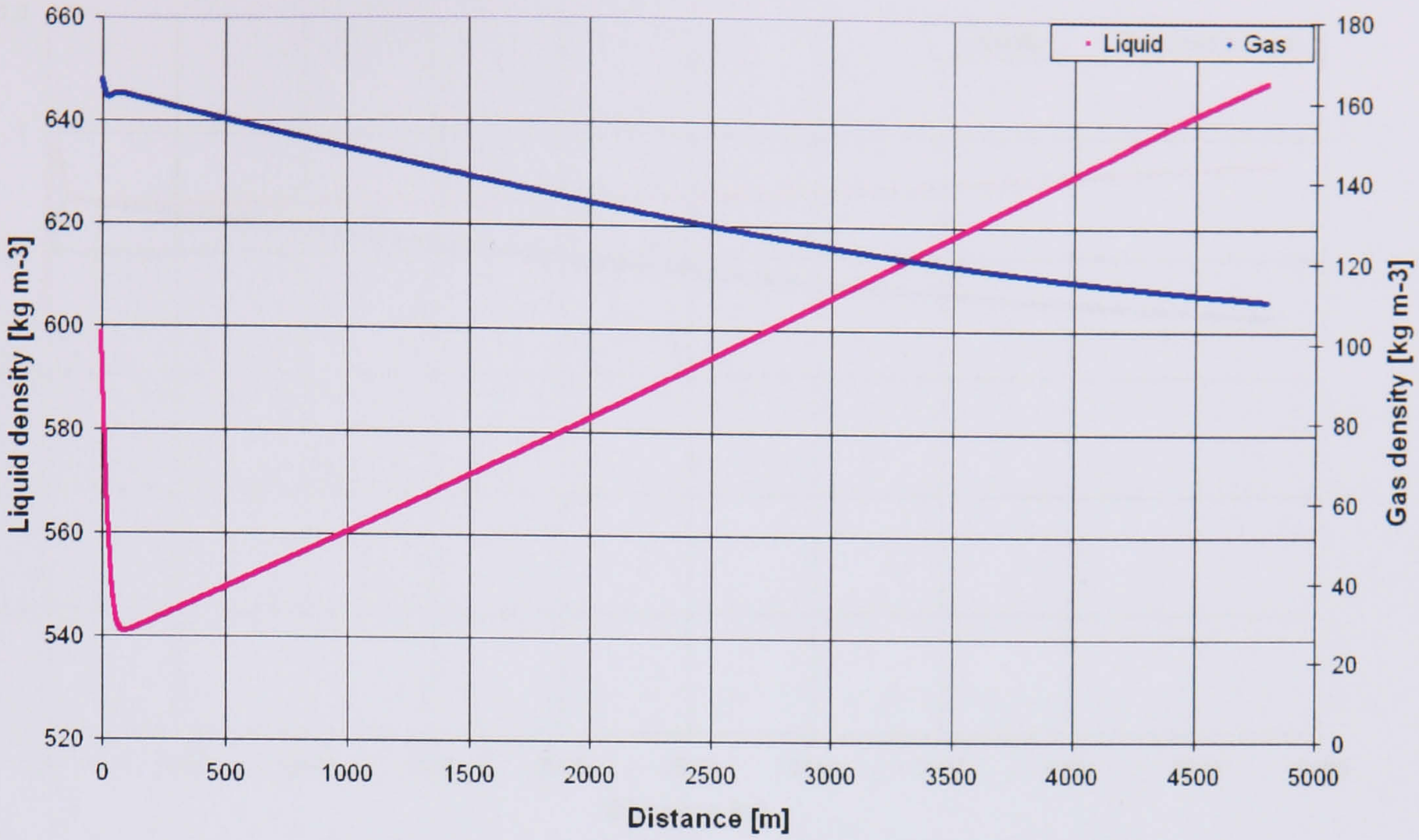


Fig. 6 –4: Simulated liquid and gas density vs. distance

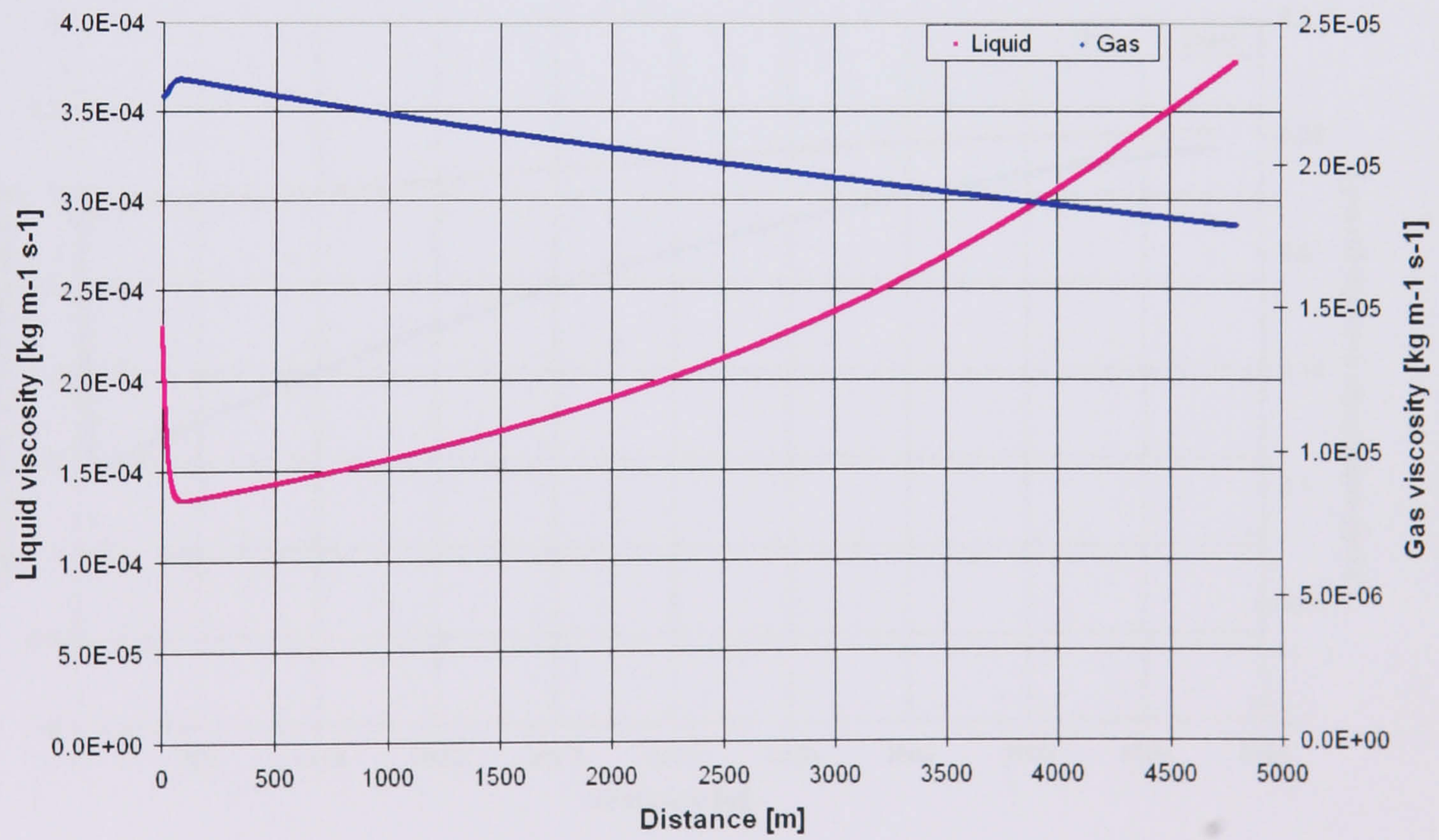


Fig. 6 – 5: Simulated gas and liquid viscosity vs. distance

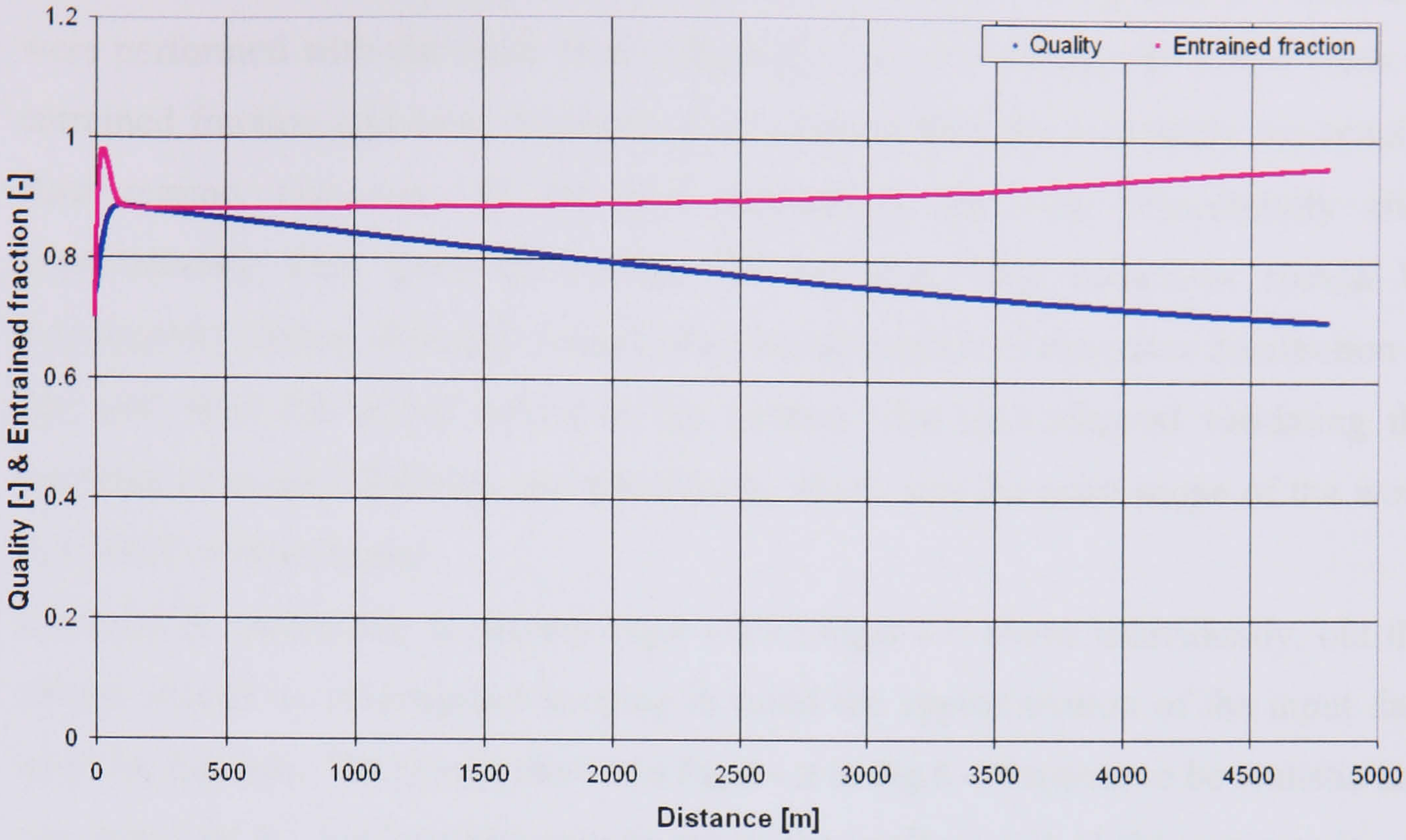


Fig. 6 –6: Simulated stream quality and entrained fraction vs. distance

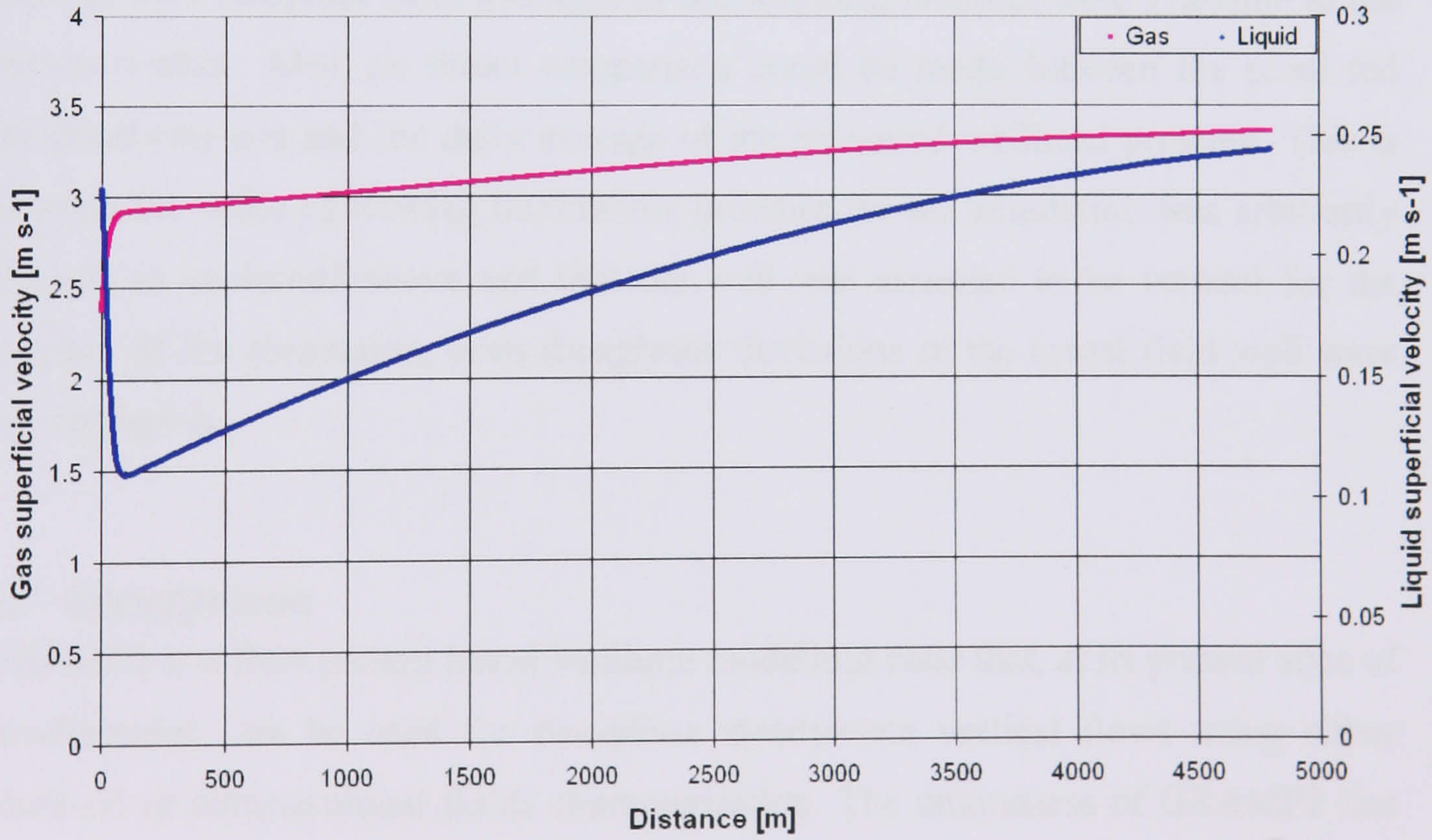


Fig. 6 – 7: Simulated liquid and gas superficial velocity vs. distance

All the parameters plotted in **Fig.6 – 2** to **Fig.6 – 7** show an abrupt change from the initial trend after the first 30m of tube length. Several runs of GRAMP2+Multiflash were performed with the input data of **Table 6 – 2**, but changing the initial value of entrained fraction and some tolerance parameters within the subroutine for annular flow regime. However, all the runs resulted in the same discontinuity after approximately 30m from the bottom of the well. This behaviour should be investigated further, although it may reflect an adjustment of the phase distribution in the well after the initial inflow at the bottom. The runs allowed validating the interface between GRAMP2 and Multiflash, which was the main scope of the work described in this chapter.

It would be interesting to discuss **Fig.6 – 2** to **Fig.6 – 7** above individually, but the results should be investigated keeping in mind the approximation of the input data used for this test. The results shown in **Fig.6 – 2** to **Fig.6 – 7** appear to be realistic and can therefore be used qualitatively to assess the performance of the new version of GRAMP2. However, it would be necessary to compare the simulations with measured pressure and temperature profiles along the well (for a given set of liquid and gas flow rates) for a quantitative analysis. Unfortunately, this was not possible during the work discussed in this thesis because only daily allocated values of liquid and gas flow rates and daily averages of the wellhead pressure were available to the present author. Also, no direct comparison could be made between the predicted wellhead pressure and the daily average of the measured wellhead pressure. This is because the value of flowing bottomhole pressure for the simulation was arbitrarily chosen, as explained above and that the well was assumed to be vertical for the purpose of the simulation, even though the deviations in the actual field well were not negligible.

6.7 Conclusions

GRAMP2 is a flow pattern based wellbore modelling code that, at its present state of development, can be used for two-phase steady-state vertical flows using either black-oil or compositional fluids characterisation. The uniqueness of GRAMP2 lies in the use of flow correlations specific to the flow regime encountered and also in the way the mass, momentum and energy conservation equations are solved, which allows for a new way of determining the temperature at each integration step.

A preliminary assessment of the performance of the new version of GRAMP2, based on a gas condensate field in the North Sea and carried out as part of the work described in this thesis, proved rather encouraging. However, it was not possible to perform a quantitative comparison between the predictions and relevant field data. More tests should be conducted in the future to fully validate this new version of GRAMP2. Particular attention should be paid to the development of a procedure to assess the sensitivity of the code to different length steps and different input parameters, and also to variations in the fluids characterisation within Multiflash. Also, a more appropriate field candidate should be chosen to extend the comparison, making sure that:

- the wells selected for the analysis are vertical;
- the PVT characterisation is optimised for reservoir as well as for wellhead pressure and temperature conditions;
- there are complete and accurate sets of bottomhole flowing pressure and temperature, wellhead flowing pressure and temperature, gas flow rate and liquid flow rate;
- there are available production logging data reporting the pressure and temperature profiles along the well for a given flowing condition.

GRAMP2 is currently implemented in FORTRAN. For the study presented here, Compaq Visual FORTRAN Standard Edition 6.1.0 was used and the interface with Multiflash was achieved by means of dedicated subroutines added to the project. **Fig.6 - 8** is a screen capture of the workspace built to run the main GRAMP2 programme and call the ancillary subroutines.

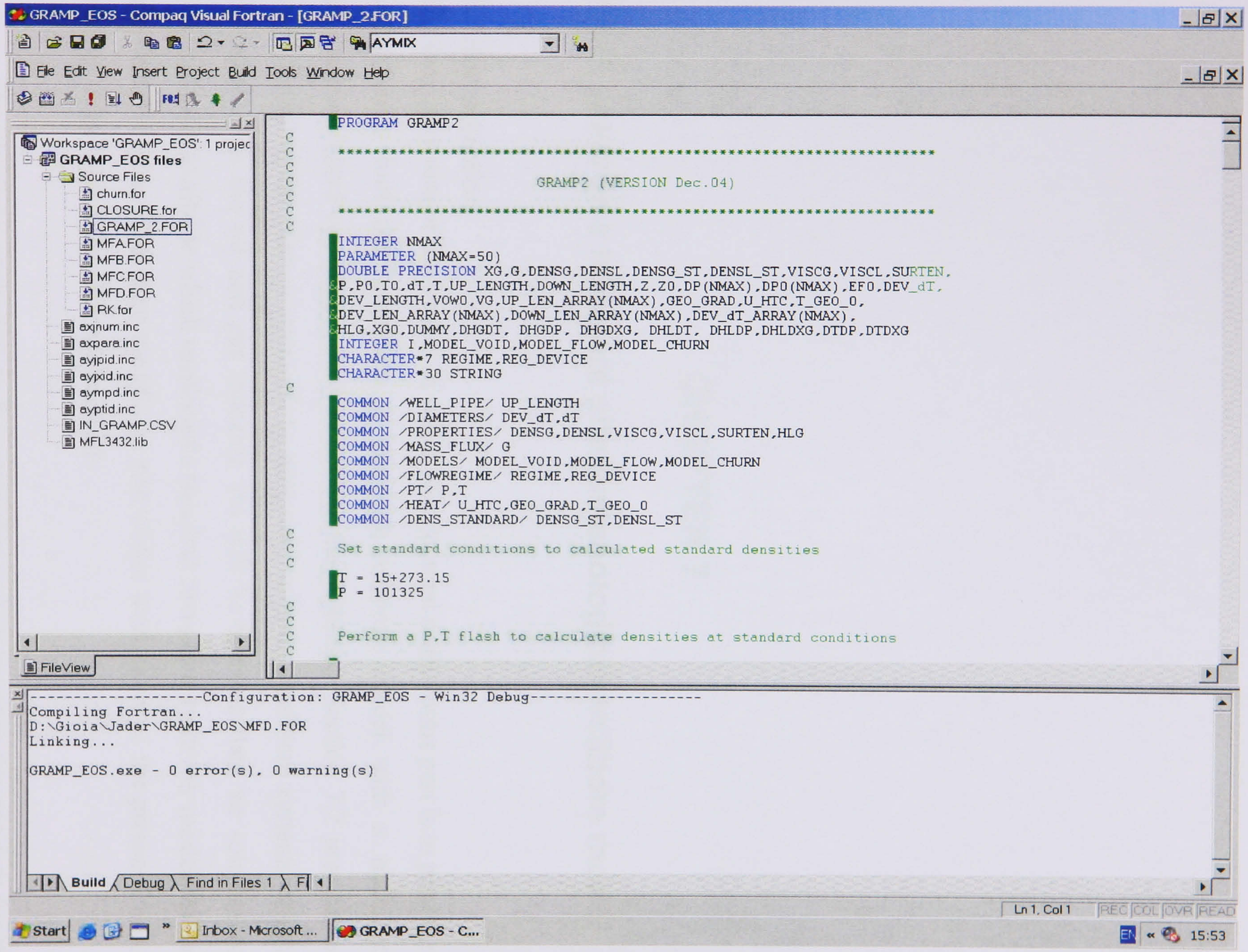


Fig.6 - 8: Compaq Visual FORTRAN workspace with GRAMP2 main programme and ancillary subroutines for the interface with Multiflash.

CHAPTER 7

Work towards a transient phenomenological wellbore model

7.1 Introduction

The long term aim of the project of which this doctoral study forms part is to produce a prediction tool that combines a transient reservoir model with a transient phenomenological two-phase flow model for the wellbore. Section 7.2 presents a brief review of the current approach to integrated reservoir-wellbore systems which are adopted in the oil and gas industry. As will be seen, to date no solution is commercially available which combines a transient two-phase reservoir model with a transient two-phase wellbore model. As part of the work done in the present Ph.D. project, three areas of work were pursued:

- Developing a methodology for establishing a link between the transient (well test) conditions at the bottom of the well and the reservoir outflow (note that this reservoir outflow can be negative if the pressure at the bottom of the well is high enough to re-inject the fluids back into the reservoir). The work carried out in this context included computational studies using the Eclipse code and is described in Section 7.3.

- Developing a set of equations for the case where the fluid in the reservoir and in the well is in the form of a single phase compressible gas. This case is a limiting one which any generic multiphase flow model should be capable of dealing with and is therefore of great interest in the path to the development of such a generic model. The work in this area is described in Section 7.4.

- Developing a set of wellbore equations for the case of transient two-phase annular flow. The equations, developed by Professor J.R. Barbosa of the University of Santa Catarina (Brazil), are presented in Appendix II.

7.2 Current approach to integrated reservoir-wellbore systems

Integrated systems (i.e. reservoir + wellbore) can be handled rather satisfactorily by existing commercial software packages in the case of steady-state flow (or pseudo-steady-state flow) (Alimonti and Falcone, 2002). This is achieved either by integrating the reservoir and wellbore mathematical codes into one unique code or by setting up a cascade workflow from the reservoir to surface. The often reported drawbacks of the first approach are convergence problems and prohibitive computer processing times. The second approach runs the risk of serious instability, which arises when coupling software packages together. In addition to these concerns, transient flows are much more complicated and PVT characterisation also plays a much more important role in the case of gas condensates.

Condensates have a tendency to drop liquids as pressure falls and to take them back into solution as pressure rises again. The PVT properties of gas condensate reservoirs are a function of time and change constantly, either in the reservoir or in the wellbore. Accurate laboratory studies of PVT and phase equilibrium behaviour of reservoir fluids are necessary to characterise gas condensate fluids.

When dealing with transient wellbore phenomena, a limited number of commercial software packages are already available to petroleum engineers (Masella et al., 1998; Bendlksen et al., 1991; Pauchon et al., 1994), but they require experienced users to identify the problem and correctly define the boundary conditions. The weakness of these packages lies in the link with the reservoir model and in the applicability of the

transient flow correlations to conditions different from those under which the correlations themselves have been validated.

To date, the following solutions have been adopted to quantify the reservoir performance and its influx into the wellbore:

- Material balance equations. These are zero-dimensional equations, which were first derived by Schilthuis (1963). They are based on a volumetric balance between the cumulative observed production and the change of volume of the fluids in the reservoir resulting from a finite decrease in reservoir pressure.
- Numerical simulators (based on the solution of the diffusivity equation with the "classic" initial and boundary conditions discussed earlier on in this chapter).
- Superposition principle (Duhamel's principle). This principle states that the addition of solutions to a linear differential equation is also a solution to the original differential equation. It can be applied to investigate the effects of multiple wells, rate change, boundaries in the reservoir and pressure change.
- Steady-state or pseudo-steady-state Inflow Performance Relationships (IPRs). Sturm *et al.* (2004) have recently presented an approach to the dynamic interaction between the reservoir and the wellbore, based on the characterisation of the near-wellbore region by means of "dynamic" inflow performance curves. The near-wellbore region can be defined as that part of the reservoir, closer to the well, where fast rate or pressure induced changes in rock compaction, permeability, skin and fluid properties cannot be captured by steady-state IPRs. The procedure proposed by Sturm et al. is based on a series of look-up IPR curves.

However, none of the above solutions is specifically tailored to fully transient cases or, as it is the case for the superposition principle, they cannot be applied to non-linear problems (i.e. compressible fluids).

The above reservoir modelling techniques have been coupled with homogeneous, separated (two fluid) or drift flux models for the well performance (Thompson et al., 1984; Xiao et al., 1995; Hasan et al., 1996 and 1997).

Most commercial steady-state wellbore simulators adopt empirical multiphase flow correlations developed from laboratory work. Some examples are the correlations by Hagedorn Brown, Duns and Ros, Orkiszeski, Beggs and Brill, etc (as described by Petroleum Experts, 2005). None of these correlations make an attempt to identify the flow regime.

To date, a fully mechanistic and integrated solution for the coupling of reservoir and wellbore, able to deal with compressible as well as incompressible fluids, steady-state and transient flows, still remains unavailable.

During transient flow conditions, most of the assumptions made for the steady-state case are no longer valid. The boundary conditions become a function of time and the dynamic interaction between the wellbore, the near-wellbore and the reservoir must be accounted for.

7.3 Link between wellbore conditions and efflux from the reservoir

One method of linking the wellbore and the reservoir is the development of Inflow Performance Relationships (IPR's) which link the inflow from the reservoir to the conditions at the bottom of the well. In a DipIng project jointly supervised by the present author, Costantini (2005) investigated IPR's using the Eclipse code. The runs with Eclipse300, without simulation of the wellbore, allowed the isolation of reservoir effects from wellbore effects during build-ups. The bottomhole pressure rather than the surface rate (converted to bottom hole conditions) was used as simulation constraint. In order to reproduce transient conditions, the pressure build ups/pressure drawdowns were simulated as fast steps up/down of the controlling constraint, with the bottom hole rates as the output. The study showed that steady-state conditions must be achieved during each time interval to avoid instabilities and to obtain reliable results. The time intervals, the calculations time steps and the bottom hole pressure changes between time intervals dictate whether steady-state conditions can be achieved. It was showed that, during the early times of a build up (wellhead rate equal to zero), the bottom hole rate is not equal to zero. As a result of

this work, a transient IPR at bottom hole conditions was derived for a given reservoir mini-model (one well, radial coordinates, homogeneous reservoir properties) and for a specific set of time intervals, time steps and bottom hole pressure changes between time intervals. However, it was not possible to verify the results against measured bottomhole rates.

Fig.7 – 1 and **Fig.7 - 2** illustrate the workflow adopted to investigate bottomhole IPR's during build-ups using Eclipse300.

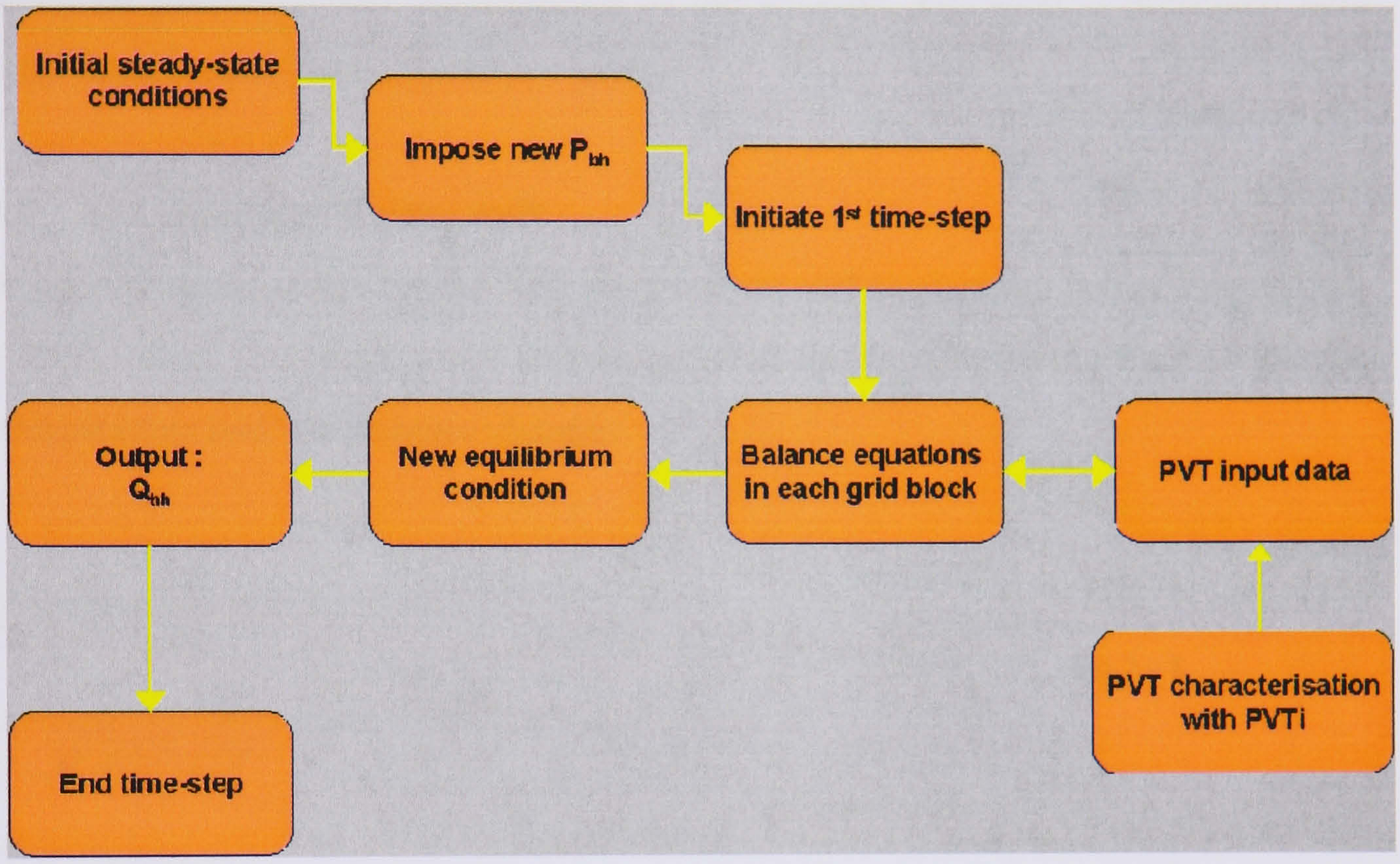


Fig.7 - 1: Workflow to investigate bottomhole IPR's during build-ups using Eclipse300 (Costantini, 2005).

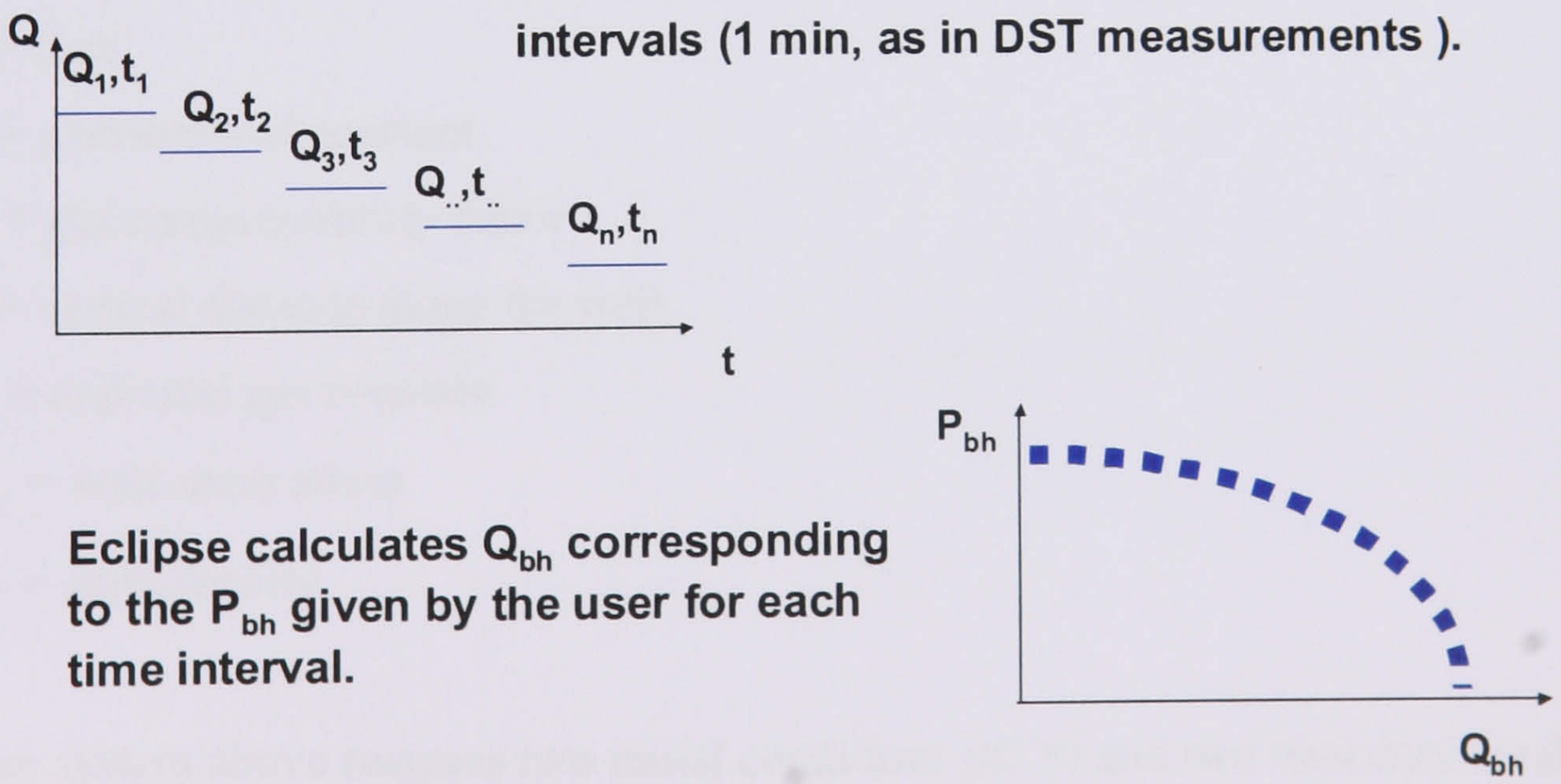


Fig.7 - 2: Typical procedure followed to simulate a build-up with Eclipse300 and corresponding output (Costantini, 2005).

7.4 Integrated approach to reservoir and wellbore equations for transient flows (single phase compressible fluid)

The ultimate objective of the project, of which the work described here is part, is to develop full transient phenomenological models for well test conditions. A limiting case (important in itself) is that of a single-phase gas flow in both reservoir and well. This case was considered analytically in the present work. This Section presents the governing equations and discusses the way in which they could be solved. Time restrictions prevented full investigation of the solution, but what is presented here should form a useful basis for future work.

7.4.1 The equations for the well

The governing equations for the well are the mass and momentum balance equations. An Equation of State (EoS) will also be required to characterise the fluid properties as the pressure and temperature change.

$$\begin{cases} \dfrac{1}{ZRT}\dfrac{\partial p}{\partial t}+\dfrac{\partial G}{\partial z}=0 \\ \left(1-\dfrac{G^2}{\rho^2 ZRT}\right)\dfrac{\partial p}{\partial z}+\dfrac{\partial G}{\partial t}+\dfrac{2G}{\rho}\dfrac{\partial G}{\partial z}=-\rho g-\dfrac{4}{d_T}\tau_w \end{cases} \qquad \textbf{Eq.7 - 1}$$

where:

G = mass flux

p = pressure

t = time

g = gravitational constant

Z = gas compressibility factor

z = vertical distance along the well

R = universal gas constant

τ_w = wall shear stress

ρ = fluid density

The system above requires two initial conditions (IC's) and two boundary conditions (BC's):

$$p(z,0) = p_0(z)$$
$$G(z,0) = G_0$$
$$p(0,t) = p_B(t)$$
$$G(L,t) = G_H(t)$$

Eq.7 - 2

where

p_B = bottmhole pressure

G_H = wellhead mass flux

G_0 = initial (steady-state) mass flux

7.4.2 The equations for the reservoir

The governing equations for the reservoir are the mass conservation equation, Darcy's law and an EoS. They result in a partial differential equation that can be linearised by introducing the real gas pseudo-pressure, as seen in Chapter 4:

$$\frac{\partial^2 m(p)}{\partial r^2} + \frac{1}{r}\frac{\partial m(p)}{\partial r} = \frac{\phi r c_t}{k}\frac{\partial m(p)}{\partial t}$$

Eq.7 - 3

where

$$m(p)\big|_{r=r_W} = 2\int_{p_{ref}}^{p_B} \frac{\tilde{p}}{\eta Z} d\tilde{p}$$

Eq.7 - 4

r_e = reservoir drainage radius

r_w = wellbore radius

p_{ref} = reference pressure (usually atmospheric)

To obtain a unique solution to **Eq.7 – 3**, it is necessary to specify one IC and two BC's:

$$m(r,0) = m_{ini}(r)$$
$$G_B = -\frac{kh}{r_w}\frac{\rho_B Z}{p_B}\frac{\partial m(p)}{\partial r}\bigg|_{r=r_w}$$

Eq.7 - 5

$$m(r_e,t) = m_\infty$$

where:

G_B = bottomhole mass flux

h = formation thickness

7.4.3 Solution procedure

The suggested solution procedure involves a numerical time-marching methodology, starting with the initial (steady-state) flow situation.

Calculation procedure (performed at each time step):

1. Guess p_B.
2. Solve the well equations and obtain G_B.
3. Using the G_B from step 2, calculate $\left.\frac{\partial m(p)}{\partial r}\right|_{r=r_W}$.
4. Solve the reservoir and obtain the *m(p)* profile and hence the new value of p_B.
5. Go back to 2 until convergence.

The well equations **Eq.7 – 1** can be written in matrix form:

$$\frac{\partial \hat{r}}{\partial t} + [C]\frac{\partial \hat{r}}{\partial z} = \hat{R}$$

$$\hat{r} = \begin{bmatrix} p \\ G \end{bmatrix} \qquad \textbf{Eq.7 - 6}$$

$$[C] = \begin{bmatrix} 0 & ZRT \\ \left(1 - \frac{G^2}{\rho^2 ZRT}\right) & \frac{2G}{\rho} \end{bmatrix}$$

$$\hat{R} = \begin{bmatrix} 0 \\ -\left(\rho g + \frac{4\tau_w}{d_T}\right) \end{bmatrix}$$

The matrix form can then be discretised as follows:

$$\frac{\hat{r}_{j+1}^{n+1}-\hat{r}_{j+1}^{n}}{\Delta t}+\left[C\right]_j\frac{\hat{r}_{j+1}^{n+1}-\hat{r}_{j}^{n+1}}{\Delta x}=\hat{R}_j^n$$

$$\frac{\hat{r}_{j+1}^{n+1}}{\Delta t}+\left[C\right]_j\frac{\hat{r}_{j+1}^{n+1}}{\Delta x}-\left[C\right]_j\frac{\hat{r}_{j}^{n+1}}{\Delta x}=\hat{R}_j^n+\frac{\hat{r}_{j+1}^{n}}{\Delta t}$$

$$\frac{1}{\Delta t}\begin{bmatrix}p_{j+1}^{n+1}\\G_{j+1}^{n+1}\end{bmatrix}+\frac{1}{\Delta z}\begin{bmatrix}C_{11}&C_{12}\\C_{21}&C_{22}\end{bmatrix}_j^n\begin{bmatrix}p_{j+1}^{n+1}\\G_{j+1}^{n+1}\end{bmatrix}-\frac{1}{\Delta z}\begin{bmatrix}C_{11}&C_{12}\\C_{21}&C_{22}\end{bmatrix}_j^n\begin{bmatrix}p_{j}^{n+1}\\G_{j}^{n+1}\end{bmatrix}=\begin{bmatrix}\hat{R}_1\\\hat{R}_2\end{bmatrix}_j+\frac{1}{\Delta t}\begin{bmatrix}p_{j+1}^{n}\\G_{j+1}^{n}\end{bmatrix}$$

Eq.7 - 7

As C_{11} and $\hat{R}_1$ are null, the equations above (**Eq. 7 - 7**) become, in matrix form:

$$-\frac{C_{12}}{\Delta x}G_j^{n+1}+\frac{1}{\Delta t}p_{j+1}^{n+1}+\frac{C_{12}}{\Delta x}G_{j+1}^{n+1}=\frac{1}{\Delta t}p_{j+1}^{n}$$ **Eq.7 - 8**

$$-\frac{C_{21}}{\Delta x}p_j^{n+1}-\frac{C_{22}}{\Delta x}G_j^{n+1}+\frac{C_{21}}{\Delta x}p_{j+1}^{n+1}+\left(\frac{1}{\Delta t}+\frac{C_{22}}{\Delta x}\right)G_{j+1}^{n+1}=\hat{R}_2+\frac{1}{\Delta t}G_{j+1}^{n}$$ **Eq.7 - 9**

Eq.7 – 8 and **Eq.7 - 9** are to be solved simultaneously in an implicit finite difference scheme. In finite difference form, the IC's and BC's in **Eq.7 - 2** become:

$$\begin{aligned}p_j^0&=p_0(j)\\G_j^0&=G_0\\p_0^{n+1}&=p_B^{n+1}(t)\\G_{j_{\max}}^{n+1}&=G_H^{n+1}(t)\end{aligned}$$ **Eq.7 - 10**

Thus, for j=0, **Eq.7 – 8** and **Eq.7 – 9** become:

$$-\frac{C_{12}}{\Delta x}G_0^{n+1}+\frac{1}{\Delta t}p_1^{n+1}+\frac{C_{12}}{\Delta x}G_1^{n+1}=\frac{1}{\Delta t}p_1^{n}$$ **Eq.7 - 11**

$$-\frac{C_{22}}{\Delta x}G_0^{n+1}+\frac{C_{21}}{\Delta x}p_1^{n+1}+\left(\frac{1}{\Delta t}+\frac{C_{22}}{\Delta x}\right)G_1^{n+1}=\hat{R}_2+\frac{1}{\Delta t}G_1^{n}+\frac{C_{21}}{\Delta x}p_0^{n+1}$$ **Eq.7 - 12**

where:

$p_0^{n+1} = p_B^{n+1}$ is the guessed value of bottomhole pressure

For j=1, **Eq.7 – 8** and **Eq.7 – 9** become:

$$-\frac{C_{12}}{\Delta x} G_1^{n+1} + \frac{1}{\Delta t} p_2^{n+1} + \frac{C_{12}}{\Delta x} G_2^{n+1} = \frac{1}{\Delta t} p_2^n \qquad \textbf{Eq.7 - 13}$$

$$-\frac{C_{21}}{\Delta x} p_1^{n+1} - \frac{C_{22}}{\Delta x} G_1^{n+1} + \frac{C_{21}}{\Delta x} p_2^{n+1} + \left(\frac{1}{\Delta t} + \frac{C_{22}}{\Delta x}\right) G_2^{n+1} = \hat{R}_2 + \frac{1}{\Delta t} G_2^n \qquad \textbf{Eq.7 - 14}$$

For j=jmax-1, **Eq.7 – 8** and **Eq.7 – 9** become:

$$-\frac{C_{12}}{\Delta x} G_{j_{\max}-1}^{n+1} + \frac{1}{\Delta t} p_{j_{\max}}^{n+1} = \frac{1}{\Delta t} p_{j_{\max}}^n - \frac{C_{12}}{\Delta x} G_{j_{\max}}^{n+1} \qquad \textbf{Eq.7 - 15}$$

$$-\frac{C_{21}}{\Delta x} p_{j_{\max}-1}^{n+1} - \frac{C_{22}}{\Delta x} G_{j_{\max}-1}^{n+1} + \frac{C_{21}}{\Delta x} p_{j_{\max}}^{n+1} = \hat{R}_2 + \frac{1}{\Delta t} G_{j_{\max}}^n - \left(\frac{1}{\Delta t} + \frac{C_{22}}{\Delta x}\right) G_{j_{\max}}^{n+1}$$

Eq.7 - 16

The system of well equations can therefore be written in the following matrix form of the type [A][x]=[d]:

$$\begin{bmatrix} -\frac{C_{12}}{\Delta x} & \frac{1}{\Delta t} & \frac{C_{12}}{\Delta x} & 0 & 0 & 0 \\ -\frac{C_{22}}{\Delta x} & \frac{C_{21}}{\Delta x} & \frac{1}{\Delta t}+\frac{C_{22}}{\Delta x} & 0 & 0 & 0 \\ & & & & & \\ & & & & & \\ & & & & & \\ & & & & & \\ & & & & & \\ 0 & & & 0 & -\frac{C_{12}}{\Delta x} & \frac{1}{\Delta t} & 0 \\ 0 & & & 0 & -\frac{C_{21}}{\Delta x} & -\frac{C_{22}}{\Delta x} & \frac{C_{21}}{\Delta x} \end{bmatrix} \begin{bmatrix} G_0 \\ p_1 \\ G_1 \\ p_2 \\ G_2 \\ .. \\ .. \\ p_{j_{\max}-1} \\ G_{j_{\max}-1} \end{bmatrix} = \begin{bmatrix} \frac{p_1^n}{\Delta t} \\ \hat{R}_2+\frac{1}{\Delta t}G_1^n+\frac{C_{21}}{\Delta x}p_0^{n+1} \\ \frac{p_2^n}{\Delta t} \\ \hat{R}_2+\frac{1}{\Delta t}G_2^n \\ .. \\ .. \\ .. \end{bmatrix}$$

In finite-difference form, the reservoir equation **Eq.7 – 3** can be written as:

$$\frac{m_{j+1}^{n+1}-2m_j^{n+1}+m_{j-1}^{n+1}}{(\Delta r)^2}+\frac{1}{r_j}\frac{m_{j+1}^{n+1}-m_{j-1}^{n+1}}{2\Delta r}=\left(\frac{\phi\eta c_t}{k}\right)^n\frac{m_j^{n+1}-m_j^n}{\Delta t} \qquad \textbf{Eq.7 - 17}$$

Let's define a diffusivity term as:

$$\vartheta=\frac{\phi\eta c_t}{k}$$

where all the parameters have been described in Chapter 4.

Eq.7 – 17 can be re-arranged as follows:

$$m_{j-1}^{n+1}\left(\Delta t-\frac{\Delta t\Delta r}{2r_j}\right)\left[-\frac{1}{\vartheta^n(\Delta r)^2}\right]+m_j^{n+1}\left[-2\Delta t-\vartheta^n(\Delta r)^2\left[-\frac{1}{\vartheta^n(\Delta r)^2}\right]+\left(\Delta t+\frac{\Delta t\Delta r}{2r_j}\right)\left[-\frac{1}{\vartheta^n(\Delta r)^2}\right]=m_j^n\right.$$

that is:

$$a_j m_{j-1}^{n+1}+b_j m_j^{n+1}+c_j m_{j-1}^{n+1}=m_j^n$$

where:

$$a_j = \left(\Delta t - \frac{\Delta t \Delta r}{2r_j}\right)\left[-\frac{1}{\vartheta^n(\Delta r)^2}\right]$$

$$b_j = \left[-2\Delta t - \vartheta^n(\Delta r)^2\right]\left[-\frac{1}{\vartheta^n(\Delta r)^2}\right] \qquad \textbf{Eq.7 - 18}$$

$$c_j = \left(\Delta t + \frac{\Delta t \Delta r}{2r_j}\right)\left[-\frac{1}{\vartheta^n(\Delta r)^2}\right]$$

The IC's and BC's can be re-written as follows:

I.C.	$m_j^0 = m_{ini}(r)$	**t=0**	**Eq.7 - 19**
B.C. 1	$m_1^{n+1} - m_0^{n+1} = -\frac{G_B \Delta r r_W p_B}{Kh\rho_B Z}$	**j=0**	**Eq.7 - 20**
B.C. 2	$m_{j_{\max}}^{n+1} = m_\infty$	**j=j_{max}**	**Eq.7 - 21**

In matrix form, the system for the reservoir becomes:

$$\begin{bmatrix} -1 & 1 & 0 & 0 & .. & 0 \\ c_1 & b_1 & a_1 & 0 & .. & 0 \\ 0 & c_2 & b_2 & a_2 & .. & 0 \\ 0 & 0 & c_3 & b_3 & a_3 & 0 \\ .. & .. & .. & .. & .. & 0 \\ 0 & 0 & 0 & 0 & c_{j_{\max}-1} & b_{j_{\max}-1} \end{bmatrix} \begin{bmatrix} m_0^{n+1} \\ m_1^{n+1} \\ m_2^{n+1} \\ m_3^{n+1} \\ .. \\ m_{j_{\max}-1}^{n+1} \end{bmatrix} = \begin{bmatrix} -\frac{G_B \Delta r r_w p_B}{Kh\rho_B Z} \\ m_1^n \\ m_2^n \\ m_3^n \\ .. \\ m_{j_{\max}-1}^n - a_{j_{\max}-1} m_\infty \end{bmatrix}$$

7.5 Transient annular flow

To obtain a complete transient phenomenological model for the multiphase flow behaviour in the well, transient models will need to be set up for all the relevant regimes. For gas-condensate systems, however, the dominant regime is likely to be

annular flow. Work carried out as part of this project was focussed on extending the steady-state annular flow model, as presented in Section 1.3.7 and embodied in the GRAMP2 code (see Chapter 6), to the case of a transient annular flow. This work was carried out in collaboration with Professor J.R. Barbosa of the University of Santa Catarina, Brazil, who developed a set of equations for the transient annular flow case. These equations are included, for completeness, as Appendix II of the present thesis.

7.6 Conclusions

The development of a transient phenomenological two-phase flow model for the wellbore, coupled with a transient two-phase reservoir model, is a challenging task. The work described in this Chapter was aimed at taking important steps towards addressing this task. The development of IPR's (see Section 7.3) seems a promising route for linking wellbore and reservoir models for the multiphase flow case. This link can be more explicit for single-phase gas flows (Section 7.4). The next stages of the work will probably be to investigate the solutions for the single-phase gas flow case and to investigate the link between multiphase IPR's and the transient annular flow equations for the gas-condensate case.

CHAPTER 8

Conclusions and recommendations for future work

8.1 Conclusions

The work described in this thesis focussed on the application of the modelling of gas-liquid flows to Multiphase Flow Metering (MFM) at high gas content and to the understanding of the phenomena occurring in transient well testing. The experimental work that was carried out to validate the analysis was presented here.

8.1.1 MFM and wet gas metering

MFM has now become an established discipline within the Oil and Gas Industry. To date, a generic solution to MFM does not exist, but adequate methodologies are available for specific applications at low gas content. The situation for high gas content ("wet gas metering") is less satisfactory. As part of the work presented here, a novel wet gas metering system, ANUMET, was developed and protected by international patent. Encouraging results were obtained from experimental tests carried out with air-water flows on the LOTUS facility at Imperial College. The ANUMET system depends on having accurate measurements of liquid film thickness

and pressure drop. Though adequate accuracy can be achieved for pressure drop, the main current limitation in the system is that of achieving the required accuracy in film thickness measurement. However, it should be possible to overcome these difficulties with further development.

8.1.2 Work towards a transient reservoir/wellbore model

A large fraction of the work described in this thesis was focussed on improving the interpretation of the pressure transient data arising in well testing. The following main steps were taken in pursuit of this ambitious long-term objective:

- Under the supervision of the present author, two experimental campaigns were carried out on the LOTUS facility at Imperial College, in which two-phase air-water flows were shut-in and the subsequent behaviour recorded. These experiments gave valuable insights into the processes occurring. A model was developed for the bubbly flow case, which gave encouraging agreement with the data.

- A two-phase phenomenological modelling code (GRAMP2) previously developed by Hawkes (1996) and Barbosa and Hewitt (2001) was adapted for use in predicting initial (steady-state) conditions in wellbores by linking it to the commercial physical property package Multiflash. The resultant combined code gave realistic predictions for a typical well case.

- Under the supervision of the present author, a study was carried out using the Eclipse code, in which the link between the pressure at the bottom of the well and the reservoir output (i.e. an Inflow performance Relationship, IPR) was established for multiphase production in a typical field.

- A full set of equations were derived for the linked system of reservoir and well in the case of single-phase gas flow and solution schemes for these equations suggested.

8.2 Recommendations for future work

Although the work carried out under this Ph.D. project progressed modelling methods for gas-liquid flow, which can be applied to wet gas metering and to the understanding of the phenomena occurring in transient well testing, recommendations can be made for further work on these topics.

8.2.1 Future work on MFM and wet gas metering

There is scope for improvement in the implementation of the fundamental technologies used in MFM and, also, in the definition of International Regulations on MFM accuracy requirements and in the integration of MFM solutions.

In the light of the encouraging results obtained from the experiments on the ANUMET metering system, it is envisaged that further tests will be carried out at Imperial College to validate this concept and build a field prototype. In particular, more work on the liquid film thickness measurements is recommended.

8.2.2 Future work towards a transient reservoir/wellbore model

The following main recommendations are made with respect to future work in the well testing interpretation area:

- The experiments described in Chapter 5 provided useful insights and could be extended. In particular, improved representation of the reservoir might be achieved by using a porous medium at the end of the LOTUS test section. **Fig.8 – 1** represents a possible basis for the design of an experimental set up that would include the effects of the near-wellbore region, simulated by a cylindrical porous medium around the bottom of the tube. A preliminary evaluation of the main design parameters was carried out by Costantini (2005). This set-up would allow the investigation of the dynamic interaction between the reservoir and the well, including phase re-injection.

- The steady-state GRAMP2/Multiflash code should be tested against a wider range of conditions and further developed to include the cases of non-vertical wells and three-phase flow.

- The transient equations for single-phase gas flow should be coded and, if possible, tested against data from an appropriate field.

- The transient two-phase annular flow equations developed by Barbosa (see Appendix II) should be implemented in the GRAMP2 code and tested against data for high gas fraction wells. Transient models should be developed for the full gamut of flow regimes.

- Further work should be done on linking the transient wellbore model to a reservoir model. The IPR's discussed in Section 7.3 would be a stating point for this work.

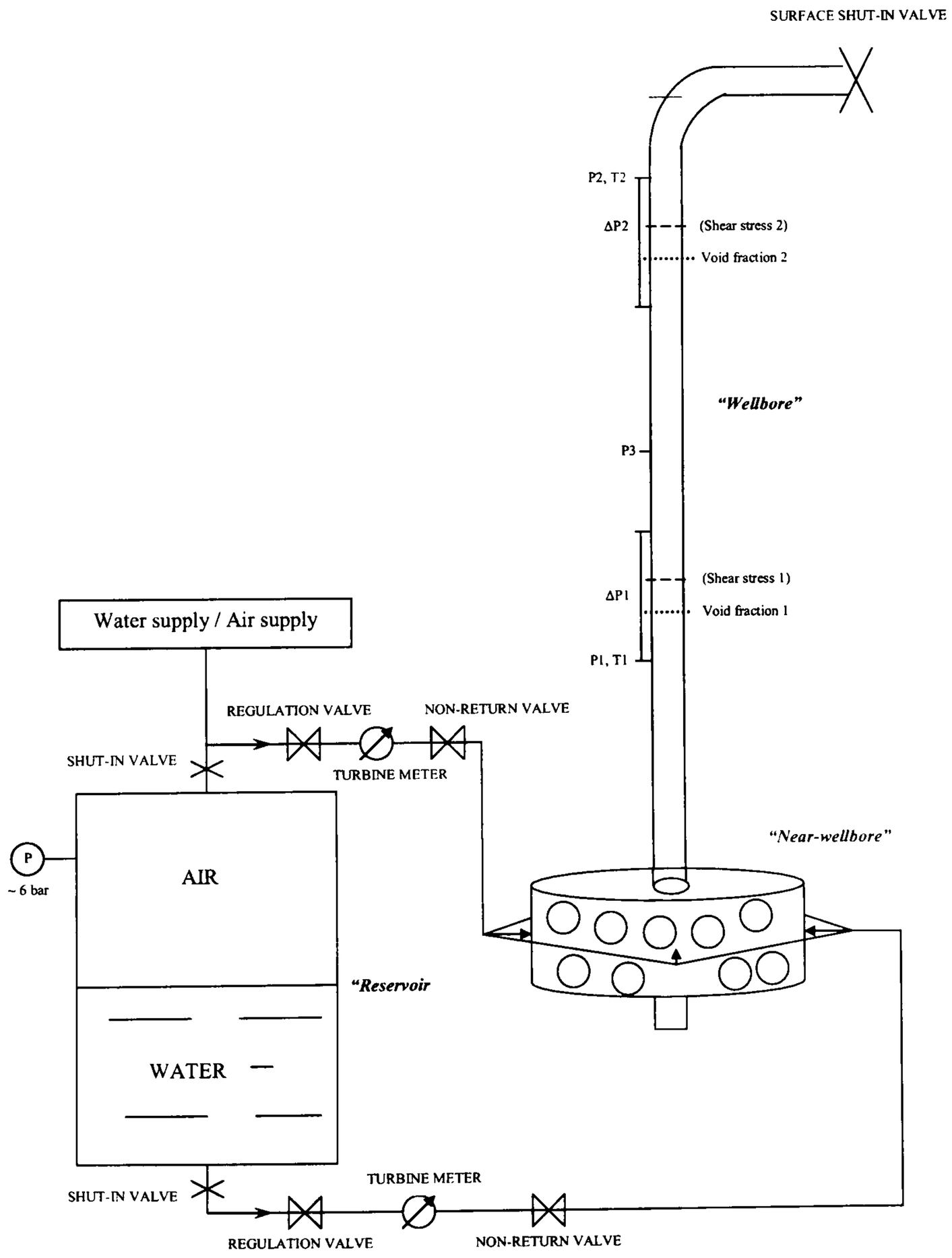


Fig. 8 – 1: Experimental layout with pressure vessel and porous medium.

NOMENCLATURE

Roman

A - cross-sectional area [m^2]

A_r - Nikuradse roughness parameter [-]

B - formation volume factor [-]

C - droplet concentration [kg m^{-3}], count rate [counts s^{-1}]

C_0 - drift-flux model distribution parameter [-]

C_D - venturi discharge coefficient [-]

c_t - total compressibility [N^{-1} m^2]

D - droplet deposition rate [kg m^{-2} s^{-1}]

D_1 - venturi upstream diameter [m]

D_2 - venturi throat diameter [m]

d, d_T - tube diameter [m]

E - droplet entrainment rate [kg m^{-2} s^{-1}]

Eö - Eötvos number [-]

e - interfacial roughness [m]

e_F - entrained fraction [-]

f - friction factor [-]

g -acceleration due to gravity [m s^{-2}]

G - mass flux [kg m^{-2} s^{-1}]

GOR - gas-oil ratio [-]

GVF - gas volume factor [-]

h - enthalpy [J kg^{-1}]

h_{LG} - latent heat of vaporisation [J kg^{-1}]

I - intensity of gamma-ray beam [counts s^{-1}]

j_{GL} - drift flux [m s^{-1}]

k - droplet deposition transfer coefficient [m s^{-1}]

k - venturi loss coefficient [-]

k - rock permeability [m^2]

k_i - equilibrium constants [-]

k_{ro} - relative oil permeability [-]

k_{rg} - relative gas permeability [-]

k_{TP} - Van Karmen constant [-]

$m(P)$ - pseudo-pressure

$\dot{m}$ - mass flux [kg m^{-2} s^{-1}]

$\dot{m}_I$ - interfacial mass flow rate per unit perimeter area [kg m^{-2} s^{-1}]

$\dot{M}$ - mass flow rate [kg s^{-1}]

M_W - molecular weight

N_C - capillary number [-]

p - pressure [N m^{-2}]

P_i - parachors [m^3 mol^{-1})(J m^{-2})$^{1/4}$]

$\dot{q}$ - heat flux [W m^{-2}]

Q - volumetric flow rate [m^3 s^{-1}]

r_0 - wall radius [m]

Re - Reynolds number [-]

S - slip ratio [-]

S_i - shift parameters [-]

t - time [s]

T - temperature [K]

u - velocity (local) [m s^{-1}]

u_{GU} - rise velocity (local) of gas bubbles relative to mean flow [m s^{-1}]

u_S - rise velocity of Taylor bubble in static liquid [m s^{-1}]

u_∞ - rise velocity of a single gas bubble in liquid [m s^{-1}]

U - velocity (superficial) [m s^{-1}]

U - heat transfer coefficient [W m^{-2} K^{-1}]

V - velocity (actual) [m s^{-1}]

V - voltage [V]

V_i - viscosity number [-]

x - quality [-]

X - Lockhart-Martinelli parameter [-]

y - distance from the wall [m]

z - distance [m]

Z - gas compressibility factor [-]

Greek

β - coefficient of intertial resistance [m^{-1}]

Γ -mass generation rate per unit length [kg m^{-3} s^{-1}]

γ - linear attenuation coefficient [m^{-1}]

ΔP - pressure drop [N m^{-2}]

δ - film thickness [m]

$\delta\varepsilon$ - absolute error in phase fraction [-]

ε_G - void fraction [-]

ξ - area ratio [-]

η - dynamic viscosity [kg m^{-1} s^{-1}]

θ - inclination from the horizontal [rad]

ϑ - diffusivity term [s m^{-2}]

ρ - density [kg m^{-3}]

σ - surface tension [N m^{-1}]

τ - shear stress [n m^{-2}]

ϕ - rock porosity [-]

ϕ^2 - two-phase multiplier [-]

ω - acentric factor [-]

Subscript

a - accelerational / air

BH - bottom hole

c - critical

eff - effective

f - frictional

F - film

g - gravitational

G -gas

GC - gas core

GT - gas in the tube

H - homogeneous

I - interface

L -liquid

LE - entrained liquid

LF - liquid film

LO - all liquid

M - mixture

O -oil

r - reduced

res - reservoir

S - superficial

TOT - total

TP - two-phase

w - wall

W - water

WH - well head

Superscript

— - relative to homogeneous model

+ - dimensionless form

SC - standard conditions

References

Ahmed, T. (2001): "Reservoir Engineering Handbook", 2nd Edition, Gulf Professional Publishing, pp.1033-1034.

Akemu, O.A. (2001): "Wellbore Dynamics in Gas Condensate Wells", MSc thesis, Dept of Earth Science & Engineering, Imperial College, September 2001.

Al-Afaleg, N.I., Giliani, S. (2001): "Testing Configuration and Pre-Analysis Data Treatment to Eliminate the Effect of Fluid Segregation on Well-Test Interpretation", SPE 71577 presented at the SPE Annual Technical Conference and Exhibition held in New Orleans, Louisiana, 30 September-3 October, 2001.

Al-Darmaki, S. (2005): "Simulation of Transient Well Behaviour during Well Testing", MSc thesis, Dept. of Chemical Engineering, Imperial College, September 2005.

Al-Haddad, S., LeFlore, M. and Lacy, T. (1997): "Changing Wellbore Storage Effects in Gas Well Testing," SPE 38723 presented at the SPE Annual Technical Conference and Exhibition, San Antonio, Texas, October 5-8, 1997.

Al-Hussein, R., Ramey Jr., H.J., Crawford, P.B. (1966): "The Flow of Real Gases Through Porous Media", Trans. AIME, 1966, pp.237, 624.

Ali, A.M. (2004): "Experimental Investigation of Wellbore Phase Redistribution Effects on Pressure Transient Data", MSc thesis, Dept of Earth Science & Engineering, Imperial College, September 2004.

Ali, A.M., Falcone, G., Hewitt, G.F., Bozorgzadeh, M., Gringarten, A.C. (2005): "Experimental Investigation of Wellbore Phase Redistribution Effects on Pressure-Transient Data", SPE 96587 presented at the 2005 SPE Annual Technical Conference and Exhibition held in Dallas, Texas, U.S.A., 9 – 12 October 2005.

Alimonti, C., Basso, A., Bilardo, U., Pelliccia, A. (2001): "Is it really possible to use a choke valve as multiphase flow meter? The CVAF from laboratory to the field",

presented at the 10th International Conference MULTIPHASE '01, Cannes. France. 13-15 June, 2001.

Alimonti, C., Bilardo, U. (2001): "Measurement of three-phase flow rates using neural network approach", 4th Int. Conf. on Multiphase Flow. New Orleans, Lousinana, USA, May 27- June 1, 2001.

Alimonti, C., Falcone, G. (2002): "Knowledge Discovery in Databases and Multiphase Flow Metering: the integration of statistics, data mining, neural networks, fuzzy logic and ad-hoc flow measurements towards well monitoring and diagnosis", paper SPE 77407 presented at the SPE Annual Technical Conference and Exhibition conference in San Antonio, Texas, September 2002.

Almehaideb, R.A., Aziz, K and Pedrosa, O.A. (1989): "A Reservoir/Wellbore Model for Multiphase injection and Pressure Transient Analysis", SPE 17941 presented at the SPE Middle East Technical Conference and Exhibition, Manama, Bahrain, March 11-14, 1989.

API (2004) Publication 2566, First Edition: "State of the Art Multiphase Flow Metering", May 2004.

Aspelund, A., Midttveit, O., Richards, A. (1996): "Challenges in Downhole Multiphase Measurements", presented at the European Production Operations Conference & Exibition held in Stavanger, Norway, 16-17 April 1996.

Assael, M.J., Trusler, J.P.M., Tsolakis, T.F. (1996): "Thermophysical Properties of Fluids", Imperial College Press.

Atkinson, A., Theuveny, B., Berard, M., Conort, G., Lowe, T., McDiarmid, A., Mehdizadeh, P., Pinguet, B., Smith, G., Williamson, K.J. (2004-2005): "A New Horizon in Multiphase Flow Measurement", Schlumberger Oilfield Review, Winter 2004-2005, pp.52-63.

Barbosa, Jr., J.R., Hewitt (2001): "Gas-Liquid Two-Phase Flow in Vertical Pipes (A description of the models used in the GRAMP 2 Programme)", report prepared for ICON.

Barbosa, Jr., J.R., Govan, A.H., Hewitt, G.F. (2001): "Visualisation and modelling studies of churn flow in a vertical pipe", Int. J. Multiphase Flow, Vol. 27, pp. 2105-2127.

Barbosa, Jr., J.R., Hewitt, G.F., Konig, G., Richardson, S.M. (2002): "Liquid entrainment, droplet concentration and pressure gradient at the onset of annular flow in a vertical pipe", Int. J. Multiphase Flow, Vol. 28, pp. 943-961.

Bendlksen, K.H., Malnes, D., Moe, R., Nuland, S. (1991): "The Dynamic Two-Fluid Model OLGA: Theory and Application", SPE Production Engineering, May 1991.

Bentolila, Y., Constant, M. (2005): "Physical approach of volumetric phase estimation based on mixture laws for multiphase flows", presented at the 5th North American Conference on Multiphase Technology, Banff, Canada, 1-6 June 2005.

Beisheuvel, A., Gorissen, W.C.M. (1989): "Void fraction disturbances in a uniform bubbly fluid", Int. J. Multiphase Flow.

Bouman, H., van Koppen, C.W.H. and Raas, L.J. (1974): "Some investigations of influence of heat flux on flow patterns in vertical boiling tubes", European Phase Flow Group Meeting, Harwell, Paper A2, June 1974.

Bourdet, D., Ayoub, J.A., Pirard, Y.M. (1984): "Use of Pressure Derivative in Well-Test Interpretation", SPE 12777 presented at the California Regional Meeting held in Long Beach, April 11-13, 1984.

Bourdet, D. (2002): "Well Test Analysis: the use of advanced interpretation models", Hanbook of Petroleum Exploration and Production series, Elsevier, ISBN 0-444-50968-2.

Bozorgzadeh, M., Gringarten, A.C. (2004): "New Estimate for the Radius of a Condensate Bank from Well Test Data Using Dry Gas Pseudo-Pressure", SPE 89904 presented at the SPE Annual Technical Conference and Exhibition held in Houston, Texas, U.S.A., 26–29 September 2004.

Bozorgzadeh, M., Gringarten, A.C. (2005): "Application of Build-Up Transient Pressure Analysis to Well Deliverability Forecasting in Gas Condensate Reservoirs Using Single_Phase and Two-Phase Pseudo-Pressures", SPE/IADC 94018 presented at the 14th Europec Biennial Conference held in Madrid, Spain, 13-16 June, 2005.

BP Review of World Energy 2005, downloaded from the bp website.

Brauner, N., Barnea, D. (1986): "The slug/churn transition in upward gas-liquid flow", Chem. Eng. Sci., Vol. 41, pp. 159-163.

Chierici, G.L. (1989): "Principi di ingegneria dei giacimenti petroliferi", Vol. I, p.171, Agip.

Collier, J.G., Thome, J.R. (1994): "Convective Boiling and Condensation", 3rd Edition, Oxford University Press.

Costantini, A. (2005): "Dynamic interaction between the reservoir and the well during well testing", undergraduate thesis, University "La Sapienza" of Rome and Imperial College, October 2005.

Couput, J., Gajan, P., de Laharpe, V., Strzelecki, A. (2000): "Wet Gas Metering in the upstream area: needs, applications & developments", presented at the 18th North Sea Flow Measurement Workshop held in Scotland, 24-27 October 2000.

Dake, L.P. (1978): "Fundamentals of reservoir engineering", Developments in Petroleum Science series, Elsevier.

Douglas-Westwood Limited, "The World Deepwater Report 2000-2004".

DTI (2002), "Guidance Notes For Petroleum Measurement", Issue 6, March 2002.

DTI (2003), "Guidance Notes For Petroleum Measurement", Issue 7, December 2003.

Ertekin, T., Abou-Kassem, J.H., King, G.R. (2001): "Basic Applied Reservoir Simulation Textbook" Vol.7, SPE.

Fair, W.B. Jr. (1979): "Pressure Buildup Analysis with Wellbore Phase Redistribution Effects," SPE 8206 presented at the 54th SPE Annual Fall Technical Conference and Exhibition, Las Vegas, Nevada, September 23-26, 1979.

Fairuzov, Y.V., Gonzalez Guevara, J., Lobato Barradas, G., Camacho Velazquez, R., Fuentes Nucamendi, F. (2002): "A Lumped-Parameter Model for Transient Two-Phase Gas-Liquid Flow in a Wellbore", SPE 75453, published in the SPE Production & Facilities magazine, Vol 17, Number 1, February 2002, pp. 36-41.

Falcone, G., Alimonti, C., Hewitt, G.F., Harrison, B. (2001): "Multiphase Flow Metering: Current Trends and Future Developments", paper SPE 71474 presented at the 2001 SPE Annual Technical Conference and Exhibition held in New Orleans, Louisiana, 30 September-3 October 2001.

Friedel, L.(1979): "Improved friction pressure drop correlations for horizontal and vertical two-phase pipe flow", European Two-Phase Flow Group Meeting, Ispra, Italy, paper E2.

Gamio, C., Ismail, I., Zhang, Z.T., Yang, W.Q. (2004): "Review of electrical capacitance tomography for oil industry", Proc. of 4th Int. Symp. on Measurement Techniques for Multiphase Flows, Hangzhou, China, 10-12 Sept. 2004, pp.116-121.

Gill, L.E., Hewitt, G.F., Hitchon, J.W. (1963): "Sampling probe studies of the gas core in annular two-phase flow. I: The effect of length on phase and velocity distribution", Chem. Eng. Sci., Vol. 18, pp. 525-535.

Gill, L.E., Hewitt, G.F., Lacey, P.M.C. (1964): "Sampling probe studies of the gas core in annular two-phase flow: II, Studies of the effect of phase flowrates on phase and velocity distribution", Chem. Eng. Sci., Vol. 19, pp.665-682.

Gjerstad, T. (2000), "Roxar carves multiphase metering niche", Hart's E&P, April 2000, pp.87-89.

Govan, A.H., Hewitt, G.F., Owen, D.G., Bott, T.R. (1988): "An improved CHF modelling code", Proc. 2nd UK National Heat Transfer Conference, ImechE, Glasgow, paper C175.

Govan, A.H., Hewitt, G.F., Richter, H.J., Scott, A. (1991): "Flooding and churn flow in vertical pipes", Int. J. Mulitphase Flow, Vol. 17, pp. 27-44.

Gringarten, A.C., Al-Lamki, A., Daungkaew, S., Mott, R. and Whittle, T.M. (2000): "Well Test Analysis in Gas Condensate Reservoirs," SPE 62920 presented at the SPE Annual Technical Conference and Exhibition, Dallas Texas, October 1-4, 2000.

Gudmundsson, J.S., Celius, H.K. (1999): "Gas-Liquid Metering Using Pressure-Pulse Technology", paper SPE 56584 presented at the SPE Annual Technical Conference and Exhibition, Houston, Texas, 3-6 October 1999.

Gudmundsson, J.S., Durgut, I., Ronnevig, J., Korsan, K., Celius, H.K. (2001): "Pressure Pulse Analysis of Gas Lift Wells", presented at the Fall 2001 ASME/API Gas Lift Workshop, Aberdeen, 12-13 November 2001.

Hall, A.R.W., Whitaker, T.S., Millington, B.C. (1997): "Multiphase Flow Metering: Current Status and Future Developments", paper OTC 8553 presented at the 1997 Offshore Technology Conference held in Houston, Texas, 5-8 May 1997.

Hatton, G.J. (1997): "Multiphase Flow Meters and Application Trends", paper OTC 8547 presented at the 1997 Offshore Technology Conference held in Houston, Texas, 5-8 May 1997.

Hasan A.R and Kabir, C.S. (1992): "Modeling Changing Wellbore Storage During Shut-In Test", SPE 24717 presented at the SPE Annual Technical Conference and Exhibition, Washington, October 4-7, 1992.

Hasan, A.R., and Kabir, C.S. (1993): "A Mechanistic Approach to Understanding Wellbore Phase Redistribution," SPE 26483 presented at the SPE Annual Technical Conference and Exhibition, Houston, Texas, October 3-6, 1993.

Hasan, A.R., and Kabir, C.S., Wang, X. (1996):"A Wellbore/Reservoir Simulator for Testing Gas Wells in High-Temperature Reservoirs", SPE Formation Evaluation, June 1996, pp.128-134.

Hasan, A.R., and Kabir, C.S., Wang, X. (1997): "Development and Application of a Wellbore/Reservoir Simulator for Testing Oil Wells", SPE Formation Evaluation, September 1997, pp.182-188.

Hawkes, N. (1996): "Wispy-annular flow", Ph. D Thesis, University of London (Imperial College).

Hawkes, N.J., Lawrence, C.J., Hewitt, G.F. (2000): "Studies of wispy-annular flow using the transient pressure gradient and optical measurement", Int. J. Multiphase Flow, Vol. 26, pp. 1565-1582.

Hawkes, N.J., Lawrence, C.J., Hewitt, G.F. (2001): "Prediction of the transition from annular to wispy-annular flow using linear stability analysis of the gas-droplet core", Chem. Eng. Sci., Vol. 56, pp. 1925-1932.

Hegeman, P.S., Halford, D.L., and Joseph, J.A. (1991): "Well Test Analysis with Changing Wellbore Storage," SPE 21829 presented at the Rocky Mountain Regional Meeting and Low-Permeability Reservoirs Symposium, Denver, Colorado, April 15-17, 1991.

Hewitt, G.F., Wallis, G.B. (1963): "Flooding and associated phenomena in falling film in a vertical tube", Proc. Multiphase Flow Symposium, Philadelphia, PA, pp. 62-74.

Hewitt, G.F., Hall-Taylor, N.S. (1970): "Annular Two-Phase Flow", Pergamon Press.

Hewitt, G.F. (1982): "Prediction of Pressure Drop in Annular Flow by Phenomenological Modelling", Section 2.2.4 of *Handbook of Multiphase Flow System*, ed. G.Hetsroni, Hemisphere Publishing Corporation.

Hewitt, G.F., Martin, C.J., Wilkes, M.S. (1985): "Experimental and modelling studies of annular flow in the region between the flow reversal and the pressure drop minimum." Physico Chemical Hydrodynamics, Vol. 6, pp. 69-86.

Hewitt, G.F. (1990): "Non-equilibrium two-phase flow", Proc. 9th International Heat Transfer Conference, Jerusalem, Israel, Vol. 1, pp. 383-394.

Hewitt, G.F., Govan, A.H. (1990): "Phenomena and prediction in annular two-phase flow", Proc. Symposium on Advances in Gas-Liquid Flows, Dallas, Texas, 1990. ASME FED-Vol. 99, HTD-Vol. 155, pp. 41-56, 1990.

Hewitt, G.F., Harrison, P.S., Parry, S.J. (1997): "The MIXMETER flowmeter – another step towards routine multiphase flow measurement?", paper presented at the BHR Group Multiphase 1997 conference.

Hewitt, G.F., Reeks, M.W. (2005): "Computational modelling of multi-phase flows", Chapter 7 in "Prediction of Turbulent Flows", Edited by G.F .Hewitt and J.C. Vassilicos, Cambridge University Press.

Hills, J.H., Azzopardi, B.J., Barhey, A.S. (1996): "Spatial Unsteadainess, A Way Towards Intensive Gas-Liquid Reactors", Trans IchemE, Vol. 74, Part A, July 1996.

Horne, R.N. (1990): "Modern Well Test Analysis, A Computer-Aided Approach", Petroway Inc, ISBN 0-9626992-0-9.

Horne, R.N. (1995): "Modern well test analysis a computer-aided approach". Second Edition, Petroway, Inc.44.

Ismail, I., Chondronasios, A., Yang, W.Q. (2005): "Wet gas flow metering by electrical capacitance tomography", paper presented at the 4th South East Asia Hydrocarbon Flow Measurement Workshop, Kuala Lumpur, Malaysia, 7-11 March 2005.

Jamieson, A.W. (2001): "Wet Gas Metering – The Unexpected Challenge Status and Trends on Technology and Applications", paper presented at the 19th North Sea Flow Measurement Workshop 2001.

Jayanti, S., Hewitt, G.F., (1992): "Prediction of slug-to-churn transition in vertical two-phase flow", Int. J. Multiphase Flow, Vol. 18, pp. 847-860.

Jensen, M.K. (1987): "The liquid film and the core region velocity profiles in annular two-phase flows", Int. J. Multiphase Flow, 13, pp.615-628.

JIP on Well Test Analysis in Gas Condensate & Volatile Oil Reservoirs, Annual Report, Phase II, May 2005.

Kragas, K., Bostick III, F.X., Mayeu, C., Gysling, D.L., van der Spek, A.M. (2003): "Downhole Fiber-Optic Flowmeter: Design, Operating Priciple, Testing, and Field Installations", SPE Production and Facilities, November 2003, pp.257-268.

Laforgia, A. (2004): "Modelling gas-liquid annular flow at high mass fluxes", Ph.D. Thesis, University of London (Imperial College), August 2004.

Lao, L., Lawrence, C.J., Hewitt, G.F. (2002): "Flow Rate Measurement Methods in the LOTUS rig", internal status report, Imperial College, July 2002.

Lao, L. (2003): "A note on the calibration of conductance probes for liquid-film thickness measurements", internal status report, Imperial College, March 2003.

Leporcher, E. (2000): "So far, so much better!", SPE review, June 2000, p.8.

Lorentz, Bray, Clark (1964): "Calculating viscosity of Reservoir Fluids from their composition", J.Peet.Tech., p.1171, 1964.

Machado, R.T.H. (1997): "Mulitphase Flow in Venturi: An Experimental and Theoretical Study", PhD Thesis, University of London (Imperial College).

Mareuge, I.C. (2000): "Analysis and Development of Multi-Energy Gamma Densitometry Systems", internal report, TMF project, Imperial College, December 2000.

Mattar, L., Santo, M. (1992): "How Wellbore Dynamics Affect Pressure Transient Analysis". J. Can. Pet. Tech., Volume 31, No 2.

Mattar, I., Zaoral, K. (1992): "A New Diagnostic Tool in Well Test Interpretation," J. Can. Pet. Tech., Volume 31, No 4.

Masella, J.M, Tran, D.H., Ferre, D., Pauchon, C. (1998): "Transient simulation of two-phase flows in pipes", International Journal of Multiphase Flow 24, pp.739-755.

McQuillan, K.W., Whalley, P.B., Hewitt, G.F. (1985): "Flooding in vertical two-phase flow", Int. J. Multiphase Flow, Vol. 11, pp. 741-760.

Mehdizadeh, P. (1998): "Multiphase Meters: Delivering Improved Production Measurements And Well Testing Today", Hart's Petroleum Engineer International, May 1998.

Mehdizadeh, P., Marrelli, J. (2002): "Wet Gas Metering: Trends in Applications and Technical Developments", paper SPE 77351 presented at the 2002 SPE Annual Technical Conference and Exhibition held in San Antonio, Texas, 29 September-2 October 2002.

Mehdizadeh, P., Williamson, J. (2004): "Principles of Multiphase Flow Measurements", Information Document prepared for the Alaska Oil & Gas Conservation Commission to accompany "Guidelines For Qualification of Multiphase Metering Systems for Well Testing", November 30, 2004.

Milashenko, V.I., Nigmatulin, B.I., Petukhov, V.V., Trubkin, N.I. (1989): "Burnout and distribution of liquid in evaporative channels of various lengths", Int. J. Multiphase Flow, Vol. 15, pp. 393-402.

Mishima, K., Ishii, M. (1984): "Flow regime transition criteria for upward two-phase flow in vertical tubes", Int. J. Heat and Mass Transfer, Vol. 27, pp. 723-737.

Moissis, R., Griffith, P. (1962): "Entrance effects in a two-phase slug flow", J. Heat Transfer, pp. 29-39.

Morton, E.J., Luggar, R.D., Key, M.J., Kundu, A., Tavora, L.M.N., Gilboy, W.B. (1998): "Development of a High Speed X-ray Tomography System for Multiphase Flow Imaging", presented at the 1998 IEEE Nuclear Sciences Symposium and submitted for publication in IEEE Transactions on Nuclear Science.

Mus, E.A., Toskey, E.D., Bascoul, S.J.F., Norris, R.J. (2001): "Added Value of a Multiphase Flow Meter in Exploration Well Testing", paper OTC 13146 presented at the 2001 Offshore Technology Conference held in Houston, Texas, 30 April-3 May 2001.

NEL (2001), notes from "Multiphase Flow Measurement Training Course", 17th January 2001.

NFOGM (2005), Tecna,: "Handbook of multiphase metering", Revision 2, March 2005.

Nicklin, D.J., Davidson, J.F. (1962): "The onset of instability in two-phase slug flow", Proc. Symp. Two-Phase Flow, Paper 4.

Nigmatulin, B.I. (1978): "Investigation of mass transfer intensity and force interactions between core flow and liquid film in gas-and-vapour-liquid flows", Int. Seminar Momentum Heat and Mass Transfer in Two-Phase Energy and Chemical Systems, Dubrovnik, September 1978.

Olarewaju, J.S, and Lee, W.J. (1989): "Effects of Phase Segregation on Buildup Data from Gas Wells", SPE 19100 presented at the SPE Gas Technology Symposium, Dallas, Texas, June 7-9, 1989.

Olarewaju, J.S. (1990): "Detection and Interpretation of Well Test Data Distorted by Phase Segregation". J. Pet. Sci. Eng., 5, pp.201-212.

Offshore Engineer magazine (2000): "Microwaves make a case for real-time return" in Offshore Engineer, September 2000, pp.46-47.

Ong, J.T., Oyeneyin, M.B., Coutts, E.J., MacLean, I.M. (2004): "In Well Nuclear Magnetic Resonance (NMR) Multiphase Flowmeter in the Oil and Gas Industry", paper SPE 89978 presented at the SPE Annual Technical Conference and Exhibition held in Houston, Texas, 26-29 September 2004.

Owen, D.G. (1986): "An experimental and theoretical analysis of equilibrium annular flows", Ph.D. Thesis, University of Birmingham.

Pan, L. (1996): "High pressure three phase (Gas/liquid/liquid) flow", Ph.D. Thesis, University of London (Imperial College).

Pauchon, C.L., Dhulesia, H., Cirlot, G.B., Fabre, J. (1994): "TACITE: A Transient Tool for Multiphase Pipeline and Well Simulation", SPE 28545 presented at the SPE Annual Technical Conference and Exhibition held in New Orleans, USA, 25-28 September 1994.

Petroleum Experts, PROSPER manual, 2005.

Piantanida, M., Mazzoni, A., Tanzi, A., Hope, B.R. (1998): "Multiphase Metering: Experimental Results from the Analysis of Acoustic Noise Through a Choke", paper SPE 50681 presented at the 1998 SPE European Petroleum Conference held in The Hague, The Netherlands, 20-22 October 1998.

Pinguet, B., Haddad, N., Birkett, G. (2005): "Fluid Properties on the Main Path for Multiphase Meters and Wet Gas Meter Accuracy: An Analytical Approach", paper presented at the 4th South East Asia Hydrocarbon Flow Measurement Workshop, Kuala Lumpur, Malaysia, 7-11 March 2005.

Pinheiro da Silva Filho, J.A. (2000): "Multiphase Flow Metering with High Gas Content Using Successive Venturi Devices", DIC Thesis, Imperial College, August 2000.

Pitzer, S.C., Rice, J.D. and Thomas, C.E. (1959): "A Comparison of Theoretical Buildup Curves with Field Curves Obtained from Bottom-Hole Shut-in Tests," Trans., AIME 216, pp.416-419.

Qasem, F.H., Nashawi, I.S. and Mir, M.I. (2001): "A New Method for the Detection of Wellbore Phase Redistribution Effects During Pressure Transient Tests", SPE 67239 presented at the SPE Production and Operations Symposium, Oklahoma City, Oklahoma, March 24-27, 2001.

Radovcick, N.A., Moissis, R. (1962): "The transition from two-phase bubble flow to slug flow", MIT Report 7-7673-22.

Raghavan, R. (1986): "Well Test Analysis for Multiphase Flow", SPE 14098 presented at the SPE International Meeting on Petroleum Engineering, Beijin, China, March 17-20, 1986.

Rasmussen, A. (2004): "Field applications of model-based multiphase flow computing", presented at the 22nd North Sea Flow Measurement Workshop, St. Andrews, Fife, 26-29 October 2004.

Reid, Prausnitz, Sherwood (1977): "The properties of Gases and Liquids", McGraw Hill, 3rd Edition.

Ribeiro (1996): "Developments in Multiphase Metering", paper SPE 36197 presented at the ADIPEC 7th Abu Dhabi International Petroleum Exhibition and Conference held in Abu Dhabi, 13-16 October 1996.

Rushing, J.A., and Lee, W.J. (1989): "Use of Automatic History-Matching Technique To Analyse Pressure Buildup Data Affected by Wellbore Phase Segregation: Case Histories," SPE 18837 presented at the SPE Production and Operations Symposium, Oklahoma City, Oklahoma, March 13-14, 1989.

Schilthuis, R.J. (1936), in Active Oil and Reservoir Energy, Trans.,AIME,118:33-52, 1936.

Sheers, A.M., Noordhuis, B.R. (1999): "Multi-phase and Wet Gas Flow Measurement", presented at IBC's 5th Annual Multi-Phase Metering Conference held in Aberdeen, Scotland, 22-23 February 1999.

Søreide, I., Reffstrup, J., Whitson, C.H.: "Procedures for Reservoir Fluid Characterisation using an Equation of State Model", Report RE 88-8, Laboratory for Energetics, Danish Tech. Univ., Lyngby.

Stegemeier, G.L. and Matthews, C.S. (1958): "A Study of Anomalous Pressure Buildup Behaviour," J. Pet. Tech., February 1958, pp.44-50; Trans., AIME 213.

Sturm, W.L., Belfroid, S.P.C., Wolfswinkel, O. van, Peters, M.C.A.M., Verhelst, F.J.P.C.M.G. (2004): "Dynamic Reservoir Well Interaction", paper SPE 90108 presented at the SPE Annual Technical Conference and Exhibition held in Houston, Texas, 26-29 September 2004.

Taitel, Y., Dukler, A.E. (1976): "A model for predicting flow regime transitions in horizontal and near horizontal gas-liquid flow", AIChE J. Vol. 22, pp. 47-55.

Taitel, Y., Barnea, D., Dukler, A.E. (1980): "Modelling flow pattern transitions for steady upward gas-liquid flow in vertical tubes", AIChE. J., Vol. 26, pp. 345-354.

Thompson, L.G., Jones, J.R., Reynolds, A.C. (1984): "Analysis of Pressure Buildup Data Influenced by Wellbore Phase Redistribution," SPE 12782 presented at the SPE California Regional Meeting, Long Beach, California, April 11-13, 1984.

Thorn, R., Johansen, G.A., Hammer, E.A. (1997): "Recent developments in three-phase flow measurement", Meas. Sci. Technol. 8, pp.691-701.

Vasquez-Cruz, M.A., Camacho-Velasquez, R.A. (1996): "Analysis of Short Transient Tests Affected by Changing Wellbore Storage", SPE 36120 presented at the SPE Latin American and Caribbean Petroleum Engineering Conference, Port-of-Spain, 23-26 April, 1996.

Wallis, G.B. (1962): "General correlations for the rise velocity of cylindrical bubbles in vertical tubes", General Electric Company Report 62GL130.

Wallis, G.B. (1969): "One Dimensional Two-Phase Flow", McGraw-Hill, New York.

Watson, M.J. (1999): "Flow regime transitions and associated phenomena", Ph.D. Thesis, University of London (Imperial College).

Watson, M.J, Hewitt, G.F. (1999): "Pressure effects on the slug to churn transition", Int. J. Multiphase Flow, Vol. 25, pp. 1225-1241.

Webster, M., Richardson, S., Gabard-Cuoq, C., Fitzgerald, J.B., Stephenson, E. (2004): "Multiphase Well Surveillance with a Permanent Downhole Flowmeter", paper SPE 90024 presented at the SPE Annual Technical Conference and Exhibition held in Houston, Texas, 26-29 September 2004.

Whitson, C.H., Brule', M.R. (2000): "Phase Behaviour", SPE monograph Vol. 20. 13.

Williams, J. (1994): "Status of Multiphase Flow Measurement Research", paper SPE 28515 presented at the SPE 69th Annual Technical Conference and Exhibition held in New Orleans, LA, U.S.A., 25-28 September 1994.

Winterfeld, P.H. (1986): "Simulation of Pressure Buildup in a Multiphase Reservoir System", SPE 15534 presented at the 61st SPE Annual Technical Conference and Exhibition, New Orleans, Louisiana, October 5-8, 1986.

Wolf, A. (1995): "Film structure of vertical annular flow, Ph.D. Thesis, University of London (Imperial College).

Xiao, J.J., Fuentes-N, F.A., Alhanati, F., and Reynolds, A.C. (1004): " Modelling and Analysing Buildup Data Affected by Phase Redistribution in the Wellbore," SPE 26965 presented at the III Latin American/Carribean Petroleum Engineering Conference, Buenos Aires, Argentina, April 27-29, 1994.

Zimmerman, R.W. (1998-1999): "Flow in porous media" course notes, MSc in Petroleum Engineering, Imperial College.

Appendix I: Experimental data gathered in LOTUS during ANUMET tests

Experimental set No. 1

water mass flux kg/m2/s	gas mass flux kg/m2/s	DP1 kPa	DP/DZ Pa/m	DP2 kPa	PVEN1 psia	PVEN2 psia	DPAIR "H2O	PAIR psia	t film m
103.06	30.15	1.817	2264.7	19.222	18.16	15.19	2.7814	22.73	0.0006053
103.06	45.29	2.460	3116.3	32.480	20.63	15.60	5.5403	26.31	0.0005010
103.06	61.22	3.281	4194.2	51.000	24.75	16.20	8.5203	31.73	0.0004268
103.06	115.63	4.502	5801.0	102.129	40.64	18.09	18.995	51.99	0.0002867
103.06	131.48	5.043	6497.7	117.878	46.63	19.20	21.502	59.43	0.0003309
103.06	179.19	5.636	7276.0	156.242	60.29	21.43	31.278	76.83	0.0002752
103.06	209.53	5.720	7379.1	178.938	68.35	22.74	37.957	87.29	0.0003093
195.54	35.01	2.893	3632.4	32.490	21.94	15.82	3.0925	27.88	0.0008005
195.54	53.74	3.854	4897.0	54.469	27.34	16.83	5.926	34.81	0.0006979
195.54	71.24	4.574	5842.5	73.741	32.51	17.72	8.8416	41.47	0.0006296
195.54	98.70	5.475	7023.1	101.469	41.43	19.15	13.488	52.77	0.0005589
195.54	139.89	6.412	8250.3	137.155	54.16	21.42	21.008	68.94	0.0004878
195.54	163.40	6.801	8753.9	157.346	61.59	22.95	25.436	78.20	0.0005010
195.54	186.84	7.241	9336.1	179.437	69.52	24.55	29.57	88.30	0.0004328
195.54	194.49	7.409	9549.0	187.307	72.47	25.38	30.82	91.97	0.0004671
280.54	31.86	3.169	3969.7	36.110	23.18	16.18	2.4112	29.90	0.0009483
280.54	52.23	4.167	5280.6	59.720	29.64	17.33	5.2009	37.79	0.0008443
280.54	64.33	4.702	5984.1	74.845	33.84	18.17	6.9339	43.30	0.0007888
280.54	95.00	5.664	7246.9	108.191	44.56	20.09	11.701	56.63	0.0007025
280.54	129.53	6.462	8301.1	139.759	55.69	22.12	17.684	70.48	0.0005824
280.54	153.79	6.992	8986.8	161.918	63.71	23.85	21.957	80.57	0.0005957
280.54	169.05	7.313	9408.3	176.266	69.22	24.98	24.598	87.23	0.0005696
280.54	187.70	7.734	9964.9	194.801	75.85	26.72	27.776	95.60	0.0005022
371.59	27.18	3.621	4533.9	35.323	23.24	16.39	1.7375	30.53	0.0011095
371.59	42.54	5.135	6496.2	54.869	28.92	17.46	3.4628	37.85	0.0011318
371.59	58.04	4.969	6316.7	77.175	35.06	18.98	5.4143	45.43	0.0008866
371.59	77.97	5.609	7151.0	100.179	42.82	20.23	8.222	54.47	0.0008653
371.59	103.94	6.317	8080.6	128.093	52.22	22.24	12.107	66.31	0.0007955
371.59	121.26	6.646	8522.2	146.183	59.16	23.05	14.779	74.33	0.0007021
371.59	145.26	7.061	9064.7	169.935	67.62	24.91	18.697	84.88	0.0006765
371.59	166.63	7.489	9620.7	188.455	74.09	26.29	22.6	93.04	0.0006706
371.59	175.35	7.692	9880.0	197.190	77.31	27.02	24.078	97.00	0.0007054

Water mass flux: reference measurement from rotameters
Gas mass flux: reference measurement from orifice
DP1: deltaP over straight pipe section
DP/DZ: pressure gradient over straight pipe section
DP2: deltaP across the venturi (upstream-throat)
PVEN1: absolute pressure upstream of venturi throat
PVEN2: absolute pressure downstream of venturi throat
DPAIR: deltaP across orifice for air reference measurement
PAIR: absolute pressure in air line before feed to tube
t film: film thickness from gamma-ray measurement

Experimental set No. 2

water mass flux kg/m2/s	gas mass flux kg/m2/s	DP1 kPa	DP/DZ Pa/m	DP2 kPa	PVEN1 psia	PVEN2 psia	DPAIR "H2O	PAIR psia	t film m
103.06	30.37	1.499	1947.2	14.344	17.17	15.01	2.9677	21.29	0.0006925
103.06	47.19	2.279	2959.2	32.660	20.86	15.63	5.8621	26.51	0.0006186
103.06	65.62	2.859	3712.9	52.812	25.10	16.14	9.4513	32.31	0.0005200
103.06	115.84	3.950	5130.2	100.812	40.13	18.00	18.873	51.28	0.0004638
103.06	132.09	4.256	5527.4	114.439	45.09	18.68	21.911	57.60	0.0003772
103.06	179.63	5.015	6513.6	152.798	58.85	20.89	31.317	75.14	0.0003343
103.06	216.65	5.461	7091.9	181.043	68.83	22.38	39.185	87.94	0.0003874
274.48	36.59	2.951	3832.5	37.280	23.54	16.34	3.0113	30.15	0.0014502
274.48	57.19	3.813	4951.3	62.441	30.25	17.59	5.7878	38.75	0.0012164
274.48	74.09	4.328	5620.3	80.778	35.16	18.53	8.3951	45.20	0.0011138
274.48	100.56	5.040	6546.0	108.878	44.65	20.25	12.405	56.76	0.0010846
274.48	135.78	5.791	7520.5	142.144	56.23	22.46	18.14	71.35	0.0010238
274.48	159.16	6.227	8086.7	161.946	63.65	23.69	22.231	80.40	0.0009318
274.48	173.99	6.470	8403.0	175.095	68.15	24.74	24.844	86.20	0.0009683
274.48	195.81	6.884	8939.7	193.793	74.65	26.30	28.759	94.65	0.0009492
450.54	35.07	4.164	5407.1	42.603	25.71	16.90	2.4498	33.83	0.0015431
450.54	54.35	4.874	6330.3	71.542	34.33	18.76	4.5264	44.27	0.0014381
450.54	66.19	5.039	6544.1	86.936	39.01	19.86	5.957	50.06	0.0012769
450.54	97.10	5.598	7269.9	121.945	51.27	21.89	10.038	64.45	0.0012501
450.54	119.48	6.021	7819.9	145.948	58.97	24.04	13.125	74.95	0.0011777
450.54	156.86	6.517	8463.6	181.532	72.70	26.41	18.873	90.53	0.0010291
450.54	163.83	6.702	8703.7	189.153	75.25	27.03	19.852	93.94	0.0010126
769.81	36.68	6.373	8277.0	63.871	32.02	18.67	2.0601	43.75	0.0016940
769.81	48.68	6.688	8685.3	83.568	38.53	20.00	3.1189	51.04	0.0015136
769.81	52.71	6.666	8657.4	92.045	42.02	20.37	3.4343	54.35	0.0016850
769.81	69.69	7.100	9220.1	114.670	49.48	22.20	5.152	63.59	0.0015189
769.81	88.09	7.594	9862.5	137.087	57.55	23.96	7.2209	72.77	0.0014180
769.81	97.55	7.868	10218.1	151.394	61.74	25.72	8.1361	79.27	0.0014938
769.81	128.31	8.444	10966.4	184.847	74.34	28.50	11.966	93.76	0.0013014

Water mass flux: reference measurement from rotameters
Gas mass flux: reference measurement from orifice
DP1: deltaP over straight pipe section
DP/DZ: pressure gradient over straight pipe section
DP2: deltaP across the venturi (upstream-throat)
PVEN1: absolute pressure upstream of venturi throat
PVEN2: absolute pressure downstream of venturi throat
DPAIR: deltaP across orifice for air reference measurement
PAIR: absolute pressure in air line before feed to tube
t film: film thickness from gamma-ray measurement

Experimental set No. 3

water mass flux kg/m2/s	gas mass flux kg/m2/s	DP1 kPa	DP/DZ Pa/m	DP2 kPa	PVEN1 psia	PVEN2 psia	DPAIR "H2O	PAIR psia	t film m
103.06	37.16	1.826	2371.0	21.313	18.52	15.27	4.1316	23.11	0.0004442
103.06	47.45	2.294	2978.7	31.816	20.66	15.59	6.0185	26.16	0.0003727
103.06	67.19	2.971	3858.0	54.088	25.41	16.24	9.8077	32.70	0.0002696
103.06	108.12	3.966	5151.0	93.508	37.34	17.65	17.608	47.89	0.0001937
103.06	130.92	4.526	5878.4	113.046	44.52	18.70	21.776	56.95	0.0002687
103.06	179.55	5.330	6922.4	152.214	58.64	20.89	31.401	74.92	0.0001228
103.06	214.45	5.855	7603.4	180.581	68.97	22.79	38.285	87.98	0.0001201
274.48	35.00	2.837	3684.8	33.198	22.38	15.91	2.8882	28.78	0.0009275
274.48	57.51	3.796	4929.7	60.272	29.60	17.32	6.0057	37.84	0.0007236
274.48	66.09	4.123	5354.5	70.953	32.51	17.94	7.2324	41.64	0.0006813
274.48	98.33	5.099	6622.3	104.784	43.16	19.82	12.261	54.97	0.0005826
274.48	132.62	5.910	7675.8	137.319	54.76	21.94	17.815	69.34	0.0004762
274.48	158.52	6.431	8351.8	160.091	62.79	23.54	22.326	79.49	0.0006276
274.48	171.24	6.690	8688.6	171.190	66.92	24.42	24.561	84.51	0.0005031
274.48	191.02	7.044	9147.7	187.775	72.73	25.73	28.186	91.97	0.0004621
450.54	32.92	4.030	5233.6	40.602	25.26	16.67	2.2011	33.14	0.0010465
450.54	53.01	4.785	6214.5	68.882	33.39	18.35	4.4187	43.14	0.0009341
450.54	68.74	5.422	7041.9	88.544	39.53	19.68	6.3505	50.72	0.0008375
450.54	95.15	5.729	7440.4	119.068	49.80	21.70	9.8448	63.11	0.0007398
450.54	125.41	6.244	8109.7	149.476	60.76	23.90	14.22	76.42	0.0006849
450.54	149.71	6.641	8624.9	174.223	69.82	25.70	17.8	87.34	0.0007319
450.54	159.27	6.786	8812.5	184.060	73.19	26.54	19.232	91.62	0.0006372
450.54	177.05	7.047	9152.3	199.026	78.11	27.54	22.276	98.12	0.0005178
769.81	32.02	5.639	7323.0	54.963	29.48	17.69	1.714	40.03	0.0013160
769.81	46.18	6.704	8706.7	77.556	36.78	19.46	2.9164	49.09	0.0012371
769.81	52.32	7.130	9259.2	87.234	39.64	20.28	3.483	52.85	0.0012315
769.81	67.57	7.071	9183.3	110.614	48.85	21.76	4.9725	61.92	0.0011648
769.81	84.16	7.761	10078.9	131.470	55.92	23.33	6.7876	70.62	0.0012259
769.81	93.85	7.862	10210.8	143.713	59.77	24.69	7.8733	75.85	0.0011859
769.81	119.63	7.944	10316.8	173.665	70.83	27.15	10.978	88.76	0.0010709
769.81	132.99	8.207	10657.9	189.379	77.18	28.37	12.616	95.63	0.0010155

Water mass flux: reference measurement from rotameters
Gas mass flux: reference measurement from orifice
DP1: deltaP over straight pipe section
DP/DZ: pressure gradient over straight pipe section
DP2: deltaP across the venturi (upstream-throat)
PVEN1: absolute pressure upstream of venturi throat
PVEN2: absolute pressure downstream of venturi throat
DPAIR: deltaP across orifice for air reference measurement
PAIR: absolute pressure in air line before feed to tube
t film: film thickness from gamma-ray measurement

Experimental set No. 4

water mass flux kg/m2/s	gas mass flux kg/m2/s	DP1 kPa	DP/DZ Pa/m	DP2 kPa	PVEN1 psia	PVEN2 psia	DPAIR "H2O	PAIR psia	t film m
103.06	26.87	2.387	2876.4	12.999	17.01	14.97	2.4697	20.33	0.0007982
103.06	48.53	2.877	3466.5	33.278	20.93	15.58	6.4575	26.10	0.0005572
103.06	62.61	3.224	3884.8	49.573	24.45	16.05	9.2514	30.69	0.0004629
103.06	111.79	3.575	4307.3	97.203	39.34	17.65	18.82	49.00	0.0004348
103.06	127.53	3.739	4505.2	109.995	43.97	18.26	22.049	54.67	0.0004103
103.06	174.91	4.493	5413.3	148.781	57.90	20.37	31.811	71.92	0.0004620
103.06	202.35	5.014	6041.5	171.472	66.09	21.95	37.439	82.05	0.0004211
274.48	36.31	3.627	4370.4	35.011	22.99	15.95	3.1433	29.06	0.0011063
274.48	57.48	4.330	5217.2	62.015	30.37	17.30	6.0089	38.49	0.0009324
274.48	69.00	4.665	5620.9	75.455	34.19	18.04	7.8394	42.77	0.0008217
274.48	94.82	5.109	6155.5	102.991	43.11	19.60	11.907	53.63	0.0007566
274.48	128.56	5.526	6657.7	134.596	54.26	21.62	17.633	67.18	0.0006982
274.48	152.09	5.675	6837.0	155.376	61.74	23.12	21.848	76.30	0.0006277
274.48	169.38	5.991	7218.3	170.986	67.39	24.42	24.917	83.23	0.0006501
274.48	173.57	6.022	7255.1	175.501	69.12	24.79	25.559	85.21	0.0006395
450.54	29.77	3.697	4454.5	34.822	23.85	16.35	1.9665	30.89	0.0013720
450.54	55.89	4.585	5524.3	73.126	35.02	18.51	4.8725	44.38	0.0011628
450.54	69.87	4.928	5937.8	91.739	41.21	19.65	6.619	51.27	0.0011284
450.54	93.36	5.570	6711.4	119.223	50.51	21.45	9.7782	62.35	0.0010324
450.54	123.88	6.142	7399.8	150.764	61.88	23.69	14.275	75.74	0.0009841
450.54	145.52	6.548	7889.3	172.669	69.61	25.32	17.596	85.13	0.0009759
450.54	158.45	6.781	8170.3	185.805	74.27	26.39	19.582	90.87	0.0009230
769.81	32.00	4.931	5940.6	53.505	29.36	17.54	1.7871	39.10	0.0016609
769.81	42.08	4.877	5875.6	68.916	34.29	18.64	2.6876	45.09	0.0015706
769.81	52.93	5.406	6513.4	89.849	41.70	20.19	3.6041	53.28	0.0015307
769.81	72.02	5.670	6831.2	115.905	50.85	22.15	5.6032	63.74	0.0014191
769.81	83.85	5.881	7086.1	132.677	56.84	23.58	6.8818	70.48	0.0014243
769.81	98.78	6.278	7564.3	146.738	62.10	24.55	8.8828	76.12	0.0013225
769.81	117.96	6.616	7971.7	171.915	71.08	26.62	11.127	86.87	0.0012577
769.81	133.34	7.001	8434.6	190.635	78.69	28.12	13.035	94.93	0.0012348

Water mass flux: reference measurement from rotameters
Gas mass flux: reference measurement from orifice
DP1: deltaP over straight pipe section
DP/DZ: pressure gradient over straight pipe section
DP2: deltaP across the venturi (upstream-throat)
PVEN1: absolute pressure upstream of venturi throat
PVEN2: absolute pressure downstream of venturi throat
DPAIR: deltaP across orifice for air reference measurement
PAIR: absolute pressure in air line before feed to tube
t film: film thickness from gamma-ray measurement

Experimental set No. 5

water mass flux kg/m2/s	gas mass flux kg/m2/s	DP1 kPa	DP/DZ Pa/m	DP2 kPa	PVEN1 psia	Pswirl psia	DPAIR "H2O	PAIR psia	t film m
103.06	45.46	2.151	2868.3	31.338	20.53	21.02	5.5946	26.03	0.0004354
103.06	51.22	2.502	3336.4	38.300	21.96	22.49	6.5983	28.15	0.0004040
103.06	73.15	3.068	4090.7	62.545	27.48	28.06	10.827	35.48	0.0003270
103.06	114.21	3.763	5016.8	101.730	40.15	40.73	18.441	51.48	0.0002521
103.06	136.05	4.117	5489.6	119.540	46.53	47.05	22.731	59.58	0.0002294
103.06	179.45	4.726	6301.1	154.683	59.02	59.74	31.512	75.53	0.0001893
103.06	205.15	5.398	7197.8	177.362	67.35	68.15	36.12	86.30	0.0002172
274.48	39.84	3.022	4029.2	41.525	24.30	24.84	3.5103	31.11	0.0008947
274.48	66.00	4.064	5418.8	74.317	33.30	33.84	7.1194	42.52	0.0007843
274.48	76.22	4.428	5903.8	86.763	37.01	37.76	8.5724	47.25	0.0007592
274.48	104.52	5.173	6897.7	115.972	46.35	47.11	13.035	58.95	0.0007360
274.48	133.83	5.798	7731.0	143.631	56.15	56.99	17.834	71.11	0.0006929
274.48	160.97	6.361	8480.7	167.799	64.88	65.89	22.497	82.14	0.0006534
274.48	179.97	6.751	9001.2	185.278	71.43	72.44	25.678	90.17	0.0006450
450.54	39.48	4.032	5375.9	50.401	27.99	28.72	2.8803	36.79	0.0009113
450.54	63.57	4.995	6659.4	84.443	38.42	39.17	5.626	49.22	0.0008521
450.54	79.00	5.371	7161.1	103.014	44.51	45.36	7.5822	56.64	0.0008060
450.54	100.05	5.647	7529.2	126.787	53.09	53.86	10.397	66.57	0.0008260
450.54	131.26	6.197	8262.8	159.218	64.78	65.79	14.842	80.77	0.0008170
450.54	150.04	6.500	8666.9	177.608	71.22	72.19	17.69	88.85	0.0008125
450.54	155.51	6.593	8791.3	182.445	73.09	74.04	18.532	91.19	0.0008144
769.81	49.17	6.825	9099.6	84.581	39.52	40.90	3.1501	51.93	0.0008785
769.81	63.56	7.271	9694.0	104.853	46.55	47.43	4.564	60.10	0.0008312
769.81	76.98	7.608	10143.4	125.322	53.68	55.02	5.9016	68.33	0.0008487
769.81	91.90	7.918	10557.1	144.052	59.89	60.96	7.5572	76.26	0.0007891
769.81	109.77	7.953	10604.5	164.966	67.64	68.61	9.685	85.18	0.0008041
769.81	123.15	8.210	10946.2	181.201	74.31	75.76	11.26	92.36	0.0007889

Water mass flux: reference measurement from rotameters
Gas mass flux: reference measurement from orifice
DP1: deltaP over straight pipe section
DP/DZ: pressure gradient over straight pipe section
DP2: deltaP across the venturi (upstream-throat)
PVEN1: absolute pressure upstream of venturi throat
PVEN2: absolute pressure downstream of venturi throat
DPAIR: deltaP across orifice for air reference measurement
PAIR: absolute pressure in air line before feed to tube
t film: film thickness from gamma-ray measurement

Experimental set No. 6

water mass flux kg/m2/s	gas mass flux kg/m2/s	DP1 kPa	DP/DZ Pa/m	DP2 kPa	PVEN1 psia	Pswirl psia	DPAIR "H2O	PAIR psia	t film m
103.06	37.65	2.003	2743.9	28.437	19.68	20.08	4.8874	20.57	0.0005489
103.06	53.75	2.591	3549.3	47.351	23.66	24.06	7.9684	26.10	0.0004636
103.06	73.15	2.823	3866.7	61.733	27.05	28.06	10.827	35.48	0.0004078
103.06	107.81	3.634	4977.9	100.279	39.77	40.15	18.333	46.55	0.0003727
103.06	131.02	3.906	5350.4	118.665	46.36	46.74	23.121	54.85	0.0003514
103.06	169.71	4.613	6319.6	151.081	58.08	58.71	30.557	69.87	0.0003400
103.06	209.37	5.296	7254.6	183.431	69.81	70.54	38.461	84.80	0.0003280
274.48	37.74	2.785	3815.4	41.757	24.59	24.96	3.6331	27.11	0.0009638
274.48	58.92	3.591	4918.9	68.554	31.83	32.26	6.6724	36.38	0.0008448
274.48	88.41	4.424	6059.7	102.287	41.96	42.70	11.226	49.16	0.0006882
274.48	136.54	5.488	7518.4	148.551	58.07	58.83	19.242	69.18	0.0006213
274.48	156.46	5.892	8071.6	167.091	64.78	65.60	22.607	77.55	0.0005676
450.54	36.84	3.901	5343.6	50.317	27.60	28.34	2.8896	32.14	0.0010128
450.54	80.07	5.150	7054.5	109.568	46.16	46.99	8.1773	54.36	0.0008756
450.54	94.65	5.432	7441.4	125.828	51.80	52.69	10.167	61.30	0.0008579
450.54	150.09	6.307	8639.5	183.939	72.72	74.06	18.282	86.60	0.0007983
450.54	165.66	6.437	8817.4	196.426	77.22	78.12	21.077	91.89	0.0007721
769.81	53.66	6.360	8711.8	96.053	42.73	43.28	3.8151	51.42	0.0010256
769.81	90.00	7.291	9987.5	146.125	60.84	61.68	7.6979	72.20	0.0009248
769.81	117.66	7.744	10607.9	178.286	72.96	74.03	11.079	86.16	0.0008688
769.81	117.66	7.744	10607.9	178.286	72.96	74.03	11.079	86.16	0.0008718

Water mass flux: reference measurement from rotameters
Gas mass flux: reference measurement from orifice
DP1: deltaP over straight pipe section
DP/DZ: pressure gradient over straight pipe section
DP2: deltaP across the venturi (upstream-throat)
PVEN1: absolute pressure upstream of venturi throat
PVEN2: absolute pressure downstream of venturi throat
DPAIR: deltaP across orifice for air reference measurement
PAIR: absolute pressure in air line before feed to tube
t film: film thickness from gamma-ray measurement

Appendix II

EQUATIONS FOR TRANSIENT TWO-PHASE ANNULAR FLOW

Developed by Prof. J.R. Barbosa, University of Santa Catarina, Brazil

CONSERVATION PRINCIPLES

MASS CONSERVATION

Entrained droplets

$$\frac{\partial}{\partial t}\left(\rho_L A_{LE}\right)+\frac{\partial}{\partial z}\dot{M}_{LE}=\left(E-D-\dot{m}_{I,LE}\right)P_w$$

Gas

$$\frac{\partial}{\partial t}\left(\rho_G A_G\right)+\frac{\partial}{\partial z}\dot{M}_G=\left(\dot{m}_{I,LF}+\dot{m}_{I,LE}\right)P_w$$

Liquid film

$$\frac{\partial}{\partial t}\left(\rho_L A_{LF}\right)+\frac{\partial}{\partial z}\dot{M}_{LF}=\left(D-E-\dot{m}_{I,LF}\right)P_w$$

ENERGY CONSERVATION

$$\dot{q}_w P_w+\tau_w u_{LF} P_w=\frac{\partial}{\partial t}\left(\rho_L A_{LF} h_L+\rho_L A_{LE} h_L+\rho_G A_G h_G\right)+\frac{\partial}{\partial t}\left(\rho_L A_{LF}\frac{u_{LF}^2}{2}+\rho_L A_{LE}\frac{u_{LE}^2}{2}+\rho_G A_G\frac{u_G^2}{2}\right)+gz\frac{\partial}{\partial t}\left(\rho_L A_{LF}+\rho_L A_{LE}+\rho_G A_G\right)$$

$$-A\frac{\partial}{\partial t}p+\frac{\partial}{\partial z}\left(\dot{M}_{LF} h_L+\dot{M}_{LE} h_L+\dot{M}_G h_G\right)+\frac{\partial}{\partial z}\left(\dot{M}_{LF}\frac{u_{LF}^2}{2}+\dot{M}_{LE}\frac{u_{LE}^2}{2}+\dot{M}_G\frac{u_G^2}{2}\right)+g\dot{M}$$

MOMENTUM CONSERVATION

$$-A\frac{\partial}{\partial z}p - P_w\tau_w - g\left(\rho_L A_{LF} + \rho_L A_{LE} + \rho_G A_G\right) = \frac{\partial}{\partial t}\left(\rho_L A_{LF}u_{LF} + \rho_L A_{LE}u_{LE} + \rho_G A_G u_G\right) + \frac{\partial}{\partial z}\left(\dot{M}_{LF}u_{LF} + \dot{M}_{LE}u_{LE} + \dot{M}_G u_G\right)$$

Ancillary definitions:

$$A = A_{LF} + A_{LE} + A_G \qquad P_I = 2\pi r_I \qquad P_w = 2\pi R$$

Introducing the cross-sectional area fractions and mass fractions

$$\varepsilon_{LF} = \frac{A_{LF}}{A};\ \varepsilon_{LE} = \frac{A_{LE}}{A};\ \varepsilon_G = \frac{A_G}{A}$$

$$x_{LF} = \frac{\dot{M}_{LF}}{\dot{M}};\ \ x_{LE} = \frac{\dot{M}_{LE}}{\dot{M}};\ x_G = \frac{\dot{M}_G}{\dot{M}}$$

and also the definitions of the real phase velocities,

$$u_{LF} = \frac{Gx_{LF}}{\rho_L \varepsilon_{LF}}$$

$$u_{LE} = \frac{Gx_{LE}}{\rho_L \varepsilon_{LE}}$$

$$u_G = \frac{G x_G}{\rho_G \varepsilon_G}$$

the original conservation equations become:

MASS CONSERVATION

Entrained droplets

$$\frac{\partial}{\partial t}(\rho_L \varepsilon_{LE}) + \frac{\partial}{\partial z}(G\, x_{LE}) = \frac{4}{d_T}(E - D - \dot{m}_{I,LE})$$

Gas

$$\frac{\partial}{\partial t}(\rho_G \varepsilon_G) + \frac{\partial}{\partial z}(G\, x_G) = \frac{4}{d_T}(\dot{m}_{I,LF} + \dot{m}_{I,LE})$$

Liquid film

$$\frac{\partial}{\partial t}(\rho_L \varepsilon_{LF}) + \frac{\partial}{\partial z}(G\, x_{LF}) = \frac{4}{d_T}(D - E - \dot{m}_{I,LF})$$

ENERGY CONSERVATION

$$\frac{4}{d_T}\left(\dot{q}_w + \tau_w \frac{G x_{LF}}{\rho_L \varepsilon_{LF}}\right) = \frac{\partial}{\partial t}[\rho_L h_L(\varepsilon_{LE} + \varepsilon_{LF}) + \rho_G h_G \varepsilon_G] + \frac{1}{2}\frac{\partial}{\partial t}\left(\frac{G^2 x_{LF}^2}{\rho_L \varepsilon_{LF}} + \frac{G^2 x_{LE}^2}{\rho_L \varepsilon_{LE}} + \frac{G^2 x_G^2}{\rho_G \varepsilon_G}\right) + gz\frac{\partial}{\partial t}[\rho_L(\varepsilon_{LF} + \varepsilon_{LE}) + \rho_G \varepsilon_G]$$

$$-\frac{\partial}{\partial t}p + \frac{\partial}{\partial z}[G h_L(x_{LF} + x_{LE}) + G h_G x_G] + \frac{1}{2}\frac{\partial}{\partial z}\left(\frac{G^3 x_{LF}^3}{\rho_L^2 \varepsilon_{LF}^2} + \frac{G^3 x_{LE}^3}{\rho_L^2 \varepsilon_{LE}^2} + \frac{G^3 x_G^3}{\rho_G^2 \varepsilon_G^2}\right) + gG$$

MOMENTUM CONSERVATION

$$-\frac{\partial}{\partial z}p-\frac{4}{d_T}\tau_w-g[\rho_L(\varepsilon_{LF}+\varepsilon_{LE})+\rho_G\varepsilon_G]=\frac{\partial}{\partial t}G+\frac{\partial}{\partial z}\left(\frac{G^2x_{LF}^2}{\rho_L\varepsilon_{LF}}+\frac{G^2x_{LE}^2}{\rho_L\varepsilon_{LE}}+\frac{G^2x_G^2}{\rho_G\varepsilon_G}\right)$$

BOUNDARY CONDITIONS

- Pressure at pipe inlet as a function of time: $p(0,t)=p_{in}(t)$
- Pressure at pipe outlet as a function of time: $p(L,t)=p_{out}(t)$
- Inlet (or outlet) quality as a function of time: $x_G(0,t)=x_{G,in}(t)$ or $x_G(L,t)=x_{G,out}(t)$
- Inlet (or outlet) entrained fraction as a function of time: $ef(0,t)=ef_{in}(t)$ or $ef(L,t)=ef_{out}(t)$
- Inlet (or outlet) void fraction as a function of time: $\varepsilon_G(0,t)=\varepsilon_{G,in}(t)$ or $\varepsilon_G(L,t)=\varepsilon_{G,out}(t)$
- Initial total mass flux: $G(z,0)=G_0$
- Initial quality profile: $x_G(z,0)=x_{G,0}(z)$
- Initial entrained fraction profile: $ef(z,0)=ef_0(z)$; where $ef=x_{LE}/(x_{LE}+x_{LF})$
- Initial film thickness profile: $\delta(z,0)=\delta_0(z)$; *where* $\delta=d_T\varepsilon_{LF}/4$
- Initial void fraction profile: $\varepsilon_G(z,0)=\varepsilon_{G,0}(z)$

CLOSURE

The system of equations has 9 unknown variables: $(p,G,x_{LF},x_{LE},x_G,\varepsilon_{LF},\varepsilon_{LE},\varepsilon_G,\tau_w)$. We therefore require 4 additional relationships. These are as follows

- Void fraction constraint: $1=\varepsilon_{LF}+\varepsilon_{LE}+\varepsilon_G$
- Mass fraction constraint: $1=x_{LF}+x_{LE}+x_G$
- A correlation for the wall shear stress: $\tau_w=\tau_w(\tau_I,\rho_G,\rho_L,...)$

- A triangular relationship between film thickness, film flow rate and wall shear stress:

$$\dot{M}^{+}_{LF} = f\left(\delta^{+}\right); \quad \text{where } \dot{M}^{+}_{LF} = \frac{\dot{M}_{LF}}{\pi d_T \eta_L},\ \delta^{+} = \frac{\rho_L u^{*} \delta}{\eta_L},\ u^{*} = \sqrt{\frac{\tau_w}{\rho_L}}$$

In order to simplify the governing equations, the following operations were performed:

1. the void fraction and mass fraction constraints were introduced in the governing equations

$$\varepsilon_{LE} = 1 - \varepsilon_{LF} - \varepsilon_G$$

$$x_{LE} = 1 - x_{LF} - x_G$$

2. the physical properties (density, enthalpy) terms were expressed as functions of p and x_G, referring to the liquid and vapour densities of a *NOC* component mixture as an example:

$$\frac{\partial \rho_L}{\partial z} = \left.\frac{\partial \rho_L}{\partial p}\right|_{sat} \frac{\partial p}{\partial z} + \left.\frac{\partial \rho_L}{\partial T}\right|_{sat} \frac{\partial T}{\partial z} + \sum_{i=1}^{NOC-1} \left(\left.\frac{\partial \rho_L}{\partial w_{L,i}}\right|_{sat} \frac{\partial w_{L,i}}{\partial z} \right)$$

$$\frac{\partial \rho_G}{\partial z} = \left.\frac{\partial \rho_G}{\partial p}\right|_{sat} \frac{\partial p}{\partial z} + \left.\frac{\partial \rho_G}{\partial T}\right|_{sat} \frac{\partial T}{\partial z} + \sum_{i=1}^{NOC-1} \left(\left.\frac{\partial \rho_G}{\partial w_{G,i}}\right|_{sat} \frac{\partial w_{G,i}}{\partial z} \right)$$

where $w_{L,i}$ and $w_{G,i}$ are the equilibrium mass fractions of the i-th component in the liquid and vapour phases. For the simple case of a binary mixture:

$$\frac{\partial \rho_L}{\partial z} = \left.\frac{\partial \rho_L}{\partial p}\right|_{sat} \frac{\partial p}{\partial z} + \left.\frac{\partial \rho_L}{\partial T}\right|_{sat} \frac{\partial T}{\partial z} + \left.\frac{\partial \rho_L}{\partial w_L}\right|_{sat} \frac{\partial w_L}{\partial z}$$

$$\frac{\partial \rho_G}{\partial z} = \left.\frac{\partial \rho_G}{\partial p}\right|_{sat} \frac{\partial p}{\partial z} + \left.\frac{\partial \rho_G}{\partial T}\right|_{sat} \frac{\partial T}{\partial z} + \left.\frac{\partial \rho_G}{\partial w_G}\right|_{sat} \frac{\partial w_G}{\partial z},$$

where:

$$\frac{\partial T}{\partial z} = \left.\frac{\partial T}{\partial p}\right|_{sat} \frac{\partial p}{\partial z} + \left.\frac{\partial T}{\partial w_L}\right|_{sat} \frac{\partial w_L}{\partial z} \qquad \text{(for the liquid)}$$

$$\frac{\partial T}{\partial z} = \left.\frac{\partial T}{\partial p}\right|_{sat} \frac{\partial p}{\partial z} + \left.\frac{\partial T}{\partial w_G}\right|_{sat} \frac{\partial w_G}{\partial z} \qquad \text{(for the vapour)}$$

From equilibrium relationships, it is known that:

$$x_G = \frac{w_o - w_L}{w_G - w_L}$$

where w_o is the overall mass fraction. Thus, by substituting the equations above, it is possible to write:

$$\frac{\partial \rho_L}{\partial z} = \left(\left.\frac{\partial \rho_L}{\partial p}\right|_{sat} + \left.\frac{\partial \rho_L}{\partial T}\right|_{sat} \left.\frac{\partial T}{\partial p}\right|_{sat} \right) \frac{\partial p}{\partial z} + \left(\left.\frac{\partial w_L}{\partial x_G}\right|_{sat} \right) \left(\left.\frac{\partial \rho_L}{\partial w_L}\right|_{sat} + \left.\frac{\partial \rho_L}{\partial T}\right|_{sat} \left.\frac{\partial T}{\partial w_L}\right|_{sat} \right) \frac{\partial x_G}{\partial z}$$

$$\frac{\partial \rho_G}{\partial z} = \left(\left.\frac{\partial \rho_G}{\partial p}\right|_{sat} + \left.\frac{\partial \rho_G}{\partial T}\right|_{sat} \left.\frac{\partial T}{\partial p}\right|_{sat} \right) \frac{\partial p}{\partial z} + \left(\left.\frac{\partial w_G}{\partial x_G}\right|_{sat} \left(\left.\frac{\partial \rho_G}{\partial w_G}\right|_{sat} + \left.\frac{\partial \rho_G}{\partial T}\right|_{sat} \left.\frac{\partial T}{\partial w_G}\right|_{sat} \right) \frac{\partial x_G}{\partial z} \right.$$

The above results can be extended to the time derivatives:

$$\frac{\partial \rho_L}{\partial t} = \left(\left.\frac{\partial \rho_L}{\partial p}\right|_{sat} + \left.\frac{\partial \rho_L}{\partial T}\right|_{sat} \left.\frac{\partial T}{\partial p}\right|_{sat} \right) \frac{\partial p}{\partial t} + \left(\left.\frac{\partial w_L}{\partial x_G}\right|_{sat} \left(\left.\frac{\partial \rho_L}{\partial w_L}\right|_{sat} + \left.\frac{\partial \rho_L}{\partial T}\right|_{sat} \left.\frac{\partial T}{\partial w_L}\right|_{sat} \right) \frac{\partial x_G}{\partial t} \right.$$

$$\frac{\partial \rho_G}{\partial t} = \left(\left.\frac{\partial \rho_G}{\partial p}\right|_{sat} + \left.\frac{\partial \rho_G}{\partial T}\right|_{sat} \left.\frac{\partial T}{\partial p}\right|_{sat} \right) \frac{\partial p}{\partial t} + \left(\left.\frac{\partial w_G}{\partial x_G}\right|_{sat} \left(\left.\frac{\partial \rho_G}{\partial w_G}\right|_{sat} + \left.\frac{\partial \rho_G}{\partial T}\right|_{sat} \left.\frac{\partial T}{\partial w_G}\right|_{sat} \right) \frac{\partial x_G}{\partial t} \right.$$

$$\frac{\partial h_L}{\partial t} = \left(\left.\frac{\partial h_L}{\partial p}\right|_{sat} + \left.\frac{\partial h_L}{\partial T}\right|_{sat} \left.\frac{\partial T}{\partial p}\right|_{sat} \right) \frac{\partial p}{\partial t} + \left(\left.\frac{\partial w_L}{\partial x_G}\right|_{sat} \left(\left.\frac{\partial h_L}{\partial w_L}\right|_{sat} + \left.\frac{\partial h_L}{\partial T}\right|_{sat} \left.\frac{\partial T}{\partial w_L}\right|_{sat} \right) \frac{\partial x_G}{\partial t} \right.$$

$$\frac{\partial h_G}{\partial t} = \left(\left.\frac{\partial h_G}{\partial p}\right|_{sat} + \left.\frac{\partial h_G}{\partial T}\right|_{sat} \left.\frac{\partial T}{\partial p}\right|_{sat} \right) \frac{\partial p}{\partial t} + \left(\left.\frac{\partial w_G}{\partial x_G}\right|_{sat} \left(\left.\frac{\partial h_G}{\partial w_G}\right|_{sat} + \left.\frac{\partial h_G}{\partial T}\right|_{sat} \left.\frac{\partial T}{\partial w_G}\right|_{sat} \right) \frac{\partial x_G}{\partial t} \right.$$

By substituting the above relationships in the governing equations, these can be re-written as follows:

GAS MASS CONSERVATION

$$GK_{19}\frac{\partial p}{\partial t}+GK_3\frac{\partial x_G}{\partial t}+GK_5\frac{\partial \varepsilon_G}{\partial t}+GK_{10}\frac{\partial G}{\partial z}+GK_{12}\frac{\partial x_G}{\partial z}=GK_0$$

where

$$GK_3=\varepsilon_G\left(\left.\frac{\partial w_G}{\partial x_G}\right|_{sat}\right)\left(\left.\frac{\partial \rho_G}{\partial w_G}\right|_{sat}+\left.\frac{\partial T}{\partial w_G}\right|_{sat}\left.\frac{\partial \rho_G}{\partial T}\right|_{sat}\right)$$

$$GK_5=\rho_G$$

$$GK_{10}=x_G$$

$$GK_{12}=G$$

$$GK_{19}=\varepsilon_G\left(\left.\frac{\partial \rho_G}{\partial p}\right|_{sat}+\left.\frac{\partial T}{\partial p}\right|_{sat}\left.\frac{\partial \rho_G}{\partial T}\right|_{sat}\right)$$

$$GK_0=\frac{4}{d_T}\left(\dot{m}_{I,LE}+\dot{m}_{I,LF}\right)$$

LIQUID FILM MASS CONSERVATION

$$FK_{19}\frac{\partial p}{\partial t}+FK_3\frac{\partial x_G}{\partial t}+FK_4\frac{\partial \varepsilon_{LF}}{\partial t}+FK_{10}\frac{\partial G}{\partial z}+FK_{11}\frac{\partial x_{LF}}{\partial z}=FK_0$$

where

$$FK_3 = \varepsilon_{LF}\left(\left.\frac{\partial w_L}{\partial x_G}\right|_{sat}\right)\left(\left.\frac{\partial \rho_L}{\partial w_L}\right|_{sat} + \left.\frac{\partial T}{\partial w_L}\right|_{sat}\left.\frac{\partial \rho_L}{\partial T}\right|_{sat}\right)$$

$$FK_4 = \rho_L$$

$$FK_{10} = x_{LF}$$

$$FK_{11} = G$$

$$FK_{19} = \varepsilon_{LF}\left(\left.\frac{\partial \rho_L}{\partial p}\right|_{sat} + \left.\frac{\partial T}{\partial p}\right|_{sat}\left.\frac{\partial \rho_L}{\partial T}\right|_{sat}\right)$$

$$FK_0 = \frac{4}{d_T}\left(D - E - \dot{m}_{I,LF}\right)$$

LIQUID DROPLETS MASS CONSERVATION

$$DK_{19}\frac{\partial p}{\partial t} + DK_3\frac{\partial x_G}{\partial t} + DK_4\frac{\partial \varepsilon_{LF}}{\partial t} + DK_5\frac{\partial \varepsilon_G}{\partial t} + DK_{10}\frac{\partial G}{\partial z} + DK_{11}\frac{\partial x_{LF}}{\partial z} + DK_{12}\frac{\partial x_G}{\partial z} = DK_0$$

where

$$DK_3 = \left(1 - \varepsilon_{LF} - \varepsilon_G\right)\left(\left.\frac{\partial w_L}{\partial x_G}\right|_{sat}\right)\left(\left.\frac{\partial \rho_L}{\partial w_L}\right|_{sat} + \left.\frac{\partial T}{\partial w_L}\right|_{sat}\left.\frac{\partial \rho_L}{\partial T}\right|_{sat}\right)$$

$$DK_4 = -\rho_L$$

$$DK_5 = -\rho_L$$

$$DK_{10} = \left(1 - x_{LF} - x_G\right)$$

$$DK_{11} = -G$$

$$DK_{12} = -G$$

$$DK_{19} = \left(1 - \varepsilon_{LF} - \varepsilon_G\right)\left(\left.\frac{\partial \rho_L}{\partial p}\right|_{sat} + \left.\frac{\partial T}{\partial p}\right|_{sat}\left.\frac{\partial \rho_L}{\partial T}\right|_{sat}\right)$$

$$DK_0 = \frac{4}{d_T}\left(E - D - \dot{m}_{I,LE}\right)$$

ENERGY CONSERVATION

$$EK_{23}\frac{\partial p}{\partial t} + EK_1\frac{\partial G}{\partial t} + EK_2\frac{\partial x_{LF}}{\partial t} + EK_{21}\frac{\partial x_G}{\partial t} + EK_4\frac{\partial \varepsilon_{LF}}{\partial t} + EK_5\frac{\partial \varepsilon_G}{\partial t} +$$
$$EK_{20}\frac{\partial p}{\partial z} + EK_{10}\frac{\partial G}{\partial z} + EK_{11}\frac{\partial x_{LF}}{\partial z} + EK_{22}\frac{\partial x_G}{\partial z} + EK_{13}\frac{\partial \varepsilon_{LF}}{\partial z} + EK_{14}\frac{\partial \varepsilon_G}{\partial z} = EK_0$$

where

$$EK_1 = G\left[\frac{x_{LF}^2}{\rho_L \varepsilon_{LF}} + \frac{x_G^2}{\rho_G \varepsilon_G} + \frac{(1 - x_{LF} - x_G)^2}{\rho_L (1 - \varepsilon_{LF} - \varepsilon_G)}\right]$$

$$EK_2 = \frac{G^2}{\rho_L}\left[\frac{x_{LF}}{\varepsilon_{LF}} - \frac{(1 - x_{LF} - x_G)}{(1 - \varepsilon_{LF} - \varepsilon_G)}\right]$$

$$EK_3 = G^2\left[\frac{x_G}{\rho_G \varepsilon_G} - \frac{(1 - x_{LF} - x_G)}{\rho_L (1 - \varepsilon_{LF} - \varepsilon_G)}\right]$$

$$EK_4 = \frac{1}{2}\frac{G^2}{\rho_L}\left[\frac{(1 - x_{LF} - x_G)^2}{(1 - \varepsilon_{LF} - \varepsilon_G)^2} - \frac{x_{LF}^2}{\varepsilon_{LF}^2}\right]$$

$$EK_5 = \left\{(\rho_G h_G - \rho_L h_L) + \frac{1}{2}G^2\left[\frac{(1 - x_{LF} - x_G)^2}{\rho_L (1 - \varepsilon_{LF} - \varepsilon_G)^2} - \frac{x_G^2}{\rho_G \varepsilon_G^2}\right] + gz(\rho_G - \rho_L)\right\}$$

$$EK_6 = \left\{h_L (1 - \varepsilon_G) - \frac{1}{2}\frac{G^2}{\rho_L^2}\left[\frac{x_{LF}^2}{\varepsilon_{LF}}\frac{(1 - x_{LF} - x_G)^2}{(1 - \varepsilon_{LF} - \varepsilon_G)} - \right] + gz(1 - \varepsilon_G)\right\}$$

$$EK_7 = \left\{h_G \varepsilon_G - \frac{1}{2}\frac{G^2}{\rho_G^2}\frac{x_G^2}{\varepsilon_G} + gz\varepsilon_G\right\}$$

$$EK_8 = \rho_L (1 - \varepsilon_G)$$

$$EK_9 = \rho_G \varepsilon_G$$

$$EK_{10} = \left\{ \left[\left(x_G h_G - \left(1 - x_G\right) h_L \right) \right] + \frac{3}{2} G^2 \left[\frac{x_{LF}^3}{\rho_L^2 \varepsilon_{LF}^2} + \frac{x_G^3}{\rho_G^2 \varepsilon_G^2} + \frac{\left(1 - x_{LF} - x_G\right)^3}{\rho_L^2 \left(1 - \varepsilon_{LF} - \varepsilon_G\right)^2} \right] \right\}$$

$$EK_{11} = \left\{ \frac{3}{2} \frac{G^3}{\rho_L^2} \left[\frac{x_{LF}^2}{\varepsilon_{LF}^2} - \frac{\left(1 - x_{LF} - x_G\right)^2}{\left(1 - \varepsilon_{LF} - \varepsilon_G\right)^2} \right] \right\}$$

$$EK_{12} = \left\{ G\left(h_G - h_L\right) + \frac{3}{2} G^3 \left[\frac{x_G^2}{\rho_G^2 \varepsilon_G^2} - \frac{\left(1 - x_{LF} - x_G\right)^2}{\rho_L^2 \left(1 - \varepsilon_{LF} - \varepsilon_G\right)^2} \right] \right\}$$

$$EK_{13} = \frac{G^3}{\rho_L^2} \left[\frac{\left(1 - x_{LF} - x_G\right)^3}{\left(1 - \varepsilon_{LF} - \varepsilon_G\right)^3} - \frac{x_{LF}^3}{\varepsilon_{LF}^3} \right]$$

$$EK_{14} = G^3 \left[\frac{\left(1 - x_{LF} - x_G\right)^3}{\rho_L^2 \left(1 - \varepsilon_{LF} - \varepsilon_G\right)^3} - \frac{x_G^3}{\rho_G^2 \varepsilon_G^3} \right]$$

$$EK_{15} = -\frac{G^3}{\rho_L^3} \left[\frac{x_{LF}^3}{\varepsilon_{LF}^2} - \frac{\left(1 - x_{LF} - x_G\right)^3}{\left(1 - \varepsilon_{LF} - \varepsilon_G\right)^2} \right]$$

$$EK_{16} = -\frac{G^3 x_G^3}{\rho_G^3 \varepsilon_G^2}$$

$$EK_{17} = G\left(1 - x_G\right)$$

$$EK_{18} = G x_G$$

$$EK_{20} = EK_{15}\left(\left.\frac{\partial \rho_L}{\partial p}\right|_{sat} + \left.\frac{\partial T}{\partial p}\right|_{sat}\left.\frac{\partial \rho_L}{\partial T}\right|_{sat}\right) + EK_{16}\left(\left.\frac{\partial \rho_G}{\partial p}\right|_{sat} + \left.\frac{\partial T}{\partial p}\right|_{sat}\left.\frac{\partial \rho_G}{\partial T}\right|_{sat}\right) +$$
$$EK_{17}\left(\left.\frac{\partial h_L}{\partial p}\right|_{sat} + \left.\frac{\partial T}{\partial p}\right|_{sat}\left.\frac{\partial h_L}{\partial T}\right|_{sat}\right) + EK_{18}\left(\left.\frac{\partial h_G}{\partial p}\right|_{sat} + \left.\frac{\partial T}{\partial p}\right|_{sat}\left.\frac{\partial h_G}{\partial T}\right|_{sat}\right)$$

$$EK_{21} = EK_3 + EK_6\left(\left.\frac{\partial w_L}{\partial x_G}\right|_{sat}\right)\left(\left.\frac{\partial \rho_L}{\partial w_L}\right|_{sat} + \left.\frac{\partial T}{\partial w_L}\right|_{sat}\left.\frac{\partial \rho_L}{\partial T}\right|_{sat}\right) + EK_7\left(\left.\frac{\partial w_G}{\partial x_G}\right|_{sat}\right)\left(\left.\frac{\partial \rho_G}{\partial w_L}\right|_{sat} + \left.\frac{\partial T}{\partial w_L}\right|_{sat}\left.\frac{\partial \rho_G}{\partial T}\right|_{sat}\right) +$$
$$EK_8\left(\left.\frac{\partial w_L}{\partial x_G}\right|_{sat}\right)\left(\left.\frac{\partial h_L}{\partial w_L}\right|_{sat} + \left.\frac{\partial T}{\partial w_L}\right|_{sat}\left.\frac{\partial h_L}{\partial T}\right|_{sat}\right) + EK_9\left(\left.\frac{\partial w_G}{\partial x_G}\right|_{sat}\right)\left(\left.\frac{\partial h_G}{\partial w_L}\right|_{sat} + \left.\frac{\partial T}{\partial w_L}\right|_{sat}\left.\frac{\partial h_G}{\partial T}\right|_{sat}\right)$$

$$EK_{22} = EK_{12} + EK_{15}\left(\left.\frac{\partial w_L}{\partial x_G}\right|_{sat}\right)\left(\left.\frac{\partial \rho_L}{\partial w_L}\right|_{sat} + \left.\frac{\partial T}{\partial w_L}\right|_{sat}\left.\frac{\partial \rho_L}{\partial T}\right|_{sat}\right) + EK_{16}\left(\left.\frac{\partial w_G}{\partial x_G}\right|_{sat}\right)\left(\left.\frac{\partial \rho_G}{\partial w_L}\right|_{sat} + \left.\frac{\partial T}{\partial w_L}\right|_{sat}\left.\frac{\partial \rho_G}{\partial T}\right|_{sat}\right) +$$
$$EK_{17}\left(\left.\frac{\partial w_L}{\partial x_G}\right|_{sat}\right)\left(\left.\frac{\partial h_L}{\partial w_L}\right|_{sat} + \left.\frac{\partial T}{\partial w_L}\right|_{sat}\left.\frac{\partial h_L}{\partial T}\right|_{sat}\right) + EK_{18}\left(\left.\frac{\partial w_G}{\partial x_G}\right|_{sat}\right)\left(\left.\frac{\partial h_G}{\partial w_L}\right|_{sat} + \left.\frac{\partial T}{\partial w_L}\right|_{sat}\left.\frac{\partial h_G}{\partial T}\right|_{sat}\right)$$

$$EK_{23} = -1 + EK_6\left(\left.\frac{\partial \rho_L}{\partial p}\right|_{sat} + \left.\frac{\partial T}{\partial p}\right|_{sat}\left.\frac{\partial \rho_L}{\partial T}\right|_{sat}\right) + EK_7\left(\left.\frac{\partial \rho_G}{\partial p}\right|_{sat} + \left.\frac{\partial T}{\partial p}\right|_{sat}\left.\frac{\partial \rho_G}{\partial T}\right|_{sat}\right) +$$
$$EK_8\left(\left.\frac{\partial h_L}{\partial p}\right|_{sat} + \left.\frac{\partial T}{\partial p}\right|_{sat}\left.\frac{\partial h_L}{\partial T}\right|_{sat}\right) + EK_9\left(\left.\frac{\partial h_G}{\partial p}\right|_{sat} + \left.\frac{\partial T}{\partial p}\right|_{sat}\left.\frac{\partial h_G}{\partial T}\right|_{sat}\right)$$

$$EK_0 = \frac{4}{d_T}\left(\tau_w \frac{Gx_{LF}}{\rho_L \varepsilon_{LF}} + \dot{q}_w\right) - gG$$

MOMENTUM CONSERVATION

$$MK_1 \frac{\partial G}{\partial t} + MK_{20} \frac{\partial p}{\partial z} + MK_{10} \frac{\partial G}{\partial z} + MK_{11} \frac{\partial x_{LF}}{\partial z} + MK_{22} \frac{\partial x_G}{\partial z} + MK_{13} \frac{\partial \varepsilon_{LF}}{\partial z} + MK_{14} \frac{\partial \varepsilon_G}{\partial z} = MK_0$$

where

$$MK_1 = 1$$

$$MK_{10} = 2G\left[\frac{x_{LF}^2}{\rho_L \varepsilon_{LF}} + \frac{x_G^2}{\rho_G \varepsilon_G} + \frac{(1 - x_{LF} - x_G)^2}{\rho_L (1 - \varepsilon_{LF} - \varepsilon_G)}\right]$$

$$MK_{11} = 2\frac{G^2}{\rho_L}\left[\frac{x_{LF}}{\varepsilon_{LF}} - \frac{(1 - x_{LF} - x_G)}{(1 - \varepsilon_{LF} - \varepsilon_G)}\right]$$

$$MK_{12} = 2G^2\left[\frac{x_G}{\rho_G \varepsilon_G} - \frac{(1 - x_{LF} - x_G)}{\rho_L (1 - \varepsilon_{LF} - \varepsilon_G)}\right]$$

$$MK_{13} = \frac{G^2}{\rho_L}\left[\frac{(1 - x_{LF} - x_G)^2}{(1 - \varepsilon_{LF} - \varepsilon_G)^2} - \frac{x_{LF}^2}{\varepsilon_{LF}^2}\right]$$

$$MK_{14} = G^2\left[\frac{(1 - x_{LF} - x_G)^2}{\rho_L (1 - \varepsilon_{LF} - \varepsilon_G)^2} - \frac{x_G^2}{\rho_G \varepsilon_G^2}\right]$$

$$MK_{15} = -\frac{G^2}{\rho_L^2}\left[\frac{x_{LF}^2}{\varepsilon_{LF}} + \frac{(1 - x_{LF} - x_G)^2}{(1 - \varepsilon_{LF} - \varepsilon_G)}\right]$$

$$MK_{16} = -\frac{G^2 x_G^2}{\rho_G^2 \varepsilon_G}$$

$$MK_{20} = 1 + MK_{15}\left(\left.\frac{\partial \rho_L}{\partial p}\right|_{sat} + \left.\frac{\partial T}{\partial p}\right|_{sat}\left.\frac{\partial \rho_L}{\partial T}\right|_{sat}\right) + MK_{16}\left(\left.\frac{\partial \rho_G}{\partial p}\right|_{sat} + \left.\frac{\partial T}{\partial p}\right|_{sat}\left.\frac{\partial \rho_G}{\partial T}\right|_{sat}\right)$$

$$MK_{22} = MK_{12} + MK_{15}\left(\left.\frac{\partial w_L}{\partial x_G}\right|_{sat}\left(\left.\frac{\partial \rho_L}{\partial w_L}\right|_{sat} + \left.\frac{\partial T}{\partial w_L}\right|_{sat}\left.\frac{\partial \rho_L}{\partial T}\right|_{sat}\right)\right) + MK_{16}\left(\left.\frac{\partial w_G}{\partial x_G}\right|_{sat}\left(\left.\frac{\partial \rho_G}{\partial w_L}\right|_{sat} + \left.\frac{\partial T}{\partial w_L}\right|_{sat}\left.\frac{\partial \rho_G}{\partial T}\right|_{sat}\right)\right)$$

$$MK_0 = -\frac{4}{d_T}\tau_w - g\left[\rho_L\left(1-\varepsilon_G\right) + \rho_G \varepsilon_G\right]$$

TRIANGULAR RELATIONSHIP

In its simplest form (thin film assumption), the triangular relationship can be written as:

$$\dot{M}_{LF} = \pi\, d_T\, \delta \sqrt{\frac{2\tau_I \rho_L}{f_{LF}}}$$

where

$$f_{LF} = 0.001069 + 143.8\left(\log \mathrm{Re}_{LF}\right)^{4.5}$$

$$\mathrm{Re}_{LF} = \frac{G\, x_{LF}}{\eta_L}$$

By re-writing the original equation in terms of mass flux and of liquid film fraction:

$$G x_{LF} = \varepsilon_{LF} \sqrt{\frac{2\tau_I \rho_L}{f_{LF}}}$$

The above equation can be linearised as follows:

$$G x_{LF} = \varepsilon_{LF} C_T$$

where

$$C_T = \sqrt{\frac{2\tau_I \rho_L}{f_{LF}}}$$

Thus,

$$\frac{\partial \varepsilon_{LF}}{\partial t} = \frac{1}{C_T} G \frac{\partial x_{LF}}{\partial t} + \frac{1}{C_T} x_{LF} \frac{\partial G}{\partial t}$$

$$\frac{\partial \varepsilon_{LF}}{\partial z} = \frac{1}{C_T} G \frac{\partial x_{LF}}{\partial z} + \frac{1}{C_T} x_{LF} \frac{\partial G}{\partial z}$$

And by substituting in the governing equations:

GAS MASS CONSERVATION

$$GK_{19}\frac{\partial p}{\partial t}+GK_{3}\frac{\partial x_{G}}{\partial t}+GK_{5}\frac{\partial \varepsilon_{G}}{\partial t}+GK_{10}\frac{\partial G}{\partial z}+GK_{12}\frac{\partial x_{G}}{\partial z}=GK_{0}$$

LIQUID FILM MASS CONSERVATION

$$FK_{19}\frac{\partial p}{\partial t}+FK_{3}\frac{\partial x_{G}}{\partial t}+FK_{4}\left(\frac{G}{C_{T}}\frac{\partial x_{LF}}{\partial t}+\frac{x_{LF}}{C_{T}}\frac{\partial G}{\partial t}\right)+FK_{10}\frac{\partial G}{\partial z}+FK_{11}\frac{\partial x_{LF}}{\partial z}=FK_{0}$$

LIQUID DROPLETS MASS CONSERVATION

$$DK_{19}\frac{\partial p}{\partial t}+DK_{3}\frac{\partial x_{G}}{\partial t}+DK_{4}\left(\frac{G}{C_{T}}\frac{\partial x_{LF}}{\partial t}+\frac{x_{LF}}{C_{T}}\frac{\partial G}{\partial t}\right)+DK_{5}\frac{\partial \varepsilon_{G}}{\partial t}+DK_{10}\frac{\partial G}{\partial z}+DK_{11}\frac{\partial x_{LF}}{\partial z}+DK_{12}\frac{\partial x_{G}}{\partial z}=DK_{0}$$

ENERGY CONSERVATION

$$EK_{23}\frac{\partial p}{\partial t}+EK_{1}\frac{\partial G}{\partial t}+EK_{2}\frac{\partial x_{LF}}{\partial t}+EK_{21}\frac{\partial x_{G}}{\partial t}+EK_{4}\left(\frac{G}{C_{T}}\frac{\partial x_{LF}}{\partial t}+\frac{x_{LF}}{C_{T}}\frac{\partial G}{\partial t}\right)+EK_{5}\frac{\partial \varepsilon_{G}}{\partial t}+$$

$$EK_{20}\frac{\partial p}{\partial z}+EK_{10}\frac{\partial G}{\partial z}+EK_{11}\frac{\partial x_{LF}}{\partial z}+EK_{22}\frac{\partial x_{G}}{\partial z}+EK_{13}\left(\frac{G}{C_{T}}\frac{\partial x_{LF}}{\partial z}+\frac{x_{LF}}{C_{T}}\frac{\partial G}{\partial z}\right)+EK_{14}\frac{\partial \varepsilon_{G}}{\partial z}=EK_{0}$$

MOMENTUM CONSERVATION

$$MK_1 \frac{\partial G}{\partial t} + MK_{20} \frac{\partial p}{\partial z} + MK_{10} \frac{\partial G}{\partial z} + MK_{11} \frac{\partial x_{LF}}{\partial z} + MK_{22} \frac{\partial x_G}{\partial z} + MK_{13} \left(\frac{G}{C_T} \frac{\partial x_{LF}}{\partial z} + \frac{x_{LF}}{C_T} \frac{\partial G}{\partial z} \right) + MK_{14} \frac{\partial \varepsilon_G}{\partial z} = MK_0$$

Rearranging the terms:

GAS MASS CONSERVATION

$$GK_{19} \frac{\partial p}{\partial t} + GK_3 \frac{\partial x_G}{\partial t} + GK_5 \frac{\partial \varepsilon_G}{\partial t} + GK_{10} \frac{\partial G}{\partial z} + GK_{12} \frac{\partial x_G}{\partial z} = GK_0$$

LIQUID FILM MASS CONSERVATION

$$FK_{19} \frac{\partial p}{\partial t} + FK_1 \frac{\partial G}{\partial t} + FK_2 \frac{\partial x_{LF}}{\partial t} + FK_3 \frac{\partial x_G}{\partial t} + FK_{10} \frac{\partial G}{\partial z} + FK_{11} \frac{\partial x_{LF}}{\partial z} = FK_0$$

where

$$FK_1 = FK_4 \frac{x_{LF}}{C_T}$$

$$FK_2 = FK_4 \frac{G}{C_T}$$

LIQUID DROPLETS MASS CONSERVATION

$$DK_{19}\frac{\partial p}{\partial t}+DK_{1}\frac{\partial G}{\partial t}+DK_{2}\frac{\partial x_{LF}}{\partial t}+DK_{3}\frac{\partial x_{G}}{\partial t}+DK_{5}\frac{\partial \varepsilon_{G}}{\partial t}+DK_{10}\frac{\partial G}{\partial z}+DK_{11}\frac{\partial x_{LF}}{\partial z}+DK_{12}\frac{\partial x_{G}}{\partial z}=DK_{0}$$

where

$$DK_{1}=DK_{4}\frac{x_{LF}}{C_{T}}$$

$$DK_{2}=DK_{4}\frac{G}{C_{T}}$$

ENERGY CONSERVATION

$$EK_{23}\frac{\partial p}{\partial t}+EK_{24}\frac{\partial G}{\partial t}+EK_{25}\frac{\partial x_{LF}}{\partial t}+EK_{21}\frac{\partial x_{G}}{\partial t}+EK_{5}\frac{\partial \varepsilon_{G}}{\partial t}+EK_{20}\frac{\partial p}{\partial z}+EK_{26}\frac{\partial G}{\partial z}+EK_{27}\frac{\partial x_{LF}}{\partial z}+EK_{22}\frac{\partial x_{G}}{\partial z}+EK_{14}\frac{\partial \varepsilon_{G}}{\partial z}=EK_{0}$$

where

$$EK_{24}=EK_{1}+EK_{4}\frac{x_{LF}}{C_{T}}$$

$$EK_{25}=EK_{2}+EK_{4}\frac{G}{C_{T}}$$

$$EK_{26}=EK_{10}+EK_{13}\frac{x_{LF}}{C_{T}}$$

$$EK_{27}=EK_{11}+EK_{13}\frac{G}{C_{T}}$$

MOMENTUM CONSERVATION

$$MK_1 \frac{\partial G}{\partial t} + MK_{20} \frac{\partial p}{\partial z} + MK_{26} \frac{\partial G}{\partial z} + MK_{27} \frac{\partial x_{LF}}{\partial z} + MK_{22} \frac{\partial x_G}{\partial z} + MK_{14} \frac{\partial \varepsilon_G}{\partial z} = MK_0$$

$$MK_{26} = MK_{10} + MK_{13} \frac{x_{LF}}{C_T}$$

$$MK_{27} = MK_{11} + MK_{13} \frac{G}{C_T}$$

BOUNDARY CONDITIONS

$$p(0,t) = p_{in}(t)$$

$$p(L,t) = p_{out}(t)$$

$$x_G(L,t) = x_{G\,out}(t)$$

$x_{LF}(0,t) = x_{LF\,in}(t)$ this boundary condition reflects the initial entrained fraction, i.e., $ef(0,t) = ef_{in}(t)$

$$\varepsilon_G(L,t) = \varepsilon_{G\,out}(t)$$

$$G(z,0) = G_0$$

$$x_G(z,0) = x_{G,0}(z)$$

$$x_{LF}(z,0) = x_{LF,0}(z)$$

$$\varepsilon_G(z,0) = \varepsilon_{G,0}(z)$$

DISCRETISATION

TIME (explicit throughout)

$$\frac{\partial p}{\partial t} \approx \frac{p_i^{n+1} - p_i^n}{\Delta t};\ \frac{\partial G}{\partial t} \approx \frac{G_i^{n+1} - G_i^n}{\Delta t};\frac{\partial x_{LF}}{\partial t} \approx \frac{x_{LF,i}^{n+1} - x_{LF,i}^{n}}{\Delta t};\frac{\partial x_G}{\partial t} \approx \frac{x_{G,i}^{n+1} - x_{G,i}^{n}}{\Delta t};\frac{\partial \varepsilon_G}{\partial t} \approx \frac{\varepsilon_{G,i}^{n+1} - \varepsilon_{G,i}^{n}}{\Delta t}$$

SPACE (explicit for G, implicit for the other variables)

$$\frac{\partial p}{\partial z} \approx \frac{p_{i+1}^{n+1} - p_i^{n+1}}{\Delta z};\ \frac{\partial G}{\partial z} \approx \frac{G_{i+1}^{n} - G_i^{n}}{\Delta z};\frac{\partial x_{LF}}{\partial z} \approx \frac{x_{LF,i+1}^{n+1} - x_{LF,i}^{n+1}}{\Delta z};\frac{\partial x_G}{\partial z} \approx \frac{x_{G,i+1}^{n+1} - x_{G,i}^{n+1}}{\Delta z};\frac{\partial \varepsilon_G}{\partial z} \approx \frac{\varepsilon_{G,i+1}^{n+1} - \varepsilon_{G,i}^{n+1}}{\Delta z}$$

$$GK_{19}\left(\frac{p_i^{n+1} - p_i^n}{\Delta t}\right) + GK_3\left(\frac{x_{G,i}^{n+1} - x_{G,i}^{n}}{\Delta t}\right) + GK_5\left(\frac{\varepsilon_{G,i}^{n+1} - \varepsilon_{G,i}^{n}}{\Delta t}\right) + GK_{10}\left(\frac{G_{i+1}^n - G_i^n}{\Delta z}\right) + GK_{12}\left(\frac{x_{G,i+1}^{n+1} - x_{G,i}^{n+1}}{\Delta z}\right) = GK_0$$

$$FK_{19}\left(\frac{p_i^{n+1} - p_i^n}{\Delta t}\right) + FK_1\left(\frac{G_i^{n+1} - G_i^n}{\Delta t}\right) + FK_2\left(\frac{x_{LF,i}^{n+1} - x_{LF,i}^{n}}{\Delta t}\right) + FK_3\left(\frac{x_{G,i}^{n+1} - x_{G,i}^{n}}{\Delta t}\right) + FK_{10}\left(\frac{G_{i+1}^n - G_i^n}{\Delta z}\right) + FK_{11}\left(\frac{x_{LF,i+1}^{n+1} - x_{LF,i}^{n+1}}{\Delta z}\right) = FK_0$$

$$DK_{19}\left(\frac{p_i^{n+1}-p_i^n}{\Delta t}\right)+DK_1\left(\frac{G_i^{n+1}-G_i^n}{\Delta t}\right)+DK_2\left(\frac{x_{LF,i}^{n+1}-x_{LF,i}^n}{\Delta t}\right)+DK_3\left(\frac{x_{G,i}^{n+1}-x_{G,i}^n}{\Delta t}\right)+DK_5\left(\frac{\varepsilon_{G,i}^{n+1}-\varepsilon_{G,i}^n}{\Delta t}\right)+$$
$$DK_{10}\left(\frac{G_{i+1}^n-G_i^n}{\Delta z}\right)+DK_{11}\left(\frac{x_{LF,i+1}^{n+1}-x_{LF,i}^{n+1}}{\Delta z}\right)+DK_{12}\left(\frac{x_{G,i+1}^{n+1}-x_{G,i}^{n+1}}{\Delta z}\right)=DK_0$$

$$EK_{23}\left(\frac{p_i^{n+1}-p_i^n}{\Delta t}\right)+EK_{24}\left(\frac{G_i^{n+1}-G_i^n}{\Delta t}\right)+EK_{25}\left(\frac{x_{LF,i}^{n+1}-x_{LF,i}^n}{\Delta t}\right)+EK_{21}\left(\frac{x_{G,i}^{n+1}-x_{G,i}^n}{\Delta t}\right)+EK_5\left(\frac{\varepsilon_{G,i}^{n+1}-\varepsilon_{G,i}^n}{\Delta t}\right)+$$
$$EK_{20}\left(\frac{p_{i+1}^{n+1}-p_i^{n+1}}{\Delta z}\right)+EK_{26}\left(\frac{G_{i+1}^n-G_i^n}{\Delta z}\right)+EK_{27}\left(\frac{x_{LF,i+1}^{n+1}-x_{LF,i}^{n+1}}{\Delta z}\right)+EK_{22}\left(\frac{x_{G,i+1}^{n+1}-x_{G,i}^{n+1}}{\Delta z}\right)+EK_{14}\left(\frac{\varepsilon_{G,i+1}^{n+1}-\varepsilon_{G,i}^{n+1}}{\Delta z}\right)=EK_0$$

$$MK_1\left(\frac{G_i^{n+1}-G_i^n}{\Delta t}\right)+MK_{20}\left(\frac{p_{i+1}^{n+1}-p_i^{n+1}}{\Delta z}\right)+MK_{26}\left(\frac{G_{i+1}^n-G_i^n}{\Delta z}\right)+MK_{27}\left(\frac{x_{LF,i+1}^{n+1}-x_{LF,i}^{n+1}}{\Delta z}\right)+MK_{22}\left(\frac{x_{G,i+1}^{n+1}-x_{G,i}^{n+1}}{\Delta z}\right)+$$
$$MK_{14}\left(\frac{\varepsilon_{G,i+1}^{n+1}-\varepsilon_{G,i}^{n+1}}{\Delta z}\right)=MK_0$$

PAGE NUMBERING AS ORIGINAL

Appendix III

Selection of publications related to this Ph.D. work

1. Falcone, G., Hewitt, G.F., Alimonti, C., Harrison, B. (2005): "MULTIPHASE FLOW METERING: 4 YEARS ON", presented at the North Sea Flow Measurement Workshop, Norway, 18-21 October 2005-12-14

2. Ali, A.M., Falcone, G., Hewitt, G.F., Bozorgzadeh, M., Gringarten, A.C. (2005): "Experimental Investigation of Wellbore Phase Redistribution Effects on Pressure-Transient Data", SPE 96587 presented at the 2005 SPE Annual Technical Conference and Exhibition held in Dallas, Texas, U.S.A., 9 – 12 October 2005

3. Alimonti, C., Falcone, G. (2004): "Integration of Multiphase Flowmetering, Neural Networks and Fuzzy Logic in Field Performance Monitoring", paper SPE 87629 published in the SPE Production & Facilities magazine, February 2004

4. Falcone, G., Hewitt, G.F., Lao, L., Richardson, S.M. (2003): "ANUMET: A Novel Wet Gas Meter", paper SPE 84504 presented at the 2003 SPE Annual Technical Conference and Exhibition held in Denver, Colorado, U.S.A., 5 – 8 October 2003

5. Falcone, G., Hewitt, G.F., Alimonti, C., Harrison, B. (2002): "Multiphase Flow Metering: Current Trends and Future Developments", paper SPE 74689, executive version of original paper SPE 71474 published in the Distinguished Author Series of the JPT magazine, April 2002 issue

North Sea Flow Measurement Workshop
18-21 October 2005

MULTIPHASE FLOW METERING: 4 YEARS ON

G.Falcone, TOTAL E&P UK PLC and Imperial College London, UK,
G.F.Hewitt, Imperial College London, UK,
C.Alimonti, University "La Sapienza" of Rome, Italy,
B.Harrison, TriPhase Consulting Ltd, UK

1 Abstract

Since the authors' last review in 2001 [1], the use of Multiphase Flow Metering (MFM) within the oil and gas industry continues to grow apace, being more popular in some parts of the world than others. Since the early 1990's, when the first commercial meters started to appear, there have been more than 1,600 field applications of MFM for field allocation, production optimisation and mobile well testing. As the authors predicted, wet gas metering technology has improved to such an extent that its use has rapidly increased worldwide. A "who's who" of the MFM sector is provided, which highlights the mergers in the sector and gives an insight into the meters and measurement principles available today. Cost estimates, potential benefits and reliability in the field of the current MFM technologies are revisited and brought up to date. Several measurements technologies have resurfaced, such as passive acoustic energy patterns, infrared wavelengths, Nuclear Magnetic Resonance (NMR) and Electrical Capacitance Tomography (ECT), and they are becoming commercial. The concept of "virtual metering", integrated with "classical MFM", is now widely accepted. However, sometimes the principles of the MFM measurements themselves are forgotten, submerged in the sales and marketing hype.

2 Introduction

Over the past four years, MFM has come a long way from being generally recognised as an area of research, development and technology application, to representing a discipline *per se'* within the oil and gas industry. The benefits associated with MFM, as outlined in the authors' previous review [1], have been confirmed by the way MFM technology has succeeded in fitting with other technologies toward global field-wide solutions.

However, MFM has not yet achieved its full potential nor is everybody in the oil and gas industry aware of what MFM can and cannot do.

Nowadays, it is not surprising to hear of a multi-million dollar contract being signed by an Operator for a Manufacturer to supply fifty MFM's for a field development, but it is debatable whether there has been any revolutionary advancement in MFM solutions since 2001. What has undeniably improved is the confidence in the subsea versions of the MFM technology and in the hardware reliability, the stability of the sensors and the mean time to failure. Also improved is the collaboration between Operator and Manufacturer, forged by working together in the field over the past years.

However, have all the technical routes to MFM innovation been fully exploited? Are there still physical and economic constraints that prevent this technology from moving forward?

3 MFM Trends

Since 2001 there have been several published reviews on the number of MFM installations worldwide [2][3]. However, it remains difficult to establish the official figures, as it is necessary to distinguish between:

- MFM's installed and currently working;
- MFM's installed, but now discontinued;
- MFM's ordered, but not yet delivered;
- MFM's delivered, but not yet installed;
- MFM's used as portable well testing solutions.

This type of information is commercially sensitive due to the high competition in the market of commercial MFM's.

Following a market research by the authors in 2005, it appears that a total figure for MFM installations to date, as defined in the bulleted list above, is in excess of 1,600. Of these, 10% is represented by mobile well testing applications and a further 20% corresponds to wet gas metering. Western Europe, Asia-Pacific and the U.S. together represent 75% of the total number of MFM installations. Asia-Pacific has seen a sharp increase in MFM applications since 2001 and has now overtaken the North Sea, where most of the initial installations of MFM's began. However, the 1,600 figure does not account for all of the installations since the early 1990's as some Manufacturers have disappeared and some of the solutions have been discontinued. The past four years has seen mergers amongst manufacturers, but the entry of newcomers has kept the total number of commercial manufacturers at around twenty. In some ways, these mergers have helped in the disclosure of information to the public domain, but knowledge has also been lost. Some of the smaller manufacturers, who were around four years ago, have experienced mixed fortunes, becoming established "names" and setting trends with the larger providers, while others have not really "cracked" the market.

Table 1 presents a list of the current commercial MFM's, divided into "traditional" MFM's (Gas Volume Fraction, GVF<95-98%), high gas volume fraction MFM's (GVF>95-98%) and Downhole MFM's (DMFM's).

Table 2, **Table 3**, **Table 4** and **Table 5** present possible ways to classify the current commercial MFM's based on their features. Those meters that are still under development have not been included (e.g. IFP, University of Manchester, Imperial College, Robert Gordon University/QuantX). Also omitted are those MFM solutions that need to be integrated with other techniques in order to provide the three flow rates (e.g. pressure pulse, virtual metering).

Although the authors have developed their own views on the MFM solutions available, the tables of MFM's only provide an immediate overview of the MFM market today and indicate what applications the contractors claim they may be used for.

MFM's	High GVF MFM's	DMFM's
Roxar-MPFM	Roxar-WGM	QuantX
Schlumberger/Framo-Vx	Schlumberger/Framo-Vx	Weatherford/CIDRA
Flowsys/FMC-TopFlow	Petrotech-Smartvent	Schlumberger
Jiskoot-MIXMETER		
TEA Sistemi-Lyra	TEA Sistemi-VEGA	
Agar-MPFM	Agar-MPFM 400 loop	
Red Eye-REMMS	Red Eye-REMMS (?)	
Abbon-Flow Master	Abbon-Flow Master	
Haimo-MPFM	Haimo-MPFM	
ESMER	ESMER (e.g. + V-cone)	
Kvaerner-DUET	Kvaerner-CCM	
Kvaerner-CCM		
Accuflow	Accuflow	
Daniel/Emerson-MEGRA	Solartron/Emerson-Dualstream II	
Hydralift-Wellcomp		

Table 1: current commercial MFM's, WGM's and DMFM's

Flow conditioning /Homogenisation	Leave-as-it-is	In-line separation	Isokinetic sampling
Roxar-WGM	Roxar-MPFM	Agar	TEA Sistemi-VEGA
Jiskoot-MIXMETER	Schlumberger/Framo-Vx	Wellcomp	
TEA Sistemi-Lyra	Flowsys/FMC-TopFlow	Accuflow	
Daniel/Emerson-Dualstream II	Daniel/Emerson-MEGRA (for GVF<25%)	Daniel/Emerson-MEGRA (for GVF>25%)	
	Abbon-Flow Master	Red Eye-REMMS	
ESMER (+ V-cone)	ESMER	Haimo-MPFM	
	Petrotech-Smartvent		
	Kvaerner-DUET	Kvaerner-CCM	

Table 2: current commercial MFM's with/without flow conditioning

Gamma source	No Gamma source
Roxar-MPFM	Roxar-WGM
Jiskoot-MIXMETER	Red Eye-REMMS
Daniel/Emerson-MEGRA	Daniel/Emerson-Dualstream II
Kvaerner-DUET	Kvaerner-CCM
Haimo-MPFM	Agar
Schlumberger/Framo-Vx	Wellcomp
TEA Sistemi-Lyra	TEA Sistemi-LYRA (for WC>30%)
TEA Sistemi-VEGA	
Flowsys/FMC-TopFlow	
Petrotech-Smartvent	
Abbon-Flow Master	
ESMER	
Accuflow	

Table 3: current commercial MFM's with/without gamma ray source

Intrusive	Non-intrusive(*)
Roxar-WGM	Roxar-MPFM
Jiskoot-MIXMETER	Schlumberger/Framo-Vx
TEA Sistemi-VEGA	TEA Sistemi-LYRA
Kvaerner-CCM	Kvaerner-DUET
Daniel/Emerson-Dualstream II	Daniel/Emerson-MEGRA
Haimo-MPFM (flow conditioning vessel)	Petrotech-Smartvent
Accuflow	Flowsys/FMC-TopFlow
Red Eye-REMMS	Abbon-Flow Master
Agar	ESMER
Wellcomp	

Table 4: current commercial MFM's intrusive/non-intrusive
(*) Venturi's are not regarded as intrusive devices

X-correlation	No X-correlation
Roxar-MPFM	Roxar-WGM
Kvaerner-DUET	Kvaerner-CCM
Haimo-MPFM (flow conditioning vessel)	TEA Sistemi-LYRA
Flowsys/FMC-TopFlow	Schlumberger/Framo-Vx
	Daniel/Emerson-MEGRA
	Petrotech-Smartvent
	Daniel/Emerson-Dualstream II
	Abbon-Flow Master
	ESMER
	Accuflow
	Red Eye-REMMS
	Agar
	Wellcomp
	TEA Sistemi-VEGA
	Jiskoot-MIXMETER

Table 5: with/without cross-correlation

The cost of MFM's today remains in the range of US$100,000-US$500,000 (varying with onshore/offshore, topsides/subsea, the dimension of the tool and the number of units ordered), even though there has been an estimated increase of 25-50% in production facilities CAPEX since 1999 [4]. This CAPEX rise has been "cancelled out" by the fact that MFM's have become up to 50% cheaper, mainly due to the increased competition in the market and the rise in units sold.

When comparing a traditional production layout (with test separator and test lines) with an installation with MFM, it still appears that the second option involves much lower CAPEX. The installed cost of a separator varies enormously with rates, pressures, temperatures, chemistry of the fluids to be treated, onshore/offshore, but is typically in the range US$1m-5m. It may also require several instruments, depending on its complexity.

The test lines may be omitted in some MFM installations. Carbon steel flow lines of 4-6" in diameter cost approximately US$1.3m-3.6m per Km installed.

OPEX costs associated with test separators can be around US$350,000 per year for offshore installations. In 1999, it was estimated [4] that the OPEX for a MFM was likely to be 25% of the cost of the meter itself for the first year, then US$10-40,000 per year (for both onshore and topsides applications). Today, with the increased reliability of the MFM hardware and more structured training of personnel, OPEX is spread more evenly over the operating life of a MFM.

4 The MFM Community

The oil and gas industry is a global business, yet the MFM expertise is not equally distributed worldwide. Not all Operators have in-house MFM specialists and, within the Service Companies, only a select handful of people can be defined as experts in MFM. As with all in-house specialists in any particular discipline, there is reluctance to share too much of their hard-won knowledge, which can lead to them being isolated from the rest of the company.

With MFM now being accepted as a standard solution for existing and new developments, competition among MFM suppliers has intensified. Despite the existence of a global MFM community, it remains very difficult to release and share confidential data. A small/medium Operator without direct MFM experience will find it almost impossible to obtain a fair and independent view of the advantages and disadvantages of each commercial MFM from discussions with the Manufacturers or other Operators. The old trick of going to see Manufacturer A to ask about the downfalls of the product sold by Manufacturer B (and *vice versa*) only works up to a certain point.

There has been a constant rise in the availability of MFM handbooks, guidelines, recommendations and technical publications, but so far, none of them has described in detail the pros and the cons of each commercially available MFM solution. Such guidelines are usually limited to lists of MFM solutions (full separation, partial separation, in-line, etc.), MFM definitions (what GVF is, how calibration is done, etc.), standards by the International Organization for Standardization (not always directly applicable to the specific case of MFM) and ways to report the performance of a meter. This only captures the performance of a MFM as a "black box", but does not teach how to keep track of all the possible uncertainties and inaccuracies that are inherent in each individual MFM technique. Also, there is the risk of continual reference to original equations or relationships, while their actual implementation in commercial solutions is often adapted to suit a specific approach. There are very few worked examples in the public domain that do not have a "commercial agenda" and are sufficiently accurate to enable a critical and informed selection of meters.

As a result, there is an emerging class of consultants who perform studies on behalf of Operators and Government bodies and mediate between them and the Manufacturers.

5 Example of "forgotten basics"

As previously stated, the hardware and sensors have improved tremendously, but it is important not to forget the principles of the measurements themselves. Let us consider the basic concept of the gamma ray measurement of two-phase flow.

Figures 1, 2 and **3** illustrate the absolute error in phase fraction measurement in a two-phase flow system of air-water, air-oil and water oil, respectively. The calculations

are based on a 4" diameter pipe section made of Perspex material, with single-energy gamma-ray beams passing through pipe walls of 12.7mm of thickness. The sources and energy levels used in this example are those commonly adopted in commercial MFM's, namely, Americium 241 (17.8 and 59.5 KeV), Barium 133 (31, 81 and 356 KeV) and Caesium 137 (33 and 661 KeV). Assuming that all sources can provide the same initial intensity, I_0 = 5,000 counts/s, it is possible to calculate the intensity (I) of a single-energy gamma-ray beam, transmitted through the Perspex conduit in which there are two static or flowing phases, as:

$$I = I_0 \exp\left(-\gamma_{wall} x_{wall} - \gamma_1 x_1 - \gamma_2 x_2\right) \qquad \textbf{Eq. 1}$$

where:

γ_1 and γ_2 are the linear attenuation coefficients of phase 1 and phase 2, respectively;
x_1 and x_2 are the thicknesses of phase 1 and phase 2, respectively;
γ_{wall} is the linear attenuation coefficient of the conduit;
x_{wall} is the thickness of the conduit.

The absolute error in phase fractions is given by [5]:

$$\delta\varepsilon_{1,2} = \pm\frac{1}{(\gamma_1 - \gamma_2)D\sqrt{Ct}} \qquad \textbf{Eq. 2}$$

where:

D is the internal diameter of the pipe;
C is the transmitted count rate;
t is the counting time.

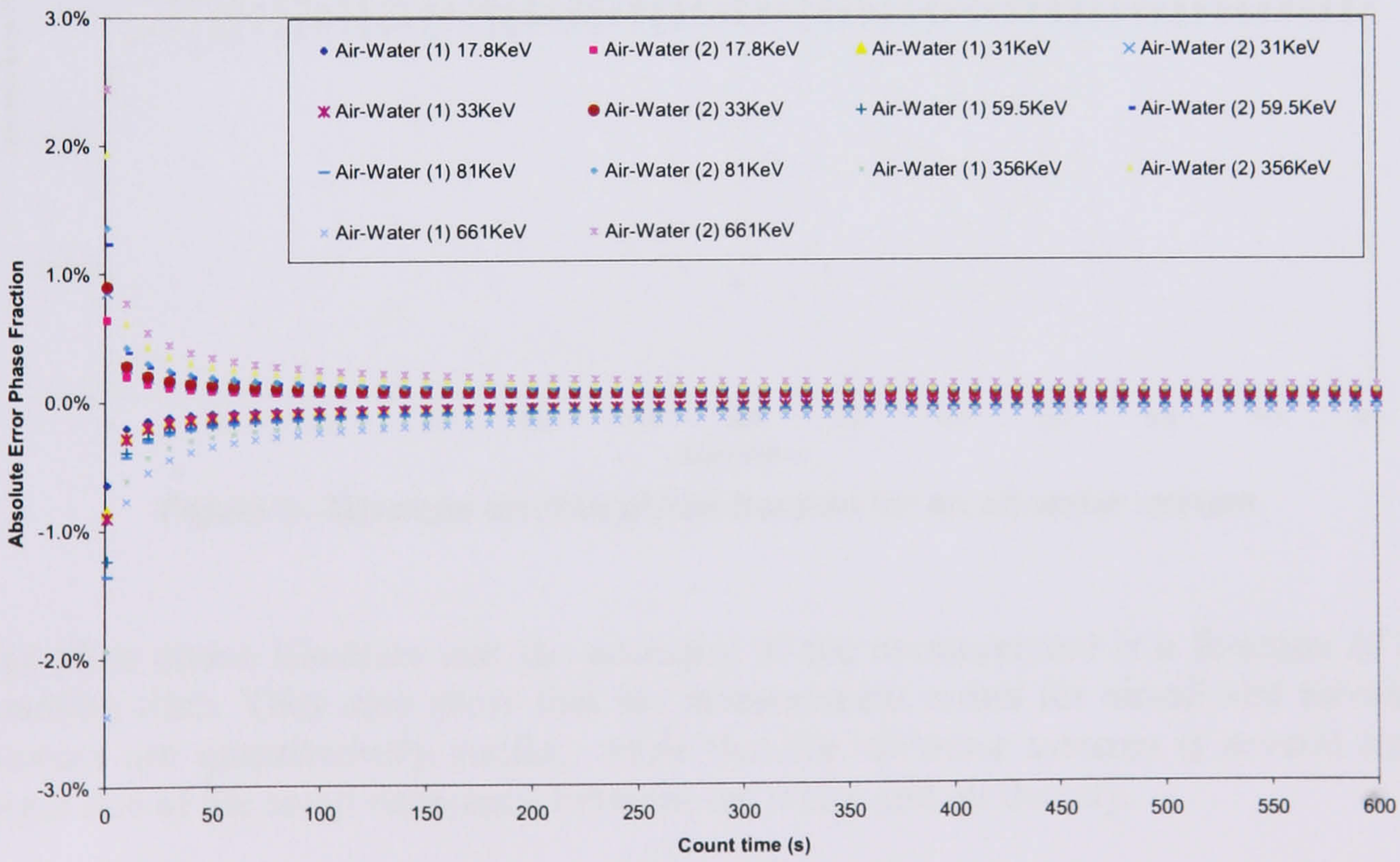


Figure1: Absolute error in phase fraction for an air-water system.

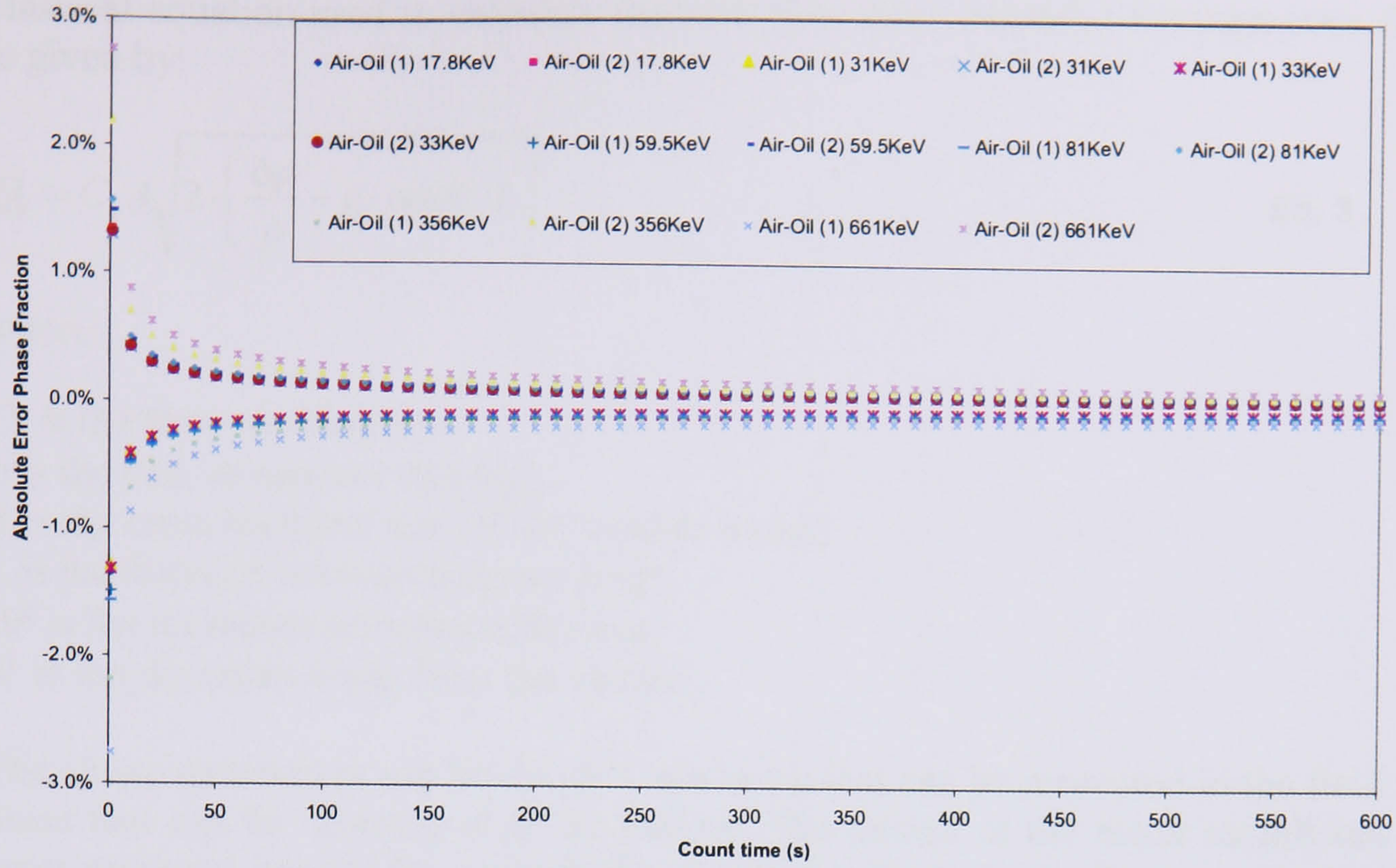


Figure 2: Absolute error in phase fraction for an air-oil system.

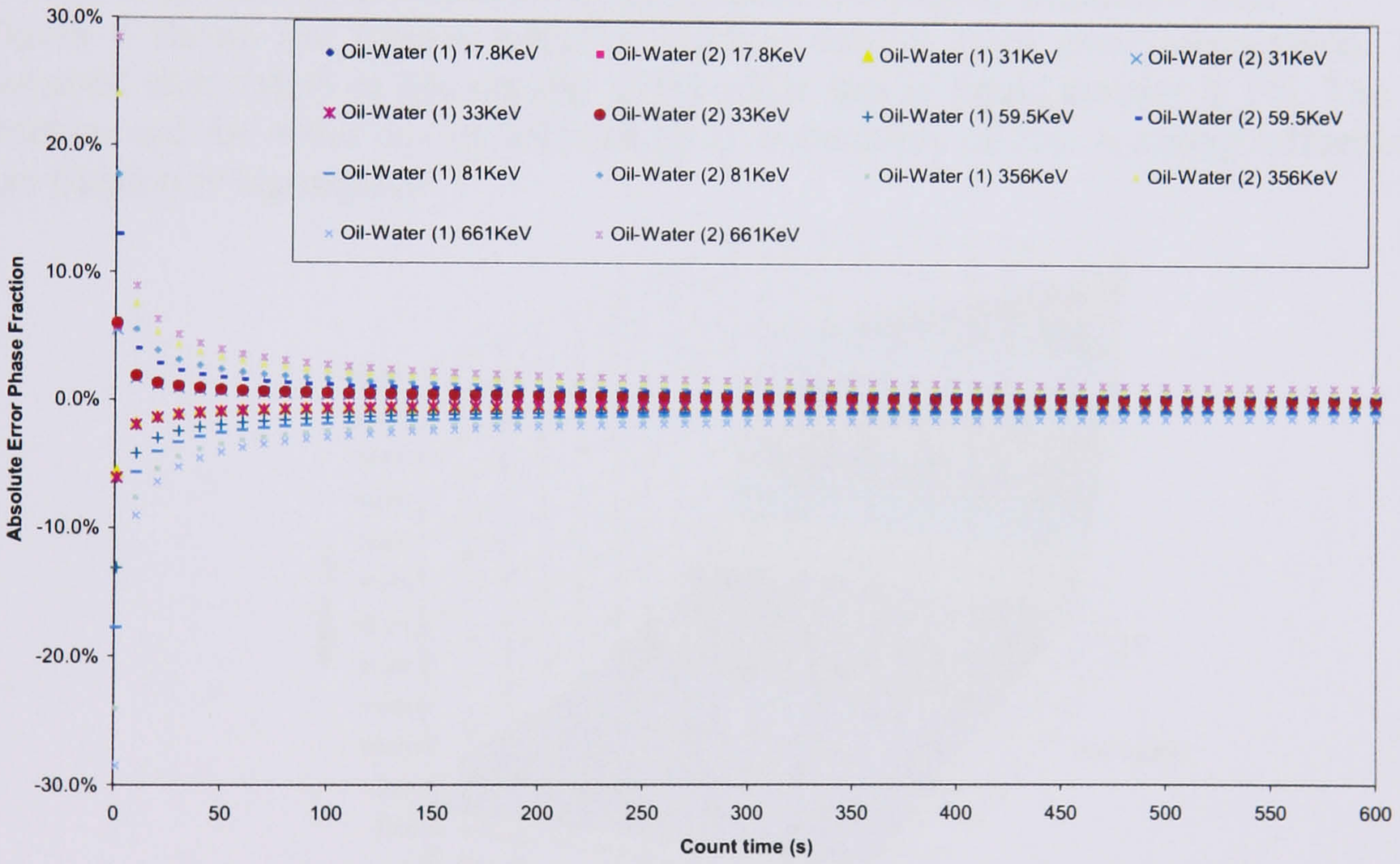


Figure 3: Absolute error in phase fraction for an oil-water system.

The plots above illustrate that the accuracy of the measurement is a function of the counting time. They also show that the measurement errors for air-oil and air-water systems are quantitatively similar, while that for oil-water systems is several times larger due to the small difference between the water and oil density.

Gamma ray measurements are usually associated with a Venturi in order to measure the total (or mixture) momentum from which the phase flow rates are calculated. The

classical equation used to calculate the total flow rate, assuming homogeneous flow, is given by:

$$Q_t = C_q A \sqrt{2 \cdot \left(\frac{\Delta p}{\rho} - g \cdot \cos\theta \cdot L \right)} \qquad \textbf{Eq. 3}$$

where:

C_q is the flow coefficient;
ρ is the bulk or mixture density;
A is the cross sectional area of the Venturi throat;
L is the distance between pressure taps;
ΔP is the measured pressure difference;
θ is the deviation angle from the vertical.

The above parameters can be divided into those that can be measured in the field and those that can be established in the factory. The design of the meter establishes the cross sectional area of the Venturi throat, the distance between the pressure tappings and the full scale of pressure transducer, while the flow coefficient can be determined in the factory by calibration. The remaining parameters are measured in the field. Of course, uncertainties in parameter determination can play an important role.
Figure 4 shows the relative error in mixture density from error propagation. The assumed uncertainty in gas density is 5% while that in liquid density is 1%. The gas fraction and the water cut are affected by an uncertainty of 3%. A strong influence of gas fraction is highlighted.

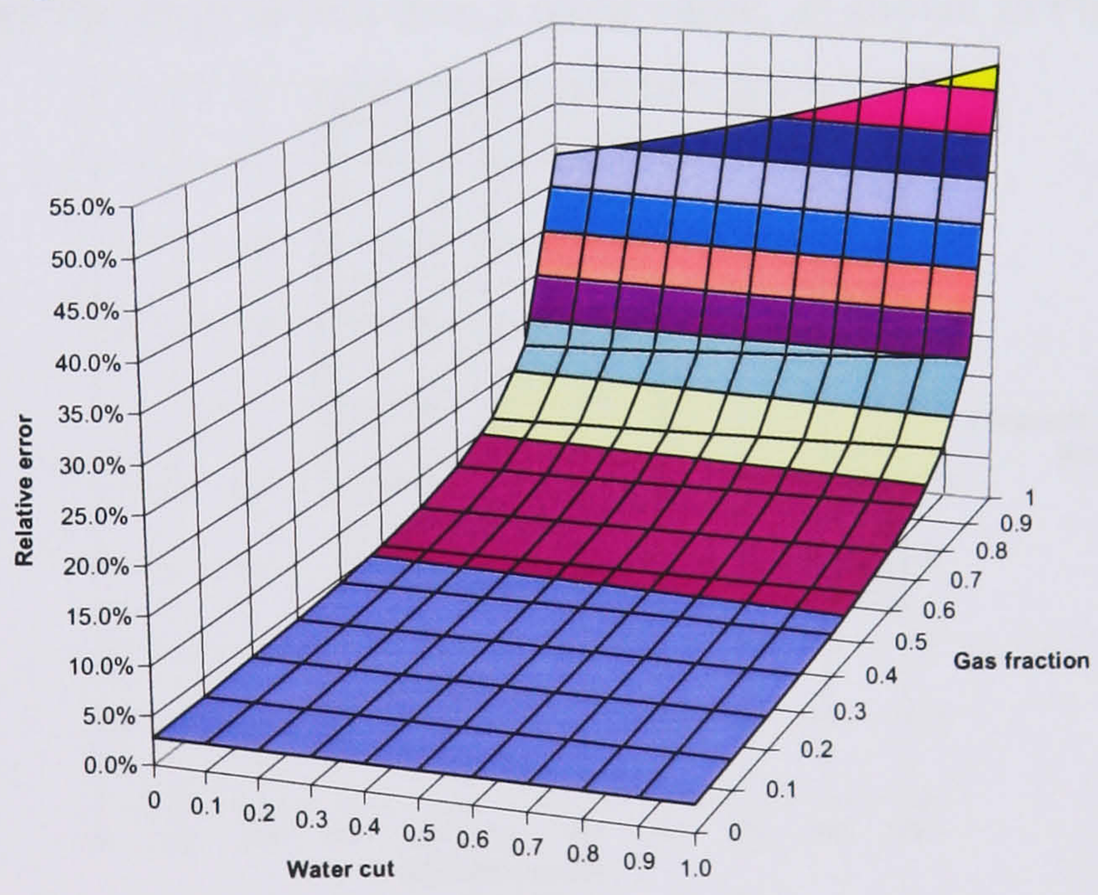


Figure 4: Relative error in mixture density for a gas-oil-water system.

The uncertainties for remaining parameters needed in the design of a 3" DN Venturi, with a cross sectional ratio of 0.5, are reported in **Table 6**.

Parameter	Uncertainty
Distance between pressure tappings	10^{-4} m
Cross sectional area	$1.2\ 10^{-5}$ m^2
Pressure difference	0.1 % of reading

Table 6: Design uncertainties of Venturi's

It is possible to estimate the error propagation from **Eq.3** and so highlight the influence of the measured parameters, pressure difference and mixture density. **Figure 5** shows the error in mixture flow rate vs. the mixture density and the pressure difference. The two parameters exert a considerable influence on the error, especially when they are relatively small in value. Errors can vary between 3.5% and 75%.

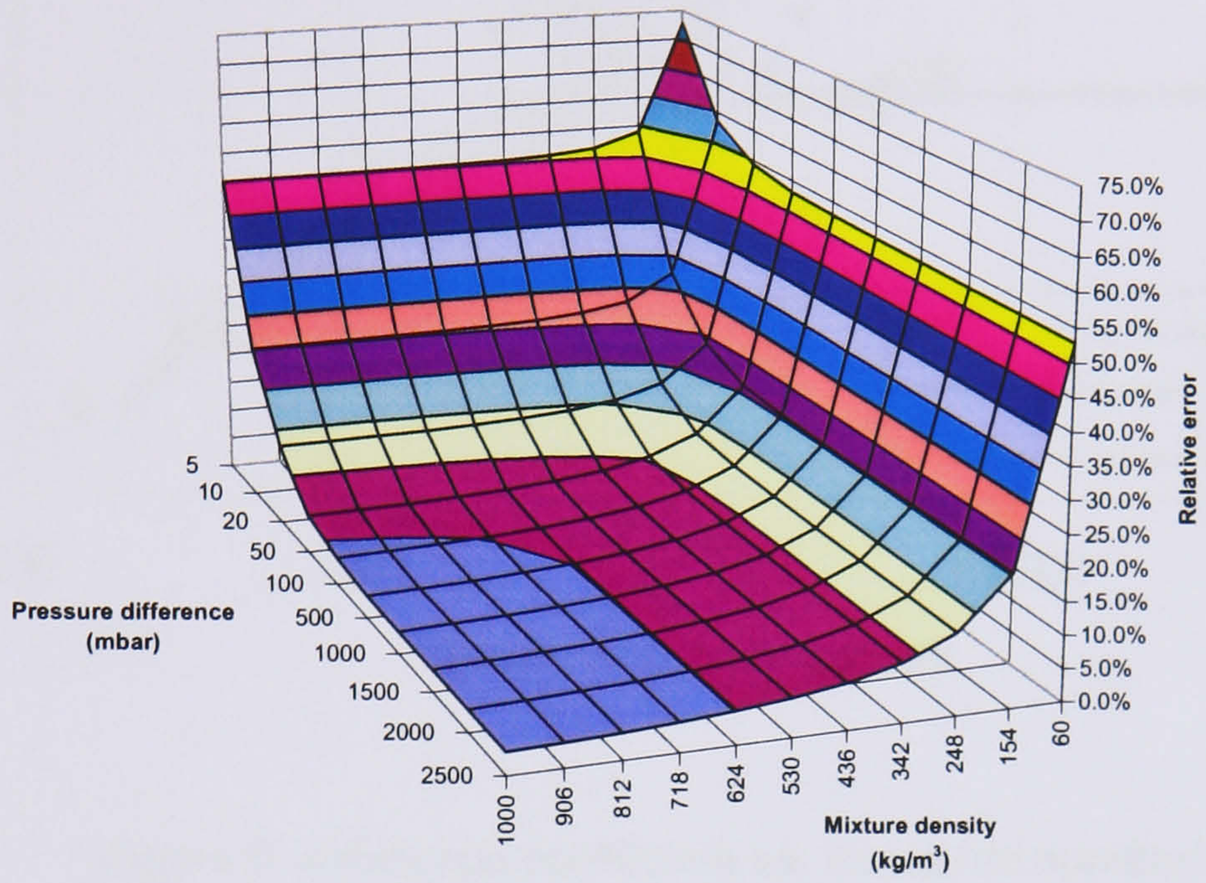


Figure 5: Relative error in mixture momentum for a gas-oil-water system.

The direct consequence of the above is the definition of an envelope of operation (rangeability), where the error is less than a fixed value, as shown in **Figure 6**.

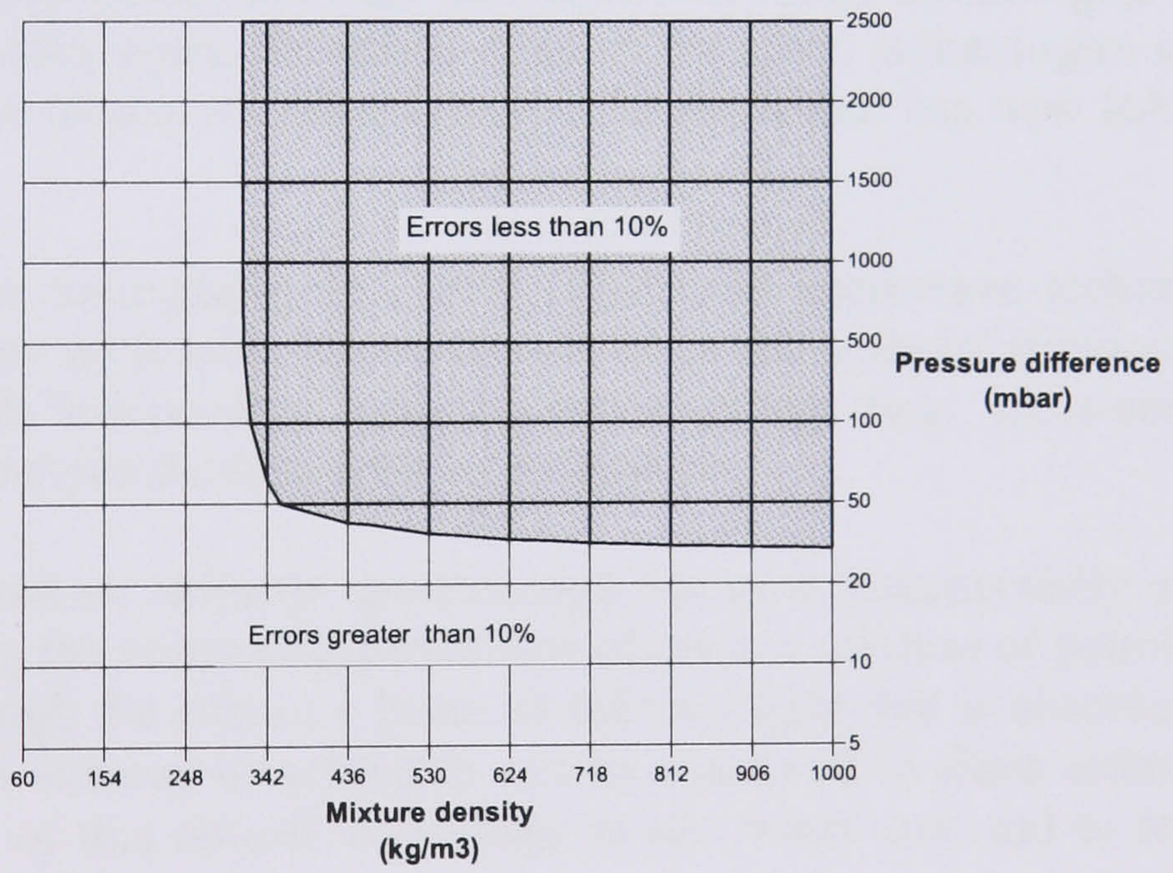


Figure 6: Envelope of operation for a mixture momentum for a gas-oil-water system.

Last but not least, the discharge coefficient is a model calibration parameter that is mainly dependent on the fluid properties. Oil viscosity can be much higher than that of water, whereas the density difference between the two phases is relatively small, so the Reynolds number of the flowing mixture will decrease as the oil fraction increases. For Reynolds numbers lower than 100,000, the discharge coefficient assumes a variable value, but this becomes constant at higher Reynolds numbers. Thus, the higher the oil viscosity, the more important it is to provide an accurate description of

the discharge coefficient pattern vs. Reynolds number. Experimental data, which exhibit this dependency, are shown in **Figure 7** [15]. The oil viscosity, in this case, was only10 mPa·s.

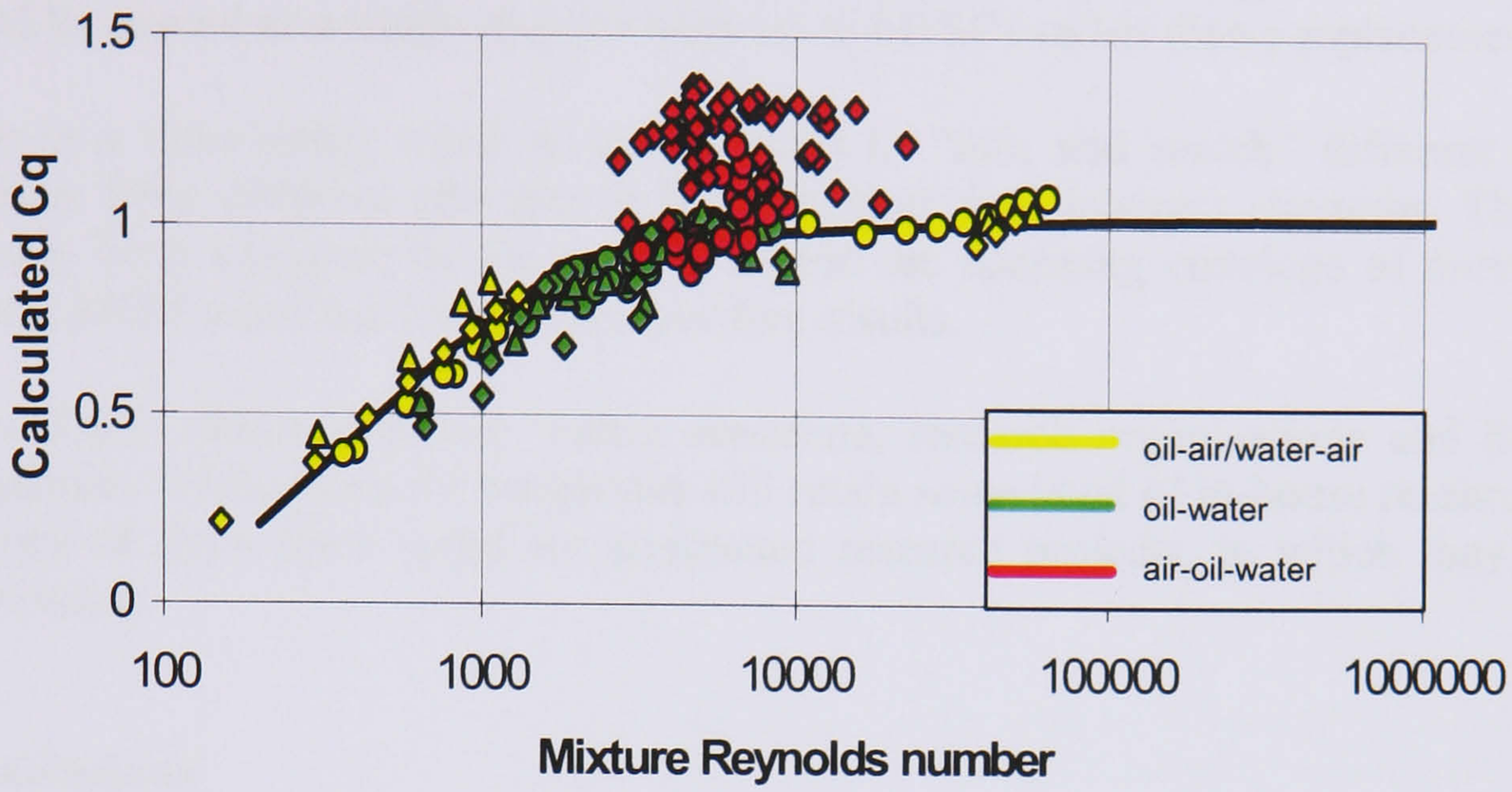


Figure 7: Discharge coefficient vs. Reynolds number.

6 Novel technologies, R&D trends

As mentioned previously, there have been no truly novel MFM technologies breaking through over the past four years. However, some of the novel technologies identified in 2001 have been the subject of rather intensive research that has now led to some significant results.

X-ray and gamma ray tomography [6], ECT [7][8] and microwave techniques [9] have already undergone noticeable improvements since the authors' previous review [1]. If combined with independent velocity measurements (e.g. cross-correlation, Venturi), they could provide the flow rates of each phase.

Water cut meters based on infrared spectroscopy are now commercially available. They aim at measuring the volumetric proportion of oil in a mixture of petroleum and water by passing through the stream a beam of infrared light that is absorbed by oil, but not water. Several infrared wavelengths can be measured to allow extending the range of applicability of this optical technology to low water cuts and to reduce the effects of the presence of gas.

Research has continued into NMR [10]. Surprisingly, Pulsed Neutron Activation (PNA) has not been the focus of any substantial studies, despite the fact that it could be the only way of directly measuring individual component velocities and fractions.

Cheaper "stand-alone" technologies such as pressure pulse [11][12] and acoustic noise interpretation [13] are now commercially available. Although there may cases

where these technologies are not suitable, they should be able to compete with other solutions on price.

The integrated monitoring and metering approach is nowadays referred to as "virtual metering" [14]. Commercial solutions are now available, although virtual metering should be treated as a supplement or back-up to MFM's rather than a replacement.

There is a developing trend in the industry to "mix and match" different MFM solutions from different provider to better exploit their inherent strengths. This has probably been triggered by the need to extend the operating envelope of previously existing MFM's and has led to some positive results.

Direct R&D efforts continue within academia, research organisations and Service Companies. While some oil companies still retain some level of in-house research, the majority of them have opted for contracted research projects, in which they share supervision.

7 Conclusions

The trends in MFM sales and installations, the establishment of wet gas metering as a special niche and the evolution of some novel technologies have been as predicted in 2001 [1]. Also, the interaction between Operators and Manufacturers has improved, but there remains a paucity of quality field data in the public domain. This is why more effort is needed to define much more specific MFM Regulations, with a special focus on the strengths and the downfalls of each MFM metering principle.

Though MFM technology has now been widely applied in hydrocarbon recovery systems, there are still unresolved questions regarding the accuracy and range of applicability of commercial meters. There is a tendency to forget some of the basic limitations, as exemplified here by the cases of gamma densitometry and Venturi meters. Even in the case of straight pipe flows, the structure and local behaviour of multiphase flows is still, in all but the simplest cases, poorly understood and certainly not predictable. Small wonder then that the developing flows through the complex geometries which occur in many metering systems are not captured by the simplified models use to interpret meter outputs. Perhaps the real surprise is that, even after discounting the sales hyperbole common in this field, the meters work even as well as they do! There is a long way to go in this field and the user should realise that MFM's are one piece of the optimised production system jigsaw.

8 References

[1] Falcone, G., Hewitt, G.F., Alimonti, C., Harrison, B.: "Multiphase Flow Metering: Current Trends and Future Developments", paper SPE 71474 presented at the 2001 SPE Annual Technical Conference and Exhibition held in New Orleans, Louisiana, 30 September–3 October 2001

[2] API Publication 2566, First Edition: "State of the Art Multiphase Flow Metering", May 2004

[3] Atkinson, A., Theuveny, B., Berard, M., Conort, G., Lowe, T., McDiarmid, A., Mehdizadeh, P., Pinguet, B., Smith, G., Williamson, K.J.: "A New Horizon in Multiphase Flow Measurement", Schlumberger Oilfield Review, Winter 2004-2005, 52-63

[4] Sheers, A.M., Noordhuis, B.R.: "Multi-phase and Wet Gas Flow Measurement", presented at IBC's 5th Annual Multi-Phase Metering Conference held in Aberdeen, Scotland, 22-23 February 1999

[5] Pan, L.: "High pressure three phase (Gas/liquid/liquid) flow", PhD Thesis, Imperial College London, 1996

[6] Johansen, G.A.: "Nuclear tomography methods in industry", Nuclear Physics A 752 (2005) 696c–705c

[7] Ismail, I., Chondronasios, A., Yang, W.Q.: "Wet gas flow metering by electrical capacitance tomography", paper presented at the 4th South East Asia Hydrocarbon Flow Measurement Workshop, Kuala Lumpur, Malaysia, 7-11 March 2005

[8] Gamio, C., Ismail, I., Zhang, Z.T., Yang, W.Q.: "Review of electrical capacitance tomography for oil industry", Proc. of 4th Int. Symp. on Measurement Techniques for Multiphase Flows, Hangzhou, China, 10-12 Sept. 2004, 116-121

[9] Bentolila, Y., Constant, M.: "Physical approach of volumetric phase estimation based on mixture laws for multiphase flows", presented at the 5th North American Conference on Multiphase Technology, Banff, Canada, 1-6 June 2005

[10] Ong, J.T., Oyeneyin, M.B., Coutts, E.J., MacLean, I.M.: "In Well Nuclear Magnetic Resonance (NMR) Multiphase Flowmeter in the Oil and Gas Industry", paper SPE 89978 presented at the SPE Annual Technical Conference and Exhibition held in Houston, Texas, 26-29 September 2004

[11] Gudmundsson, J.S., Celius, H.K.: "Gas-Liquid Metering Using Pressure-Pulse Technology", paper SPE 56584 presented at the SPE Annual Technical Conference and Exhibition, Houston, Texas, 3-6 October 1999

[12] Gudmundsson, J.S., Durgut, I., Ronnevig, J., Korsan, K., Celius, H.K.: "Pressure Pulse Analysis of Gas Lift Wells", presented at the Fall 2001 ASME/API Gas Lift Workshop, Aberdeen, 12-13 November 2001

[13] Piantanida, M., Mazzoni, A., Tanzi, A., Hope, B.R.: "Multiphase Metering: Experimental Results from the Analysis of Acoustic Noise Through a Choke", paper SPE 50681 presented at the 1998 SPE European Petroleum Conference held in The Hague, The Netherlands, 20-22 October 1998

[14] Rasmussen, A.: "Field applications of model-based multiphase flow computing", presented at the 22nd North Sea Flow Measurement Workshop, St. Andrews, Fife, 26-29 October 2004

[15] Alimonti, C., Annunziato, M., Cerri, M.: "Using a Venturi Meter in Multiphase Metering Systems", 5th International Conference on Multiphase flow in Industrial Plants, Amalfi, Italy, 26-27 September 1996

SPE 96587

Experimental Investigation of Wellbore Phase Redistribution Effects on Pressure-Transient Data

A.M.Ali, Imperial College; G.Falcone, SPE, TOTAL E&P UK PLC and Imperial College; G.F.Hewitt, Imperial College; M.Bozorgzadeh, SPE, Imperial College; A.C.Gringarten, SPE, Imperial College

Copyright 2005, Society of Petroleum Engineers

This paper was prepared for presentation at the 2005 SPE Annual Technical Conference and Exhibition held in Dallas, Texas, U.S.A., 9 – 12 October 2005.

This paper was selected for presentation by an SPE Program Committee following review of information contained in a proposal submitted by the author(s). Contents of the paper, as presented, have not been reviewed by the Society of Petroleum Engineers and are subject to correction by the author(s). The material, as presented, does not necessarily reflect any position of the Society of Petroleum Engineers, its officers, or members. Papers presented at SPE meetings are subject to publication review by Editorial Committees of the Society of Petroleum Engineers. Electronic reproduction, distribution, or storage of any part of this paper for commercial purposes without the written consent of the Society of Petroleum Engineers is prohibited. Permission to reproduce in print is restricted to a proposal of not more than 300 words; illustrations may not be copied. The proposal must contain conspicuous acknowledgment of where and by whom the paper was presented. Write Librarian, SPE, P.O. Box 833836, Richardson, TX 75083-3836, U.S.A., fax 01-972-952-9435.

Abstract

Pressure transient analysis is a well established reservoir evaluation method. By analysing pressure and pressure derivative curves from build-up and drawdown tests, it is possible to identify reservoir characteristic parameters and heterogeneities. However, much of the pressure data recorded during a well test may be dominated by wellbore effects that can mask reservoir characteristics and lead to erroneous well test interpretations. This is particularly true when the well production rate is controlled at surface and more than one phase is flowing. These effects, which are transient in nature, include phase change, flow reversal, and re-entry of the denser phase into the producing zone.

This paper presents the results of experiments carried out at Imperial College to investigate the effects of phase redistribution and phase re-injection on pressure build-up data. Single-phase and two-phase flow tests were conducted with air and water. An experimental rig was designed to emulate a reservoir connected, via a resistance, to the base of a flowing well. The "reservoir" is recreated by a pressurised vessel, while the "well" is simulated by a vertical pipe. The "well" was flowed at controlled rates to mimic those encountered in gas condensate reservoirs. After steady-state conditions had been attained, the "well" was shut-in at the top of the rig (i.e. at surface) and the associated transient phenomena monitored via distributed measurements of pressure, temperature, liquid hold-up and wall shear stress. Pressure build-up data were interpreted using established well test analysis techniques.

The experiments provide a qualitative and quantitative understanding of the effects of gas rates, liquid rates and rising gas bubbles on wellbore phase redistribution and re-injection. The results yield an insight into the corresponding impact on well test transient pressure behaviour.

Introduction

Wellbore phase redistribution (WPR) occurs in wells where more than one phase flows and has an impact on the quality of recorded pressure data. WPR may cause an increase in the wellbore storage coefficient in both drawdowns and build-ups. Phase change, on the other hand, causes the wellbore storage coefficient to decrease during build-ups and to increase during drawdowns. While the impact of phase change on the pressure behaviour is usually limited to early times, WPR may dominate a well test for several hours. When WPR occurs, derivative shapes can be easily misinterpreted as being due to double porosity, partial penetration or composite behaviour. Typical derivative shapes (for gas condensate fields) due to WPR are reported in **Fig.1**, where curve 5 is typical of situations where the denser phase re-enters into the formation.

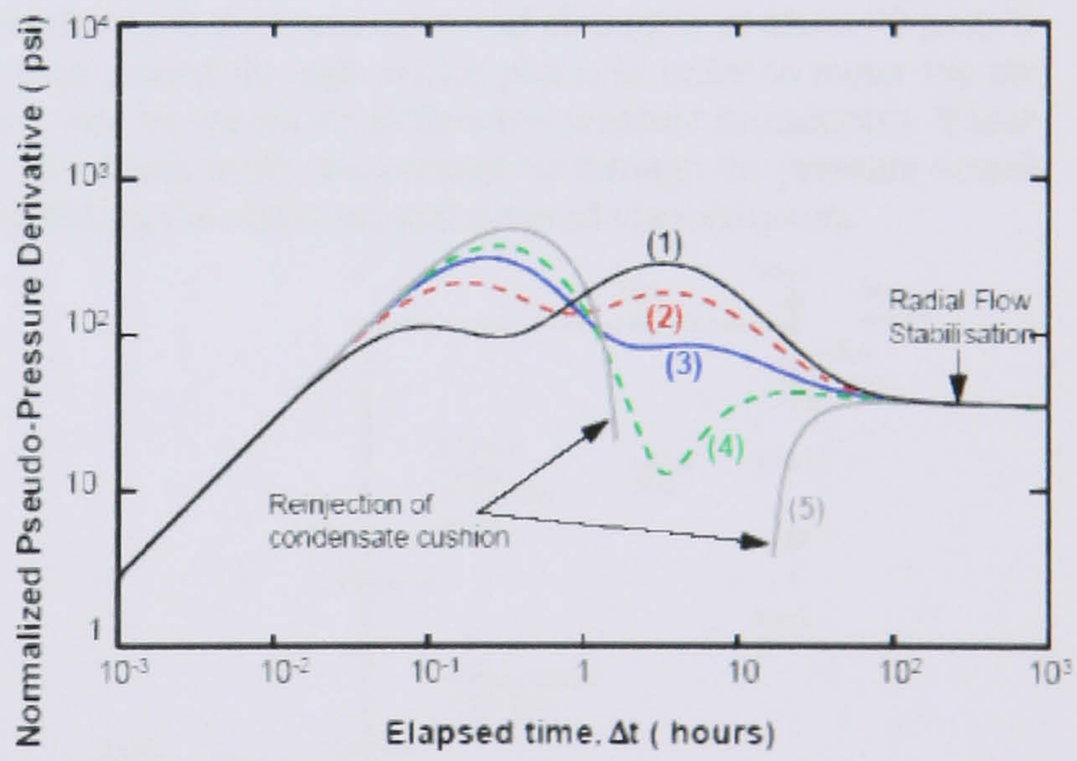


Fig.1: Log-log derivative plots, increasing wellbore storage due to phase redistribution in the wellbore[1].

Pressure transients in a wellbore imply transient multiphase flows, opposite the producing reservoir zones and higher up in the tubing. Gravity, friction and acceleration effects play an important role in this scenario, as they determine the pressure profile and the flow regime in the well. To date, there has been limited research into wellbore phenomena during well testing. Initial research has focused on empirical models to identify and match WPR, but these models do not account for the underlying physical mechanisms that cause it. More recently, robust mechanistic

modelling of multiphase flows has been proposed to characterise wellbore phenomena.

Stegemeier *et al.*[2] were the first to provide a physical explanation for the anomalous pressure hump observed in build-up data from South Texas oil fields. 75% of wells showed the effects of WPR. **Fig.2** shows the relationship between the size of the pressure hump and the productivity index. The extent of the pressure hump was found to be higher in wells with low productivity index, associated to low permeability and skin.

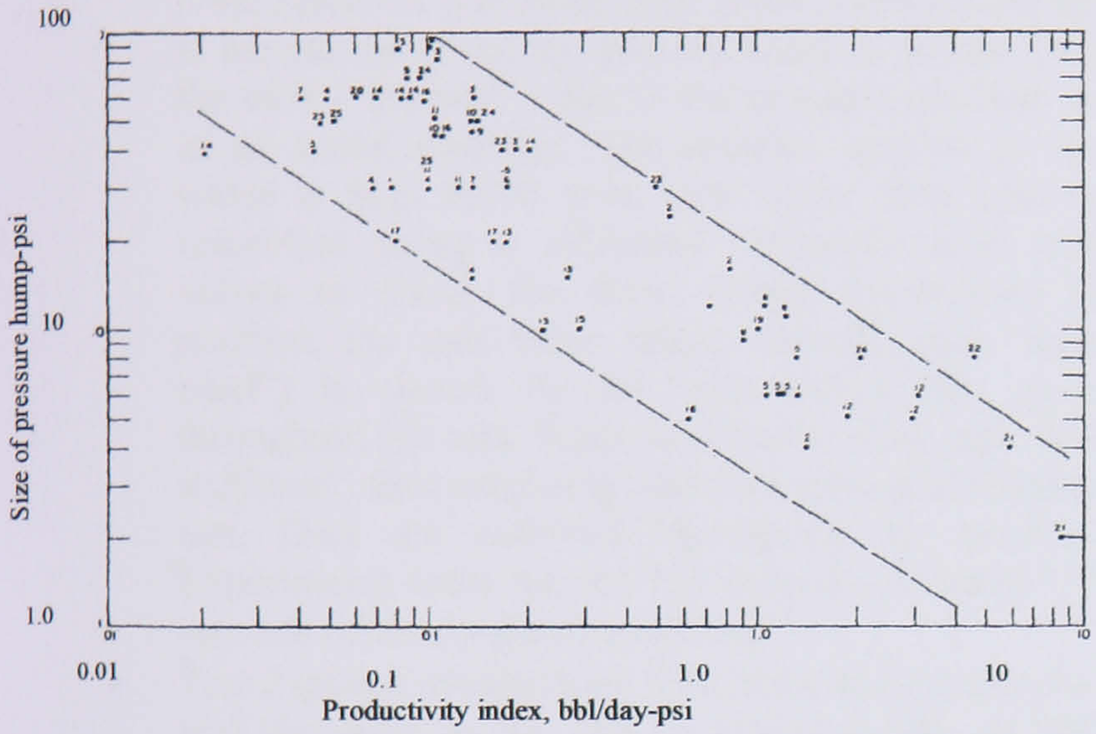


Fig.2: Size of pressure hump as a function of productivity index for South Texas oil wells[2].

When a two-phase (liquid and gas) fluid is flowing in a well which is shut-in at surface, the denser phase will travel toward the bottom of the well while the lighter phase will rise to the surface. Due to compressibility effects, this wellbore phase redistribution causes a net increase of wellbore pressure. In build-up tests, the increased pressure is dissipated through the formation until there is equilibrium between reservoir and wellbore. However, in low permeability reservoirs, it may take some time for this overpressure to be dissipated and this causes the anomalous pressure hump at early times.

Pitzer *et al.*[3] validated and extended the considerations made by Stegemeier and Matthews. They suggested that the size of the pressure hump is related to the amount of gas in the wellbore. Pitzer *et al.* also identified downhole shut-in as the way forward to eliminate the effect of afterflow and wellbore phase redistribution on well test data.

Since the papers of the 1950's, no further relevant investigations were done on the subject of WPR.

Gas-condensate and volatile oil reservoirs have become more important as more fields enter maturity and the worldwide production of condensates and NGL's grows[4,5].

Objectives

The main objective of this study was the development of an experimental system capable of simulating the effects of WPR on pressure-transient data. The aim was to investigate WPR effects during build-up tests as a function of the production rate prior to shut-in. Such investigations may produce a method of eliminating or at least reducing WPR.

An added benefit of this study has been the gathering of experimental data for future WPR mechanistic modeling Imperial College.

To achieve these objectives, an experimental rig was designed and tests performed, the results of which were then analysed using a commercial well test interpretation package.

Experimental setup and procedure

The experiments described in this paper were carried out in the LOTUS (LongTUbeSystem) facility at Imperial College. A simplified diagram of the rig is shown in **Fig.3**. LOTUS is a vertical two-phase air-water system that was originally built at the Harwell Laboratory of the UKAEA in the early 1960's. It was relocated to the pilot plant area of the Chemical Engineering Department of Imperial College in 1992. The vertical tube is mounted over three floors of the pilot plant and the test spools for data collection are located at the top and bottom of the rig. The tube is attached to a vertical fixed beam, carefully aligned to guarantee the alignment and straightness of the tube. LOTUS measurements include pressure, liquid film thickness, wall shear stress and temperature. The tube section used to simulate the wellbore has an internal diameter of 31.8mm and an active length of 10.3m. Various flanged pipes were used to accommodate all the necessary test sections and all the data gathering tappings. The reservoir is simulated by a pressure vessel of dimensions 1500mm in length and 508mm in diameter. Air and water are both introduced into the system at the bottom of the tube. Air into the rig is from a compressed air supply at about 90 psia. It is then passed through orifice plates in order to meter the air flow rate by means of differential pressure transducers. Water is introduced using compressed air through the pressure vessel simulating the reservoir, and metered via rotameters.

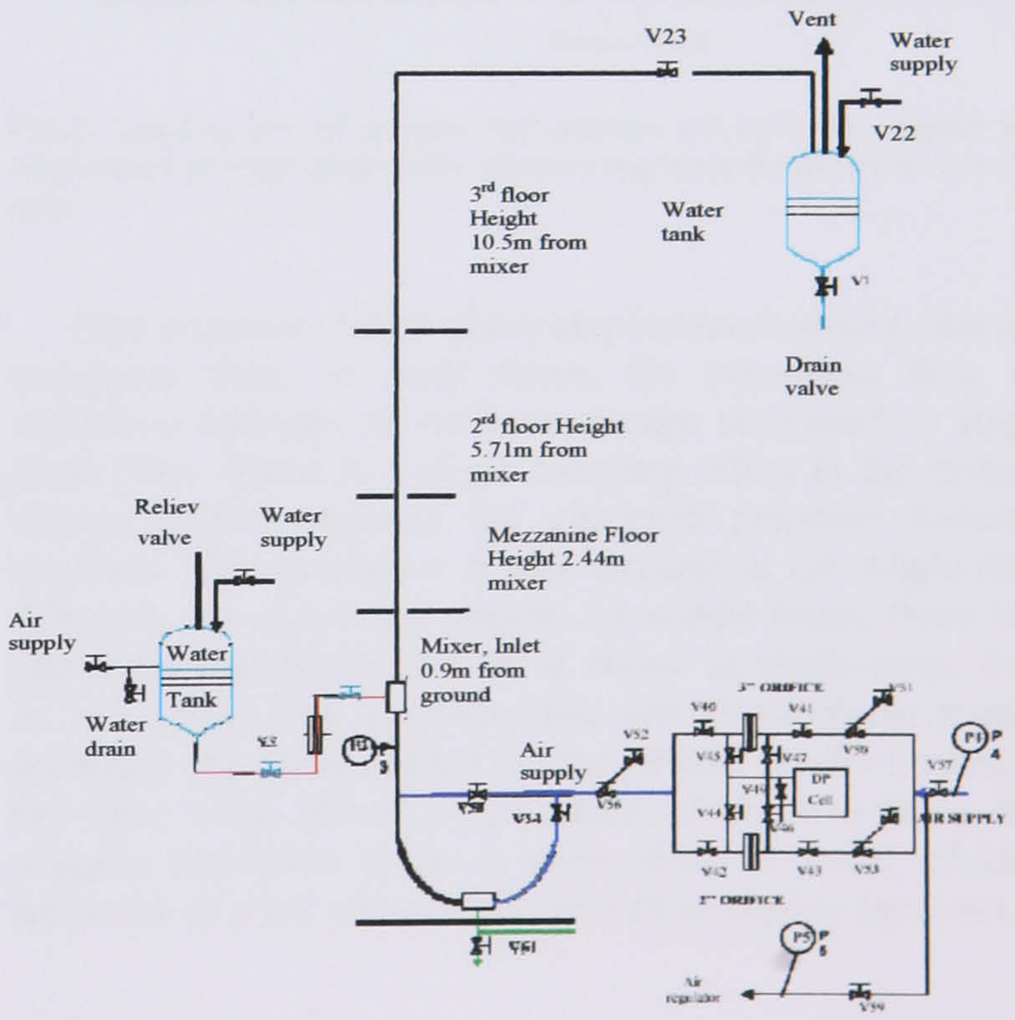


Fig.3: Experimental set-up.

The experiments were organised into three groups: (1) single- and two-phase flow tests to illustrate phase redistribution; (2) phase re-injection tests and (3) closed system tests to investigate the effects of gas migration on bottomhole pressure.

Fluids (air and water) are flowed through the tube at a steady-state surface rate prior to "the well" being shut-in at surface. To see WPR, the results are compared with those obtained with single-phase flow.

- *Test 1* (phase redistribution). The pressure vessel ("the reservoir") is filled with water, compressed air is introduced at the top and the water is pushed into the tube ("the well") due to the pressure gradient as in an actual reservoir. The pressure applied to the water is kept at 40 psia. The water flow rate is controlled using a calibrated rotameter with two valves to choke the flow. When steady-state is reached, the exit valve (**Fig.3**, valve23, the "well head") is closed. As the inlet valves stay open throughout the test, fluids continue to flow into "the wellbore", thus emulating afterflow during a build-up test. Data are recorded throughout the process. Experiments were run for 150 seconds, of which 20 seconds of steady-state conditions.
- *Test 2* (phase re-injection). The procedure for this test was the same as for Test 1. However, the air and water flow rates were kept constant while varying the vessel pressure ("reservoir" pressure). See **Table1** for more details on these experiments.
- *Test 3* (closed system). This test was designed to illustrate the relationship between bubble migration and bottomhole pressure. Three cases were investigated: single-phase water, bubble flow and slug flow. These were qualitative as no flow rate measurements were taken. Both air and water were introduced into the well using same procedure as for Test 1 and 2. After establish the desired steady-state flowing conditions, the data were logged and valves v52, v23 and v5, shown in **Fig.3**, were simultaneously closed.

For Test 1 and Test 2, annular flow conditions were established prior to shut-in, while Test 3 was conducted at different flow regimes.

Results

The experimental data were analysed using a commercial well test interpretation package. Pressure change and pressure derivative are used to illustrate the effect of WPR. The viscosity and compressibility of real gases are strongly related to pressure. The pseudo-pressure concept is used to account for these effects.

$$m(p) = 2\int_{p_0}^{p} \frac{p}{Z\mu}\, dp \qquad [1]$$

The integral of this equation yields:

$$m(p) = 2\sum_{i=2}^{n} \frac{1}{2}\left[\left(\frac{p}{\mu Z}\right)_{i-1} + \left(\frac{p}{\mu Z}\right)_{i}\right](p_i - p_{i-1}) \qquad [2]$$

where the base pressure p_0 is an arbitrary pressure (usually the lowest end of the range of pressure of interest during the test), μ is viscosity, Z is the compressibility factor. For the analysis of single-phase air tests and annular flow tests, rate normalised pseudo-pressure was used.

Single-phase flow pressure transients were conducted to illustrate the deviation of pressure change and pressure derivative in two-phase flow.

Test 1 (phase redistribution). To illustrate the effect of WPR, single-phase pressure transient build-up tests were performed. Both single-phase air and single-phase water experiments were carried out. **Fig.4** shows the pressure build-up results for single-phase water. At early times, wellbore storage, characterised by a unit slope, was observed, followed by stabilization and boundary effects. As the water flow rate increases, the wellbore storage decreases. This was found to be consistent throughout the range of flow rates investigated.

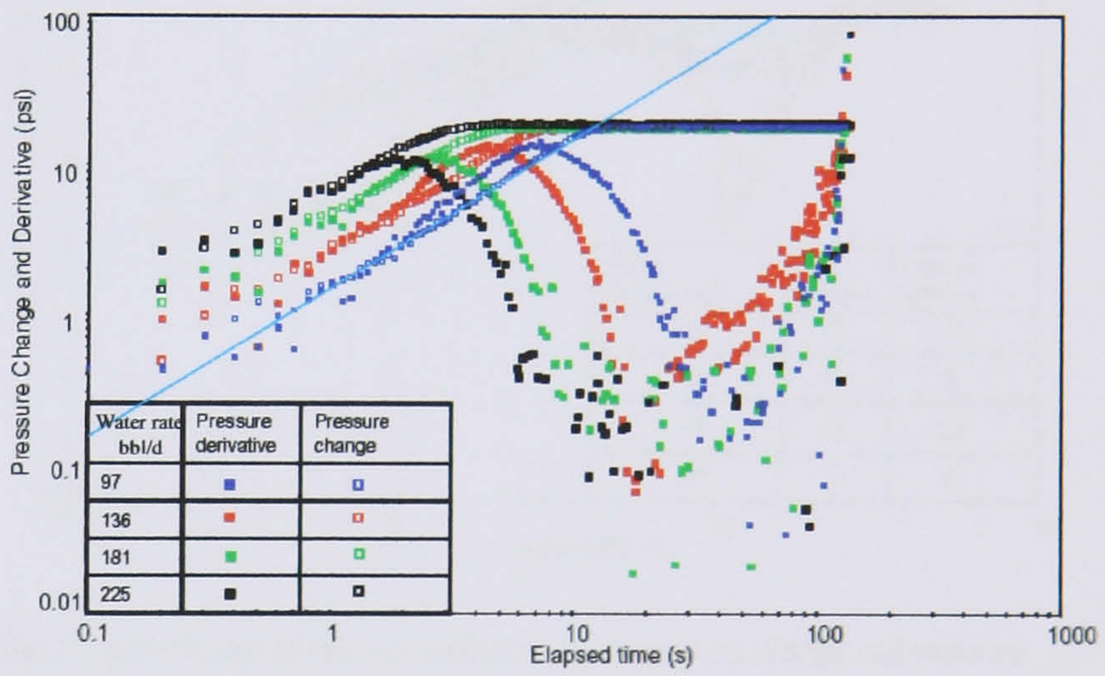


Fig.4: Log-Log plot of pressure and pressure derivative vs. elapsed time. Comparison of single-phase water pressure responses for different water flow rates.

Fig.5 compares single-phase air pressure transient data with two-phase data. At early times, the two-phase flow test exhibits a decrease in wellbore storage compared to single-phase flow. There is a slight humping effect in the pressure change, which explains the observed pressure derivative response. This behaviour is also present in the single-phase flow test, but to a lesser degree. At middle times, there is an additional stabilisation, which is absent in single-phase flow. At late times, both the two-phase and single-phase pressure derivative responses show a similar upward trend with roughly the same slope. Close examination of the two-phase flow pressure derivative shows a rather sharp V-shape, which is indicative of a late phase redistribution or even re-injection.

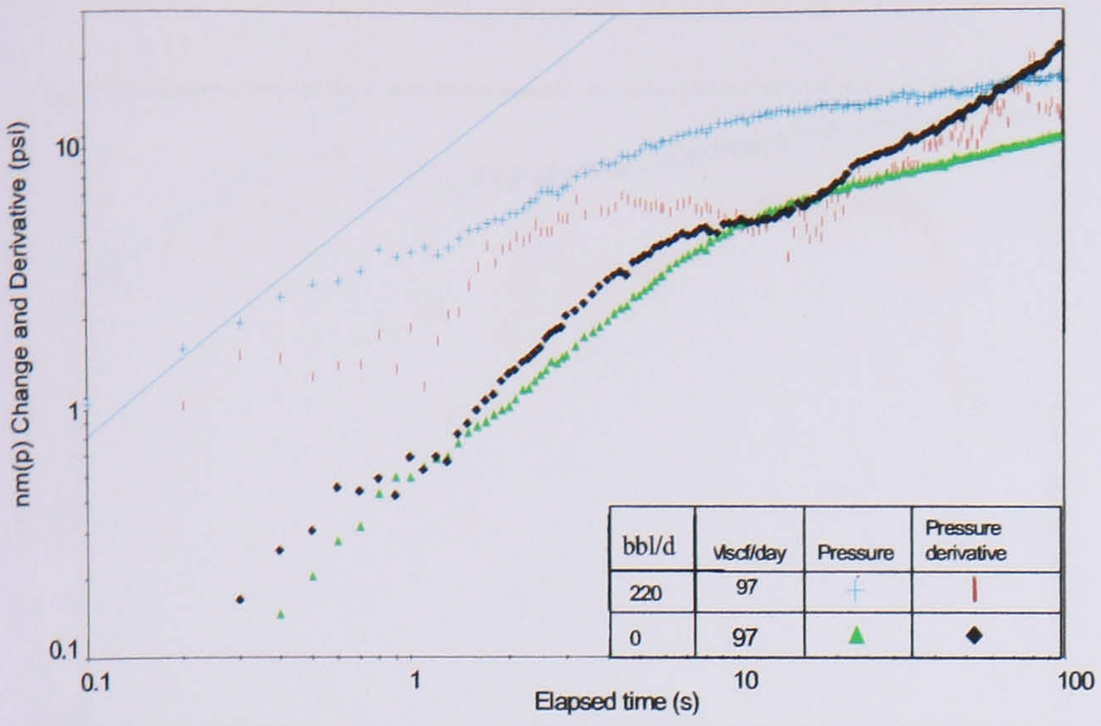


Fig.5: Log-log plot of rate normalised pseudo-pressure change and pressure derivative vs. elapsed time. The comparison between single- and two-phase flow shows WPR.

Fig.6 illustrates the effect of reduced gas flow rate compared to that shown in **Fig.5**. The pressure change and pressure derivative responses exhibit similar shapes in both cases. However, for single-phase air flow, the lower the rate, the smoother the response. For two-phase flow, the lower the air rate, the less pronounced the V-shape (which is indicative of WPR) in the pressure derivative. At late times, for two-phase flow, the pressure derivatives show similar slope in both cases (high and low air rate).

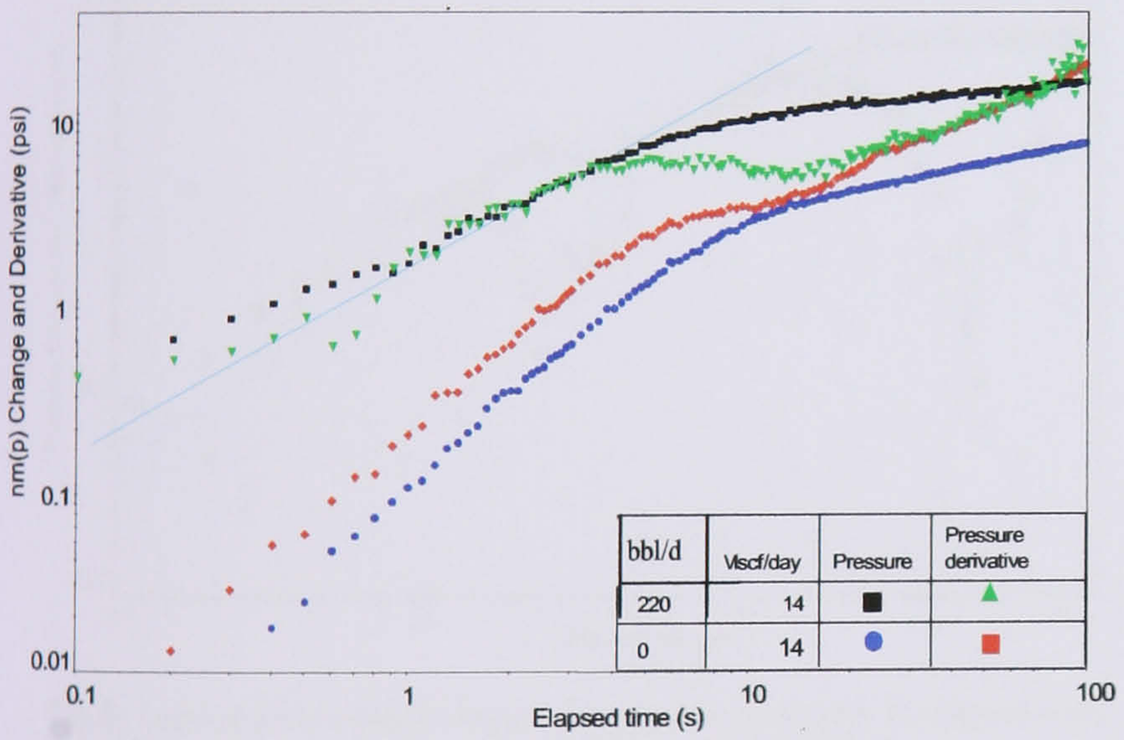


Fig.6: Log-log plot of rate normalised pseudo-pressure change and pressure derivative vs. elapsed time. Single- and two-phase flow rate at low air rate.

Test 2 (phase re-injection). Phase re-injection is a major problem in well dynamics. It has been noted in the literature to have a significant effect on the pressure profile. The following experiments were designed to illustrate the effects of phase re-injection. The methodology and procedure were the same as before, the only change was the pressure at which the vessel (the "reservoir") was kept, which was manipulated as shown in **Table 1**. All of the other test procedures stayed the same.

Run	Liquid rate (bbl/d)	Gas rate Mscf/d	Reservoir Pressure (psia)
1	220	115	35
2	220	115	40
3	220	111	45
4	220	114	50

Table 1: Rates and vessel pressures used in Test 2.

Fig.7 compares runs 1 to 4 shown above in **Table 1**. At early times, the data show WPR, illustrated by the hump in the pressure change. Phase re-injection is clearly illustrated by the V-shape in the pressure derivative and was also visually observed at the pressure vessel. The magnitude of the V-shape depression is much deeper and occurs earlier at lower vessel pressures than at higher vessel pressures. The humping effect, which is indicative of phase re-injection, is only visible at low vessel pressures. At late times, all derivative responses are seen to follow the same trend and slope.

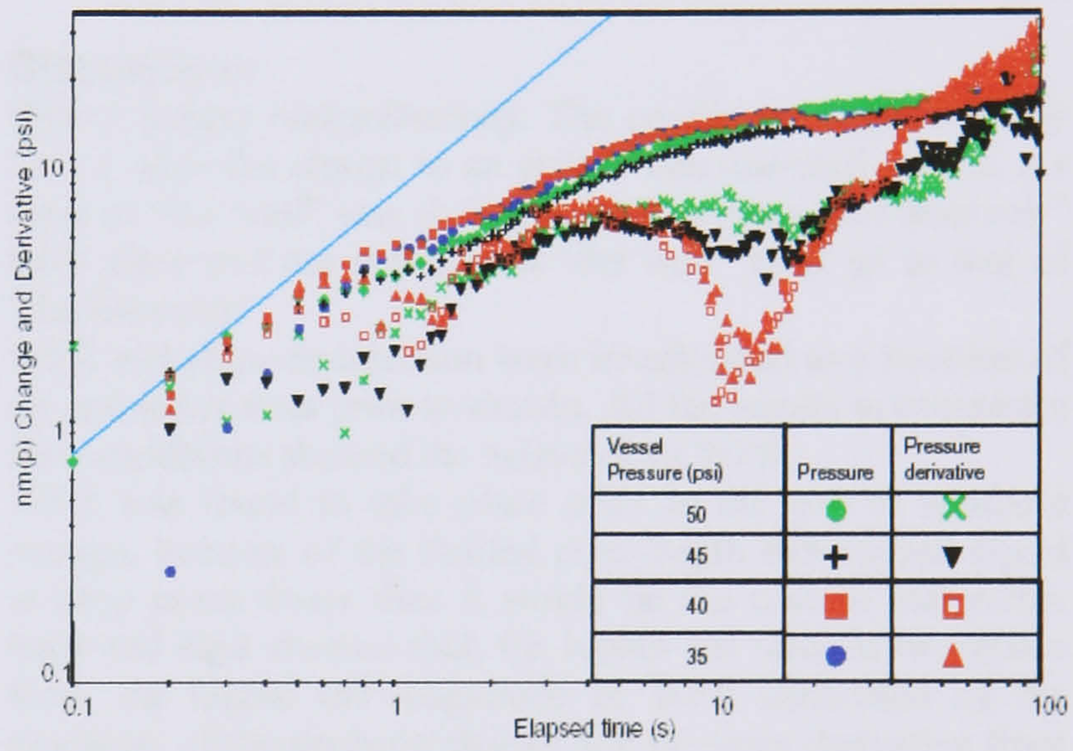


Fig.7: Log-log plot of rate normalised pseudo-pressure change and pressure derivative. Two-phase flow, phase re-injection.

Test 3 (closed system). Three different cases were investigated with Test 3: two-phase bubble flow, two-phase slug flow and single-phase (water) flow.

Fig.8 shows the results obtained with bubble flow regime, with water as the dominant phase. Normal pressure is used instead of normalized pseudo-pressure for the interpretation of the results. Bubble flow regime is unlikely in gas condensate reservoirs. However, this test was intended to illustrate the impact that rising gas bubbles could have on the pressure gauge.

During the first seconds after shut-in, a straight line with a unit slope (which is indicative of wellbore storage) is observed in the log-log plot, followed by a wave-type response that causes instability in the pressure derivative. At middle times, the pressure change data become less noisy and increase steadily, as does the pressure derivative. At late times, no further pressure change takes place and the pressure derivative goes to zero, as in a closed system.

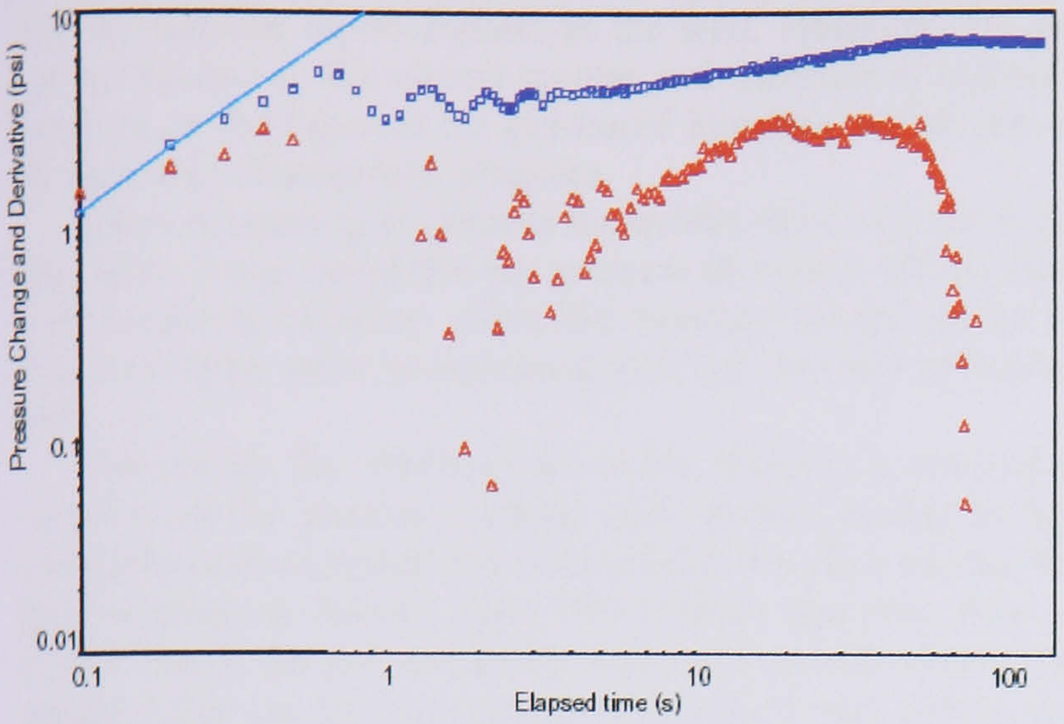


Fig.8: Log-log plot pressure change and pressure derivative vs. elapsed time. Bubble flow regime, phase redistribution without afterflow effect.

Fig.9 shows shows the results obtained with slug flow regime. The pressure rise takes longer to stabilise than for the case of bubble flow and the magnitude of WPR is greater. This is illustrated by the continuous fluctuation of the pressure change and by the sharper V-shape in the pressure derivative. At late times, no further pressure change takes place and the pressure derivative goes to zero, as in a closed system

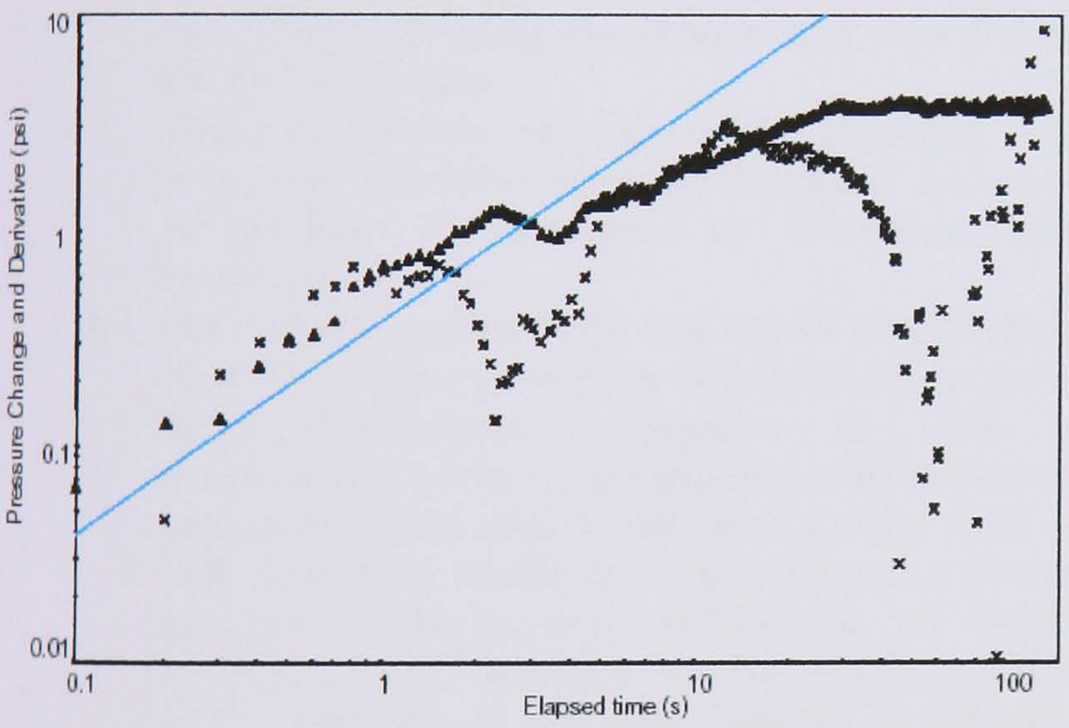


Fig.9: Log-log plot pressure change and pressure derivative vs. elapsed time. Slug flow regime, phase redistribution without afterflow effect.

Fig.10 shows results from a shut-in test with single-phase water. The purpose of this test was to illustrate the significance of sudden momentum changes, called water hammering in hydraulics.

During the first seconds after shut-in, the pressure change increases and then decreases with a wave-type response, due to the incompressibility of the fluid, and is typical of water hammering. The pressure stabilises after the hump.

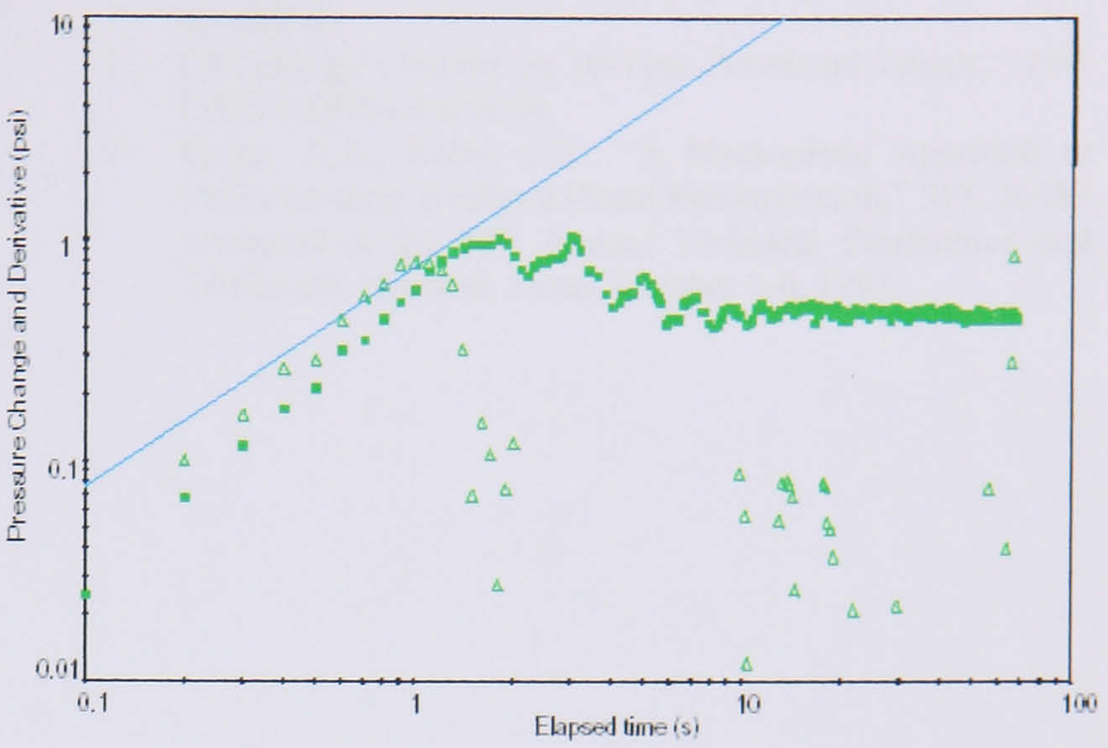


Fig.10: Log-log plot of pressure change and pressure derivative vs. elapsed time. Single-phase water, hammering effect.

Discussions

Test 1 (phase redistribution). The conditions reproduced by Test 1 were the closest to an actual reservoir-well system. As soon as "the well" was shut-in, afterflow from "the reservoir" took place and the pressure in "the well" built up to that of "the reservoir".

WPR and phase re-injection were investigated as a function of air and water rates prior to shut-in. All the results in two-phase flow conditions showed the existence of WPR.

WPR was found to take place prior to the end of wellbore storage, because of the limited pipe length that caused liquid to drop much faster than it would be the case in real wells. **Fig.5** and **Fig.6** showed that, the higher the rates in two-phase flow, the higher the magnitude of WPR (indicated by the deviation of the pressure change and pressure derivative from the single-phase air case). In particular, WPR was found to be a strong function of air rate, for a given water rate. It is difficult to draw a firm conclusion from the data collected during Test 1, but it is believed that the behaviour observed is a consequence of the fact that annular flow was the predominant flow regime for the experiments.

One important anomaly to report is that, at high air rates, even the single-phase air tests showed pressure change and pressure derivative deviations. Similar anomalies were also reported by Gringarten *et al.*[1] for a dry gas well in Canada.

Test 2 (phase re-injection). Test 2 investigated the effects of phase re-injection, which usually takes place in damaged wells and in low-permeability formations. In these experiments, the pressure at the vessel was manipulated to simulate a low-productivity reservoir. **Fig.7** showed higher phase re-injection at lower vessel pressures, in agreement with the findings by Stegemeier *et al.*[2].

Test 3 (closed system). The tests with the closed system allowed the investigation of WPR without afterflow and without re-injection.

The results for bubble flow were found to be consistent with what reported by Stegemeier *et al.*[2] and, more recently,

by Kabir *et al.*[6]. In bubble flow build-up tests, the gas bubbles rise through the liquid column in the well. However, the gas cannot expand in the closed system and therefore it exterts a pressure on the liquid at the gas-liquid interface, which causes an increase in bottomhole pressure.

When comparing the results for bubble flow with those for slug flow, it was noted that the pressure change in bubble flow took longer to stabilise. Also, the pressure waves shown in slug flow were more pronounced than for the case of bubble flow.

The results for single-phase water showed a wave-type response in the pressure change after shut-in similar to that caused by water hammering. The results also showed that the rise in pressure change, seen with bubble and slug flow at middle times, did not take place with single-phase water. This suggests that the rise in pressure change seen with bubble and slug flow was only due to gas rise.

Conclusions and recommendations for future work

- An effective experimental set-up and methodology was developed for the study of WPR. A pressure vessel was found to represent the reservoir satisfactorily.
- WPR was found to occur in two-phase flow tests before the end of wellbore storage.
- Air flow rate was found to have a higher effect than water flow rate on WPR. This was most probably due to annular flow being the predominant flow regime for the experiments.
- Phase re-injection was successfully simulated. The lower the "reservoir" pressure, the higher the liquid re-injection, an analogue to low-permeability reservoirs.
- For a closed system, WPR was shown to take place. Rising gas causes an increase in bottomhole pressure.
- More experimental investigation of WPR is necessary for a better understanding of its impact on pressure-transient data. In particular, a wider range of flow conditions should be considered and a porous medium should be used to simulate the "near-wellbore region" between "the reservoir" and "the well". Research is currently ongoing at Imperial College to combine the experimental investigation of WPR with the modelling of the associated transient flow phenomena.

References

1. Gringarten, A.C., Al-Lamki, A., Daungkaew, S., Mott, R. and Whittle, T.M.: "Well Test Analysis in Gas Condensate Reservoirs," SPE 62920 presented at the SPE Annual Technical Conference and Exhibition, Dallas Texas, October 1-4, 2000.
2. Stegemeier, G.L. and Matthews, C.S.: "A Study of Anomalous Pressure Buildup Behaviour," J. Pet. Tech. (February 1958) 44-50; Trans., AIME 213.
3. Pitzer, S.C., Rice, J.D. and Thomas, C.E.: "A Comparison of Theoretical Buildup Curves with Field Curves Obtained from Bottomhole Shut-in Tests," Trans., AIME 216, 416-419, 1959.
4. BP Review of World Energy 2005, downloaded from the bp website.
5. IHS Energy's Report on 10-Year Petroleum Trends, 1994-2003, published in 2004.
6. Hasan, A.R., Kabir, C.S.: "A Mechanistic Approach to Understanding Wellbore Phase Redistribution," SPE 26483 presented at the SPE Annual Technical Conference and Exhibition, Houston, Texas, October 3-6, 1993.

Integration of Multiphase Flowmetering, Neural Networks, and Fuzzy Logic in Field Performance Monitoring

C. Alimonti, SPE, U. of Rome, La Sapienza, and **G. Falcone,** SPE, Enterprise Oil UK plc*

Summary

The usual approach to the interpretation of producing wells is based on mechanistic models for the simulation of steady-state and transient flow regimes. However, there are significant reservations about convergence problems, computational limits, the need for extensive tuning on field data, the instability of boundary conditions, the limited applicability of existing multiphase flow models, and the uncertainties associated with choke-valve models. The current industry standards are critically reviewed within this framework.

The real-time monitoring of producing wells is recognized as the best way of optimizing field performance. Monitoring a producing well implies the ability to track any changes in fluid composition, flow rates, or pressure and temperature profiles in real time. Multiphase flowmetering (MFM) plays a key role in this scenario. Such information, combined with the critical analysis of historical data from the well itself or from analog wells, allows diagnosis of the system and prediction of future trends. However, field data *per se* do not necessarily generate knowledge. This is particularly true for large databases, which are difficult to manipulate to provide suitable inputs for wellbore simulators.

This paper suggests how MFM, knowledge discovery in databases (KDD), and fuzzy logic (FL) can offer an alternative approach to analyzing producing wells. KDD is the automated extraction of patterns representing knowledge implicitly stored in large information repositories. Distributed, *ad hoc* field measurements (including MFM and downhole measurements) can be processed by means of data cleaning, data integration, data mining, artificial intelligence (AI), and pattern evaluation. FL can then manage the resulting information in terms of flow assurance and production optimization.

The same techniques can also be extended to the reservoir and production network for an integrated approach to production-system analysis.

Introduction

Production wells are the physical connection between the reservoir and the surface facilities. As such, they are part of a production system, which is a network of components through which underground hydrocarbons must flow to reach the surface. It includes and is characterized by the following.

- The reservoir, with its geological and petrophysical properties, and the properties of the fluids stored within it.
- The production wells, particularly their completions and any artificial-lift solutions.
- The flow-control valves, such as the wellhead chokes.
- The flowlines and any flow-assurance solutions associated with them (such as single or multiphase pumping, thermal isolation, and chemical injection).
- The separation and treatment facilities, both subsea and at surface.

Besides this hardware, the properties of multiphase flows within the reservoir and through the production network must also be taken into account for the production system to be fully characterized. It is common knowledge that variations of any of the previous characteristics are reflected in the rest of the system; therefore, none of the system elements can be considered physically disconnected from the others. This means that the production system can be regarded as integrated.

There are several levels of integrated analysis that can be carried out on a production system, depending on what sorts of results are needed. The short-, medium-, and long-term optimization of field management certainly are the main reasons oil companies put so much effort into simulating integrated production systems. Short-term optimization means finding the optimum operational conditions—choke settings, rate and allocation per well of gas lift gas and chemical injection, separator pressure—that maximize the day-to-day production and honor any physical constraints dictated by the system itself (overall capacity of the network, availability of compressors, slug-handling capacity, and flaring restrictions). Medium-term optimization includes planning startups and shutdowns so that the effects of transients can be smoothed and handled throughout the system. Long-term optimization aims at maximizing the recoverable reserves from the system and may include debottlenecking and topsides modifications to handle larger amounts of water or gas from depleting fields.

Optimization can be achieved only by monitoring the field closely and critically reviewing any significant trend in the main parameters of the system. The frequency at which the information must be retrieved from the field is a function of the time dependency of the events being analyzed. Monitoring provides a feel for the lag time between the moment a variation occurs in the system and the moment it is felt by any of the parameters characterizing the system. Thus, *una tantum* measurements can be enough for steady-state conditions, while real-time monitoring is necessary for accurate verification or prediction of fast-changing conditions.

Different levels of analysis may be needed at different stages of field development. The design stage and the early life of a field are the most critical in terms of development planning because very little is known about the potential performance of the field. However, late-life solutions may be critical as well because of the likelihood of more unstable flow conditions associated with depleting systems.

Having introduced the concept of integrated production systems, it follows that the best approach to their interpretation and optimization is the simultaneous integration of information from their individual components. Well monitoring and diagnosis, in particular, are the most direct ways of detecting variations in any key parameter of an integrated production system. However, how can we discern what parameters are most representative of significant changes in system properties? Are variations predictable? Can we measure these in the field? Can the information be inferred from standard software packages when it is not possible to get all the necessary data from the field?

State of the Art

Standard Approach to Integrated Production Systems. To date, several models have been developed to simulate the behavior of multiphase flows within the reservoir and through individual components of a production system. A number of commercial

* Now with TOTAL E&P UK plc, London

Copyright © 2004 Society of Petroleum Engineers

This paper (SPE 87629) was revised for publication from paper SPE 77407, first presented at the 2002 SPE Annual Technical Conference and Exhibition, 29 September–2 October. Original manuscript received for review 20 January 2003. Revised manuscript received 10 November 2003. Paper peer approved 9 December 2003.

TABLE 1—SUMMARY OF OIL PROPERTIES		
Density	Viscosity	Associated GOR
34.5 API	7 mPa • s at 20°C	1,288 to 1,400 scf/stb

simulators are available that can separately model reservoirs, wellbores, gathering systems, and the process plant, and the manufacturers claim they can handle steady-state as well as transient conditions. There are also extensive compositional and black-oil models for simulating the pressure/volume/temperature (PVT) properties of produced fluids and empirical and thermodynamic models for simulating flow through wellhead choke valves. However, compatibility problems often arise when different software packages from different vendors are coupled together.

Because different mathematical codes and convergence procedures are adopted for simulating different elements of a production system, there is always the risk of serious instability when coupling software packages together. In this modular approach to simulating production systems, special attention also must be paid when defining the so-called boundary conditions.[1] These dynamic interactions between different parts of the system guarantee the conservation of mass, energy, and momentum from the reservoir to the process plant. For instance, the multiphase flow correlations must be smooth and consistent throughout the system and the entire range of production conditions, but this is not always possible because of the high complexity and unpredictability of multiphase flows and their strong dependence on the history of the flow. Because of this dynamic interrelation between the various elements of an integrated production system, it is important to account for the overall effects caused by wellhead chokes and other control valves in the process plant.[2,3] Only when critical flow occurs can a wellhead choke decouple the reservoir from the production facilities (although a simulation run with the network model is still needed to establish whether the flow is critical). When the flow is subcritical, the choke must be regarded as a key element of the production system, which creates a pressure drop, affects the upstream/downstream flow, and controls the total production rate.

Another approach to the study of integrated production systems is to combine the equations for the reservoir and the production facilities in a single system and solve them simultaneously.[3] However, despite the need for full-field models that can couple surface facilities to reservoir simulators, no satisfactory solution has been found yet because of the prohibitive computer-processing times associated with conventional techniques. Implicit methods can be computationally intensive if not supported by the use of parallel machines and/or the implementation of acceleration techniques, such as domain decomposition.[3] To treat a system implicitly means to solve the production network first, then use the results as boundary conditions for the reservoir simulator and see if convergence of pressure and flow rate at downhole conditions can be achieved. If not, an iterative process is generated by assuming new well rates as boundary conditions for the production network, but convergence may be very slow for large models and may not be achieved in some cases, especially if choke valves are included. An alternative to implicit methods is represented by explicit methods in which the convergence point at the bottomhole is set at the beginning of the simulation. Although this procedure saves the central processing unit (CPU) time, it may be less accurate, especially when the operating conditions of the system change rapidly.

Both approaches to the study of surface facilities, wells, and reservoirs as integrated systems have the inherent uncertainty of the accuracy of the flow models adopted for simulating the various elements. Each code has its own merits for particular conditions, and it is left to the engineers to judge which combination of tools is the most suitable for simulating a given production system.

With regard to reservoir simulators, it is not unusual to get different answers to the same problem, depending on whether an analytical, deterministic, or streamline-based model is used or whether the reservoir fluids have been characterized by compositional or black-oil techniques.

A similar situation may occur when modeling multiphase flows through wells and pipelines. In this case, mechanistic models, as opposed to empirical ones, can provide more reliable solutions.[4] However, no universal multiphase flow correlations have been developed that can cover any inclination and pipe diameter or be applied to any flow regime. Furthermore, closure laws are generally needed to solve the system of equations, but because they are flow-regime dependent, an error in predicting the flow regime may invalidate the final answer. This is particularly true for transient conditions in which terrain-induced effects and the history of the flow may cause a nonunique solution to the identification of the flow regime, even though the boundary conditions remain unchanged. Because transient simulators are indeed specialized tools, they can generate misleading results unless they are used by a dedicated engineer or group of engineers with experience on the pipeline system under examination.

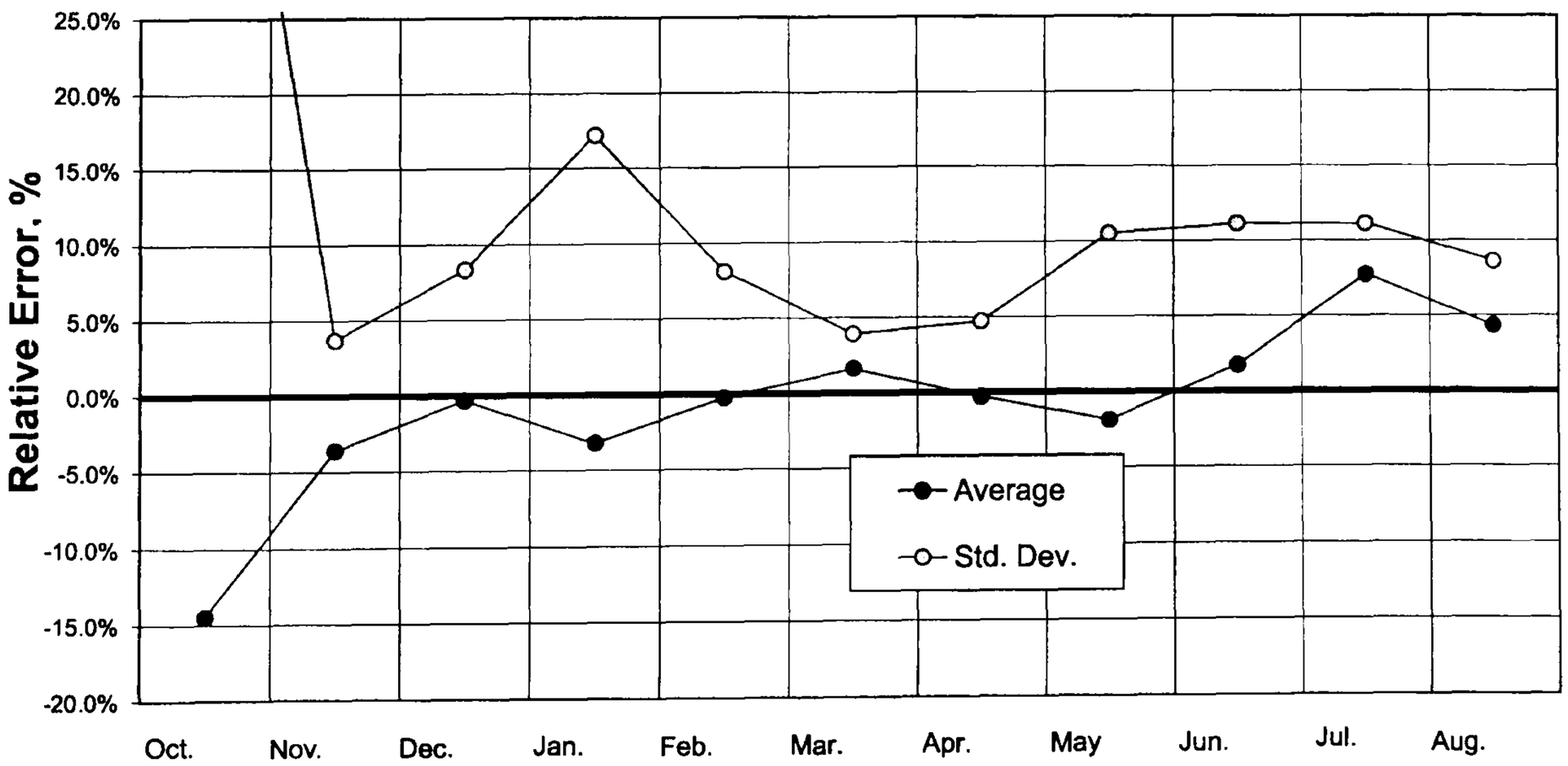


Fig. 1—ANN model vs. field data—relative error in oil flow rate.

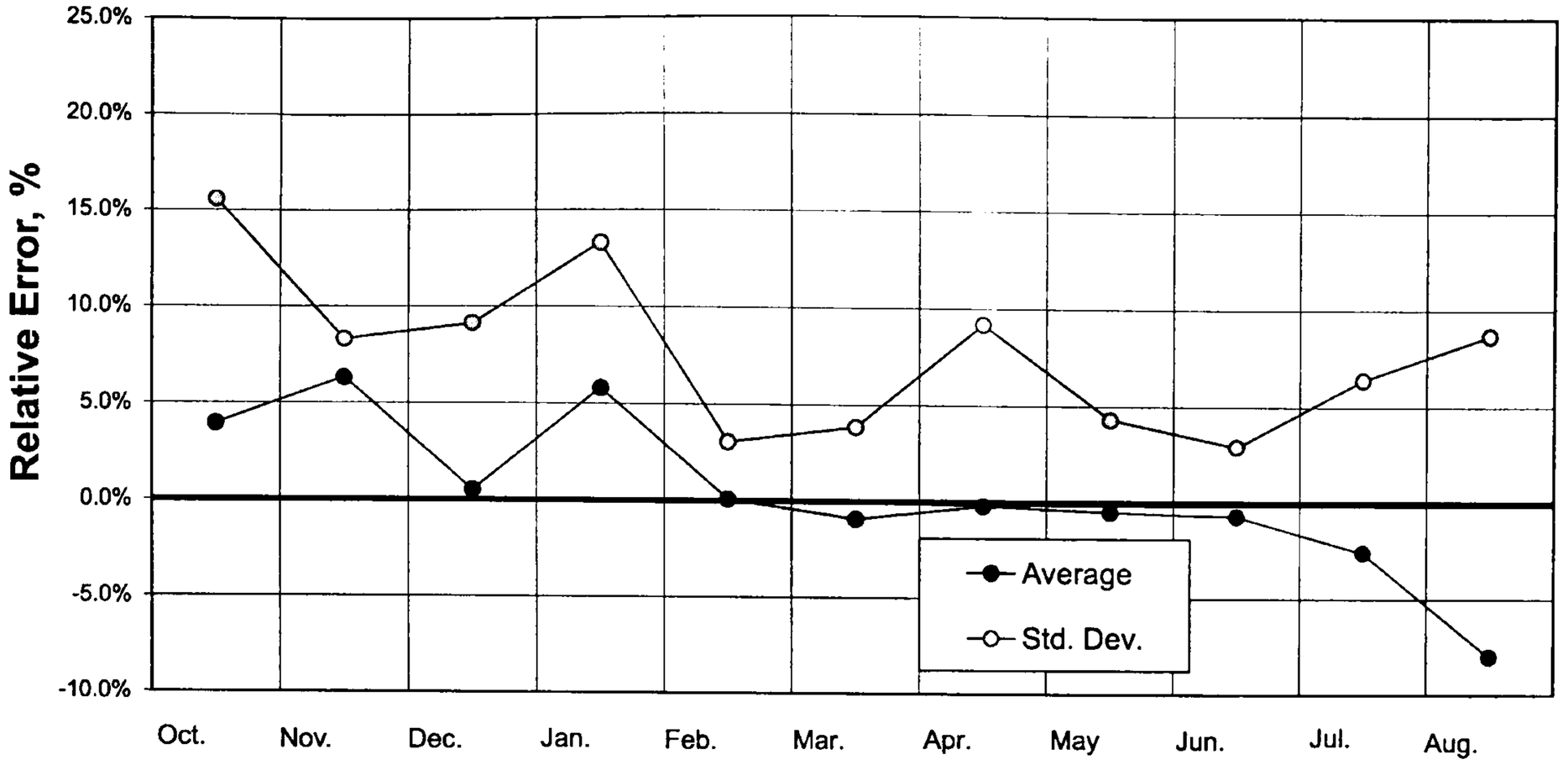


Fig. 2—ANN correction model vs. field data—relative error in oil flow rate.

Tuning Models With Field Data. Another drawback with the two approaches described previously is the need for extensive tuning of the model with field data. This makes the overall process of simulating integrated production systems even longer.

Matching vertical-lift performance curves to measured data and generating families of curves for a large enough water-cut range, gas/oil ratio (GOR), and tubing-head pressure requires long running times and powerful computers. History matching a reservoir model can be very time consuming, especially for fully compositional fluid models and refined simulation grids. Sometimes it is necessary to edit out part of the reservoir, generally part of the aquifer, and assume that its contribution to the pressure support is negligible, at least until depletion becomes significant in the main reservoir. Even when a detailed tuning on historical data is performed, there is no guarantee that the model can run safely in predictive mode.

Multiphase flow correlations also need extensive tuning with field data, yet there may be flow conditions (in the wells, in the pipelines, or through the chokes) that are not satisfied by any of the available correlations.

Data Handling. It is essential that the data gathered from the field contain the information needed for a consistent match of the integrated production system as a whole. The location of reservoir and production monitoring devices throughout the system must be strategic, as must the sampling frequency and any adopted data-filtering technique. Unfortunately, this is not always the case. Many pressure and temperature sensors in the field are not in the desired location to get the necessary information for the multiphase flow models of wells, pipelines, and chokes, usually because of retrofitting (i.e., adding sensors to a field already under development). Also, it is not unusual that downhole pressure gauges are retrieved from the wells long after their memory has become full and are only rarely replaced with new gauges, leaving inference methodologies to estimate pressure values. Thus, retrieved information may be useless unless it is combined with other information from different elements of the system for the same period.

Even when enough instrumentation is put on site, it may become technically challenging to transmit and store large amounts of information to databases from which historical information can be extracted when needed.[5] There may be the risk of storing "noise" or nonessential data along with key information if no filtering techniques are used between the field and the database. However, data can only be filtered when the users know in advance what kind of frequency is to be expected from a given phenomenon, and this frequency may vary during the field's life.

In the last decade, many efforts have been made to offer reliable control tools that provide real-time information for field surveillance. Fiber-optic-based sensors are being used for temperature, pressure, pH, acoustic noise, and strain measurements.[6] So-called intelligent completions have been developed that include not only permanent temperature and pressure downhole sensors but also remote control of downhole chokes for real-time flow control of different producing zones.[7] Continuous measurement of the formation conductivity is now possible by means of water-monitoring radar, which is based on the electromagnetic field generated between a transmitter and two receivers.[7] Permanent geophones are being considered as a potential option for continuously monitoring the fluid migration in the reservoir. Multiphase flowmeters are becoming standard practice for the development of tieback, deepwater, and marginal fields, and they provide invaluable well diagnostics.[8]

Internet-based databases that can retrieve real-time information from the field, make it available to users worldwide, and plot it under different formats, as required, are available to the oil and gas industry. Also, data collected in this way can be downloaded into standard software packages for production allocation and produc-

TABLE 2—SUMMARY OF AVERAGE RELATIVE ERRORS AND STANDARD DEVIATIONS FOR DIFFERENT FLOW-RATE ESTIMATION MODELS

	Oil		Gas	
	Error (%)	Standard Deviation (%)	Error (%)	Standard Deviation (%)
FDM	–3.4	16	2.5	19
ANN	–0.8	13	0.8	7.8
ANN corrector	0.3	7.7	1.8	7.0

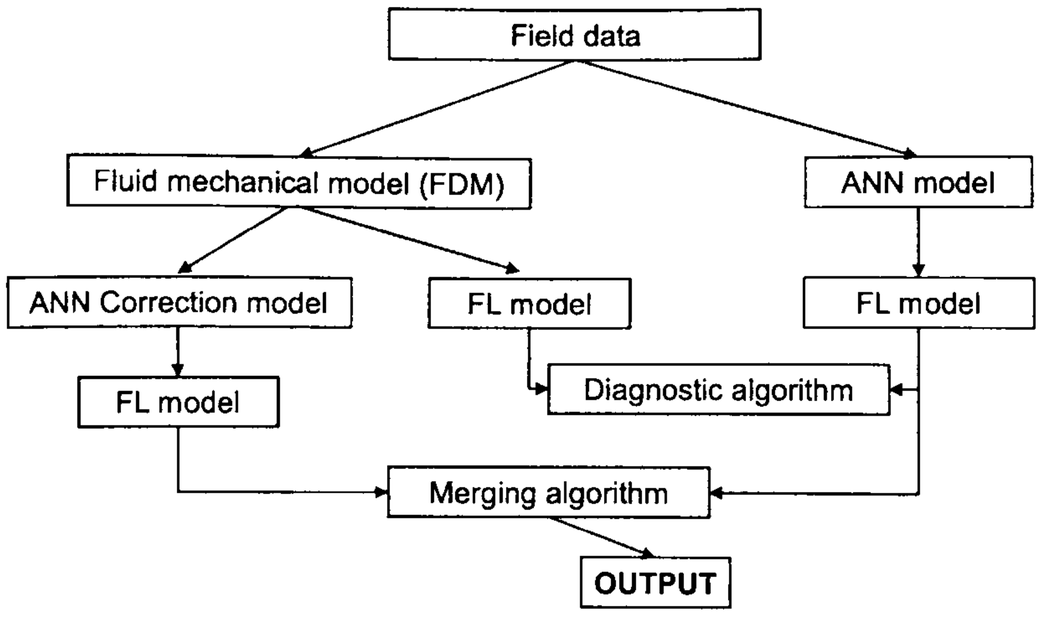


Fig. 3—Flow chart of the data-processing sequence.

tion forecast purposes. A note of caution: such procedures can be quite time consuming, rely on powerful machines, and imply that data are processed and interpreted only after they have been acquired and stored in a databank.

Finally, statistical and probabilistic analysis of reservoir properties (Monte Carlo simulation) and production data (prediction methods such as the linear model fit by least squares and the *k*-nearest-neighbors prediction rule) can now be performed by commercial software packages. Probability theory allows us to model the uncertainty of any process in which the outcomes of any particular realization of it are strictly a matter of chance. This is fine for random processes in which a precise description is available of the statistics of the long-run averages of the process. However, the uncertainty associated with nonlinear, complex systems (and, hence, with integrated production systems) is not random. In such cases, the information available to solve the problem is more qualitative than quantitative and can only be incorporated in engineering models with some tolerance for imprecision.

An Alternative Approach to Well Monitoring and Diagnosis

In the following, we introduce the implementation of AI techniques with the standard methodologies described previously for a more flexible and meaningful approach to interpreting integrated production systems. Although it is not possible to go away without making use of traditional tools, such as reservoir, wellbore, and pipeline simulators, we shall show how key parameters measured at the wellhead and fluid dynamic models can be harmonized by AI to provide real-time information on a flowing system.

In particular, we describe the integrated use of online MFM, *ad hoc* measurements at the wellhead, and AI for a critical approach to well monitoring and diagnosis.

Review of AI Techniques

Knowledge Discovery in Databases: Data Mining and Artificial Neural Networks (ANNs). Data mining, an essential step in the KDD process, is defined as "the automated extraction of patterns representing knowledge implicitly stored in large databases."[9] Thus, data *per se* do not necessarily mean knowledge, and, therefore, some way of uncovering data patterns is usually needed.

KDD has developed continuously since the 1960s, when data collection and database-creation techniques began to make significant progress. The rapid evolution of KDD would not have happened without incredible advances in computing, making it possible to handle huge amounts of data. Hence, now there is the ability to process such data potentially at the same speed at which they are gathered. The KDD process can be summarized as follows:

- Noise and spurious data are removed from the database by means of cleaning/filtering techniques.
- Data that are stored in different databases but belong to the same phenomenon are combined.
- Basic statistics or aggregation techniques are applied to the data for consolidation.
- Patterns are extracted from the data by means of data mining operations, which includes techniques such as machine learning, spatial data analysis, database technology, pattern recognition, and ANNs.
- Once the patterns have been extracted, they must be evaluated to discern new or interesting information from nonessential information.

The previous steps are not necessarily in the order described because they must be tailored to each individual application and its features.

Data mining is not just a deductive database system or a statistical data-analysis tool; it involves an integration of different techniques that rely on the interaction between users and the data mining system. This is particularly true when ANN learning is adopted, because direct user involvement is required to interpret the qualitative meaning behind the learning weights associated with the connections in the network. ANNs, which employ nonlinear functions of linear combinations ("derived features") from the inputs,[10] represent a very general approach to regression and classification problems. Because of their characteristics, ANNs best apply to situations with a high signal-to-noise ratio. ANNs are useful for classification in data mining because of their nonlinear statistical models, from which rules can be extracted and incorporated within FL applications.

FL. The concept of FL was introduced in 1965 by Prof. Lofti Zadeh.[11] FL is a problem-solving control-system methodology that provides a simple way to arrive at a definite conclusion based on vague, ambiguous, imprecise, noisy, or missing input information. It mimics how a person would make decisions, only much faster. In 1973, Prof. Zadeh stated: "As the complexity of a system increases, our ability to make precise and yet significant statements about its behaviour diminishes until a threshold is reached beyond which precision and significance (or relevance) become almost mutually exclusive characteristics."[12]

While it does not bring much improvement in the case of simple linear systems or naturally automated processes, FL best

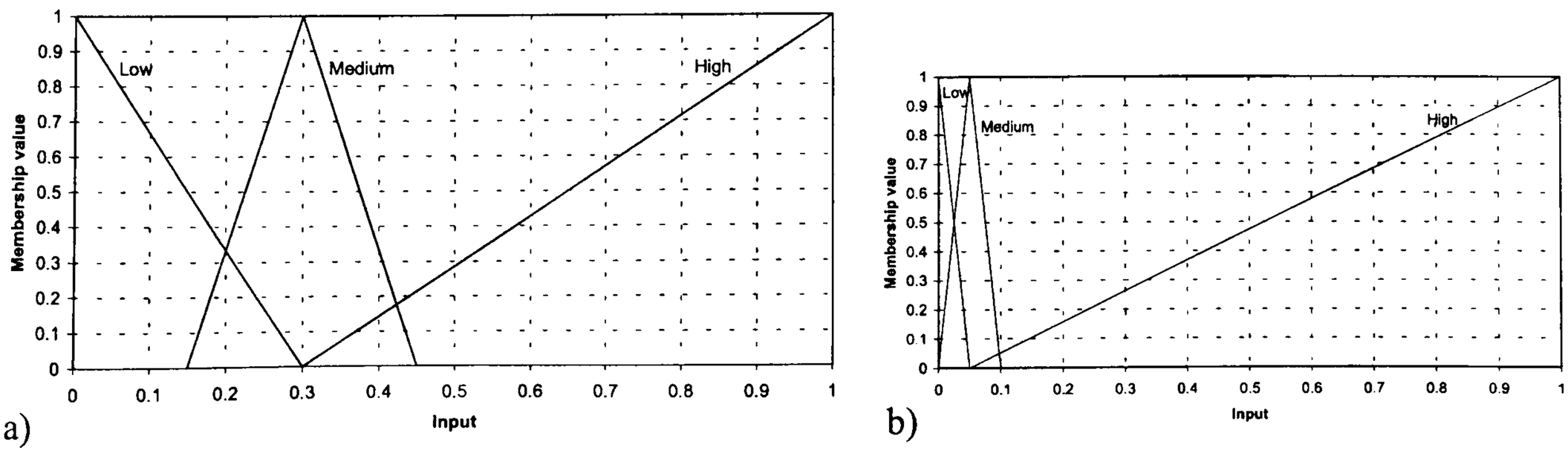


Fig. 4—Membership functions for error Q_o: (a) FDM and (b) ANN model.

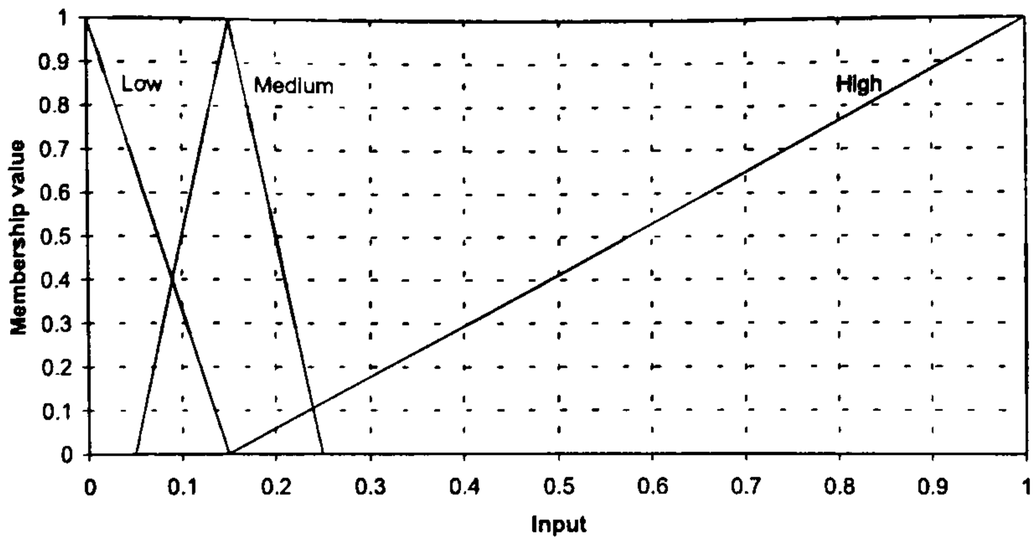


Fig. 5—Membership function for input error GOR.

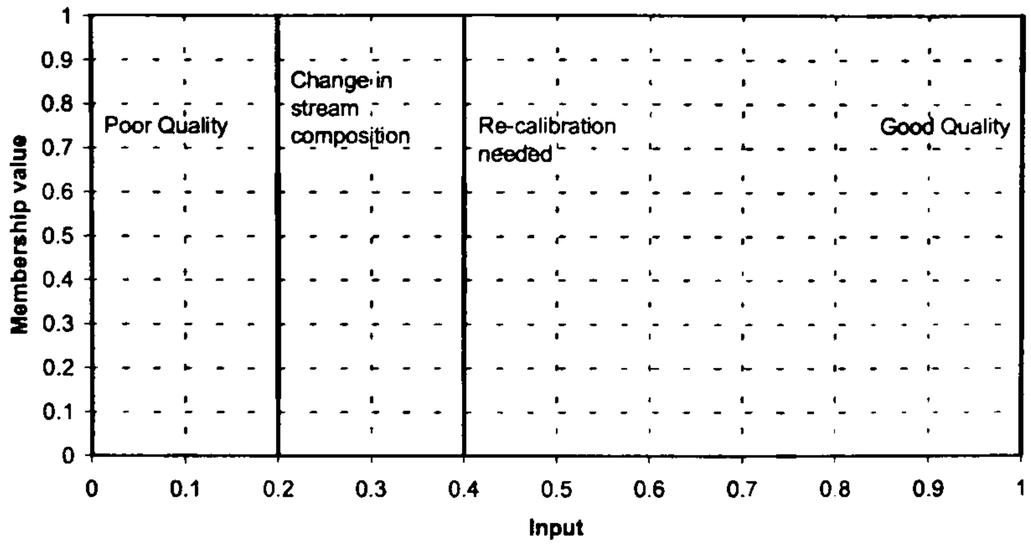


Fig. 6—Membership function for output. Crisp membership function.

applies to areas in which intuition and judgment still play a fundamental role. In Japan, FL is now part of day-by-day life, being successfully implemented to train scheduling, videography, stock tracking on the Nikkei stock exchange, robotics, and domestic appliances.

FL is an infinite-valued logic that allows for degrees of set membership. The three logic operations AND, OR, and NOT return a degree of membership that is a real number between 0 and 1, in contrast to the traditional Boolean values of TRUE, 1, and FALSE, 0.[13]

For a certain number of input parameters, FL identifies the fuzzy variables associated with each parameter of an event. Membership functions, which are assigned to the fuzzy variables to judge the magnitude of their participation in the event, are defined by shape, height, width, shouldering, center points, and overlap. They can be generated in several ways, including use of the so-called genetic algorithms (based upon the concept of Darwin's theory of evolution) and ANNs. Rules that use the input membership values as weighting factors to determine their influence on the final fuzzy output sets are then defined.

The final step in the FL process is so-called defuzzification, converting the fuzzy sets into scalar, single quantities. Defuzzification methods are context-dependent; hence, they may vary from case to case.

Applications of AI to the Oil and Gas Industry. The application of AI techniques to the petroleum industry has been evaluated since the early 1990s. ANNs and FL have already been developed in the following areas.[9, 13–21]

- Geology and geophysics (e.g., reserves estimation, seismic pattern recognition, and sequence stratigraphy).
- Formation evaluation (e.g., porosity and permeability prediction, fracture delineation, and pore pressure determination from log data).
- Drilling [e.g., measurement-while-drilling (MWD) data analysis].
- Production and facilities (e.g., gas-lift optimization, topsides processes optimization, diagnosis and maintenance, and multiphase flowmetering).
- Reservoir engineering (e.g., automatic history matching, pattern recognition of pressure-transient data, and reservoir properties prediction).
- Petroleum economics (e.g., risk analysis and portfolio optimization).

ANNs best reproduce nonlinear phenomena, while fluid dynamic models can be scaled to different flow conditions. Thus, an FL-based integration of both solutions proved to be more accurate than using ANNs and fluid dynamic models separately.

Results

In this section, we present the results obtained from the analysis of the production data gathered during a 10-month extended production test (EPT) on a well of the Val d'Agri field (Italy) carried out between October 1999 and August 2000. The Val d'Agri field is currently being developed in a joint venture between ENI-Agip and Enterprise Oil.** The well considered for this study is located in the northern area of the field and produces oil with the properties shown in **Table 1.**

** Now Shell Italia E&P.

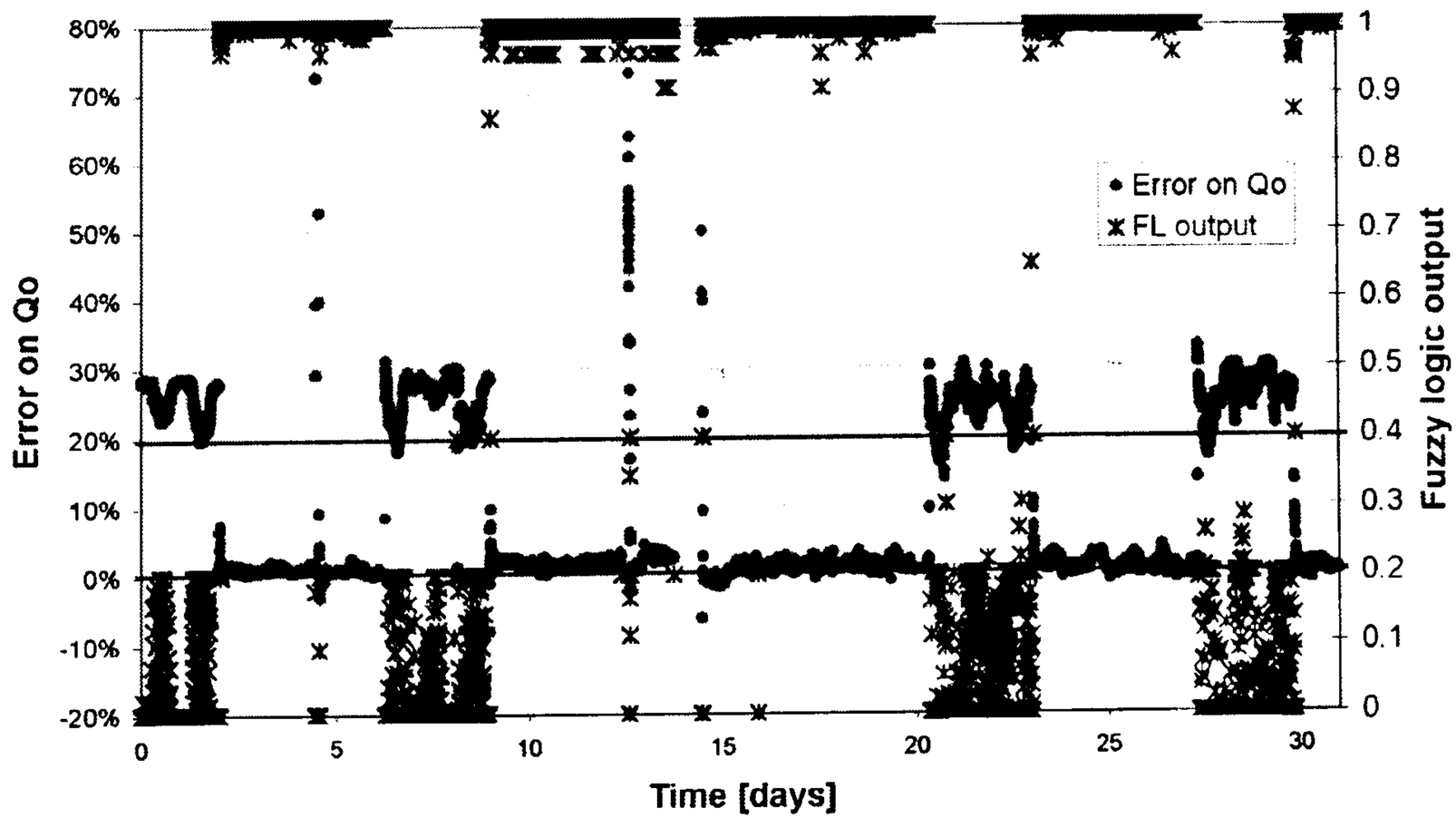


Fig. 7—FL applied to the ANN model—data refer to July 2000.

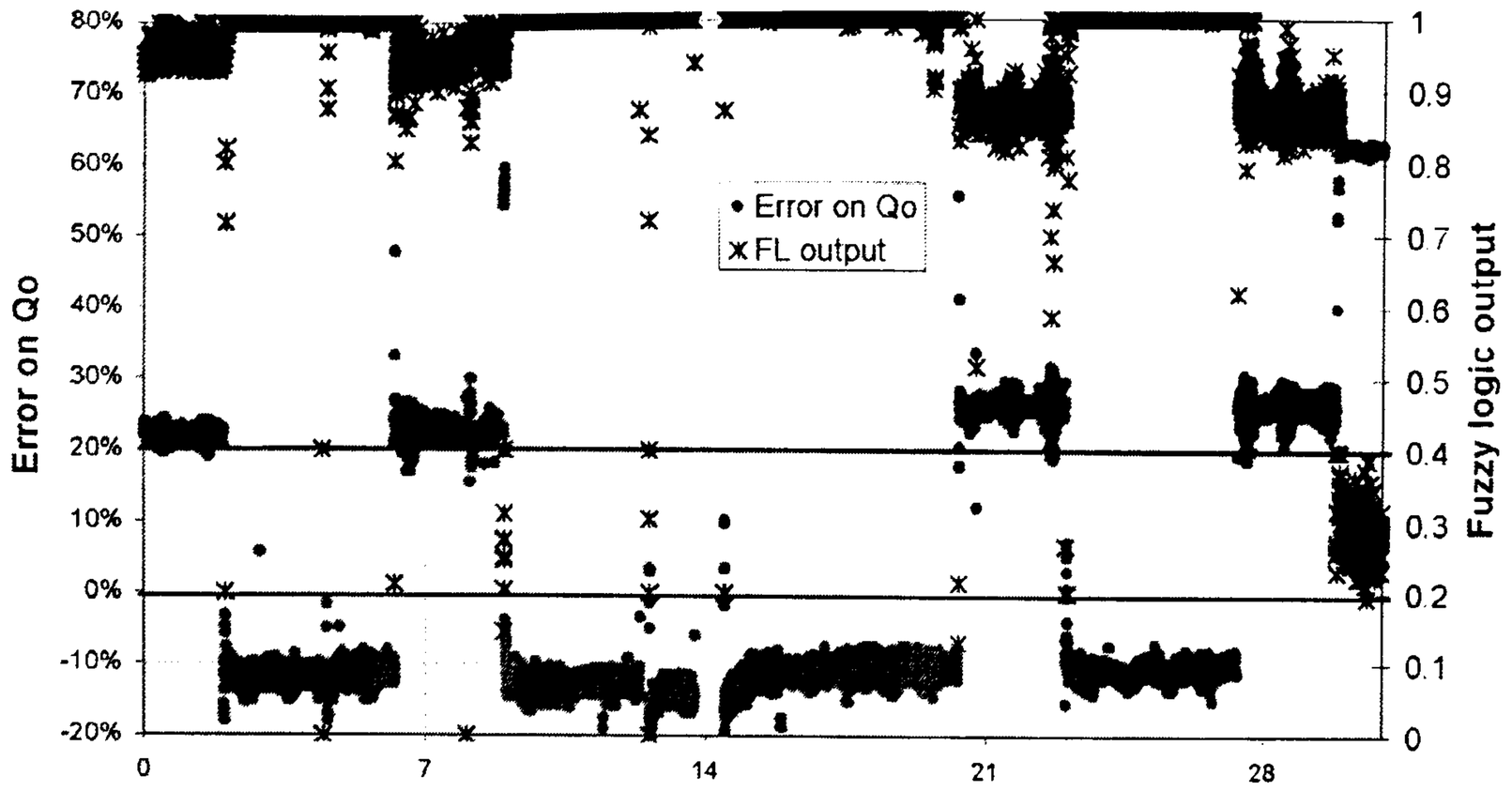


Fig. 8—FL applied to the FDM—data refer to July 2000.

The original aim of the study was to integrate the data measured at the wellhead with the flow rates estimated by a fluid dynamic model (FDM). In particular, an online system based on the existing wellhead choke valve was used together with *ad hoc* measurements of pressure and temperature upstream and downstream of the choke. The results showed that the metering system had achieved the functionality of a multiphase flowmeter. Acceptable oil flow-rate predictions were obtained during the 10-month period, with an average relative error of –3.4% and a standard deviation of 16%. A similar performance was obtained for the gas flow-rate prediction, with an average error of 2.5% and a standard deviation of 19%. A detailed analysis of the results is reported in Alimonti *et al.*[22]

On the basis of those results and previous experience with Venturi meters for the prediction of single and multiphase flow rates,[14] it was decided to try to improve system performance with ANNs. This allowed a critical analysis of data quality as well as process diagnosis. Two approaches were attempted. The first (and more traditional) approach was based on an ANN model that used the same inputs as the FDM to give the flow rates of oil and gas as outputs. The ANN was trained with the data gathered in December 1999 and then used to estimate the flow rates for 9 more months. The results for the oil rates are reported in **Fig. 1,** which shows the mismatch between the measured and predicted oil flow rate. By grouping the errors per month, starting from the data gathered every 5 minutes, an average error of –0.8% and a standard deviation of 13.0% were obtained. It was also possible to observe the effects of opening/closing the well on the model's final response.

The second approach was based on implementing an ANN as a correction algorithm to the FDM. Such an ANN used the flow rates predicted by the FDM as inputs, providing corrected flow rates as outputs. This ANN was trained with the data from February 2000, and the results are presented in **Fig. 2. Table 2** summarizes the relative errors and the standard deviations for the two approaches.

Both ANN approaches lead to a reduced bias and half the standard deviation of the results from the FDM.

For both cases, the higher errors seen for October 1999 and January, July, and August 2000 can be explained as follows. The first 2 months reflected production startups, characterized by high contents of CO_2, and production restarts, characterized by high GORs. The other 2 months reflected the presence of water in the stream, while water production was nil for the data set used to train the ANNs.

Thus, the same kind of information (flow rates, in this case) can originate from different sources (the FDM, the "traditional" ANN model, and the ANN correction model), so that the system becomes redundant. A similar situation occurs when different flowmeters, based on different metering principles, are used at the same time.

On the basis of the previous considerations, a methodology was developed to obtain the most reliable flow-rate values. The idea is to use an FL model to evaluate the performance of different flow-rate-prediction models and adopt a strategic approach from its results. **Fig. 3** shows the flow chart of the data-processing sequence that was followed in this study. Basically, a diagnostic module is obtained by comparing the results of the FL models applied to the FDM and ANN models.

As mentioned previously, FL was adopted to build a model able to perform a quality check on the field data as well as a critical diagnosis of both the production and the online metering systems. To accomplish that, the flow rates measured at the test separator in the field were taken as reference values. The FL model used two inputs (namely, the relative errors in oil and gas flow rate) to give an output parameter ranging between 0 and 1 (0 for low data quality and 1 for high data quality). Besides the output parameter, two more values were selected to represent the need for recalibration of the online metering system (0.4) and a potential change of stream composition (0.2). **Figs. 4 through 6** show the membership functions for this application. **Figs. 7 through 9** show the results of the FL model applied to the ANN and FDM models.

Hence, it remains to define which are the most accurate oil and gas flow-rate values to adopt. The best estimate of flow rates was obtained by a weighted average of the values obtained from the two ANN models, with the weight being the FL output. The results, reported in **Table 3,** are strongly encouraging because they show a strong reduction in the standard deviation (less than 3% for both the oil and gas flow rate).

Conclusions

From the results presented previously, it appears that ANNs and FL can be combined with MFM to provide not only a real-time monitoring of produced flow rates and stream composition but also a valid quality check of this same information.

Field and predicted data can be checked against each other so that it becomes possible, by applying AI techniques, to distinguish between changes in the actual flow conditions of the production system and recalibration issues related to the metering devices.

It also appears that many more combinations of AI techniques and field data can be achieved to perform well diagnosis and monitoring. From a preliminary analysis of the data, the authors believe that the same procedure can be applied, with the well productivity index input in place of the oil rate.

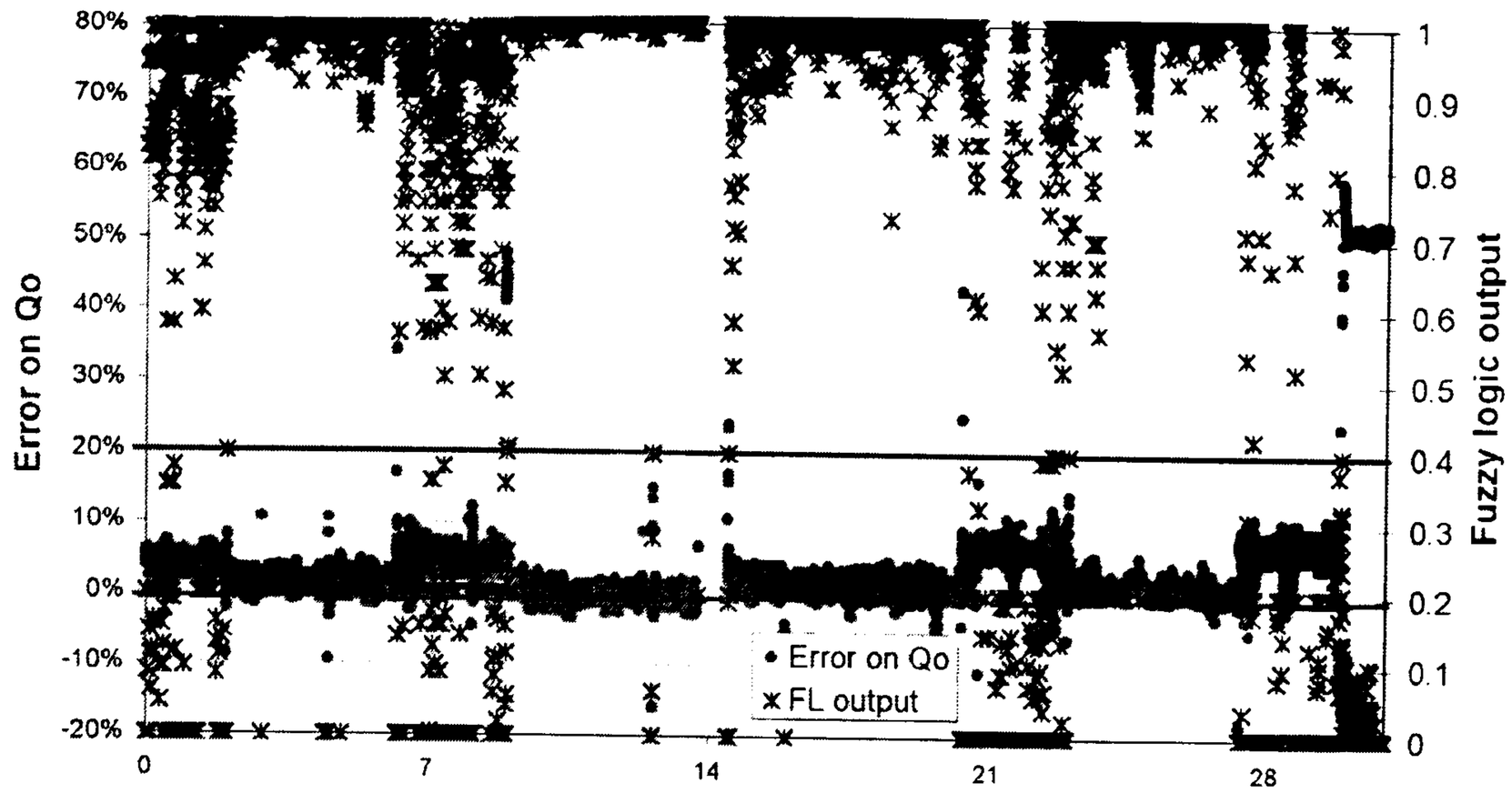


Fig. 9—FL applied to the ANN correction model data refer to July 2000.

To date, no solution has been delivered that integrates all the previously described AI methodologies with regard to integrated production systems as a whole, from reservoir to surface. This may be because expertise in both petroleum engineering and computational techniques is needed to appropriately use AI in the petroleum industry. The dynamic behaviors of oil and gas developments have their own physical characteristics, and the ANNs and FL models must be tailored to such applications. Also, each AI method handles uncertainty differently, and the sequence of steps to be followed when applying AI solutions is not unique. However, these are exactly why an integration of KDD and AI can be expected to be extremely flexible and improve computational speed and imprecision tolerance.

Nomenclature

k = text
Q = oil flow rate

Subscripts

o = oil phase

References

1. Xu, Z.G. and Shea, D.: "Important tips for setting up simulation models for multiphase flow in pipelines," paper presented at the 2001 10th Intl. Conference Multiphase, BHR Group, Cannes, France, 13–15 June.
2. Schiozer, D.J. and Aziz, K.: "Effect of Chokes on Simultaneous Simulation of Reservoir and Surface Facilities," paper SPE 26308 available from SPE, Richardson, Texas (1993).
3. Schiozer, D.J. and Aziz, K.: "Use of Domain Decomposition for Simultaneous Simulation of Reservoir and Surface Facilities," paper SPE 87876 presented at the 1994 SPE Western Regional Meeting, Long Beach, California, 23–25 March.
4. Lopez, D. and Duchet-Suchaux, P.: "Performances of Transient Two-Phase Flow Models," paper SPE 39858 presented at the 1998 SPE International Petroleum Conference and Exhibition of Mexico, Villahermosa, Mexico, 3–5 March.
5. Hunt, A.P. *et al.*: "Real time modelling of multiphase flow systems," paper presented at the 2001 10th Intl. Conference Multiphase, BHR Group, Cannes, France, 13–15 June.
6. Guaita, P.: "Development of a New Fiber-Optic Based Offshore Structural Monitoring System," paper SPE 56435 presented at the 1999 SPE Annual Technical Conference and Exhibition, Houston, 3–6 October.
7. Boe, H.S., Nordtvedt, J.-E., and Schmidt, H.S.: "Integrated Reservoir and Production Management: Solutions and Field Examples," paper SPE 65151 presented at the 2000 SPE European Petroleum Conference, Paris, 24–25 October.
8. Falcone, G. *et al.*: "Multiphase Flow Metering: Current Trends and Future Developments," paper SPE 71474 presented at the 2001 SPE Annual Technical Conference and Exhibition, New Orleans, 30 September–3 October.
9. Han, J. and Kamber, M.: *Data Mining—Concepts and Techniques,* Morgan Kaufmann (2001) ISBN 1-55860-489-8.
10. Hastie, T., Tibshirani, R., and Friedman, J.: *The Elements of Statistical Learning—Data Mining, Inference, and Prediction,* Springer (2001).
11. Zadeh, L.: "Fuzzy Sets," Information and Control 8:338-353 (1965).
12. Ross, T.J.: *Fuzzy Logic with Engineering Applications,* McGraw-Hill Inc. (1995).
13. Ali, J.K.: "Neural Networks: A New Tool for the Petroleum Industry?," paper SPE 27561 presented at the 1994 SPE European Petroleum Computer Conference, Aberdeen, 15–17 March.
14. Alimonti, C. and Bilardo, U.: "Measurement of three-phase flow rates using neural network approach," paper presented at the 2001 4th Intl. Conference on Multiphase Flow, New Orleans, 27 May–1 June.
15. Toral, H. *et al.*: "Esmer Field Tests Multiphase Flow Meter," paper presented at the North Sea Flow Measurement Workshop (1998).
16. Fang, J.H. and Chen, H.C.: "Fuzzy Modelling and the Prediction of Porosity and Permeability from the Compositional and Textural Attributes of Sandstone," *J. of Petroleum Geology* (1997) **20,** No. 2, 185.
17. Rogers, S.J. *et al.*: "Predicting Permeability from Porosity Using Artificial Neural Networks," The American Assoc. of Petroleum Geologists (July 1995)

TABLE 3—SUMMARY OF AVERAGE RELATIVE ERROR AND STANDARD DEVIATION FOR THE MERGING ALGORITHM

	Oil		Gas	
	Error (%)	Standard Deviation (%)	Error (%)	Standard Deviation (%)
Merging algorithm	0.9	2.6	–1.5	2.9

18. Murray, A. *et al.:* "The Applications of Advanced Computing Techniques to Oil and Gas Facility Optimisation," paper SPE 56904 presented at the 1999 SPE Offshore Europe Conference, Aberdeen, 7–9 September.
19. Jansen, B. *et al.:* "Automatic Control of Unstable Gas Lifted Wells," paper SPE 56832 presented at the 1999 SPE Annual Technical Conference and Exhibition, Houston, 3–6 October.
20. Vázquez, M. *et al.:* "Global Optimisation of Oil Production Systems, A Unified Operational View," paper SPE 71561 presented at the 2001 SPE Annual Technical Conference and Exhibition, New Orleans, 30 September–3 October.
21. Annunziato, M. *et al.:* "High Accuracy and Data Fusion in the on-line Measurement of Multiphase Flowrate." paper presented at the 2000 7th Intl. Conference of Multiphase Flow in Industrial Plants, Bologna, Italy, 14–16 September.
22. Alimonti, C., Basso, A., and Pelliccia, A.: "Is it really possible to use a choke valve as multiphase flowmeter? The CVAF from laboratory to the field," paper presented at the 2001 10th Intl. Conference Multiphase, BHR Group, Cannes, France, 13–15 June.

SI Metric Conversion Factors

bbl × 1.589 873	E–01	= m^3
ft^3 × 2.831 685	E–02	= m^3
°API 141.5/(131.5+°API)		= g/cm^3

Claudio Alimonti is an Assistant Professor with the U. of Rome "La Sapienza." e-mail: claudio.alimonti@uniroma1.it. His research interests include multiphase flow modelling and metering. Alimonti holds a first-class degree in mining engineering from the U. of Rome "La Sapienza" and a Ph.D. degree in mechanical engineering from the U. Catholique de Louvain, Belgium. **Gioia Falcone** is currently a Research Reservoir Engineer with Total E&P UK in London. e-mail: gioia.falcone@total.com. She was previously employed as a petroleum engineer with Enterprise Oil UK plc, Aberdeen. Falcone holds a first-class degree in petroleum engineering from the U. of Rome "La Sapienza" and an MSc degree in petroleum engineering from Imperial College, London.

Society of Petroleum Engineers

SPE 84504

ANUMET: A Novel Wet Gas Flowmeter

G.Falcone, SPE, TOTAL E&P UK plc, Imperial College; G.F.Hewitt, L.Lao, S.M.Richardson, Imperial College

Copyright 2003, Society of Petroleum Engineers Inc.

This paper was prepared for presentation at the SPE Annual Technical Conference and Exhibition held in Denver, Colorado, U.S.A., 5 – 8 October 2003.

This paper was selected for presentation by an SPE Program Committee following review of information contained in an abstract submitted by the author(s). Contents of the paper, as presented, have not been reviewed by the Society of Petroleum Engineers and are subject to correction by the author(s). The material, as presented, does not necessarily reflect any position of the Society of Petroleum Engineers, its officers, or members. Papers presented at SPE meetings are subject to publication review by Editorial Committees of the Society of Petroleum Engineers. Electronic reproduction, distribution, or storage of any part of this paper for commercial purposes without the written consent of the Society of Petroleum Engineers is prohibited. Permission to reproduce in print is restricted to an abstract of not more than 300 words; illustrations may not be copied. The abstract must contain conspicuous acknowledgment of where and by whom the paper was presented. Write Librarian, SPE, P.O. Box 833836, Richardson, TX 75083-3836, U.S.A., fax 01-972-952-9435.

Abstract

Wet gas metering is rapidly establishing itself as a special problem area within the more general area of multiphase flow metering. In fact, while attempts are being made across the Oil and Gas Industry to define the boundaries between humid gas, gas-condensate and high GVF (gas volume fraction) multiphase systems, a few commercial wet gas meters are already available for specific field applications.

A major interest of Imperial College has been the development of metering schemes for three-phase (oil-gas-water) flows in oil-field production systems. Imperial College has already developed a flow meter (MIXMETER)[1], which performs satisfactorily in the range of gas volume fractions of 0 to 90%. Imperial College has therefore been recently developing a new concept (ANUMET), which shows some promise for measuring two-phase flows at much higher gas volume fractions.

The technical description of the ANUMET wet gas meter is outlined in this paper. Preliminary experiments on this new metering concept have been carried out with air-water flows in a 32 mm diameter tube in the LOTUS (LongTUbeSystem) facility at Imperial College. Encouraging results have been obtained and they are presented here.

Introduction

The total world gas production has increased from 200.4 bcf/d in 1991 to 241.9 bcf/d in 2001 and the total world gas consumption has increased from 194.1 bcf/d to 232.4 bcf/d during the same period of time[2]. For the Gulf of Mexico, it is expected that deepwater gas production will peak at around 5.3 bcf/d in 2004[3]. Compared with oil fields, gas fields tend to be more environment-friendly because of lower carbon dioxide emissions and a cleaner combustion. However, the production of gas is, in most cases, associated with the production of liquid hydrocarbons (that form in the reservoir, in the wellbore and at surface as pressure and temperature drop), free formation water and condensed vapour. This is why, from a metering point of view, the techniques normally implemented for dry gas metering cannot be always applied.

Now that operators have become aware of the potential benefits in using multiphase flow meters for metering the produced streams of oil fields, in terms of cost savings, production optimization, field monitoring and reservoir management[4,5,6], it is almost straightforward to extend the same considerations to wet gas and gas condensate fields. However, before generalising the problem of multiphase flow metering and deciding which techniques can be applied for the case of wet gas metering, it is necessary to first define "wet gas".

Definition of wet gas and wet gas metering issues. To date, several definitions of wet gas have been proposed within the Oil and Gas industry, all of them equally important in covering the full range of possible stream compositions, operating pressures and temperatures, and flow regimes. Wet gas metering, in fact, may apply to gas condensate fields, high GOR fields and wet gases. Accordingly to the definition given in the SPE monograph volume 20[7] and as illustrated in **Fig.1**, a reservoir fluid is classified as dry gas when the reservoir temperature is greater than the cricondertherm and surface/transport conditions are outside the two-phase envelope; as wet gas when the reservoir temperature is greater than the cricondertherm but the surface conditions are in the two-phase region; as gas condensate when the reservoir temperature is less than the cricondertherm and greater than the critical temperature; and as an oil (volatile or black oil) when the reservoir temperature is less than the mixture critical temperature

A general definition of wet gas is that of a stream with liquid volume fractions between 5 and 10% at metering conditions[8]. Following this definition, wet gas metering can be seen as the top boundary of multiphase flow metering (oils with high gas volume fractions) and the bottom boundary of gas metering (gases with high liquid volume fractions). This implies that by pushing either multiphase flow metering or gas metering to their extremes, wet gas metering solutions could, in theory, be found. However, due to the complexity and peculiarity of wet gas flows, wet gas metering may necessitate a dedicated effort.

The occurrence of slip between the liquid and the gas, the difficulties in predicting the transition between flow regimes in horizontal as well as in vertical currents, and the uncertainties related to the PVT characterization of gas condensate fields are among the problems still associated with

wet gas metering. In addition to the above, the liquid phase of wet gas streams may be a combination of hydrocarbons and water, in which case wet gas metering becomes a problem in three-phases and the oil/water inversion point may have a big impact on the multiphase flow correlations used to calculate pressure drops and boundaries between flow regimes. Finally, solids may also be present in the stream, so that the problem of wet gas metering extends to four phases.

The importance of working in mass fractions rather than volume fractions when characterising wet gas fields has been highlighted in the literature[9,10]. The operator may be interested in metering wet gas streams for a variety of reasons: thus, the main focus may be economics and/or reservoir management, on allocation issues, on metering the produced gas only or on metering both the liquid and the gas. Depending on the specic requirement (or requirements), different metering accuracies may be required and thus different wet gas metering solutions sought. For this reason, multiphase mass fraction triangles have been produced for different fluids densities, showing the possible percentages of gas, oil and water in a wet gas stream[9]. Also, in order to account for the joint effects of flow regime, operating pressure and temperature, and liquid content of the gas, a revised classification for wet gas, based on the Lochart-Martinelli parameter, has been recently presented[11].

From the above brief description of wet gas, it is possible to infer that a unique metering solution for all gas condensate, high GOR and wet gas fields, based on the technologies available to date and able to satisfy every requirement in the wish list of operators, may not exist. Some wet gas meters have already been developed and made commercially available, but the majority of them are still under a testing and validation phase, both in flow loops and in the field.

The ANUMET system

The ANUMET system was conceived as a follow up from previous works on multiphase flow metering carried out at Imperial College. In particular, several Ph.D. thesis and one DIC thesis[12,13,14,15,16] had already been written on the validation of various methods and instruments for the measurement of key parameters in vertical upward gas-liquid flow. The development of the ANUMET system is still ongoing and is being sponsored by the Oil and Gas industry under a part-time Ph.D. project.

Briefly, the concept behind the ANUMET meter is that of deducing the liquid flow rate from measurements on annular flow in a straight pipe section and then using this liquid flow rate in the interpretation of of pressure drop data from a venturi placed downstream of the straight pipe section in order to deduce the gas flow rate.

Technical description. The measurements are made in vertical upwards flow and are specifically for annular flow, the dominant regime involved. In sequence, the steps are as follows:

1. The annular flow flows up a tube and through a twisted tape device (with "fish tails" at its upper end) as shown in **Fig. 2**.
2. Downstream of the twisted tape device, nearly all the liquid phase has been separated into the annular film on the tube wall. It continues to flow as an annular film in a straight pipe section downstream of the swirl device. Of course, re-entrainment of the droplets will occur but this process is relatively slow[16] and there is an opportunity of making measurements in this region immediately downstream of the swirler in order to determine the liquid flow rate in the film and hence the total liquid flow rate if all the liquid has been separated. The liquid flow rate is determined by measuring the liquid film thickness (δ) and the pressure gradient (dp/dz) along the straight pipe section. The pressure gradient can be measured using standard transducer systems (taking care to avoid problems of ambiguity of the line fluid) and the film thickness can be measured by a variety of techniques. In the validation tests at Imperial College, gamma densitometry and conductance probes were used to measure the film thickness, but viable alternatives might be ultrasonics or fluorescence, depending on the system. The liquid film flow rate M_{LF} is obtained from the "triangular relationship" which has the form[17,18,19]:

$$[1] \quad \dot{M}_{LF} = fn[\delta, (dp/dz)]$$

Basically, in this relationship, the interfacial shear stress and wall shear stress (often approximately equal) are calculated from the pressure gradient and the local shear stress τ (often approximately constant in the liquid film) is related to the gradient of liquid velocity in the film (du_L/dy) by the expression:

$$[2] \quad \tau = \mu_{eff}\left(\frac{du_L}{dy}\right)$$

where μ_{eff} is the effective viscosity calculated from a suitable turbulence model. Equation [2] is integrated to give the velocity profile in the film, which, in turn, is integrated to give the total liquid flow rate. Early experiments at Harwell[20], in which all three quantities ($\dot{M}_{LF}$, δ and (dp/dz)) were measured, showed that the triangular relationship fitted the data remarkably well. Thus, the film flow rate can be determined from measurements of film thickness and pressure gradient. The comparisons obtained by Gill et al.[20] are shown in **Fig. 3**, expressed in terms of a non-dimensional film flow rate W+, which is defined as follows:

$$[3] \quad W^+ = \frac{\dot{M}_{LF}}{\pi D \eta_L}$$

where D is the tube diameter and η_L the liquid viscosity. An assumption of the method is that ($\dot{M}_{LF} \approx \dot{M}_L$). Measurements by Hills et al.[21] indicated very efficient removal of the droplets by the device shown in **Fig. 2**, with less than 5% of the liquid remaining as droplets after the device. Measurements at Imperial College[16] confirmed that good separation was possible under some circumstances,

though the separation was less favourable at higher gas velocities as illustrated in **Fig. 4**. The development of improved separation devices could be an area for further development. Nevertheless, there are significant regions in which the separation is better than 90%.

3. Following the straight pipe section in which the film thickness and pressure gradient are measured, (leading to an evaluation of $\dot{M}_L$), the next step is to re-entrain all of the droplets into the gas stream before passing this stream into a venturi (step 4.). The objective is to homogenise the gas and the liquid. Experiments carried out during the development of the MIXMETER flow meter, with parallel development of the mixing devices, led to a device which gave satisfactory homogenisation of the flow over a gas volume flow fraction range of 0-90%. For higher gas fractions, it is not possible to maintain such mixing and a large fraction of the liquid phase flows on the surface of the mixer and on the channel wall downstream of the mixer. This fact was demonstrated in experiments carried out at Imperial College in 1997[14], which indicated that, with the MIXMETER mixer, the in-situ liquid fraction downstream of the mixer was very much larger than the purely mixed value for liquid volume fractions less than around 5-10%. This led to a search for mixing devices, which can more satisfactorily homogenise the flow in this low liquid fraction, high gas fraction region. This work was continued in 2000[16]. A wide range of homogenising devices was studied and it was found that the device that gave the best atomisation of the liquid was a simple expansion contraction system as shown in **Fig. 5**. Measurements of liquid film flow rates downstream of this device indicated a large increase in the fraction entrained compared to measurements in the absence of the device as illustrated in **Fig. 6**. Although the device does not give complete entrainment, it certainly increases the entrained fraction to over 70% over a wide range of gas velocities as seen.

4. The final stage is to pass the homogenised flow through a venturi. The most widely used relationships for two-phase pressure drop calculations in Venturi meters are perhaps those of Chisolm[8], which relate the two-phase pressure drop Δp to the pressure drops Δp_L or Δp_G for the liquid and gas phase respectively flowing alone through the device. These relationships can be written as:

$$[4] \quad \frac{\Delta p}{\Delta p_L} = 1 + \frac{C}{X} + \frac{1}{X^2}, \qquad \frac{\Delta p}{\Delta p_G} = 1 + CX + X^2$$

where X is the Lockhart-Martinelli parameter defined as follows:

$$[5] \quad X = \sqrt{\frac{\Delta p_L}{\Delta p_G}}$$

A widely -used trelationship for C is as follows:

$$[6] \quad C = \left(\frac{\rho_L}{\rho_G}\right)^n + \left(\frac{\rho_G}{\rho_L}\right)^n$$

where ρ_L and ρ_G are the liquid and gas densities. For a homogeneios flow, the exponent n is ½.

The pressure drops Δp_L or Δp_G for the liquid and gas flowing alone through the venturi are given by:

$$[7] \quad \Delta p_L = -k\frac{\dot{m}_L^2}{2\rho_L}, \qquad \Delta p_G = -k\frac{\dot{m}_G^2}{2\rho_G}$$

where m_L and m_G are the liquid and the gas mass fluxes respectively.

The venturi loss coefficient k is given by:

$$[8] \quad k = \frac{1-\left(\frac{D_2}{D_1}\right)^4}{C_D{}^2\left(\frac{D_2}{D_1}\right)^4}$$

where C_D is the discharge coefficient (usually taken as 0.984 for a venturi with flow at high Reynolds numbers) and D_2 and D_1 are the throat diameter and the upstream diameter respectively.

Combining equations [5] and [7] leads to the following expression for the Lockhart-Martinelli parameter:

$$[9] \quad X = \frac{\dot{m}_L}{\dot{m}_G}\left(\frac{\rho_G}{\rho_L}\right)^{\frac{1}{2}}$$

Combining the above equations leads to a quadratic expression for the gas flow rate as follows:

$$[10] \quad a\dot{m}_G^2 + b\dot{m}_G + c = 0$$

where:

$$a = 1$$

$$[11]\quad b = C\dot{m}_L\sqrt{\frac{\rho_G}{\rho_L}}$$

$$c = \left(1 + \frac{2\rho_L \Delta p}{k\dot{m}_L^2}\right)\frac{\rho_G}{\rho_L}\dot{m}_L^2$$

Of course, Eq. [10] is a quadratic equation, which has two solutions for M_G. However, one of the solutions is usually negative and therefore unphysical.

For n=0.5, the above Chisolm equation for homogeneous flow gives the same results as the general equation for a homogeneous two-phase gas-liquid flow written as follows:

$$[12]\quad \Delta p = -k\frac{(\dot{m}_L + \dot{m}_G)^2}{2\rho_H}$$

where ρ_H is the mixture density given by, in terms of quality x:

$$[13]\quad \rho_H = \frac{\rho_L\rho_G}{(1-x)\rho_G + x\rho_L}$$

Pinheiro da Silva Filho[16] studied the performance of the expansion/contraction device placed upstream of a venturi and his results are illustrated in **Fig. 7** where the ratio of the measured pressure drop to that calculated from the homogeneous theory is shown as a function of mass flow quality (fraction by mass of the gas phase in the total flow) for a constant total mass flow. As will be seen, this form of homogenisation device does, indeed, lead to a much closer agreement with the homogeneous model than that obtained in the absence of the device ("No inserts").

Experimental equipment and test procedure

The LOTUS rig. The experiments described in this paper were carried out in the LOTUS (LongTUbeSystem) facility at Imperial College. A simplified diagram of the rig is shown in **Fig. 8**. LOTUS is a vertical two-phase air-water system that was originally built at the Harwell Laboratory of the UKAEA in the early nineteen-sixties. It was relocated to the pilot plant area of the Chemical Engineering Department of Imperial College in 1992. It consists of a long vertical, 31.8mm (1.25 inch) copper tube, originally of around 19m active length at Harwell but now with a shorter active length of 10.8m. The vertical tube is mounted over three floors of the pilot plant and the test spool for the ANUMET was arranged almost entirely on the top floor (test section). The tube is attached to a vertical fixed beam, carefully aligned to guarantee the vertical alignment and straightness of the tube. Air from the college supply (operating at a pressure of up to 6 bar) is passed through orifice plates in order to meter the air flow rate by means of differential pressure transducers. The air is then fed into the system at the bottom of the tube via a U-bend. Water from a tank can be pumped through the system by either a 1.5kW or an 8 kW pump. It is then metered via rotameters located on the top floor and fed into the tube at either 0.9 m or 5.4 m above the air U-bend. For these experiments, both feed points were used at the same time, as it was noted that such configuration drastically reduces the pressure drop between the rotameter outlet and the bottom of the text section, compared with the cases when only one of the two feed points is used[22].

The flow envelope for the LOTUS rig is shown in **Fig. 9**.

The experimental set up. A picture of the test section as built on the third floor of the LOTUS rig is showed in **Fig. 10**.

Calculation of the liquid mass flux. The location for the liquid-film thickness measurements was chosen on the basis of the results previously obtained by Pinheiro da Silva Filho[16] and summarized in **Fig. 4**. Although the point of minimum entrained fraction (i.e. the point that corresponds to the peak of the film thickness) increases with increasing air flow rate and decreases with increasing water flow rate, an optimal location was considered to be that at approximately ten diamers downstream the outlet of the swirler.

For the majority of the experiments described here, the film thickness was measured using a 45milliCurie Americium 241 gamma source with a scintillation crystal detection system linked via an amplifier to a computer counting system reading the radiation count at frequencies set by the user. The 59.5 keV energy window was chosen for these experiments. The film thickness was calculated as follows:

$$[14]\quad \delta = \frac{D}{2}\frac{\ln\frac{I}{I_a}}{\ln\frac{I_w}{I_a}}$$

where D is the internal diameter of the pipe, I_a and I_w are the intensities of the transmitted photons when the pipe is filled with air and water respectively, and I is the intensity of the transmitted photons with the two-phase air-water stream flowing in the pipe. It must be noted that the ratio between the calibration values of air and water is very important because it affects the ability of the photons to 'see' the difference between a pipe full of air and a pipe full of water[23]. This ratio can be written as:

$$[15]\quad \frac{I_a}{I_w} = e^{(\gamma_w - \gamma_a)D}$$

where γ_w and γ_a are the attenuation coefficients of water and air respectively. For the 59.5 keV energy and for the water and air densities encountered during the experiments presented here, the ratio between the calibration values of air and water was about 1.9.

Two sets of experiments were carried out with conductance probes in place of the gamma densitometry system. The geometry of the probes used for these experiments and the calibration procedure carried out with the Americium 241 source are described by Lao[24]. As a result of the calibration,

the liquid-film thickness was expressed as a function of the normalized output voltage, V^*, given by:

$$[16] \qquad V^* = \frac{(V - V_0)}{(V_s - V_0)},$$

where V is the output voltage measured during the two-phase experiments, V_s is the output voltage when the pipe is filled with water and V_0 is the output voltage when the pipe is filled with air.

The pressure drop to be used, together with the liquid-film thickness, in the triangular relationship described in Eq. [1] was measured over a straight length of approximately 80 cm, from the oulet of the swirler to the inlet of the expansion contraction device.

Calculation of the gas mass flux. A Venturi meter, 20 cm long and with a β-ratio of 0.493, was placed immediately downstream of the expansion contraction section. A differential pressure transducer was used to measure the pressure drop between the inlet and the throath of the Venturi, while two absolute pressure transducers were used to measure the inlet and outlet pressure. The inlet and outlet temperatures were also recorded. The inlet pressure and inlet temperature were used to calculate the inlet fluid properties, while the outlet pressure was measured to allow the investigation of the relationship between the total pressure loss across the Venturi and the liquid fraction (this has not been done under this present work).

Test matrix. The water mass flux was varied between 103 and 770 kg/m2 s, and for each water mass flux the air mass flux was varied between approximately 30 and 200 kg/m2 s. This corresponded to gas volume fractions between 96 and 99.7% (calculated with the assumption of homogeneous flow).
A check was made to confirm that the flow was in annular regime and not in churn regime (flow reversal of the falling film). The annular regime is likely to exist if[25]:

$$[17] \qquad U_G^* = U_G \sqrt{\frac{\rho_G}{gD(\rho_L - \rho_G)}} \succ 1$$

where U_G is the gas superficial velocity. All of the current tests lay in the region $U_G^* > 1$.

At very low liquid film flow rate ($\dot{m}_{LF}$), liquid entrainment does not occur. Of course, there would be no need to use a swirl device to move liquid back into the film in this case. The value of film flow rate ($\dot{m}_{LFC}$) at which entrainment starts is given by: [26]:

$$\dot{m}_{LF} \le \dot{m}_{LFC} \longrightarrow E = 0$$

$$[18] \qquad \dot{m}_{LFC} = \frac{\eta_L}{D} \exp(5.8504 + 0.4249 \frac{\eta_G}{\eta_L} \sqrt{\frac{\rho_L}{\rho_G}})$$

where η_L and η_G are the liquid and gas viscosities and E stands for entrainment. For all of the tests reported here, the flows were such that significant entrainment would be expected.

Results

The results presented here were obtained from six experimental campaigns, carried out under a part-time PhD study still ongoing. However, a reasonable number of experimental points were collected and a critical review of the results is presented below, in an attempt to differentiate between the effects due to the instrumentation available in the LOTUS rig, the effects due to the main assumptions behind the ANUMET concept and also the intrinsic difficulties associated with wet gas metering.

Liquid mass flux. The liquid mass fluxes calculated from the film thickness and pressure gradient in the straight pipe section are compared with the rig input values in **Fig. 11**. Though the results are qualitatively encouraging, it has to be recognised that the accuracy in liquid flow estimation is significantly worse than the $\pm 20\%$ expected from the early results[20] on the triangular relationship illustrated in **Fig. 3**.

The reasons for these higher errors may lie in both measurement uncertainties and in physical phenomena which are not accounted for in transforming the results for straight tube pressure gradient and film thickness into an estimate of film flowrate. A sensitivity analysis of the equations implemented for the calculation of the liquid mass flux was performed in order to quantify the effects of potential measurement errors on the final liquid mass flux prediction. It was found that the errors in film film thickness and pressure gradient would be reflected approximately proportionately in errors in the calculated film liquid flow rate.

Measurement of pressure gradient is a well-established procedure in multiphase flow research (though good practice is still necessary) and the errors from this source are likely to be small (less that a few percent, say). However, physical effects such as acceleration pressure losses occurring due to the re-entrainment of the film liquid and residual effects of the swirl may occur and need to be further quantified. However, the largest source of error is likely to be in the measurement of film thickness.

The principal problem in using gamma densitometry to measure film thickness is that the result depends on accurately determining the small difference between count rates in the absence and presence respectively of the film. The errors are of two types, namely *statistical* and *systematic*. The statistical relative error in film thickness is given by:

$$[19] \qquad \frac{d\delta}{\delta} = \frac{1}{\ln(N/N_A)} \frac{dN}{N} - \frac{1}{\ln(N_L/N_A)} \frac{dN_L}{N_L} + \frac{\ln(N/N_L)}{\ln(N_L/N_A)\ln(N/N_A)} \frac{dN_A}{N_A}$$

where: δ is the film thickness; N the number of counts during the counting period t ,N_A the number of counts during counting counting period t with the pipe full of air, N_L the number of counts during counting counting period t with the pipe full of water and D the inner diameter of the pipe.

By using a long counting period, the statistical errors calculated from Eq.[19] could be reduced to a few percent. However, a more serious source of error was the systematic

effects of drift in the basic count rate due to time variations in the electronics and investigations revealed that these errors could be the cause of the errors revealed in **Fig. 11**. This is clearly an area in which further development is required. Improvemnets in the stability of the electronics, in calibration and in optimisation of the choice of radioactive source would be expected to yield the required precision. Thus, there is no reason to believe that adequate accuracy could not be achieved in a developed system.

Gas mass flux. Gas mass fluxes were calculated from the input liquid flow rate and the measured upsteam-to-throat pressure drop in the venturi using the methodology described above. The results were corrected for compressibility effects using the standard compressibility factor given by EN ISO 5167-1:1995. These calculated values are compared with the input values in **Fig. 12**. Consistent with the earlier results shown in Figure 7, the agreement between measured values is rather encouraging.

Conclusions

The metering concept presented in this framework introduces a novel approach to wet gas metering. In fact, although the individual devices used in ANUMET and the basic equations applied for annular flow and for homogeneous flow have been known to the Oil & Gas community for some decades now, the novelty lies in the way they have been combined towards a wet gas metering solution.

The limitations of the ANUMET concept, at its present stage of development, have been identified. They mainly relate to the instrumentation chosen for the measurements and in particular to the method used for film thickness measurement, namely gamma densitometry. Nevertheless, encouraging results have been obtained which lead to the conclusion that the system has good potential for development leading to an adequate solution to this difficult measurement problem.

References

1. G.F.Hewitt, P.S.Harrison, S.J.Parry, "The MIXMETER flowmeter – another step towards routine multiphase flow measurement?", paper presented at the BHR Group Multiphase 1997 conference.
2. *BP Review of World Energy 2002*, downloaded from the bp website.
3. "Pipelines under pressure", Petroleum Review (May 2003), 14
4. A.M.Scheers, B.R.Noordhuis, "Business Impact of Multi-phase and Wet Gas Flow Measurement", paper presented at the IBC's 5th Annual Multi-phase Metering conference held in Aberdeen, 22-23 February 1999.
5. L.Scheers, C.Wolff, "Production Measurement Management", paper presented at the 20th North Sea Flow Measurement Workshop, 22-25 October 2002.
6. G.Falcone, G.F.Hewitt, C.Alimonti, B.Harrison, "Multiphase Flow Metering: Current Trends and Future Developments", paper SPE 71474 presented at the 2001 SPE Annual Technical Conference and Exhibition held in New Orleans, Louisiana, 30 September-3 October 2001.
7. C.H.Whitson, M.R.Brule': *Phase Behaviour*, SPE monograph **Vol. 20**, (2000), 13.
8. Department of Trade and Industry (Oil and Gas Division): *Guidance Notes for Petroleum Measurement Under the Petroleum (Production) Regulations*, issue 6, March 2002
9. J.Couput, P.Gajan, V. de Laharpe, A.Strzelecki, "Wet Gas Metering in the Upstream Area: Needs, Applications & Developments", paper presented at the 18th North Sea Flow Measurement Workshop 2000
10. A.W.Jamieson, "Wet Gas Metering – The Unexpected Challenge Status and Trends on Technology and Applications", paper presented at the 19th North Sea Flow Measurement Workshop 2001
11. P.Mehdizadeh, J.Marrelli, "Wet Gas Metering: Trends in Applications and Technical Developments", paper SPE 77351 presented at the 2002 SPE Annual Technical Conference and Exhibition held in San Antonio, Texas, 29 September-2 October 2002.
12. A.Wolf: *Film structure of vertical annular flow*, PhD Thesis, Imperial College, 1995.
13. N.Hawkes: *Wispy-annular flow*, Ph. D Thesis, Imperial College, 1996.
14. R.T.H.Machado: *Mulitphase Flow in Venturi: An Experimental and Theoretical Study*, PhD Thesis, Imperial College, 1997.
15. M.J.Watson: *Flow regime transitions and associated phenomena*, Ph. D Thesis, Imperial College, 1999.
16. J.A.Pinheiro da Silva Filho: *Multiphase Flow Metering with High Gas Content Using Successive Venturi Devices*, DIC Thesis, Imperial College, August 2000.
17. G.F.Hewitt: *Analysis of Annular Two Phase Flow*, UKAEA Report AERE-R3680
18. G.F.Hewitt, N.S.Hall-Taylor: *Annular Two-Phase Flow*, Pergamon Press, (1970).
19. G.F.Hewitt: *Prediction of Pressure Drop in Annular Flow by Phenomenological Modelling*, Section 2.2.4 of *Handbook of Multiphase Flow System*, ed. G.Hetsroni, Hemisphere Publishing Corporation (1982)
20. L.E.Gill, G.F.Hewitt, P.M.C.Lacey: *Sampling probe studies of the gas core in annular two-phase flow: II, Studies of the effect of phase flowrates on phase and velocity distribution*, Chem. Eng. Sci., **19**, (1964), 665-682
21. J.H.Hills, B.J.Azzopardi, A.S.Barhey: *Spatial Unsteadainess, A Way Towards Intensive Gas-Liquid Reactors*, Trans IchemE, **vol. 74**, Part A, July 1996
22. L.Lao, C.J.Lawrence, G.F.Hewitt: *Flow Rate Measurement Methods in the LOTUS rig*, internal status report, Imperial College, July 2002
23. I.C.Mareuge: *Analysis and Development of Multi-Energy Gamma Densitometry Systems*, internal report, TMF project, Imperial College, December 2000
24. L.Lao: *A note on the calibration of conductance probes for liquid-film thickness measurements*, internal status report, Imperial College, march 2003
25. G.F.Hewitt, G.B.Wallis: *Flooding and associated phenomena in falling film in a vertical tube*, Proc. Multiphase Flow Symposium, Philadelphia, PA, 1963, **p. 62-74**
26. A.H.Govan, G.F.Hewitt, D.G.Owen, T.R.Bott: *An improved CHF modelling code*, Proc. 2nd UK National Heat Transfer Conference, ImechE, Glasgow, paper C175, 1988

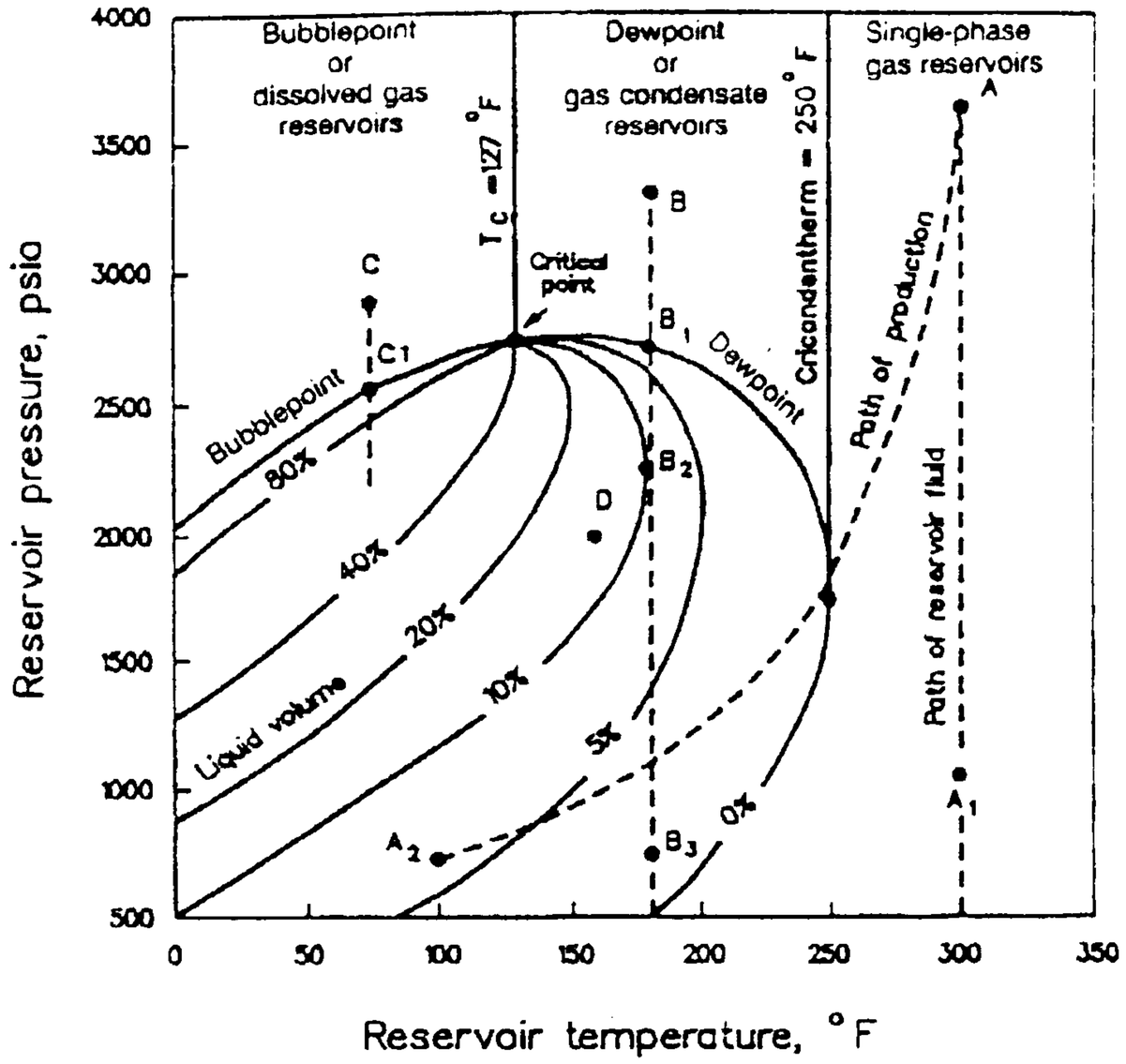


Fig.1: Classification of reservoir fluids[7]

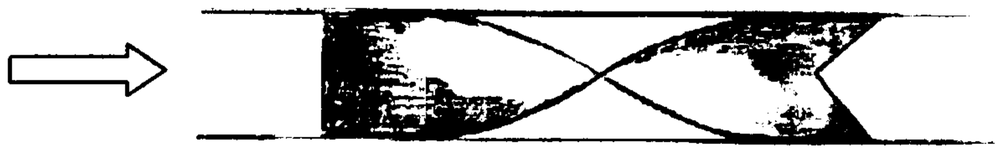


Fig.2: Twisted tape with "fish tail" end for separation of liquid drops in annular flow.

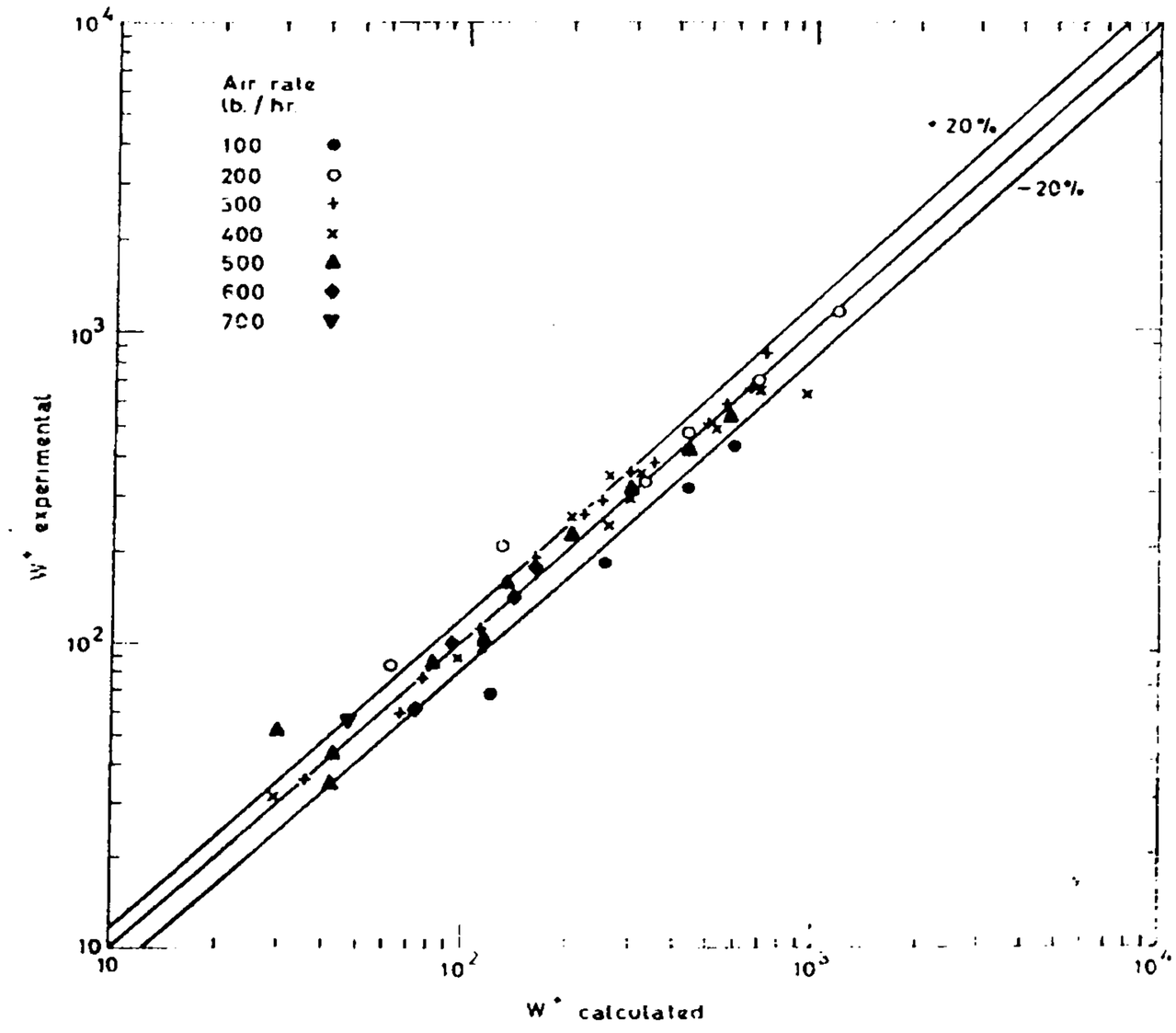


Fig. 3: Comparison of experimental dimensionless film flow rates with three calculated from the "triangular relationship"[20]

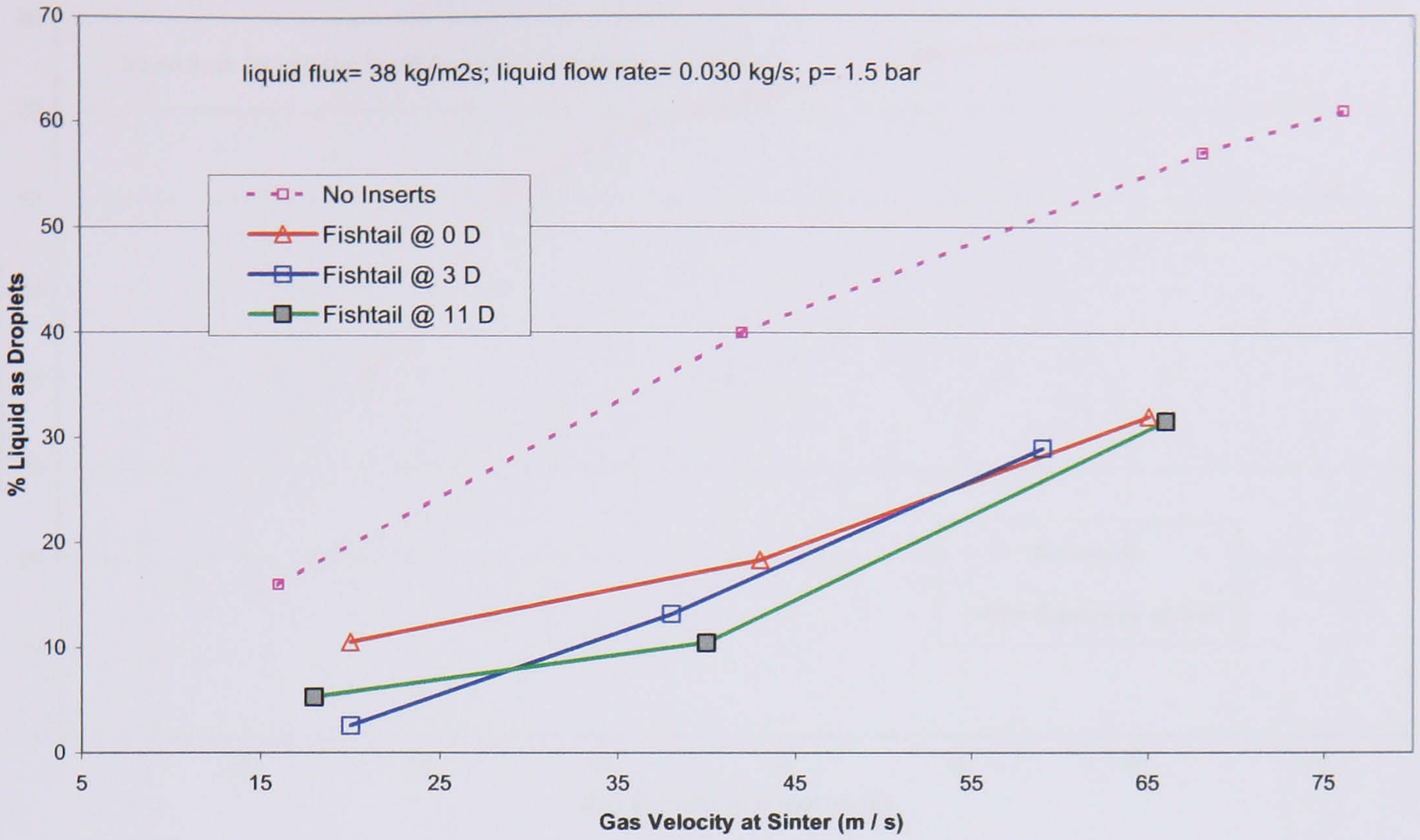


Fig. 4: Droplet separation by a "fish-tail" twisted tape device[16]

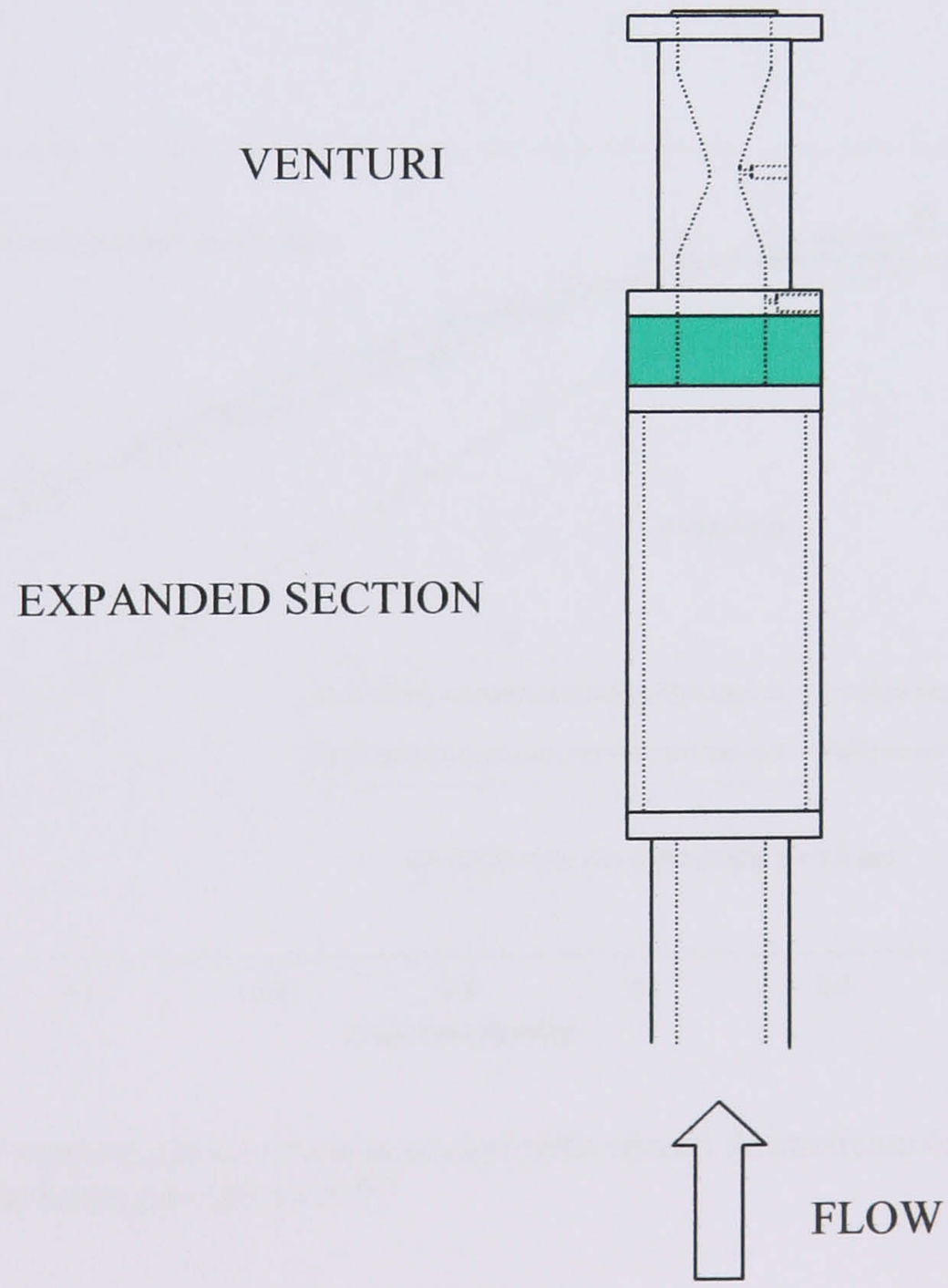


Fig. 5: Expansion / contraction device

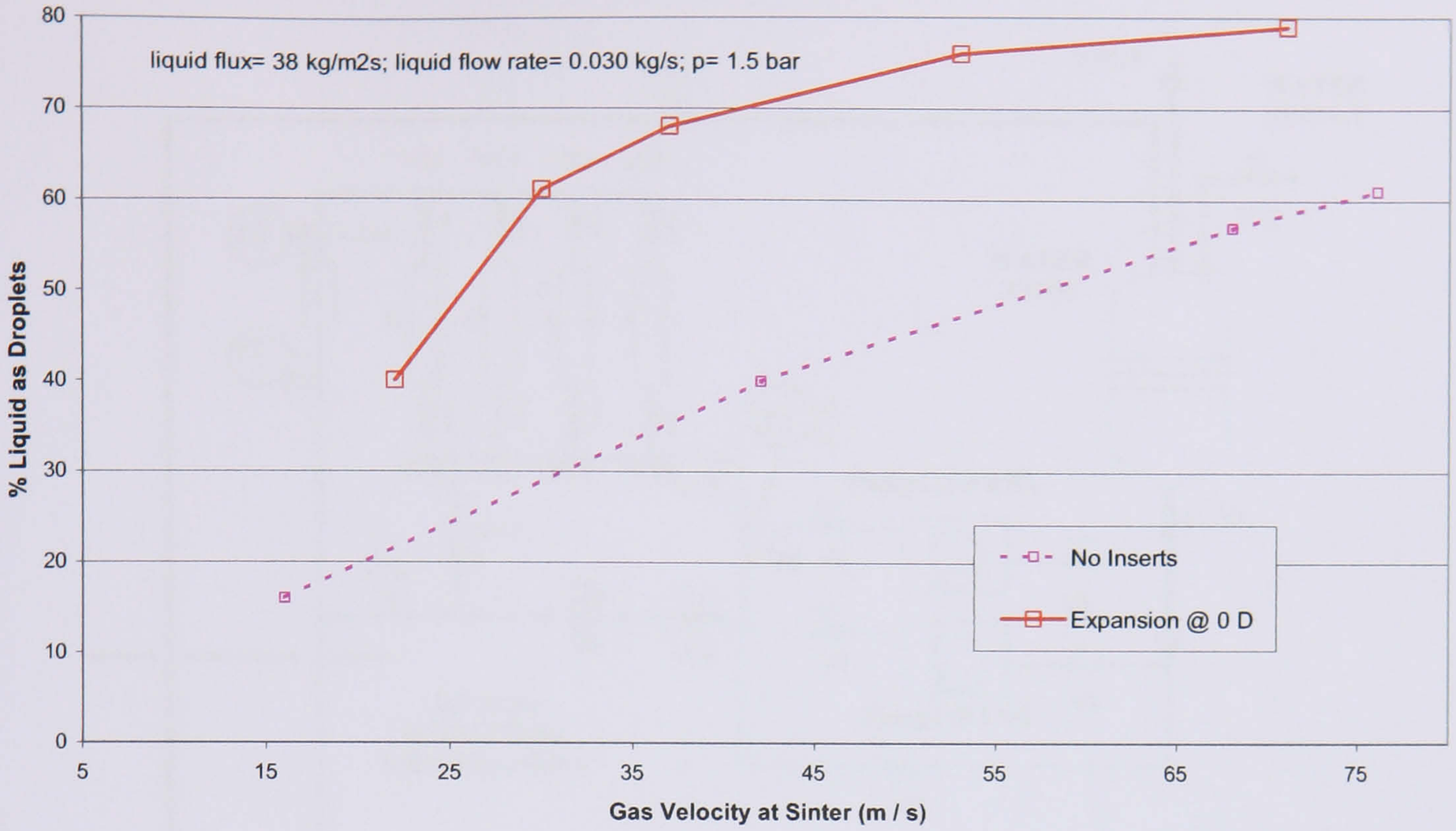


Fig. 6: Effect of expansion/contraction device on entrained fraction[16]

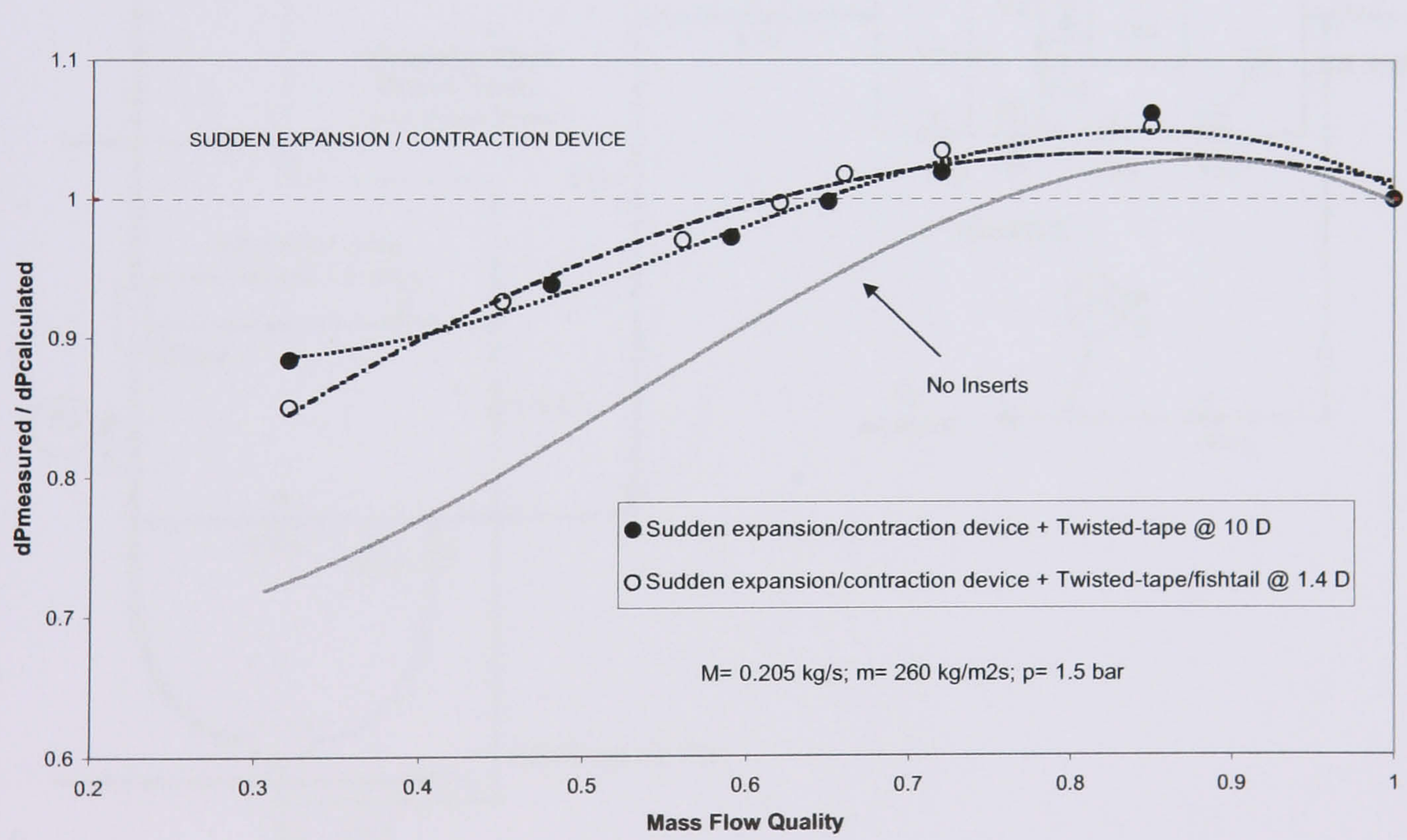


Fig. 7: Comparison of venturi pressure drop measured with venturi downstream of expansion/contraction device with that calculaed from the homogeneous model[16]

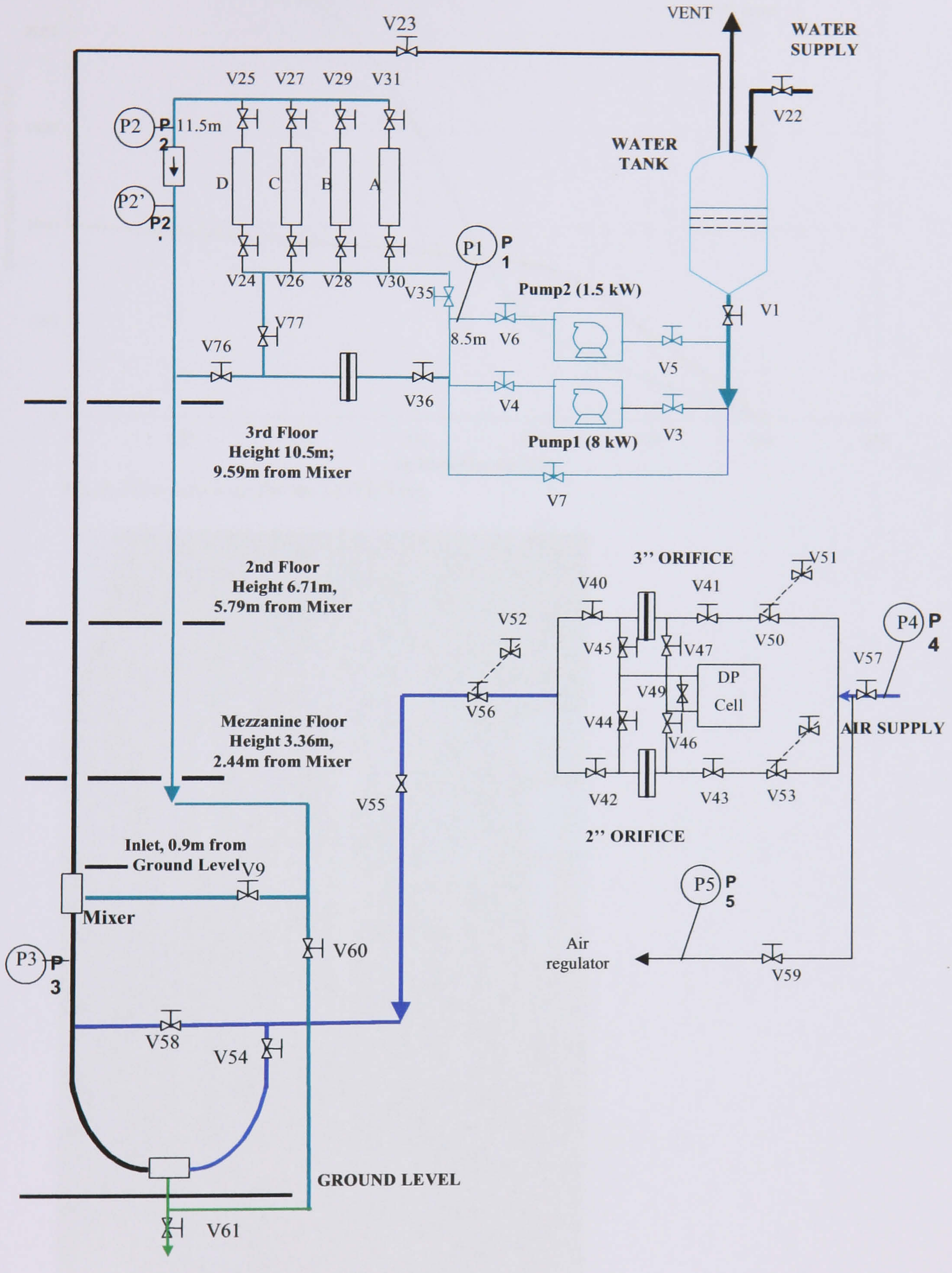


Fig. 8: The LOTUS rig.

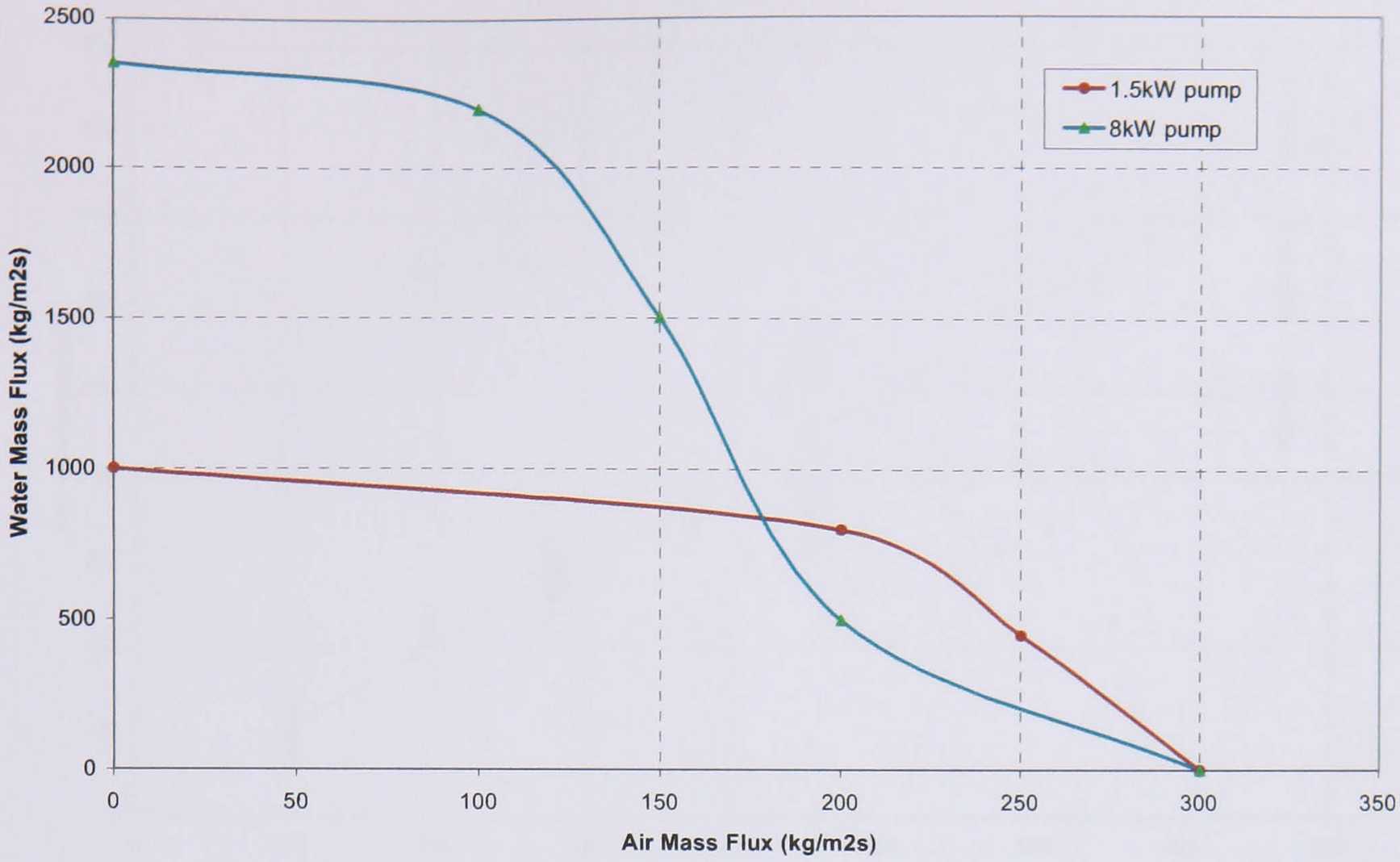


Fig. 9: Flow envelope for the LOTUS rig.

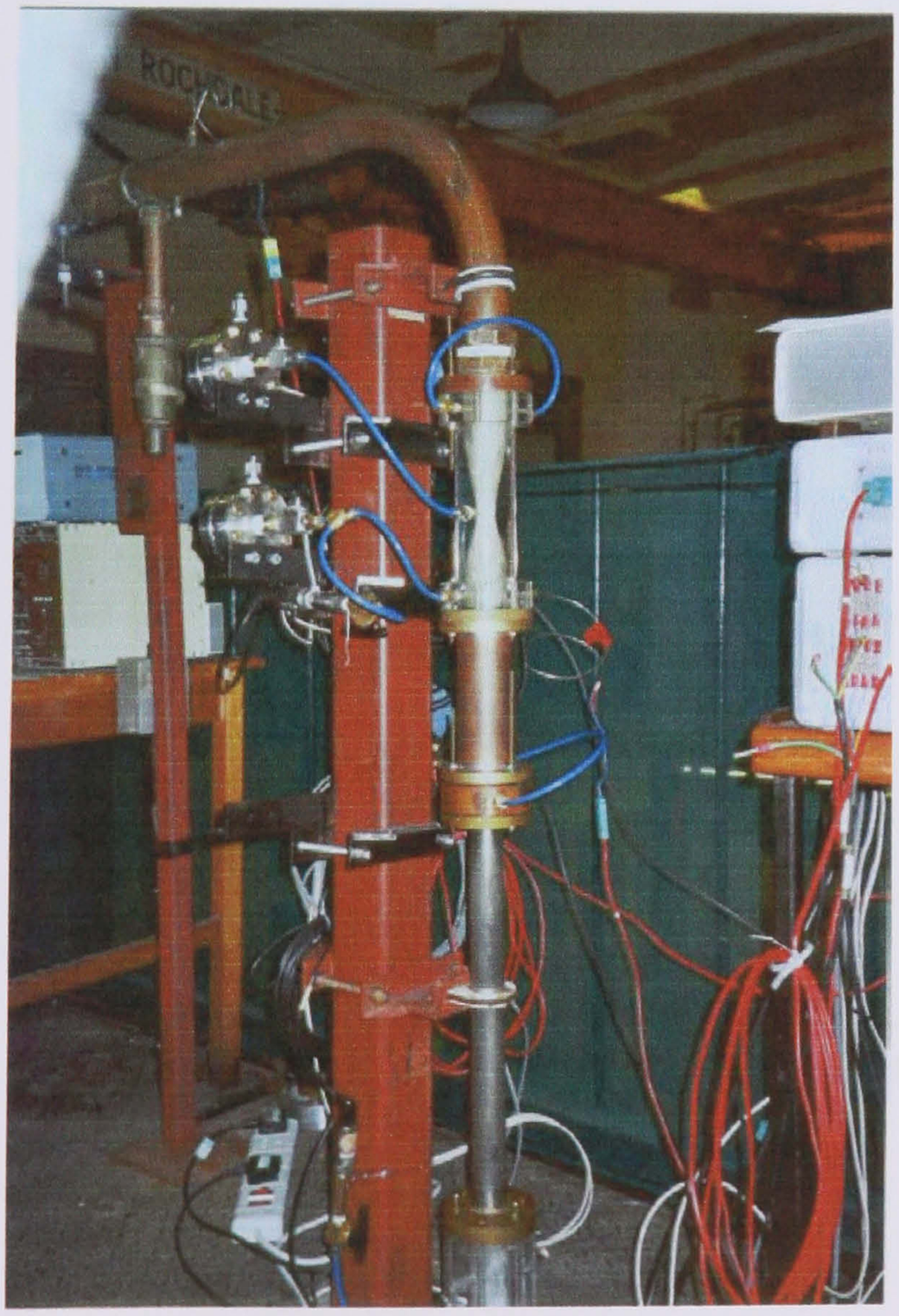


Fig. 10: The test section in the LOTUS rig.

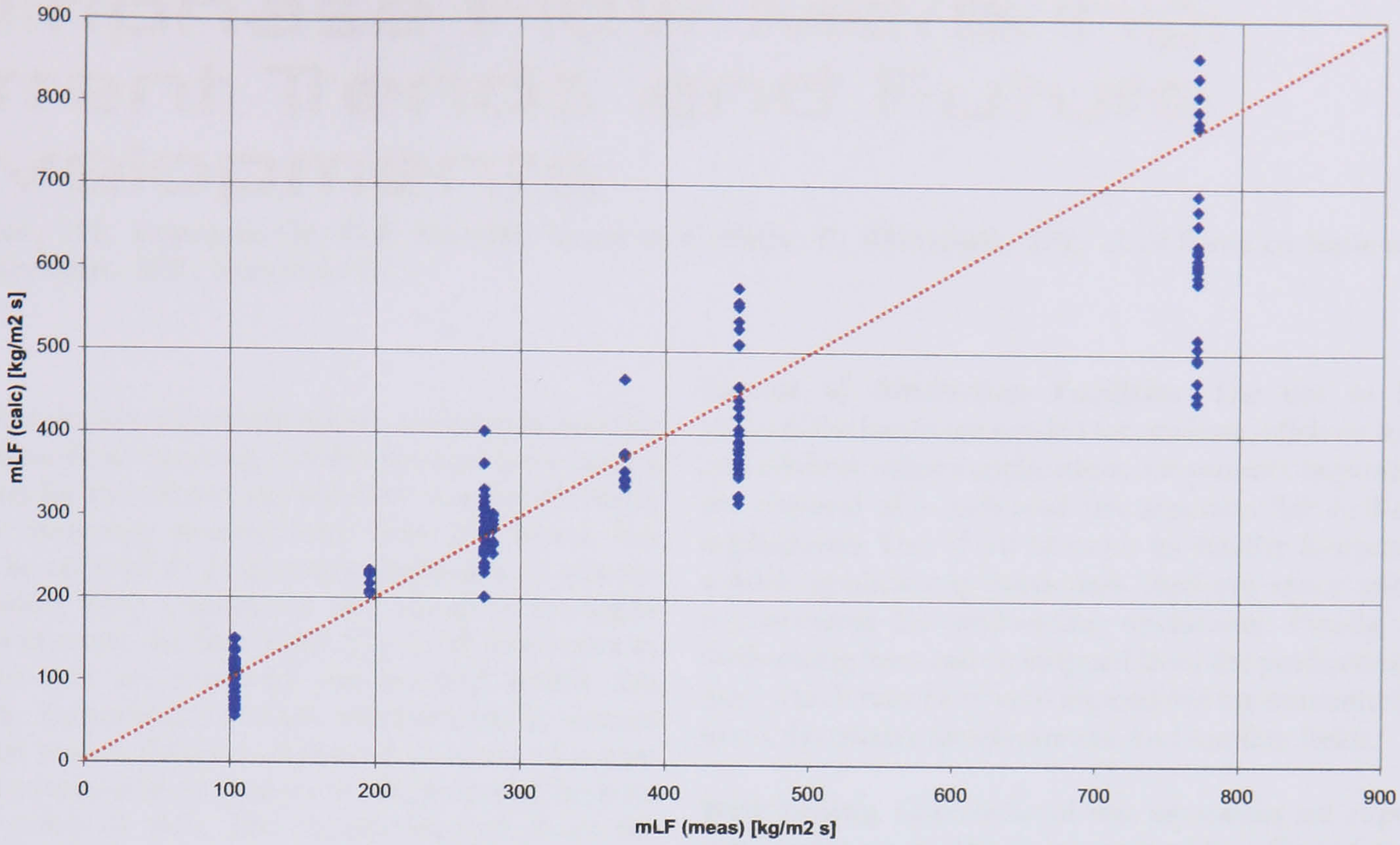


Fig. 11: Calculated vs. measured liquid mass flux.

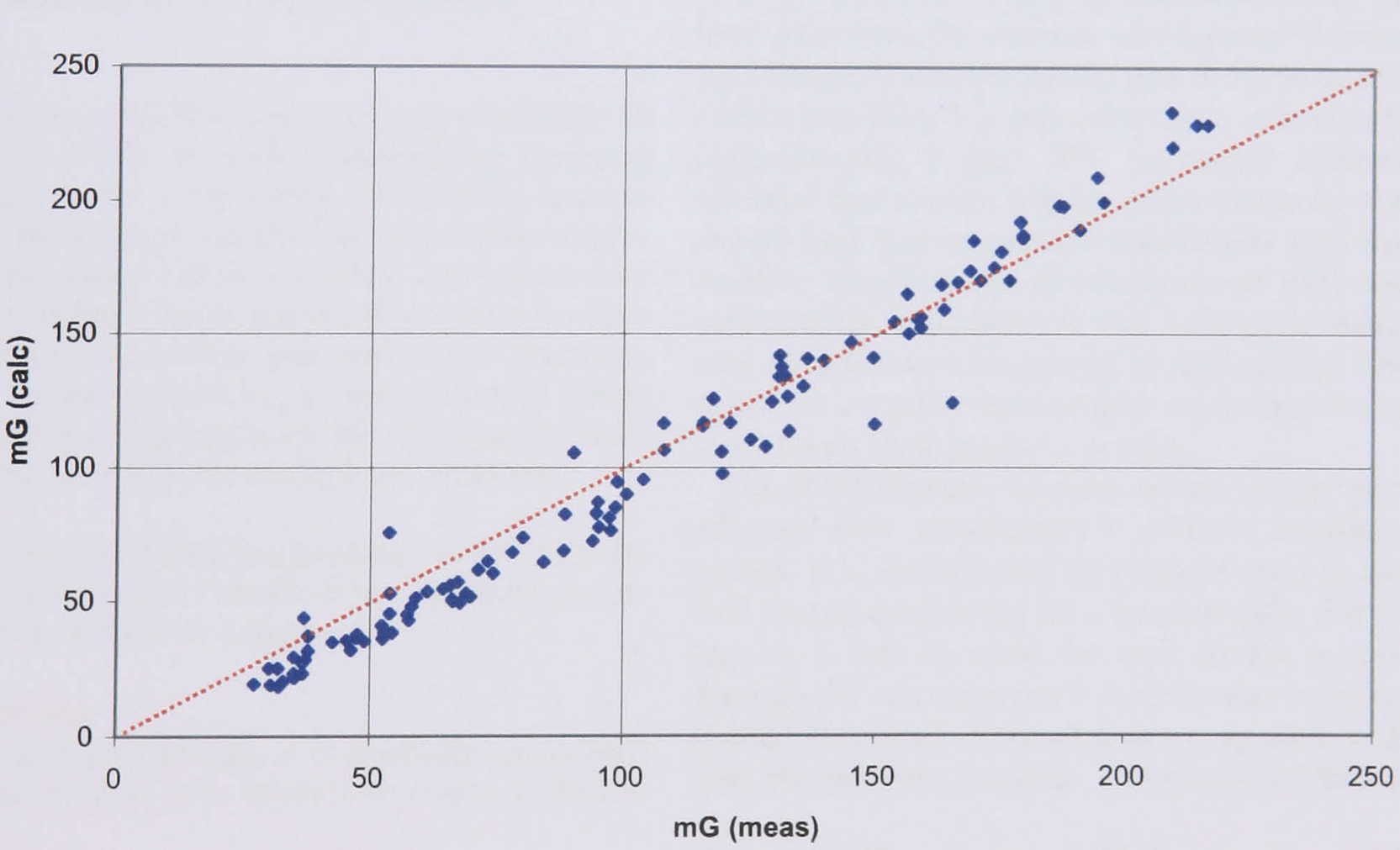


Fig. 12: Calculated vs. measured gas mass flux.

Multiphase Flow Metering: Current Trends and Future Developments

G. Falcone, SPE, Enterprise Oil; **G.F. Hewitt,** Imperial College; **C. Alimonti,** SPE, U. of Rome La Sapienza; and **B. Harrison,** SPE, Enterprise Oil

Abstract

Over the last decade, the development, evaluation, and use of multiphase-flow-metering (MFM) systems have been a major focus for the oil and gas industry worldwide. Many alternative metering systems have been developed, but none can be referred to as generally applicable or universally accurate. Both established and novel technologies suitable to measure the flow rates of gas, oil, and water in three-phase flow are reviewed and assessed within this framework. Technologies already implemented in various commercial meters then are evaluated in terms of operational and economical advantages or shortcomings from an operator's point of view. The lessons learned about the practical reliability, accuracy, and use of available technology are discussed. As operators now realize, use of MFM systems (MFMSs) is essential in exploiting marginal fields. A new approach to flow assurance, deepwater developments, downhole/seabed separation systems, and wet-gas fields is foreseen. The authors suggest where additional research to develop the next generation MFM devices will be focused to meet the as yet unsolved problems.

Brief History

The first commercial MFMSs appeared approximately 10 years ago, as a result of several multiphase metering research projects in the early 1980s. The driving force to develop MFM technology was the forecast decline of production from the major North Sea fields, accompanied by the necessity to tie back future smaller discoveries to existing infrastructure. Increasing gas and water fractions, inherent in a mature producing province, would create more-unstable flow conditions in existing production facilities and require more-flexible multiphase solutions.

In less than a decade, MFM has become accepted in the field and is beginning to be considered as a primary metering solution for new field developments.

MFM Applications

Within the oil and gas industry, it is generally recognized that MFM could lead to great benefits in terms of the following.[1,2,3]

Copyright 2002 Society of Petroleum Engineers

This paper, SPE 74689 is based on paper SPE 71474 originally presented ath the SPE 2001 Annual Technical Conference and Exhibition, New Orleans, 30 September–3 October. **Distinguished Author Series** articles are general, descriptive representations that summarize the state of the art in an area of technology by describing recent developments for readers who are not specialists in the topics discussed. Written by individuals recognized as experts in the area, these articles provide key references to more definitive work and present specific details only to illustrate the technology. **Purpose:** to inform the general readership of recent advances in various areas of petroleum engineering.

Layout of Production Facilities. The use of MFMs reduces the hardware needed for onshore, offshore topside, and offshore subsea applications. Of primary importance is the removal of a dedicated test separator for well-testing applications. Use of MFM (with its smaller footprint) for topside applications minimizes platform space and load requirements for well-testing operations. Finally, costly well-testing lines can be stripped from the production facilities, which may be of vital importance for unmanned locations, deepwater developments, and satellite fields.

Well Testing. Conventional test separators are expensive and require much time to monitor each well's performance because of the time required to reach stabilized flow conditions. It is particularly important in deepwater developments, because of the exceptional length of the flowlines. In such cases, production from individual wells connected to the same manifold may be monitored by use of a dedicated test line to avoid shutting down all the wells, then testing them one by one (with considerable production loss). However, the expense of a separate flowline may be prohibitive, hence the advantages of MFM installed in the subsea manifold. Test separators have an accuracy between approximately 5 and 10% (currently achievable with MFMSs) but require regular intervention by trained personnel and cannot provide continuous well monitoring. Another disadvantage of conventional well testing with conventional separators is that well performance suffers after shutdown cycles related to well testing. Often, wells tested on a regular basis require more-frequent workovers to maintain their production rates.

Use of MFMSs for exploration-well testing[4] provides satisfactory flow measurements without separation of the phases. It is claimed that they can be used to monitor the well during its cleanup flow (traditionally, this flow information is lost because the well stream is not directed through the test separator). Added value is represented by improved control of the drawdown applied to the formation, the pressure transient, and shortened flow periods

Reservoir Management. MFMSs provide real-time, continuous data to enable operators to characterize field and reservoir performance better and react faster. Changes in gas/oil ratio or water cut can be detected and quantified immediately, whereas traditional test separators provide information about only cumulative volumes at discrete points in time.

Production Allocation. Any situation where production from different wells and fields owned by different operators is commingled in the same pipeline for export to a common processing facility requires allocation metering. Without MFMSs, the production from each well must flow through a test separator before commingling with the other produced streams.

Production Monitoring. MFMSs provide real-time information on variations in the gas and liquid flow rates, so that well-slugging effects or gas-lift problems may be detected as they occur. This allows production optimization and extension of field life.

Capital and Operating Expenses. When operators must decide between a traditional approach to the production facilities and one including MFMSs, they must compare the capital and operating expenses of each solution. While it is relatively easy to estimate costs for hardware components, it is very difficult to predict the operating expenses. This difficulty results from the relatively low number of MFM applications worldwide and the very limited operational history. In general, it is recognized that MFM capital expense is significantly lower than that of conventional metering hardware,[5] but operators underestimate the operating expenses associated with MFM, especially for the commissioning phase and first year of operation. It is hoped that after more operational history is gained in the field, MFMSs will require less maintenance after installation and, therefore, operating expenses will be reduced.

It has been estimated that, for a subsea development 10 km from the host platform, use of a subsea MFM could represent a 62% cost reduction through the elimination of test lines.[6] In addition, MFM could improve system management with a 6 to 9% gain in the value of the oil recovered.

Fiscal Metering or Custody Transfer. Unfortunately, current MFMSs are not (and may never be) accurate enough to satisfy fiscal-metering requirements, although such an application would guarantee the future of MFMSs.

MFM Accuracy

To date, no international regulation for MFM accuracy has been delivered, which makes it very difficult for an operator to identify scenarios in which MFM can be implemented. Essentially, three main accuracy requirements exist for metering multiphase fluids: approximately 5 to 10% for reservoir management, approximately 2 to 5% for production allocation, and approximately 0.25 to 1% for fiscal metering.

Because the results from production measurements are used in the reservoir modeling or production optimization processes, it is clear that the accuracy of such measurements will affect the prediction of ultimate recovery from a reservoir. It also is clear that different levels of uncertainty may be acceptable, depending on parameters such as overall field reserves, oil price, and production lifetime. Therefore, different levels of MFM accuracy may be tolerated, without necessarily being those indicated above. With current MFM solutions, it is claimed possible to measure total liquid flow rate and gas flow rate with a relative error of less than approximately 5 to 10%, and water cut with an absolute error less than approximately 2%. [Note: Relative error=(measured−actual)/actual; Absolute error=(measured−actual).] However, because of the high complexity of multiphase mixtures, it may be optimistic to claim that the above ranges of accuracy apply to any flow regime and for any chemistry of the fluids.

Misunderstandings may occur when defining the level of uncertainty associated to different types of MFMSs. In the case of differential-pressure devices, which present a constant absolute error, the concept of "rangeability" should be taken into account if the accuracy is referred to the measurement itself **(Fig. 1)**.

Special attention must be paid to error propagation. For MFM techniques based on interdependent measurements, the errors associated to the individual measurements are combined and propagate through to the final result. Because multiphase-flow modeling is complex, tracking error propagation through the algorithm can be extremely difficult, which is why MFMSs may need to be characterized by experimental testing. Characterization can be done with tests and field trials. Laboratory tests use fluids having well-known properties. Controlled flow rates can be achieved such that operating envelopes and associated errors can be defined. Field tests then are required to identify potential operational problems. Compared with laboratory tests, field trials generally introduce more sources of error, such as the use of real fluids, the effects of changing upstream conditions, and the need for pressure/volume/temperature correlations to reconcile readings at operating conditions with readings at reference points. Some of these uncertainties may be reduced in a field flow loop, although flow instabilities or malfunctioning of the test separator can occur. In a field environment, where the reference measurements are usually taken at the test separator, crucial concerns include "Just how accurate are the measurements at the test separator?" and "Are the uncertainties in measurements from MFM and test separator comparable?"

Worldwide MFM Installations

The technical and economical advantages of MFMSs stated above are behind the increasing number of MFM field installations worldwide over the last decade. In addition, some of the major operators have made multiple orders of

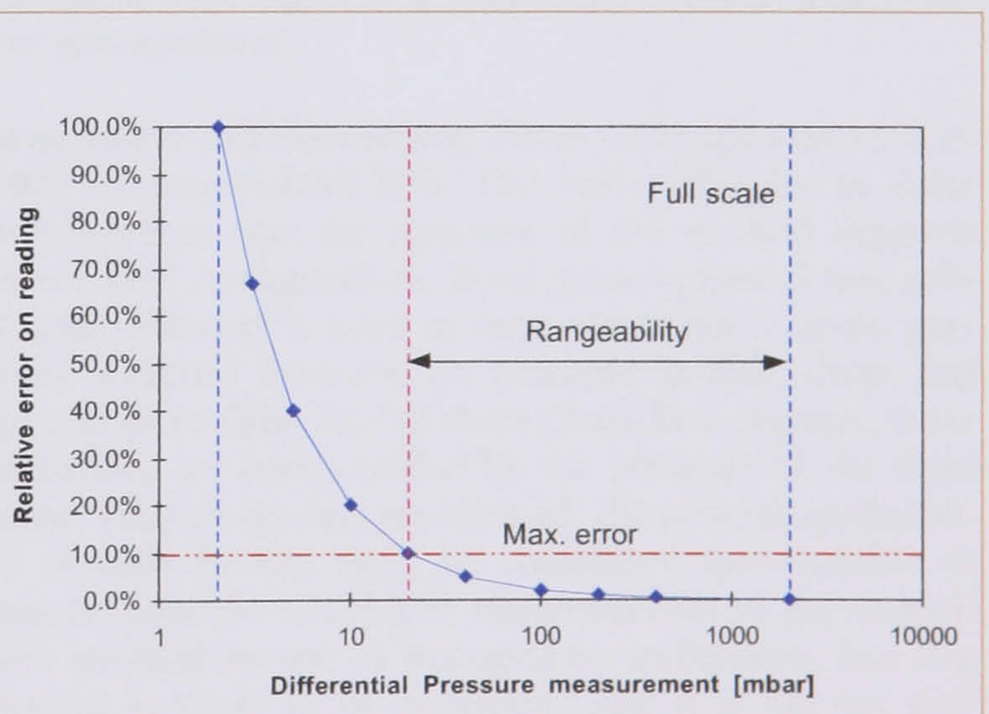
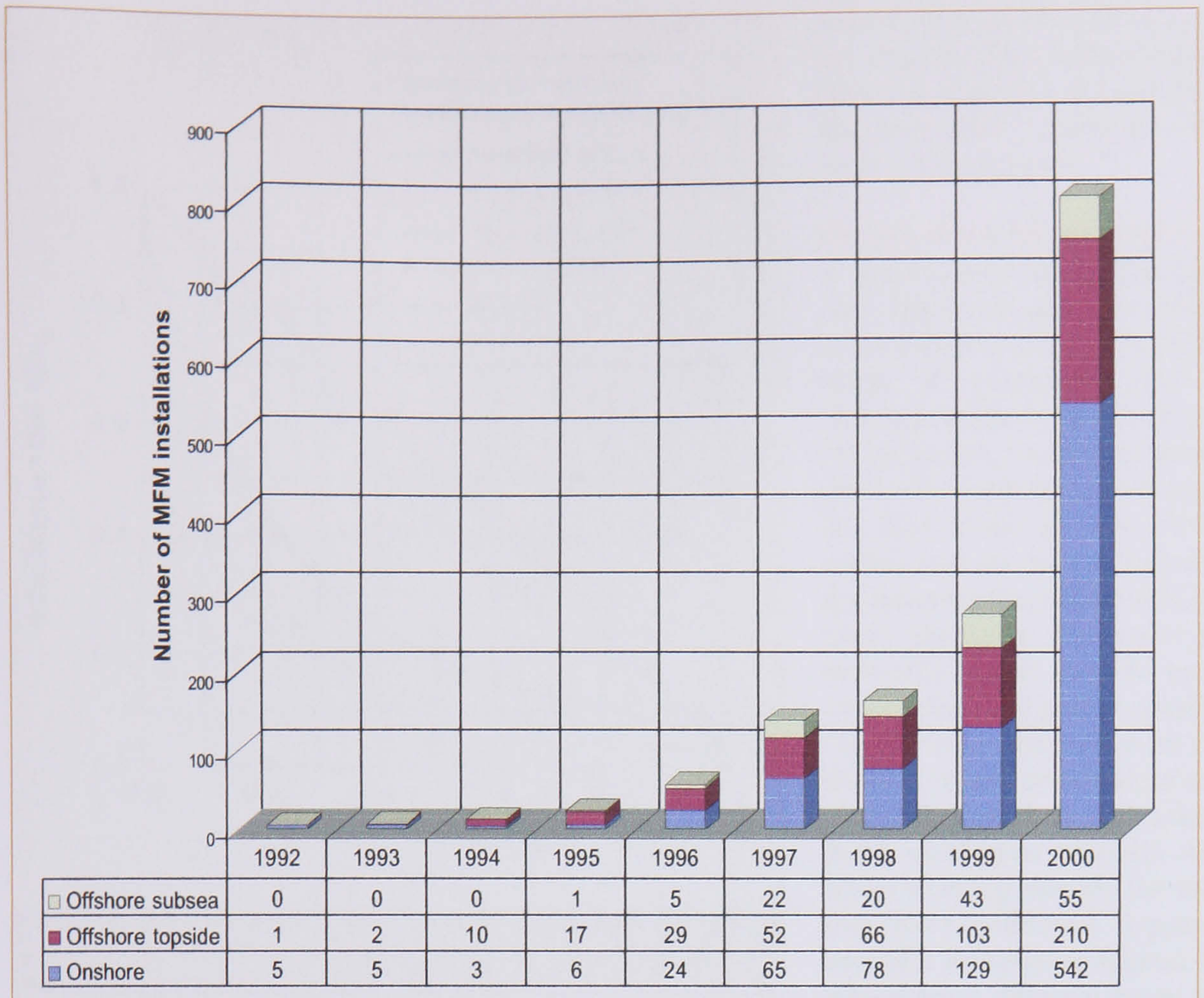


Fig. 1—The concept of "rangeability" for differential pressure devices.



	1992	1993	1994	1995	1996	1997	1998	1999	2000
Offshore subsea	0	0	0	1	5	22	20	43	55
Offshore topside	1	2	10	17	29	52	66	103	210
Onshore	5	5	3	6	24	65	78	129	542

Fig. 2—Growth rate of MFM installations.

up to 40 MFMSs for full-field application. However, the actual growth rate of MFM installations has been lower than initial industry forecasts suggested. **Fig. 2** shows the actual trend up to and including 1999,[6,7,8] plus a 2000 forecast published in 1997.[7]

Fundamentals of MFM Technologies

Basically, two approaches exist to measure flow rates of three-phase flow. In the first approach, parameters of the flow are measured that are functions of the three flow rates. For example, a pressure drop across a Venturi, the attenuation of a gamma beam, and the impedance of the mixture can be determined and relationships established between these measurements and the flow rates of the respective phases, three independent measurements are required to establish the three flow rates. These relationships cannot be predicted theoretically; therefore, they must be established by calibration. Unfortunately, it usually is not possible to calibrate the full range of conditions over which the measurement technology is to be applied, and this approach is not always a productive one.

The second approach involves measuring the basic parameters of phase velocities and phase cross-sectional fractions (holdups) or quantities that can be unequivocally related to these. To measure the volume flows (and hence the mass flows) of oil, water, and gas in a pipe, three mean velocities and three phase cross sections must be established. Therefore, five measurements are required (three velocities and two phase fractions—the third phase fraction is obtained by difference between unity and the sum of the two measured ones). Separation or homogenization can reduce this measurement requirement. By separating the phases, the need for cross-sectional holdup measurements disappears, and the three volume flows can be established by conventional single-phase metering technology. However, separation is expensive and difficult to achieve in many cases. The measurement requirement also can be reduced to three if the velocities are equalized by homogenizing the mixture. This method is a much more economic option. However, the range over which satisfactory homogenization can be achieved is always limited (e.g., it is less feasible at very high gas fractions).

Dual-Energy Gamma Densitometry. This method uses a gamma source (or sources) with different energies. It is possible to determine the holdups of the three phases, and these measurements can be coupled with velocity measurements to yield the required phase flow rates. Problems involved with this technique include shielding, source decay, averaging over the cross section, fundamental statistical inaccuracies, limitations in detection equipment, effects of changing water salinity, and the normal problems of operating sophisticated electronics for subsea applications. Nevertheless, development work on this technique has made it a reasonably reliable and effective measurement.

Impedance and Microwave. These techniques are used in many commercial MFMSs. The basic difficulty in these techniques is that the response of the method depends on the flow configuration. Even in two-phase flows, substantial differences exist in impedance (for a given gas-phase fraction) between, for example, bubble, drop, and annular flows **(Fig. 3).** For three-phase flow regimes, these difficulties are compounded by the presence of the third phase. Despite the success claimed, the general applicability of such devices must be considered questionable. It may be possible to achieve improvements in the impedance method by use of tomography techniques, but this method is likely to be expensive, and it is not yet well established for three-phase flow. Another drawback of dielectric measurements is that they are affected by the continuous phase and perform poorly in the inversion region (usually between 40 and 60% water cut).

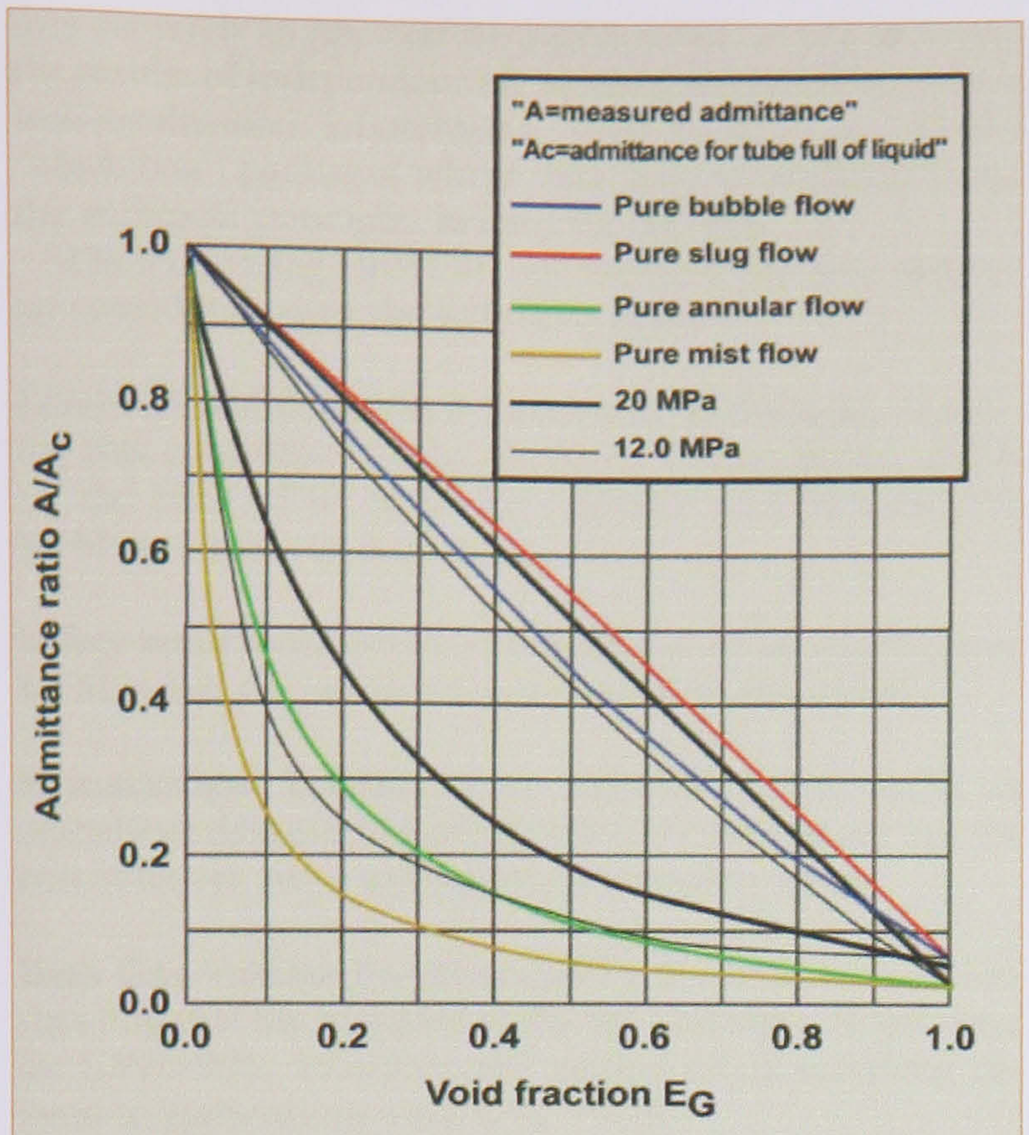


Fig. 3—Effects of flow regime and void fraction on theoretical response.

Differential Pressure. These devises are commonly used in single-phase and multiphase flow measurements. The device most commonly used for multiphase flows is the Venturi, but other devices such as orifices or chokes are sometimes used. Generally, the response of such devices for multiphase flows depends on upstream flow conditions.

The effective liquid viscosity depends on the continuous phase, the dispersed-phase fraction, and the degree to which they are mixed. An increased flow viscosity increases the differential pressure through the meter and may affect calculation of the flow velocity.

There are no general relationships for differential pressure across Venturis and other devices in multiphase flow. The best approach is to attempt to get as close as possible to a homogeneous flow. Recent work at Imperial College has concentrated on developing better homogenization schemes for high gas fractions (typically greater then 0.9).

Cross Correlation. The correlation between signals obtained at two positions along a pipe is used in several MFMSs. Thus, the peak in the cross-correlation function between the two measurements represents the "time of flight" of a flow feature between the two measurement positions. Measurement techniques to which this method can be applied include differential pressure, impedance, gamma attenuation, and acoustic transmission. Although the cross-correlation method has the advantage of directly measuring a velocity (and is, therefore, not as dependant on calibration), it suffers from several problems. The most important is that, to measure the velocity, a distinct flow feature is required. Almost always, this flow feature is a slug. Differential pressure, gamma, or impedance devices readily detect slugs. Therefore, their velocity can be determined. The problem here is that of relating this velocity to the fluid velocity with sufficient accuracy. The relationship between slug velocity and fluid velocity is highly complex and particularly severe around the phase inversion point in three-phase systems.

Novel MFM Technologies

A generic solution to the MFM problem has proved elusive. However, adequate solutions are emerging for specific applications. If regular calibration is feasible over the full range of conditions, then many alternative metering schemes could be made to work. In this case, it probably is best to select relatively inexpensive technologies and use methods, such as neural-network processing, to deduce the flow rates. To date, flow-pattern-identification techniques that use neural networks have been applied to conductance-probe, differential-pressure, and gamma-densitometer methods. The main advantage of artificial neural networks is that they do not use predefined rules (as do conventional signal-processing techniques), but rather "learn" from experience on training data sets. This feature enables neural networks to cope with the nonlinear nature of multiphase flow and achieve high accuracy. However, these intelligent systems may fail to reproduce reality when working outside the range of conditions over which they were calibrated. A possible solution is implementation of a fuzzy-logic approach. Briefly, independent sets of results from different types of measurements (or physical models) are each interpreted with neural networks. Then, on the basis of the reliability of each physical and neural-network model with regard to a particular flow configuration, the most accurate solution is selected by use of a decision-tree approach. It has been shown that such integrated solutions tend to be more accurate than those derived from a single neural-network model.[9]

Volume-fraction measurements (such as X-ray[10] or capacitance tomography, microwave techniques,[11] or grab or isokinetic sampling) are undergoing noticeable improvements and could provide the phase flow rates when combined with independent velocity measurements.

Alternatively, new stand-alone technologies are under development. Some can be highly complex, difficult to achieve, and may imply safety considerations, such as nuclear magnetic resonance (NMR) and pulsed neutron activation (PNA).[12] However, these are the only methods based on direct measurement of individual component velocities and fractions. Therefore, if available, NMR and PNA meter technology could satisfy the requirements for fiscal metering and, hence, guarantee the future of MFM. Less expensive stand-alone technologies are pressure-pulse[13] and acoustic-noise interpretation.[14] Although very attractive in terms of field applicability, these techniques may offer only limited operating ranges.

Review of Commercial MFMSs

A critical review of the MFM solutions currently available in the market is far from being an easy task. Most MFM research projects are now driven by the oil and gas industry and usually result in a patented solution. Thus, scientific and commercial interests often tend to overlap in a sector of the oil and gas market where competition is intense. Therefore, a very limited amount of public information is available on MFMS performance. Unless opera-

tors are ready to pay non-negligible sums to gain access to the results of independent MFM assessments carried out at well-established laboratories, they usually are offered "black-box" packages where very little is unveiled about the technical principles behind the MFMSs.

When choosing an MFM, operators should give particular consideration to the following items.

Level of Confidence in a Particular Technique. Acquiring this confidence is the operator's responsibility, and is on the basis of its in-house expertise and liaisons with MFM specialists or academia.

Safety and Environmental Issues. For some applications, MFMSs that use nuclear sources must be discarded.

Measurement Intrusiveness. Whenever wax, scale, or asphaltene deposition is likely, intrusive devices are not the best solution. Also, intrusiveness is a safety issue.

High Gas-Volume Fraction (GVF). It is common understanding that the majority of the MFMSs show larger error for GVF>90%. However, the market offers solutions tailored to applications with GVF>95%.

Operating Range. No tool exists that is able to cope with the entire range of GVFs, flow rates, pressure, water cuts, and flow patterns. Therefore, the window in which conditions allow accurate tool operation must be identified.

Tool Size. Most manufacturers claim that they can deliver tools between 2-in. and 10 to 12-in. in diameter with the same level of metering accuracy. However, because of the highly unpredictable nature of multiphase flow, it is very dangerous to scale up small-diameter results without performing dedicated tests on large-diameter tools. The main limitation is that large-diameter facilities are not able to guarantee the same kinds of tests as those already possible with small-diameter flow loops.

Calibration Level Needed Over Field Life. Although manufacturers tend to state that their products do not need further calibration after the factory calibration, the dangers have been illustrated of not accounting for the dependence of MFMS performance on the range of conditions (e.g., upstream conditions and fluid properties) over which they have been certified.

Capital and Operating Costs. This statement may seem obvious, but operators tend to not see the long-term advantages associated with MFM installations. Also, MFM manufacturers tend to hide the real order of magnitude of operating costs.

Level of Manufacturer Assistance. When buying MFMSs, operators also will buy other services from the manufacturers, including personnel training. It is very important to guarantee some long-term technical assistance and cooperation in case of failure or malfunction of any part of the system.

Marine Experience. Previous experience with subsea installation is a plus for manufacturers.

Vertical or Horizontal Installation. Some MFMSs must be installed vertically and others horizontally. For a particular layout of flowlines, one option may be better than the other.

Stand-Alone MFMSs vs. Integrated Packages. Some manufacturers now offer MFMSs as part of a larger package of integrated solutions for reservoir management and production optimization. Operators must evaluate whether such solutions or separate components are prefered.

Tables 1 to 4 suggest possible ways to classify current commercial MFMSs on the basis of their features. Meters still under development are not included (JNOC, IFP, Cranfield U., AEA Technology, Cidra). Also omitted are MFM solutions that must be integrated with other techniques to provide the three flow rates (isokinetic sampling—Petrotech choke-valve models).

Future of MFM

In times of low oil price, operators tend to focus efforts on short-term rather than long-term investment. Therefore, young technologies, such as MFM, that are not yet 100% proven in the field, tend to be classified as too risky and, therefore, are temporarily neglected. This neglect probably contributed to slower uptake of MFM between 1999 and 2000. With the oil price at approximately U.S. $20/bbl, the MFM market has resumed its exponential trend. The recently established Roxar Flow Measurement AS (which comprises the metering divisions of Roxar and Fluenta), in only the first four months of 2001, sold approximately the same number of MFMSs as the combined sales figures for Roxar and Fluenta for the whole of 2000. Shell predicts the MFM growth rate will settle at as many as 1,000 installations per year. Because the cycles of the oil and gas industry are notoriously difficult to predict, it may be ambitious to attempt a 5- or 10-year MFM forecast. The future of MFM depends very much on how it will fit with other technologies toward global fieldwide solutions, as well as on whether relevant scientific contributions will become mature for technical applications. Nonetheless, it is possible to address some MFM goals for the new millennium.

Better Accuracy, Repeatability, and Reliability. Because of the increasing demand for MFMSs for field installations, dedicated tests should become more frequent, allowing the manufacturers to gain a better understanding of the strengths and weaknesses of their devices and lead to improved technologies. The operating ranges of each particular solution would become clearer to the operators, who could then look at the MFM market and pick the most appropriate options for their applications.

Clamp-on Solutions for Topsides and Seabed Applications. Retrofitting existing installations is a main issue for MFM. Subsea manifolds where MFM options were not taken into account in the design may need major intervention to accept current MFMSs, causing production loss. Remote onshore fields would benefit from clamp-on MFMSs also, enabling easy moves from one flowline to another, without having to flange-connect the tool or to periodically rent a portable MFM.

TABLE 1—FLOW CONDITIONING

Homogenisation	Leave-as-it-is	In-line separation	Isokinetic sampling
Jiskoot-Mixmeter	Schlumberger-VX	Agar	TEA-Vega
Schlumberger-Framo	Roxar AS-Fluenta	WellComp	
TEA-Lyra	Roxar AS-MFI	Accuflow	
ISA-Scrollflow	Kvaerner-DUET	Kvaerner-CCM	
ISA-Solarton	Megra (for GVF<25%)	Megra (for GVF>25%)	
	Esmer	Haimo	
	Yokogawa	Jiskoot-Starcut	

International Regulation on MFM Accuracy Requirements. Although MFM is recognized and accepted by the oil and gas industry, it still must be established as a separate branch of oil and gas metering. Therefore, MFM still lacks officially approved guidelines on testing, validation and certification tools, which, unfortunately, creates many misunderstandings in the MFM community (manufacturers, operators, and governmental bodies). Reporting-accuracy standards are still absent, as are international regulations indicating which level of accuracy MFMSs must satisfy for each particular application. In some cases, MFM may be the only viable, technical, and economical solution to develop a new field. It is recognized that MFMSs cannot always achieve the same performance as single-phase meters. However, in the North Sea, as well as in other major producer countries, the only available legislation on metering requirements still requires a stream to be measured with single-phase metering accuracy, which implies separation of the phases. To date, relevant efforts in this direction have been made by the U.K. Department of Trade and Industry (DTI), the Norwegian Society for Oil and Gas Measurement,[15] and the National Engineering Laboratory, which have tried to standardize definition, classification, qualification procedure, and implementation of MFM.

TABLE 2—GAMMA SOURCE

Used	Not Used
Roxar AS-Fluenta	Agar
Schlumberger-Framo	Esmer
Schlumberger-VX	WellComp
TEA-Lyra	Accuflow
ISA-Scrollflow	Jiskoot-Starcut
Roxar AS-MFI	Kvaerner-CCM
Kvaerner-DUET	TEA-Vega
Megra	ISA-Solarton
Haimo	TEA-Lyra (for WC>30%)
Jiskoot-Mixmeter	FlowSys
	Yokogawa

TABLE 3—INTRUSIVE

Yes	No*
Jiskoot-Mixmeter	Schlumberger-VX
Agar	Roxar AS-Fluenta
Schlumberger-Framo	Roxar AS-MFI
Accuflow	KvaernerDUET
WellComp	Esmer
Kvaerner-CCM	Megra
ISA-Scrollflow	TEA-Lyra
ISA-Solarton	FlowSys
TEA-Vega	Yokogawa
Jiskoot-Starcut	
Haimo (flow conditioning vessel)	

*Venturi's are not regarded as intrusive devices.

Flow Assurance Through Technologies Integration. Marginal and deepwater fields will only be commercialized if costs are kept to a minimum, so a tendency exists to develop them by use of subsea tiebacks to existing host facilities when possible. Use of MFM avoids the need for a dedicated test line and allows metering of the produced stream before it is commingled with production from other fields. The advantages of MFM can be combined with the following technologies that enhance the feasibility of a deepwater or marginal field development.

Subsea and Downhole Separation. This technology improves vertical lift to the surface, reduces the processing load on the topside facilities, allows use of simpler flowline networks, and provides less-severe slugging. It also helps prevent corrosion, formation of hydrates and unstable emulsions, and asphaltenes deposition. Thus, many flow-assurance issues will be eased by the introduction of subsea and downhole separation, coupled with MFM to optimize field recovery.

Subsea and Downhole MFM. MFM is easier with lower GVFs, lower potential for hydrate, scale or asphaltene formation, and higher density contrast between oil and water. Downhole MFM appears best suited for intelligent wells, where streams from different producing intervals require monitoring. Otherwise, intelligent-well completions would require running wireline interventions. Downhole

TABLE 4—CROSS CORRELATION

Yes	None
Roxar AS-MFI	Jiskoot-Mixmeter
Kvaerner-DUET	Agar
Roxar AS-Fluenta	Accuflow
FlowSys	WellComp
Yokogawa	Jiskoot-Starcut
Haimo	Kvaerner-CCM
	ISA-Scrollflow
	ISA-Solarton
	Esmer
	Megra
	Schlumberger-VX
	TEA-Lyra
	Schlumberger-Framo
	TEA-Vega

MFM also allows continuous optimization of artificial-lift systems (electrical submersible pumps and gas lift) by use of real-time detection of well performance change.[16] In the future, it may be possible to achieve satisfactory metering accuracy such that, when combined with seabed multiphase pumping, topside metering will be redundant.

Multiphase Pumping. Multiphase pumping technology is used to boost production to the delivery point.[17] It can be applied without phase separation or after seabed or downhole separation to knock out water from the main hydrocarbon stream.

There are numerous ways to combine the above technologies to optimize development of a particular field. Each development scenario will vary according to the number of wells, number of fields commingled, produced-fluid properties, and distance from the delivery point. The only real drawback to all this new subsea and downhole technology is the lack of operational history and the concerns about reliability in the field.

Integrated Solutions To Optimize Field Recovery. An integrated monitoring and metering approach that enables better management of producing fields also helps improve the recovery of oil and gas. From a flow-rate-measurement point of view, it is fundamental to obtain continuous information from each producing well or producing layer in the reservoir. A distributed-metering approach enables real-time diagnosis of a well's health, because changes in well operating parameters can indicate deposition of wax, scale, or asphaltene, changes in the fluid properties, or water break through. This information then can be integrated with stock-tank measurements and reservoir modeling for nodal analysis to verify the chosen production strategy for the field. Research carried out at La Sapienza U., Rome, on the use of wellhead choke valves to monitor and predict well performance, has lead to promising results, especially when the system is integrated with MFMSs or test separators. Such a field-wide monitoring and metering approach, from downhole to stock tank, gives a real-time picture of what is happening in the reservoir and, therefore, provides the best support to reservoir simulation.[18]

Wet-Gas Metering. There seems to be a point where MFM and gas metering cross paths. Pushing the MFM operational envelope toward high GVFs (above 95%) and that of gas metering toward small liquid content (1 vol% or less), leads to what is now referred to as wet-gas metering. This general definition may change slightly depending on whether some economic value is associated with liquid recovery (in which case it may be more appropriate to talk about high-gas-fraction MFM).[19] Possible applications of wet-gas metering are gas/condensate, wet-gas, very-high-GOR, or depleted fields that are moving from moderate to very-high GOR (in which case it may be necessary to replace any MFM previously installed with dedicated wet-gas meters). Therefore, wet-gas metering is likely to become an important area of investigation in the near future. Commercial solutions are available for wet-gas metering. Although partial separation, isokinetic sampling, vortex meters, and ultrasonic meters may offer satisfactory results in some cases, the oil and gas industry seems to favor Venturi meters.

Conclusions

After more than 20 years of dedicated research and a decade of field trials, MFM has become an established discipline in the oil and gas industry. Although, to date, a generic solution to MFM does not exist, adequate methodologies are emerging for specific applications. The quality of the results achievable with existing commercial MFM solutions depends on the appropriateness of the work that operators must undertake during the pre-engineering phase of an MFM application. Throughout this period, open dialogue with the MFM manufacturers is crucial.

With respect to deepwater and marginal field developments, there is an anticipated increase in demand for accurate MFM solutions. For MFM to meet these expectations, more technical and scientific contributions are needed and more proactive communication between the oil and gas industry and governmental organizations worldwide must be established.

References

1. Williams, J.: "Status of Multiphase Flow Measurement Research," paper SPE 28515 presented at the 1994 SPE Annual Technical Conference and Exhibition, New Orleans, 25–28 September.
2. Ribeiro, A.: "Developments in Multiphase Metering," paper SPE 36197 presented at the 1996 Abu Dhabi International Petroleum Exhibition and Conference, Abu Dhabi, U.A.E., 13–16 October.
3. Thorn, R., Johansen, G.A., and Hammer, E.A.: "Recent Developments in Three-Phase Flow Measurement," *Measurement Sci. Technology, 8* (1997) 691–701.
4. Mus, E.A. *et al.*: "Added Value of a Multiphase Flow Meter in Exploration Well Testing," paper OTC 13146 presented at the 2001 Offshore Technology Conference, Houston, 30 April–3 May.
5. Sheers, A.M. and Noordhuis, B.R.: "Multiphase and Wet Gas Flow Measurement," presented at the 1999 IBC Annual Multiphase Metering Conference, Aberdeen, 22–23 February.
6. "The World Deepwater Report 2000–2004," Douglas-Westwood Ltd.
7. NEL (National Engineering Laboratory), notes from "Multiphase Flow Measurement Training Course", 17 January 2001.
8. Hatton, G.J.: "Multiphase Flow Meters and Application Trends," paper OTC 8547 presented at the 1997 Offshore Technology Conference held in Houston, 5–8 May.
9. Alimonti, C. and Bilardo, U.: "Measurement Of Three-Phase Flow Rates Using Neural Network Approach," presented at the 2001 International Conference on Multiphase Flow, New Orleans, 27 May–1 June.
10. Morton, E.J. *et al.*: "Development of a High Speed X-ray Tomography System for Multiphase Flow Imaging," presented at the 1998 IEEE Nuclear Sciences Symposium.
11. "Microwaves Make a Case for Real-Time Return," *Offshore Engineer,* September 2000, 46–47.
12. Hall, A.R.W., Whitaker, T.S., and Millington, B.C.: "Multiphase Flow Metering: Current Status and Future Developments," paper OTC 8553 presented at the 1997 Offshore Technology Conference, Houston, 5–8 May.
13. Gudmundsson, J.S. and Celius, H.K.: "Gas-Liquid Metering Using Pressure-Pulse Technology," paper SPE 56584 presented at the 1999 SPE Annual Technical Conference and Exhibition, Houston, 3–6 October.

14. Piantanida, M. *et al.*: "Multiphase Metering: Experimental Results From the Analysis of Acoustic Noise Through a Choke," paper SPE 50681 presented at the 1998 SPE European Petroleum Conference, The Hague, 20–22 October.
15. Amdal, J. *et al.*: *Handbook of Multiphase Metering*, prepared for The Norwegian Society for Oil and Gas Measurement.
16. Aspelund, A., Midttveit, O., and Richards, A.: "Challenges in Downhole Multiphase Measurements," paper SPE 35559 presented at the 1996 European Production Operations Conference and Exibition, Stavanger, 16–17 April.
17. Leporcher E.: "So far, so much better!," *SPE review*, June 2000, 8.
18. Gjerstad, T.: "Roxar Carves Multiphase Metering Niche," *Hart's E&P*, 2000 April, 87–89.
19. Couput, J. *et al.*: "Wet Gas Metering in the Upstream Area: Needs, Applications & Developments," presented at the 18th North Sea Flow Measurement Workshop, Scotland, 24–27 October 2000.

Gioia Falcone *is a petroleum engineer in the technical group of Enterprise Oil plc, Aberdeen. Falcone holds a Laurea degree in petroleum engineering from the U. of Rome, La Sapienza, and an MS degree in petroleum engineering from Imperial College, London.* ***Geoffrey F. Hewitt*** *is Emeritus Professor of chemical engineering and Senior Research Fellow at Imperial College, London.* ***Claudio Alimonti*** *is Assistant Professor at the U. of Rome, La Sapienza. He previously worked at the U. Catholique Louvain as a researcher. Alimonti holds a Laurea degree in mining engineering from the U. of Rome, La Sapienza, and a PhD degree from the U. Catholique Louvain, Louvain-la-neuve.* ***Bob Harrison*** *is a senior-staff petroleum engineer with Enterprise Oil plc, London. He holds a BS degree in electrical engineering from the U. of Science and Technology in Manchester, an MS degree in petroleum engineering from Imperial College, and an executive MBA from Cranfield School of Management.*

BRL. LONDN. UNIV